UNIVERSIDADE FEDERAL DO RIO GRANDE DO SUL
INSTITUTO DE GEOCIÊNCIAS
PROGRAMA DE PÓS-GRADUAÇÃO EM GEOCIÊNCIAS

ORIGEM E SIGNIFICADO TECTÔNICO DOS COMPLEXOS METAVULCANO-SEDIMENTARES DO CINTURÃO IRUMIDE SUL NA PROVÍNCIA DE TETE, NW DE MOÇAMBIQUE

THALES SEBBEN PETRY

ORIENTADOR: Prof. Dr. Ruy Paulo Philipp

Porto Alegre - 2023

UNIVERSIDADE FEDERAL DO RIO GRANDE DO SUL
INSTITUTO DE GEOCIÊNCIAS
PROGRAMA DE PÓS-GRADUAÇÃO EM GEOCIÊNCIAS

ORIGEM E SIGNIFICADO TECTÔNICO DOS COMPLEXOS METAVULCANO-SEDIMENTARES DO CINTURÃO SOUTHERN IRUMIDE NA PROVÍNCIA DE TETE, NW DE MOÇAMBIQUE

THALES SEBBEN PETRY

ORIENTADOR: Prof. Dr. Ruy Paulo Philipp

BANCA EXAMINADORA

Prof. Dra. Carla Cristine Porcher – Instituto de Geociências, Universidade Federal do Rio Grande do Sul (UFRGS)

Prof. Dr. Edinei Koester – Instituto de Geociências, Universidade Federal do Rio Grande do Sul (UFRGS)

Prof. Dr. Roberto Sacks de Campos – Departamento de Geologia, Universidade Federal de Santa Catarina (UFSC)

Tese de Doutorado apresentada como requisito parcial para a obtenção do título de Doutor em Ciências

Porto Alegre - 2023

Petry, Thales Sebben

Origem e significado tectônico dos complexos metavulcanossedimentares do Cinturão Irumide Sul na província de Tete, NW de Moçambique. / Thales Sebben Petry. - Porto Alegre: IGEO/UFRGS, 2023.

[136 f.] il.

Tese (Doutorado). - Universidade Federal do Rio Grande do Sul. Programa de Pós-Graduação em Geociências. Instituto de Geociências. Porto Alegre, RS - BR, 2023.

Orientador: Ruy Paulo Philipp

1. Cinturão Irumide Sul. 2. Complexos Metavulcanossedimentares. 3. Zircão detrítico. 4. Datação U-Pb. 5. Isótopos Lu-Hf. 6. Título.

CDU 550.42

Catalogação na Publicação
Biblioteca Instituto de Geociências - UFRGS
Renata Cristina Grun CRB 10/1113

Universidade Federal do Rio Grande do Sul - Campus do Vale Av. Bento Gonçalves, 9500 - Porto Alegre - RS - Brasil

CEP: 91501-970 / Caixa Postal: 15001.

Fone: +55 51 3308-6569 Fax: +55 51 3308-6337

E-mail: bibgeo@ufrgs.br

AGRADECIMENTOS

Início meus agradecimentos enaltecendo o papel da Universidade Federal do Rio Grande do Sul e do Instituto de Geociências em minha formação acadêmica. Graduação, mestrado e doutorado, mais de uma década de aprendizado e convivência em uma instituição de excelência. A todos que compõem a UFRGS, professores, técnicos e servidores, reconheço e agradeço sua dedicação na formação de pessoas e expansão do conhecimento. Um agradecimento ao CNPq e a nação brasileira, que financiou o trabalho, estejam certos de que irei retribuir e contribuir para o crescimento do nosso belo país. Um agradecimento especial à equipe do PPGGEO pelo importante suporte no desenvolvimento da tese. Agradeço a colaboração e o suporte da Universidade Eduardo Mondlane, de Maputo, Moçambique, e do Instituto Nacional de Minas (INAMI), que representam os alicerces de uma cooperação científica iniciada em 2011 a partir da integração proposta pelo Instituto de Geociências da Universidade de São Paulo através do Prof. Dr. Umberto Giuseppe Cordani.

Agradeço ao meu orientador Ruy Paulo Philipp pela oportunidade de participar do projeto Pró-África e conhecer Moçambique. Foi um tempo de muito aprendizado científico e crescimento pessoal e profissional que só um doutorado pode proporcionar. O teu apoio e empenho foram imprescindíveis para conclusão da tese, muito obrigado Ruy! Agradeço ao Prof. Marcio Pimentel por ter viabilizado o projeto, embora não esteja mais presente para ver os resultados. Agradeço aos parceiros de campo e aventura na África, prof. Dr. Rômulo Machado (IG-USP), Prof. Dr. Daud Liace Jamal, Msc. Matheus Philippe Bruckmann pirita, ao técnico em mineração Sr. Antonio Rizzo Alface, e a Dra. Fátima Chaúque, pela colaboração e pelo resgate no vilarejo de Fíngoè. Agradeço ao Laboratório de Geocronologia, do Departamento de Geologia da Universidade Federal de Ouro Preto, e aos pesquisadores Prof. Dr. Cristiano de Carvalho Lana (Coordenador) e a geóloga e técnica Ana Ramalho Alkmim, por todo o apoio na obtenção dos dados geocronológicos e isotópicos.

Agradeço a todos os amigos que foram assertivos nos incentivos e compreensivos nos momentos de ausência ou pouca paciência. Agradeço a minha família, mãe Juvenilda, pai Mário e irmã Madalena, por toda a segurança e suporte nessa longa jornada acadêmica. Vocês foram um esteio e nada disso teria sido possível sem o apoio de vocês. Por fim, agradeço a minha esposa Juliana, que sem dúvida foi quem mais me apoiou

nesses anos de doutorado, principalmente no final da tese com todo o cuidado e dedicação de mãe ao nosso amado Miguel. O tempo que estive ausente ou disperso não podemos voltar, mas estarei com vocês para curtir tudo o que virá. Esse trabalho é dedicado a vocês dois!

RESUMO

Nesta tese foi investigada a origem e evolução dos complexos metavulcano-sedimentares do Cinturão Irumide Sul na Província de Tete, noroeste de Moçambique. Os complexos Zâmbuè, Fíngoè, Cazula e Chidzolomondo foram selecionados para o estudo de proveniência de zircão detrítico com a datação U-Pb e avaliação das composições isotópicas Lu-Hf, geoquímica de rocha total e química mineral. O Cinturão Irumide Sul consiste em um cinturão de idade Mesoproterozoica formado a margem norte do Cráton do Zimbábue e que compõem o conjunto de cinturões orogênicos do Ciclo Grenviliano na região sudeste da África. A sua evolução registra um Ciclo de Wilson completo com a abertura e o fechamento de um oceano existente entre os crátons Zimbabwe e Bangweulu entre 1400-1000 Ma, caracterizando a Orogênese Irumide. Os complexos supracrustais do cinturão foram interpretados como bacias de margem passiva e bacias de arco deformadas e metamorfizadas durante a colisão entre os dois crátons. O Supergrupo Zâmbuè compreende uma sucessão de ortoquartzitos e meta-arcóseos com a ocorrência subordinada de xistos calci-silicaticos, mármores e um complexo basal de orto e paragnaisses. Os complexos Fíngoè e Cazula são compostos por meta-arenitos, xistos calci-silicáticos e metapelitos intercalados com rochas metavulcânicas félsicas, máficas e ultramáficas. O Complexo Chidzolomondo compreende gnaisses básicos a intermediários de origem vulcânica, gnaisses pelíticos, calci-silicáticos e quartzo-feldspáticos migmatíticos, metamorfizados na fácies granulito. A datação U-Pb em zircão detrítico de cinco amostras metassedimentares dos complexos estudados mostraram áreas fonte principais mesoproterozoicas com idades entre 1360 e 1080 Ma. As determinações isotópicas Lu-Hf em zircão mostraram valores de εHf(t) predominantemente positivos entre +2 e +10 e ~~as~~ idades modelo Hf_{TDM} entre 2,0 e 1,2 Ga, indicando uma assinatura isotópica juvenil, relacionada ao magmatismo de arco do cinturão. As contribuições menores de cristais de zircão Arqueano e do Paleoproterozoico evidenciam a proximidade do arco com um núcleo cratônico, ou mesmo a existência de um embasamento ensiálico para o cinturão. As idades máximas de deposição variaram entre 1121 e 1077 Ma, caracterizando um padrão de proveniência marcado por picos de idade muito próximos às idades máximas de deposição, atestando que os complexos foram formados como bacias relacionadas ao arco magmático. A datação das bordas dos cristais de zircão obtidas em amostras de gnaisse pelítico, metagabro e gnaisses charnoquíticos do Complexo Chidzolomondo evidenciaram a ocorrência de ao menos três eventos

metamórficos no cinturão. Estes eventos registram a transição da fase acrescionária para a fase colisional da Orogênese Irumide. O evento M_1 é relacionado a fase acrescionária e ao magmatismo sin-colisional com idade de 1092 Ma. O evento M_2 registra o metamorfismo do pico da colisão continental em ~1060 Ma. O evento M_3 registra o metamorfismo de contato associado à intrusão dos corpos gabróicos e charnoquíticos no ambiente pós-colisional com idades de magmatismo e metamorfismo em ~1025 Ma.

ABSTRACT

This thesis investigated the origin and evolution of the metavolcano-sedimentary complexes of the Southern Irumide Belt in Tete Province, northwest Mozambique. The Zâmbuè, Fíngoè, Cazula and Chidzolomondo complexes were selected for evaluation of the source areas through detrital zircon U-Pb dating and Lu-Hf isotopic determination, whole-rock geochemistry and mineral chemistry. The Southern Irumide Belt consists of a Mesoproterozoic orogenic belt formed to the north of the Zimbabwe Craton which makes up the Grenvillian orogenic Cycle in southeastern Africa. The evolution of the belt records the opening and closure of an ocean between the Zimbabwe and Bangweulu cratons between 1400-1000 Ma, characterizing the Irumide Orogeny. The supracrustal complexes of the belt were interpreted as deformed and metamorphosed passive margin and arc-related basins. The Zâmbuè Supergroup comprises a succession of orthoquartzites and meta-arkoses with subordinate occurrence of calcic-silicatic schists, marbles and a basal complex of ortho and paragneisses. The Fíngoè and Cazula complexes are composed of metasandstones, calcic-silicatic schists and metapelites interlayered with felsic, mafic and ultramafic metavolcanic rocks. The Chidzolomondo Complex comprises basic to intermediate granulitic gneisses of volcanic origin, pelitic, calcic-silicatic and quartz-feldspathic gneisses. U-Pb detrital zircon dating from five metasedimentary samples of the complexes show similar source areas, with ages between 1360 and 1080 Ma. The Lu-Hf zircon isotopic determinations showed predominantly positive εHf(t) values between +2 and +10 and the Hf_{TDM} model ages between 2,0 and 1,2 Ga showed predominantly juvenile isotopic signatures related to the arc magmatism of the belt. Minor Archean and Paleoproterozoic ages evidence the proximity of the arc to a cratonic core or even the existence of an ensialic basement for the belt. Maximum depositional ages vary between 1121 and 1077 Ma. The provenance pattern marked by age peaks very close to the maximum depositional ages shows that the complexes were formed as arc-related basins. The dating of metamorphic rims in zircon crystals from a pelitic gneiss, a metagabbro and a charnockitic gneiss of the Chidzolomondo Complex evidenced the occurrence of at least three metamorphic events in the belt. These events record the transition from the accretionary phase to the collisional phase of the Irumide Orogeny. The M_1 event is related to the accretionary phase and syn-collisional magmatism at ca. 1092 Ma. The M_2 event records the peak metamorphism of the continental collision at ~1060 Ma. The M_3 event records the thermal metamorphism

related to the intrusion of gabbroic and charnockitic bodies in the post-collisional setting with metamorphism and magmatism ages at ~1025 Ma.

SUMÁRIO

CAPÍTULO I

1. Introdução

Esta tese de doutorado está estruturada em um capítulo introdutório e integrador dos resultados e um capítulo contendo dois artigos científicos submetidos ao periódico internacional Precambrian Research (Qualis-CAPES A1), conforme as normas estabelecidas pelo Programa de Pós-Graduação em Geociências da Universidade Federal do Rio Grande do Sul. O projeto de pesquisa foi apoiado através de bolsa de doutorado (CNPq, processo nº 141319/2017-8), além de projeto de pesquisa Pró-África "Evolução tectônica da porção norte do Cinturão Moçambique, região de Tete" (CNPq, processo nº 440126/2015-0).

1.1. Objetivos

Esta tese teve como objetivo principal determinar a origem, os ambientes tectônicos e a evolução dos complexos metamórficos Zâmbuè, Fíngoè, Cazula e Chidzolomondo no contexto do cinturão Mesoproterozoico Irumide Sul na Província de Tete. A integração das diferentes metodologias permitiu uma reavaliação sobre a história evolutiva dos complexos, desde o ambiente de formação da bacia sedimentar, as relações estratigráficas com as unidades adjacentes, as condições de metamorfismo e o seu contexto litoestratigráfico no cinturão. Os objetivos específicos foram:

- Determinar a proveniência das rochas metassedimentares através da datação U-Pb;
- Determinar as fontes do magmatismo através da determinação das razões Lu-Hf em cristais de zircão detrítico;
- Determinar a idade de cristalização U-Pb em zircão e a composição química e mineralógica das rochas metavulcânicas para definir a idade e a natureza do vulcanismo da bacia;
- Determinar as idades de metamorfismo dos complexos através da datação U-Pb das bordas metamórficas em cristais de zircão;
- Determinar a idade de cristalização U-Pb em zircão e a composição química e mineralógica dos charnockito e gabros intrusivos nos complexos metamórficos para definir a idade e as características do magmatismo pós-colisional;
- Determinar as condições de P-T do metamorfismo através de estudos de geotermobarometria por pseudoseção;
- Avaliar as condições de captura das associações vulcano-sedimentares pelas suítes

graníticas encaixantes através de relações estratigráficas de campo e da literatura, como tipo de relações de contato, relações de intrusão e inclusão, cronologia relativa de estruturas, entre outras.

1.2. Contexto geológico

Esta tese inivestigou os complexos metavulcano-sedimentares do Cinturão Irumide Sul situados na Província de Tete, região noroeste de Moçambique, que se insere no contexto tectônico da região sudeste da África. O arcabouço geológico do embasamento Pré-Cambriano da região SE da África é caracterizado por núcleos cratônicos de idade arqueana (~~ex.~~ Zimbabwe, Bangweulu, Tanzânia, entre outros) envoltos por cinturões orogênicos de idade paleoproterozoica (ex. Magondi, Ubendian), mesoproterozoica (ex. Nampula, Namaqua, Irumide) e neoproterozoica (ex. Zambezi, Moçambique, Damara). O Cinturão Irumide Sul tem idade mesoproterozoica, e sua formação resultou da convergência entre os crátons Zimbabwe e Bangweulu (Fig. 1). O cinturão tem um formato triangular com dimensões aproximadas de 600 x 300 km e tem sua maior extensão nas regiões sudeste da Zâmbia e noroeste de Moçambique, com uma pequena porção ao norte do Zimbábue e ao oeste do Malawi. É delimitado por zonas de cisalhamento dúcteis de escala crustal, ao norte e noroeste a Zona de Cisalhamento Mwembeshi, ao sul a Zona de Cisalhamento Sanangoè e a leste a Zona de Cavalgamento Angónia. O cinturão é composto principalmente, por complexos metavulcano-sedimentares cercados por suites granitoides sin- a tardi-orogênicas (pós-colisionais).

A evolução tectônica do Cinturão Irumide Sul registrou a formação de crosta oceânica a partir de ~1400 Ma, a deposição de bacias de margem passiva, a convergência e subducção de crosta oceânica com formação e evolução de arcos magmáticos (intra-oceânicos e/ou de margem continental) entre ~1328 e 1080 Ma. Os processos colisionais e pós-colisionais que se seguiram, ocorreram entre 1080 e 1000 Ma. Os eventos de subducção e a acresção do magmatismo juvenil ocorreram ao norte do Cráton Zimbábue, e a colisão continental envolveu a margem passiva ao sul do Cráton Bangweulu, o Cinturão Irumide. Esta sequência de eventos caracteriza a Orogênese Irumide, que registrou um Ciclo de Wilson completo ao longo do Mesoproterozoico. O Cinturão Irumide Sul integra o sistema de cinturões orogênicos Mesoproterozoicos que circundam o Cráton Kalahari (ex. Nampula, Namaqua) e remontam a formação do supercontinente Rodínia. As associações petrotectônicas do Cinturão Irumide Sul foram retrabalhadas por eventos relacionados as orogêneses Pan-Africanas (880-470 Ma) e, de um modo geral, a deformação e o metamorfismo são limitados as proximidades das grandes zonas de cisalhamento dúcteis e o magmatismo granítico é restrito a batólitos graníticos de

pequena expressão.

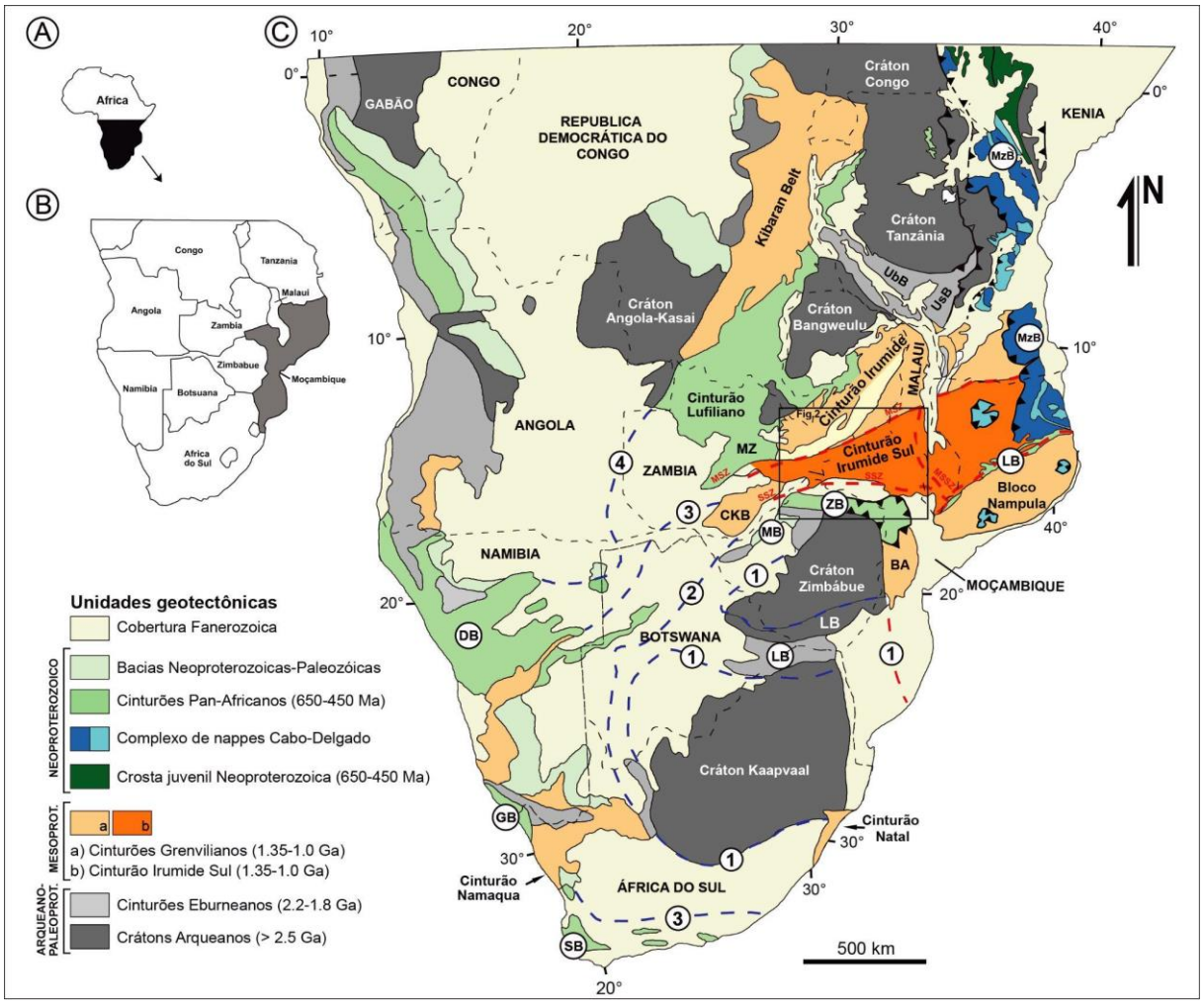

Figura 1. Mapa tectônico simplificado do sul da África, adaptado de Hanson (2003). (A) Mapa de localização no continente Africano; (B) Localização de Moçambique na porção sul da África; (C) Mapa geotectônico com as principais unidades da África central e do sul. CKB – Bloco Choma-Kalomo; LB – Cinturão Lúrio; MB – Cinturão Magondi; MzB – Cinturão Moçambique; ZB – Cinturão Zambezi; BA – Arco Bárue; UsB – Cinturão Usagaran; UbB – Cinturão Ubendian.

O mapeamento geológico mais recente da Província de Tete, realizado pelo Serviço Geológico da Finlândia (GTK Consortium, 2006) e pelo Conselho de Geociências (CGS), África do Sul em colaboração com a Direção Nacional de Geologia (DNG) e com o Ministério dos Recursos Minerais e Energia (MIREME) da República de Moçambique (CGS, 2007), resultou na individualização e caracterização das unidades litoestratigráficas com base nas relações de campo e suas especificidades litológicas, metamórficas, estruturais, geoquímicas e geocronológicas. O mapeamento foi realizado na escala de 1:250.000 e é uma das poucas referências disponíveis sobre a geologia da região e sobre os complexos estudados. A região

compreende complexos metavulcano-sedimentares metamorfizados em condições de fácies xisto-verde a granulito, envoltos e suportados por suítes granitoides de natureza sin- a tardi-orogênicas (Fig. 2). O magmatismo pós-colisional do cinturão inclui o magmatismo bimodal do complexo acamadado gabro-anortosítico da Suite Tete e dos charnockitos da Suite Castanho, além de intrusões de corpos menores de gabros.

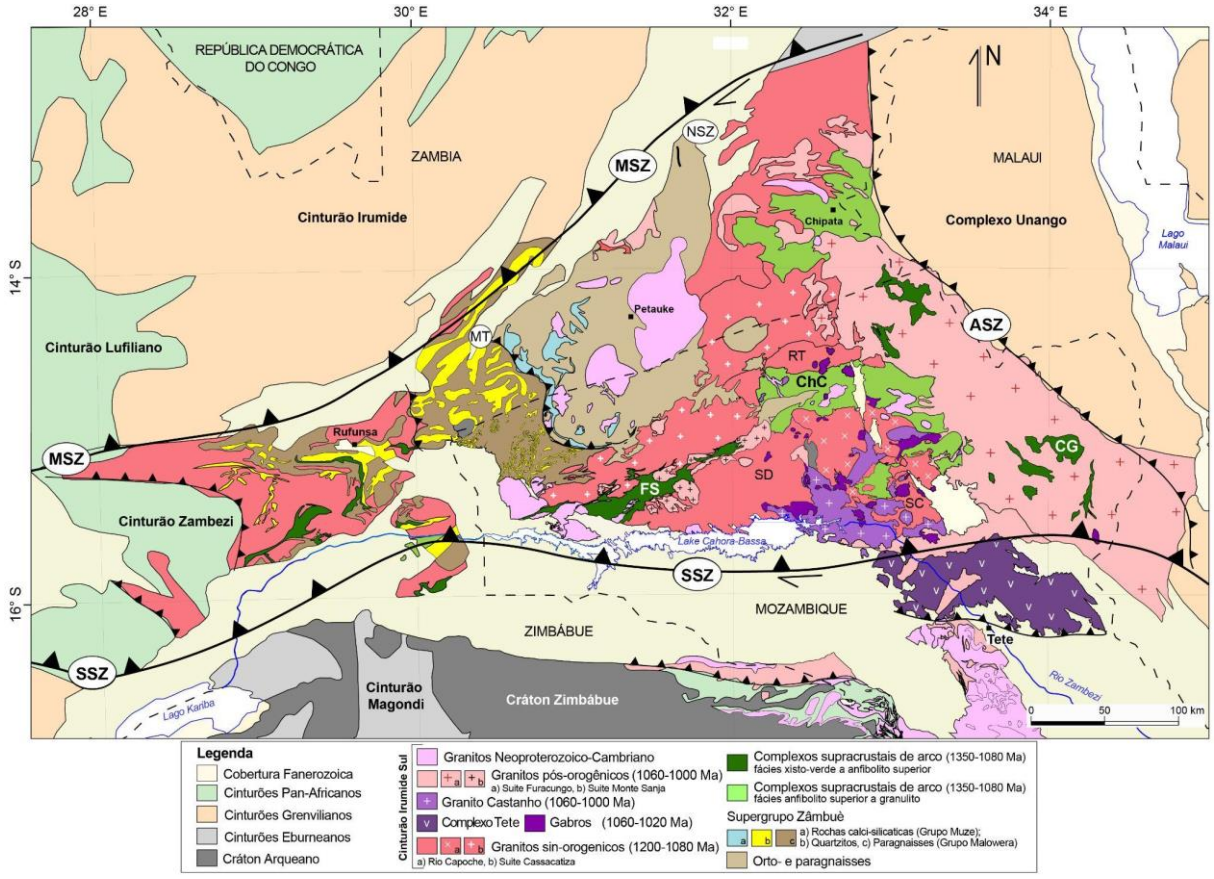

Figura 2. Mapa tectônico simplificado do Cinturão Irumide Sul com as unidades litológicas adaptadas e modificadas de Johnson et al. (2006, 2007) e GTK Consortium (2006). CG – Grupo Cazula; ChC – Complexo Chidzolomondo; FS – Supergrupo Fíngoè; MT – Zona de Cavalgamento Mchimadzi; MSZ – Zona de Cisalhamento Mwembeshi; NSZ – Zona de Cisalhamento Nyamadzi; RT – Granito Rio Tsafuro; RD – Granito Serra Danvura; SC – Granito Serra da Chiúta; SSZ – Zona de Cisalhamento Sanangoè.

Para a realização dos estudos desta tese e inserção das sequências supracrustais no contexto tectônico do Cinturão Irumide Sul foram selecionados quatro complexos metavulcano-sedimentares da Província de Tete, incluindo os supergrupos Zâmbuè e Fíngoè, o Grupo Cazula e o Complexo Chidzolomondo. A escolha dos complexos e o trabalho de campo foram orientados com base nas informações e nos mapas geológicos de GTK Consortium (2006) e CGS (2007), também levando em consideração as limitações de acesso em cada região.

A seguir apresentamos uma descrição detalhada dos complexos estudados nesta tese.

1.3.1. Supergrupo Zâmbuè

As rochas do Supergrupo Zâmbuè afloram ao extremo norte da Província de Tete, junto à fronteira com a Zâmbia, sob a forma de um cinturão contínuo com 140 km de comprimento e 60 km de largura. O supergrupo compreende a sequência metassedimentar basal de natureza siliciclástica do Grupo Malowera, que inclui meta-arcóseos, quartzitos, gnaisses pelíticos, gnaisses migmatíticos e, subordinadamente rochas metavulcânicas. No topo ocorre uma sequência carbonática de mármores e gnaisses calci-silicáticos compondo o Grupo Muze, que tem sua ocorrência controlada por estruturas N-S.

O Grupo Malowera é composto pelas formações Rio Mese, Metamboa e Sale-Sale. A Formação Rio Mese é a unidade basal do supergrupo e compreende uma assembleia de orto e paragnaisses migmatíticos muito deformados. A Formação Metamboa é a unidade litoestratigráfica de maior ocorrência no Supergrupo Zâmbuè, composta por uma sequência de meta-arcóseos, com foliação metamórfica bem desenvolvida e granitizados nas porções de borda junto aos granitoides intrusivos da Suite Cassacatiza. No topo do Grupo Malowera ocorre a Formação Sale-Sale, que consiste em sequência de ortoquartzitos, quartzitos arcoseanos e metapelitos. As rochas do Grupo Malowera encontram-se fortemente deformadas e metamorfizadas na fácies anfibolito, localmente anfibolito superior.

O Grupo Muze é composto pelas formações Musamba e Caduco, que ocorrem restritos a um cinturão de forma alongada e arqueada com direção aproximada N-S. A Formação Musamba consiste em mármores puros de granulometria média a grossa, enquanto a Formação Caduco compreende gnaisses calci-silicáticos. As sequência de rochas siliciclásticas do Supergrupo Zâmbuè é interpretada como uma bacia de margem passiva depositada entre 1400 e 1250 Ma antes da formação dos arcos magmáticos do Cinturão Irumide Sul. É considerada a hipótese da sequência carbonática do Grupo Muze ter idade neoproterozoica.

1.3.2. Supergrupo Fíngoè

O Supergrupo Fíngoè compõem um cinturão de dobramentos e cavalgamentos de direção NE-SW (N50°E) com cerca de 150 km de comprimento e até 25 km de largura. O supergrupo é subdividido nos grupos Monte Messuco, composto predominantemente por uma sequência basal de rochas vulcânicas básicas a intermediárias, e o grupo Monte Tchicombe, que compreende uma sequência sedimentar siliciclástica. As rochas estão deformadas e metamorfizadas na fácies anfibolito e, localmente, na fácies granulito. Observa-se que as

unidades do Supergrupo Fingoè foram afetadas por dois eventos principais de metamorfismo com formação da foliação metamórfica S1. Esta foliação está deformada por um evento de deformação mais jovem e constitui dobras F2 recumbentes do tipo isoclinais e apertadas de escala regional. Este evento gera uma intensa crenulação e transposição da foliação S1, gerando a foliação metamórfica S2. As foliações anteriores estão afetadas por dobras F3 com formas abertas a fechadas e normais, com eixos de disposição sub horizontal e superfícies axiais subverticais. As dobras F3 estão deformadas, com preservação parcial, comumente afetada por falhas normais mais jovens. Os contatos com os granitoides das suites Cassacatiza e Monte Sanja indica que são intrusivos no supergrupo e tem seu posicionamento controlado pelas estruturas subverticais mais jovens.

O Grupo Monte Messuco compreende as formações Monte Rupanjaze e Monte Muinga, além de mármores e paragnaisses indiferenciados (GTK Consortium, 2006). A Formação Monte Rupanjaze é composta por rochas metavulcânicas máficas a félsicas intercaladas com mica xistos e metatufos. As rochas metavulcânicas máficas ocorrem principalmente na porção central do Supergrupo Fíngoè e compreendem anfibolitos e xistos anfibolíticos de protólito basáltico composto por plagioclásio e hornblenda com quartzo, epidoto e biotita como minerais acessórios. A Formação Monte Muinga consiste de rochas metavulcânicas máficas a intermediárias e félsicas e, subordinadamente, brechas e aglomerados vulcânicos, intercalados com rochas metassedimentares clásticas. Os metatufos félsicos predominam e ocorrem intercalados com as rochas metavulcânicas máficas, que consistem de anfibolitos foliados e bandados com epidoto e, localmente, porfiroblastos de granada. O Grupo Monte Tchicombe compreende as formações Rio Mucanba e Monte Puéque, além de mármores e rochas metavulcânicas indiferenciadas (GTK Consortium, 2006). A Formação Rio Mucanba é composta por quartzitos, metarenitos e metaconglomerados. Os metarenitos são finos e tem composição quartzo-feldspática, com estrutura xistosa e/ou pouco bandada. Os metaconglomerados são clasto suportados, polimíticos e possuem clastos bem arredondados com mais de 40 cm de diâmetro de quartzitos, metarenitos e granitos, e provavelmente podem representar um conglomerado intraformacional do topo da sequência vulcano-sedimentar. A Formação Monte Puéque é composta por xistos e gnaisses calcisilicáticos. Os gnaisses apresentam um bandamento irregular e pouco desenvolvido, localmente refletindo o acamadamento primário. Os xistos são muito foliados e não apresentam estruturas primárias. São compostos por plagioclásio, quartzo e epidoto e, localmente, contêm fragmentos de rochas vulcânicas félsicas.

A composição geoquímica das rochas metavulcânicas do Supergrupo Fíngoè das

formações Monte Rupanjaze e Monte Muinga mostram uma série expandida incluindo basaltos, andesitos, riodacitos e riolitos subalcalinos e compostos por um grupo de rochas de afinidade toleítica, com feições composicionais de arcos de ilhas, e outro cálcico-alcalino relacionado a arcos continentais.

1.3.2. Grupo Cazula

As litologias do Grupo Cazula ocorrem como seis corpos de formato irregular com até 40 km de comprimento e 15 km de largura em meio aos granitoides pós-colisionais da Suite Furacungo. Os contatos dos xenólitos com os granitoides encaixantes são interlobados e foram definidos principalmente através da geofísica, caracterizada pelos baixos valores nos mapas de aerogamaespectroscopia. Devido ao isolamento e escassez dos afloramentos, poucos dados de campo estão disponíveis e não existe uma subdivisão interna do grupo. O Grupo Cazula é composto por metarenitos, quartzitos, gnaisses quartzo-feldspáticos, gnaisses calci-silicáticos e anfibolitos. As litologias predominantes são os metarenitos quartzosos e quartzo-feldspáticos, com estrutura xistosa ou gnáissica e textura granoblástica equigranular fina a média. Os anfibolitos têm cor preta e estrutura maçica, com textura blastoporfirítica definida por fenocristais reliquiares de feldspatos. Os corpos de anfibolitos constituem lentes deformadas e contínuas, com ocorrência irregular e espessuras centimétrica a métrica. É observado o incremento da deformação nas rochas para leste, onde são mais afetadas por zonas de cisalhamento de direção NW-SE, que também afetam as rochas da Suite Furacungo e são relacionadas aos cavalgamentos sentido oeste das orogêneses Pan-Africanas.

Os xistos do Grupo Cazula possuem uma foliação regional com direção média segundo NW-SE, com planos de cisalhamento sub-horizontais com abundantes injeções dos granitos intrusivos da Suite Furacungo. Estes granitos apresentam uma foliação ígnea pouco desenvolvida, paralela ao contato com os xistos, o que indica que a colocação dos granitoides ocorreu em um estágio tardi-cinemático da deformação que afetou os xistos (GTK Consortium, 2006). Estas relações indicam que a intrusão dos granitoides da Suite Furacungo (~1040 Ma) foi sin-cinemática em relação a deformação do Grupo Cazula.

1.3.3. Complexo Chidzolomondo

O Complexo Chidzolomondo está situado na porção norte da região de estudo e ocorre sob a forma de dois cinturões alongados com orientação N70°E. O grupo corresponde a um terreno metamórfico de alto grau composto principalmente por gnaisses de composição básica

e intermediária de origem vulcânica (GTK Consortium, 2006). Em campo, os gnaisses apresentam um bandamento metamórfico irregular, com níveis finos e descontínuos definidos por agregados de minerais máficos, principalmente, piroxênio e anfibólio. O bandamento tem direção NE-SW e apresenta estreitas zonas de cisalhamento concordantes e com uma lineação de estiramento do tipo dip. Estas estruturas sugerem que o bandamento metamórfico foi gerado por processos tectônicos associados a eventos de metamorfismo orogênico colisional. As relações de contato com os granitoides encaixantes revela a sua natureza intrusiva em relação aos gnaisses do complexo. A forma alongada dos corpos graníticos e a presença de uma foliação magmática concordante sugere que os mesmos foram posicionados durante a fase sin- a tardi-cinemática. Os dados aerogeofísicos radiométricos e magnéticos mostram uma compartimentação do Complexo Chidzolomondo entre as suas porções norte e sul (GTK Consortium, 2006). A porção norte consiste de um corpo alongado de direção E-W com cerca de 120 km de comprimento e 30 km de largura. Nas imagens de satélite e de aerogeofísica são identificadas estruturas lineares de direção ENE-WSW a E-W e um forte sinal magnético associado a uma baixa assinatura gamaespectrométrica, o que indica uma composição básica para os granulitos. Neste corpo predominam as litologias de composição gabroica com granulação média a grossa e textura equigranular maciça. Foram descritos piroxênio granulitos, anfibólio granulitos e granulitos tonalíticos com ortopiroxênio, clinopiroxênio, biotita, hornblenda e plagioclásio. Os granulitos com bandamento gnáissico e veios pegmatíticos quartzo-feldspáticos são mais comuns na porção leste do corpo. A porção sul do Grupo Chidzolomondo é composta por quatro corpos com dimensão total de cerca de 30 km de comprimento e 15 km de largura, que ocorrem envoltos por granitoides mesoproterozoicos. O corpo situado ao leste compreende rochas metassedimentares quartzo-feldspáticas, localmente muito deformadas e cisalhadas, com intercalações de rochas metavulcânicas de origem piroclástica e rochas calci-silicáticas (GTK Consortium, 2006). Na sua porção oeste são descritos granulitos migmatizados de composição intermediária associados com quartzitos laminados. Também são descritos gnaisses granulíticos de protólitos pelíticos com cordierita, granada, biotita, plagioclásio e ortopiroxênio na porção sul do grupo. Pequenos corpos graníticos intrusivos da Suite Castanho ocorrem dispersos cortando os gnaisses do Grupo Chidzolomondo.

Os gnaisses granulíticos básicos do Grupo Chidzolomondo foram classificados a partir de sua composição geoquímica, como uma série de composição expandida incluindo basaltos, andesitos, riodacitos e riolitos de afinidade subalcalina com afinidade toleítica dominante, com um grupo subordinado de rochas calcico-alcalinas (GTK Consortium, 2006). Os gnaisses

granulíticos básicos da porção norte do grupo são interpretados como rochas metavulcânicas básicas a intermediárias geradas em um ambiente de arco de ilhas imaturo (GTK Consortium, 2006).

2. Estado da arte

O escopo desta tese consistiu no posicionamento estratigráfico e no significado tectônico dos complexos Zâmbuè, Fíngoè, Cazula e Chidzolomondo no Cinturão Irumide Sul da Província de Tete. O estado da arte elaborado apresenta uma síntese sobre os trabalhos anteriores e as hipóteses propostas sobre a origem e evolução do Cinturão Irumide Sul em Moçambique e na Zâmbia.

Os primeiros estudos geológicos em Moçambique foram desenvolvidos ainda no século XIX com foco principal nas ocorrências de carvão, importante recurso energético na época e abundante na região da Província de Tete. A partir da década de 20 passaram a ser realizados levantamentos geológicos pelo Serviço Geológico de Moçambique, os quais resultaram em uma primeira síntese da geologia de Moçambique somente em 1976. Com a independência do país em 1975 passaram a ser implementadas campanhas sistemáticas de reconhecimento geológico do território moçambicano em colaboração com instituições e organizações internacionais como o Serviço Geológico da França (BRGM) e da Finlândia (GTK). Os primeiros trabalhos tinham foco na prospecção de recursos minerais, logo se valeram principalmente de técnicas como mapeamento geológico, geofísica e geoquímica.

O mapeamento geológico sistemático da Província de Tete permitiu a Hunting (1981, 1984) e BRGM (1987) propor a primeira divisão litoestratigráfica da região, através da identificação e individualização de sequências supracrustais e suites graníticas. Nesta divisão os complexos supracrustais foram interpretados como as unidades mais antigas do cinturão, desconsiderando os gnaisses do embasamento, e o Supergrupo Fíngoè foi tomado como um marcador estratigráfico, sendo os granitos subdivididos como pré ou pós-Fíngoè. Nesta época já havia conhecimento da idade das rochas da região e, com base em escassas e esparsas idades K-Ar e Rb-Sr, BRGM (1987) subdividiu o embasamento cristalino em três períodos:

- Arqueano e Paleoproterozoico - unidades situadas no extremo oeste junto à fronteira com o Zimbábue, compostas por *greenstone belts* e associações granito-gnáissicas;
- Mesoproterozoico-Neoproterozoico - unidades formadas ao final do Mesoproterozoico, correlacionadas ao Cinturão Irumide da Zâmbia (1300 Ma) e retrabalhadas durante as orogêneses do Cinturão Moçambique (1100 - 850 Ma);

- Neoproterozoico - unidades relacionadas ao ciclo orogênico Pan-Africano (850 - 450 Ma).

Concomitantemente, na década de 80 o Serviço Geológico da Zâmbia realizava o mapeamento geológico de reconhecimento do seu território. Diversos relatórios foram gerados, que resultaram nos trabalhos publicados de Barr et al. (1977, 1978), Daly et al. (1982, 1984), Daly (1986), Johns et al. (1989), entre outros. Dentre eles, o trabalho de Johns et al. (1989) sintetiza os relatórios gerados para o Cinturão Irumide Sul na Zâmbia e apresenta um esboço da estratigrafia com base nas relações de campo e nas feições estruturais identificadas na região. Neste trabalho é reconhecida a descontinuidade entre o Cinturão Irumide e o Cinturão Irumide Sul, que até então era interpretado como a sua extensão ao sul. A diversidade litológica do Cinturão Irumide Sul, contrastante da monotonia de metassedimentos (Supergrupo Muva) e granitos intrusivos do Cinturão Irumide, era atribuída ao retrabalhamento durante as orogêneses Pan-Africanas, sendo este incorporado ao Cinturão Moçambique em alguns trabalhos (ex. Daly et al., 1984). Foram descritos cinco eventos deformacionais e os autores propuseram a existência de três sequências estratigráficas de orto e paragnaisses no cinturão separadas por zonas de alta deformação, correlacionando a sua extensão no Malawi e em Moçambique. A sequência "complexo do embasamento" foi descrita como a sequência mais antiga do cinturão composta por granulitos, charnockitos, quartzitos, orto e paragnaisses de médio a alto grau e com ocorrência restrita a região de Chipata (Fig. 2). A sequência dos "Xistos Chitundula e Formação de quartzitos" eram atribuídas principalmente às rochas metassedimentares do cinturão como mármores, xistos pelíticos e calci-silicáticos, anfibolitos e gnaisses quartzo-feldspáticos. Esta sequência foi correlacionada aos metasedimentos do Supergrupo Muva do Cinturão Irumide. A sequência mais jovem a "Formação Mwami" compreende os metapelitos, metarenitos e mármores. Estas rochas são as mais jovens da região, correlacionadas ao Cinturão Zambezi.

A troca de conhecimento geológico entre os dois países durante estas campanhas de mapeamento geológico parece ter sido limitada, apesar da evidente continuidade das unidades para além de suas fronteiras. Grande parte destes trabalhos não foi publicada e disso resultou o conhecimento fragmentado do Cinturão Irumide Sul entre as regiões na Zâmbia e em Moçambique. Esta fragmentação persiste até hoje mesmo com o grande volume de dados geocronológicos, geoquímicos e isotópicos disponíveis.

Uma das primeiras datações U-Pb em zircão disponíveis para o Cinturão Irumide Sul foi de um plagiogranito de 1393±22 Ma intrudido em uma sequência ofiolítica no extremo oeste do cinturão e publicada por Oliver et al. (1998). Esta é a idade mesoproteozoica mais antiga

reportada para o cinturão e foi interpretada como a idade de formação de um oceano marginal e início da formação de arcos de ilhas. Esta hipótese foi suportada pelos artigos de Johnson e Oliver (2004) e Johnson et al. (2005) ambos definindo a idade de magmatismo de arco entre 1090-1040 Ma na região oeste do cinturão. Estes foram os primeiros trabalhos publicados que dissociaram definitivamente os cinturões Irumide e Irumide do Sul, mostrando de forma clara os ambientes tectônicos distintos entre os dois. Johnson e Oliver (2004) propõem um modelo de evolução para a região com a formação de arcos de ilhas a partir de 1400 e sua acresção à margem sul do Craton Bangweulu em 1040 Ma.

Uma proposta de subdivisão do Cinturão Irumide Sul na Zâmbia foi apresentada por Johnson et al. (2006, 2007), sendo amplamente adotada nos trabalhos realizados na região desde então. O artigo faz referência a dois trabalhos apresentados em congressos (Mapani et al. 2001, 2004) e um artigo submetido à revista *Tectonophysics,* que teriam concebido a subdivisão do cinturão em terrenos amalgamados à margem sul do Cráton Bangweulu. A proposta de subdivisão do cinturão em terrenos foi mantida por Johnson et al. (2006, 2007) apesar dos dados indicarem uma evolução síncrona entre 1100 e 1040 Ma e ambientes correlatos de margem continental ativa e/ou arcos intra-oceânicos para estas regiões do cinturão. A proposta respeita a fronteira da Zâmbia e desconsidera a região da Província de Tete. Foram propostos quatro terrenos distintos com base nas associações de rocha encontradas, sendo eles (de oeste a leste): Chipata, Petauke-Sinda, Luangwa-Nyimba e Chewore-Rufunsa.

O Terreno Chipata ocorre na porção oeste da região, próximo a fronteira entre a Zâmbia e o Malawi, e apresenta uma ampla diversidade litológica compreendendo granulitos máficos, félsicos e pelíticos, hornblenda-biotita gnaisses, granitoides deformados e sienitos. Os granitoides são atribuídos a um ambiente de arco magmático continental com idade entre 1080 e 1040 Ma. A presença de granulitos com granada e cordierita e granitos charnockiticos indica o metamorfismo de alta temperatura no terreno e a datação de monazitas metamórficas resultou em idades entre 1050-1010 Ma. As idades apresentadas evidenciaram a sincronicidade entre o magmatismo e o metamorfismo de alta temperatura na região, suportando o ambiente de margem continental ativa segundo os autores.

O Terreno Petauke-Sinda é composto principalmente por paragnaisses e ortognaisses deformados a muito deformados. Os ortognaisses são calci-alcalinos formados em um ambiente de arco de ilhas com idade de cerca de 1120 Ma e ambiente de margem continental ativa até 1040 Ma. Estes ortognaisses são recobertos por paragnaisses e ortognaisses graníticos de aproximadamente 740 Ma. O terreno conta com batólitos graníticos de dimensões variáveis de natureza pós-tectônica do ciclo Pan-Africano, como a Suite Sinda.

O Terreno Luangwa-Nyimba compreende uma sequência de metapelitos migmatíticos e quartzitos com horizontes subordinados de metavulcânicas máficas a intermediárias (Johnson et al., 2006). A avaliação da proveniência de zircões detríticos de duas amostras apresentou picos de frequência em 2.6, 2.2 e 2.0 Ga, com a predominância das áreas fonte do embasamento paleoproterozoico (Johnson et al., 2006). A datação dos sobrecrescimentos dos zircões resultou em uma idade metamórfica de 1060 Ma, com isso a deposição dos sedimentos ocorreu entre 2.0 e 1.06 Ga (Johnson et al., 2006).

O Terreno Chewore-Rufunsa situa-se no extremo oeste do Cinturão Irumide Sul. O terreno é composto por xistos e gnaisses calci-alcalinos máficos a félsicos, rochas metavulcânicas, metapelitos e quartzitos (Johnson et al., 2007), além da sequência ofiolítica do Complexo Chewore (1393 Ma). Foi proposto o ambiente de margem continental ativa com idade entre 1090 e 1040 Ma. O magmatismo do terreno foi atribuído a um ambiente de margem continental ativa com idades entre 1090 e 1040 Ma e expressiva contribuição de crosta paleoproterozoica. O metamorfismo varia da fácies xisto verde a granulito com o aumento do grau metamórfico para sul controlado por estruturas relacionadas ao Cinturão Zambezi. O metamorfismo mais jovem da região (~550-500 Ma) é restrito às proximidades destas zonas de cisalhamento e evidencia a sobreposição de estruturas relacionadas às orogêneses Pan-Africanas com magmatismo subordinado.

Uma breve comparação das associações de rocha do Cinturão Irumide Sul na Zâmbia com as associações da Província de Tete evidencia as semelhanças e correlações mais evidentes. Por exemplo, o terreno Luangwa-Nyimba e o Supergrupo Zâmbuè, ou os granulitos e charnockitos da região de Chipata e os granulitos do Complexo Chidzolomondo e adjacências (antigo Grupo Luia).

Os trabalhos realizados por GTK Consortium (2006), resultado das atividades de pesquisa realizadas entre 2002 a 2007 em parceria entre os Serviços Geológicos de Moçambique e da Finlândia (GTK), apresentaram uma caracterização detalhada do território de Moçambique, definidos em folhas geológicas em escala 1:250.000. Neste projeto foram integrados todos os dados geológicos disponíveis, combinados com dados geofísicos, de imagens de satélites, análises geoquímicas e dados isotópicos (U-Pb com TIMS e SHRIMP e análises Sm-Nd). De um modo geral a estratigrafia proposta anteriormente por Hunting (1984) foi mantida, apenas com a adequação da nomenclatura litoestratigráfica. Destacam-se duas alterações relacionadas no tema da tese. As rochas de alto-grau metamórfico, incluindo granulitos, migmatitos, ortognaisses e granitos que próximos à região de Tete e então incorporadas ao Grupo Luia foram desmembradas em novas unidades, o Grupo

Chidzolomondo, Granito Rio Capoche, Grupo Cazula e Granito Mussata. Além disso o critério de classificação dos granitos como "pré- ou pós-Fíngoè", que tinha como base a suposta relação estratigráfica dos granitoides com o Supergrupo Fíngoè, que foi substituída por uma análise embasada na idade absoluta e/ou relativa das intrusões e o seu ambiente de formação inferido através da petrologia dos granitos.

Os dados geocronológicos obtidos durante este projeto são pouco representativos, dispersos e não atendem as dimensões e a complexidade da geologia na região de estudo. Diversas unidades tiveram seu posicionamento estratigráfico definido a partir de observações de campo e dados geofísicos. Foram reconhecidas por GTK Consortium (2006) na Província de Tete, sequências de rochas supracrustais metamorfisadas, rochas plutônicas de arco de ilhas ou de margem continental ativa (~1.3-1.08 Ga), granitoides sub-alcalinos sin-tectônicos (~1.05-1.04 Ga) e subordinadamente, por suites intrusivas relacionadas a orogênese Pan- Africana.

Com base nos aspectos composicionais, petrográficos, estruturais e geocronológicos, os granitoides foram subdivididos em nove suítes intrusivas que compõe as Suítes Intrusivas Irumides (GTK Consortium 2006). As suites são: (1) Serra Chiúta; (2) Rio Capoche (~1.2 Ga); (3) 46 Rio Tchafuro (~1.12 Ga); (4) Serra Danvura; (5) Monte Capirimpica (~1.09 Ga); (6) Cassacatiza (~1.08 Ga); (7) Monte Sanja (~1.05 Ga); (8) Mussata e (9) Furacungo (~1.04 Ga). Além das suítes graníticas, o Bloco Tete-Chipata também inclui as rochas máficas estratiformes da Suite Tete e as rochas intrusivas associadas, descritas como uma associação anortosito-mangerito-charnockito-granito.

A síntese das pesquisas geológicas realizadas por GTK Consortium (2006) foi publicada no volume de artigos Special Paper 48 de 2008, do Serviço Geológico da Finlândia. A partir da conclusão e publicação do resultados do consórcio GTK, alguns trabalhos de autoria dos pesquisadores que fizeram parte da equipe têm sido publicados em revistas internacionais de prestígio. Contudo, estes trabalhos têm foco principalmente na região NE de Moçambique, agregando novos dados geocronológicos aplicados à evolução das entidades geotectônicas regionais e bacias Neoproterozóicas relacionadas a elas (Viola et al., 2008; Bingen et al., 2009; Thomas et al., 2010; Grantham et al., 2013; Macey et al., 2010; 2013).

3. Análise integradora

Os trabalhos de pesquisa desenvolvidos para a elaboração desta tese resultaram em dois artigos submetidos à revista *Precambrian Research*, os quais apresentam resultados coerentes entre si e contribuem significativamente para o entendimento do Cinturão Irumide

Sul. O ARTIGO 1 apresenta os resultados do estudo de proveniência pelos métodos U-Pb e Lu-Hf em zircão detrítico dos complexos Zâmbuè, Fíngoè e Cazula. Os resultados de proveniência mostraram áreas fonte principais relacionadas ao arco magmático com idades entre e assinaturas isotópicas Hf predominantemente juvenis com limitada contribuição crustal. As contribuições subordinadas de áreas fonte arqueanas e paleoproterozoicas, inclusive nas idades modelo Hf_{TDM}, mostram uma limitada participação de material crustal para o arco, ao menos no registro sedimentar. Os resultados obtidos sugerem a deposição em bacias de arco magmatico, possivelmente arcos de ilhas intra-oceânicos.

O ARTIGO 2 apresenta os resultados das análises isotópicas U-Pb e Lu-Hf em zircões detríticos, ígneos e metamórficos dos granulitos do Complexo Chidzolomondo e de zircões ígneos de plútons intrusivos de charnockitos e gabros, além da avaliação das condições de metamorfismo e a comparação geoquímica com os charnockitos da Suite Castanho. Os resultados permitiram estabelecer a temporalidade dos eventos de transição da fase acrecionária para a fase colisional do orógeno, através da idade de deposição das bacias de arco, da idade do magmatismo e metamorfismo sin-orogênico, do metamorfismo colisional e do magmatismo e metamorfismo pós-colisional.

4. Conclusões

- Os dados de proveniência de zircão detrítico dos complexos estudados mostraram a ampla predominância (>95%) de áreas fontes constituídas por rochas do Mesoproterozoico com idades entre 1250 e 1090 Ma, e participação subordinada de áreas fontes paleoproterozoicas e arqueanas.
- Os complexos Zâmbuè, Fíngoè, Cazula e Chidzolomondo apresentaram padrões de proveniência de zircão detrítico muito similares e marcados pelo pico principal com idade muito próxima a idade máxima de deposição estimada para a bacia. Este é um padrão típico de bacias de arco como os complexos estudados;
- O ambiente de arco magmático, provavelmente arcos de ilhas intra-oceânicas, também é suportado pela assinatura das razões Lu-Hf dos zircões detríticos, caracterizadas por valores positivos de $\varepsilon Hf(t)$, indicando fontes juvenis com pouca influência crustal;
- As idades de metamorfismo obtidas nos granulitos do Complexo Chidzolomondo evidenciam três eventos metamórficos no cinturão. Evento M_1 relacionado a fase acrescionária; Evento M_2 registrando o metamorfismo do pico da colisão continental e do magmatismo sin-colisional; Evento M_3 registrando o metamorfismo de contato relacionado aos corpos intrusivos

de gabros e charnockitos que marcam o período pós-colisional;

- A integração dos mapas geológicos disponíveis, acrescidos das observações obtidas durante e fase de campo, resultou em um novo mapa geológico integrado para a região de Tete,
- A integração do conhecimento e da cartografia geológica disponíveis para os países limítrofes com a Provincia de Tete, que caracteriza a porção NW de Moçambique (Zâmbia, Zimbábue e Malawi), resultou em um novo mapa integrado do Cinturão Irumide Sul, com a correlação regional entre unidades e eventos nas diferentes regiões do cinturão e unidades tectônicas adjacentes;
- Os dados obtidos nesta tese, com a compilação e integração dos dados geocronológicos e isotópicos disponíveis para o Cinturão Irumide Sul, permitiu propor um modelo evolutivo inédito no qual o Cinturão Irumide Sul preserva o registro de um Ciclo de Wilson completo durante o Mesoproterozoico. Os eventos são: (i) abertura de um oceano e deposição de sequências de margem passiva entre 1393 e 1327 Ma; (ii) subducção da crosta oceânica e formação de arcos de ilhas intra-oceânico entre 1327 e 1133 Ma; (iii) evolução do edifício do arco com o magmatismo sin-orogênico intrudindo e metamorfizando as sequências vulcano-sedimentares; (iv) colisão continental em ~1080 Ma com o pico do metamorfismo colisional em ~1060 Ma; (v) magmatismo plutônico máfico e ácido pós-colisional, com gabros, anortositos, charnockitos e granitos CA alto-K com idades entre 1060 e 1020 Ma.

5. Referências bibliográficas

Bingen, B., Jacobs, J., Viola, G., Henderson, I.H.C., Skår, Ø., Boyd, R., Thomas, R.J., Solli, A., Key, R.M., Daudi, E.X.F., 2009. Geochronology of the Precambrian crust in the Mozambique belt in NE Mozambique, and implications for Gondwana assembly. Precambr. Res. 170, pp. 231–255.

Chaúque, F.R., Cordani, U.G., Jamal, D.L., Onoe, A.T., 2017. The Zimbabwe Craton in Mozambique: A brief review of its geochronological pattern and its relation to the Mozambique Belt. J. Afr. Earth Sci. 129, 366-379.

Chaúque, F.R., Cordani, U.G., Jamal, D.L., 2019. Geochronological systematics for the Chimoio-Macossa frontal nappe in central Mozambique: Implications for the tectonic evolution of the southern part of the Mozambique belt. J. Afr. Earth Sci. 150, 47-67.

GTK Consortium, 2006. Map Explanation, Volume 4, Sheets Inhamambo (1430), Maluwera (1431), Chifunde (1432), Zumbo (1530), Fíngoè-Mágoè (1531), Songo (1532), Cazula (1533) and Zóbuè (1534). Unpubl. Report, National Directorate of Geology, Maputo, Mozambique, pp. 457.

Grantham, G.H., Ingram, B.A., Cronwright, M.C., Roberts, M.P., Macey, P.H., Manhica, V., Matola, R., Fernando, S., Cune, G., Correa, E., 2007. Explanatory notes of the 1:250.000 geological maps of sheets Furacungo (1433) and Ulongue (1434). Unpubl. Report, National Directorate of Geology, Maputo, Mozambique, pp. 174.

Hunting Geology and Geophysics Limited (1984). Mineral Inventory Project. Unpubl. Rept., National Directorate of Geology, Maputo, Mozambique, pp. 329.

Johnson, S.P., Oliver, G.J.H., 2004. Tectonothermal history of the Kaourera Arc, northern Zimbabwe: implications for the tectonic evolution of the Irumide and Zambezi Belts of South Central Africa. Precambr. Res. 130, 71–97.

Johnson, S.P., Rivers, T., De Waele, B., 2005. A review of the Mesoproterozoic to early Palaeozoic magmatic and tectonothermal history of south-central Africa: implications for Rodinia and Gondwana. J. Geol. Soc. 162, 433-450.

Johnson, S.P., De Waele, B., Liyungu, A., 2006. U-Pb sensitive high-resolution ion microprobe (SHRIMP) zircon geochronology of granitoid rocks in eastern Zambia: Terrane subdivision of the Mesoproterozoic Southern Irumide Belt. Tectonics 25 (6), TC6004.

Johnson, S.P., De Waele, B., Tembo, F., Katongo, C., Tani, K., Chang, Q., Iizuka, T., Dunkley, D., 2007. Geochemistry, geochronology and isotopic evolution of the Chewore-Rufunsa terrane, southern Irumide belt: a Mesoproterozoic continental margin arc. J. Petrol. 48, pp. 1411-1441.

Oliver, G., Johnson, S., Williams, I., Herd, D., 1998. Relict 1.4 Ga oceanic crust in the Zambezi Valley, northern Zimbabwe: evidence for Mesoproterozoic supercontinental fragmentation. Geology. 26, 571-573.

Thomas, R.J., Roberts, N.M.W., Jacobs, J., Bushi, A.M., Horstwood, M.S.A., Mruma, A., 2013. Structural and geochronological constraints on the evolution of the eastern margin of the Tanzania Craton in the Mpwapwa area, central Tanzania. Precam. Res. 224, 671–689.

Westerhof, A.P., Lehtonen, M.I., Mäkitie, H., Manninen, T., Pekkala, Y., Gustafsson, B., Tahon, A., 2008a. The Tete-Chipata Belt: a new multiple terrane element from western Mozambique and southern Zambia. Geol. Surv. Finl., Spec. Paper 48, 145-166.

CAPÍTULO II

6. Artigos científicos

6.1. ***U-Pb and Lu-Hf zircon data of the grenvilian arc-related Zâmbuè, Fíngoè and Cazula supracrustal complexes, Southern Irumide Belt, NW Mozambique*** **- Publicado na revista Precambrian Research, v. 381, outubro de 2022, 106860**

Precambrian Research 381 (2022) 106860

Contents lists available at ScienceDirect

Precambrian Research

journal homepage: www.elsevier.com/locate/precamres

U-Pb and Lu-Hf zircon data of the grenvilian arc-related Zâmbué, Fíngoè and Cazula supracrustal complexes, Southern Irumide Belt, NW Mozambique

T.S. Petry [a,*], R.P. Philipp [a], D.L. Jamal [b], C. Lana [c], A.R. Alkmim [c]

[a] Programa de Pós-Graduação em Geociências, Instituto de Geociências, Universidade Federal do Rio Grande do Sul, Av. Bento Gonçalves, 9500, Porto Alegre 91500-000, RS, Brazil
[b] Departamento de Geologia, Universidade Eduardo Mondlane, Av. Moçambique km 1.5, Caixa Postal 257, Maputo, Mozambique
[c] Departamento de Geologia, Universidade Federal de Ouro Preto (UFOP), Morro do Cruzeiro, Ouro Preto, Minas Gerais 35400-000, Brazil

ARTICLE INFO

Keywords:
Detrital zircon
Metavolcano-sedimentary complexes
Juvenile magmatism
Irumide Orogeny
Rodinia assembly

ABSTRACT

The supracrustal rocks from the Zâmbuè and Fíngoè Supergroups and the Cazula Group in the Mesoproterozoic Southern Irumide Belt (SIB) of NW Mozambique provides a sedimentation record associated with the Rodinia supercontinent. The Zâmbuè Supergroup comprises a succession of thick massive orthoquartzites and *meta*-arkoses, with minor calc-silicatic schists, marble, and a basal complex of ortho- and paragneisses. The Fíngoè Supergroup and Cazula Group are composed of metasandstones, calc-silicatic schists, and metapelites interlayered with felsic, mafic, and ultramafic metavolcanic rocks. U-Pb and Lu-Hf isotopic determinations of detrital zircon from five key samples show similar ages for the main source rocks. Detrital zircon from the Zâmbuè Supergroup range between 1208 and 1086 Ma in age, with a restricted contribution of Paleoproterozoic source rocks. The maximum depositional age was established at 1110 ± 2 Ma. The Fíngoè Supergroup shows zircon ages between 1233 and 1106 Ma, with a subordinate contribution of Paleoproterozoic and NeoArchean zircon grains. The calculated maximum depositional age of 1142 ± 6 Ma is similar to the crystallization age of 1094 ± 9 Ma obtained from a *meta*-andesite, and indicates the *syn*-orogenic nature of these volcanism. In the Cazula Group samples, the zircon ages range between 1164 and 1076 Ma, with minor Paleoproterozoic contributions. The maximum depositional ages were established at 1076 ± 1 Ma and 1139 ± 1 Ma. The Lu-Hf data show predominantly positive $\varepsilon Hf_{(t)}$ values (+2 and +10) and T^{2}_{DM} ages ranging between 1.75 and 1.50 Ga, indicating isotopic signatures of juvenile sources, with limited older continental crust contributions. The age results, the well-defined young age modes of the detrital zircon associated with the arc magmatism of the Southern Irumide Belt and the Hf isotopic composition demonstrate that the Zâmbué and Fíngoè Supergroups and Cazula Group represent arc-related basins. Structural data indicate a complex and polyphasic evolution, with the development of the metamorphic foliations associated with Mesoproterozoic transpressional oblique tectonics, related to accretionary and collisional phases of the Irumide Orogeny (1200–1000 Ma).

1. Introduction

Comparable to other continental regions, the geology of the central and southern portions of Africa is characterized by Archean-Paleoproterozoic cratonic cores, surrounded, and aggregated by Mesoproterozoic orogenic belts. The Southern Irumide Belt (SIB) is one of these belts, located between the Zimbabwe and the Central African cratons in a key area for the understanding of the regional tectonic evolution related to accretionary and collisional processes of the Irumide Orogeny (~1330–1000 Ma) that refers to the Rodinia Supercontinent formation (Johnson et al., 2006).

The SIB extends as an N70°E trending belt through the southeast portion of Africa from SE Zambia and NW Mozambique to NW Zimbabwe and W Malawi. The belt is composed of low- to medium-grade metavolcano-sedimentary and metasedimentary complexes, high-grade para- and orthogneisses immersed and surrounded by *syn*-orogenic granitic suites (ca. 1200–1080 Ma). These units were intruded by a wide late- to post-collisional magmatism, including suites of

* Corresponding author.
E-mail address: thales.petry@ufrgs.br (T.S. Petry).

https://doi.org/10.1016/j.precamres.2022.106860
Received 9 May 2022; Received in revised form 12 September 2022; Accepted 13 September 2022
Available online 7 October 2022

granites, charnockites, and gabbros ca. 1060–1020 Ma. The SIB has been interpreted as an assembly of exotic terranes (intra-oceanic and continental arcs) accreted to the southeastern margin of the Central African Craton (Bangweulu, Tanzania and Angola-Kasai cratons) during the Irumide Orogeny (Johnson et al., 2006, 2007; Westerhof et al., 2008a).

In the Tete Province, NW region of Mozambique, the Fíngoè supracrustal rocks are exposed in a WSW-ENE trending fold belt extending along approximately 180 km, from Monte Atchiza to the west to about 30 km east of Fíngoè town. The eastern part of this supracrustal belt includes a continuous and fragmented set of exposures, as roof pendants supported by the *syn*-orogenic granites of the Cassacatiza and Monte Capirimpica suites. To the northwest of the Fíngoè supracrustal belt, the Zâmbuè Supergroup includes a thick and massive package of orthoquartzite interlayered with *meta*-arkoses. These units are involved in the extreme west and east, by the high-grade para- and orthogneisses of the Rio Meze Formation.

The supracrustal rocks from Zâmbuè and Fíngoè Supergroups and the Cazula Group were interpreted as Mesoproterozoic arc-related associations of the SIB. Their successions of clastic and chemical sedimentary rocks interlayered with volcanic associations (basalts, andesites and acid pyroclastic rocks) are characteristic of arc-related basins (GTK Consortium, 2006; Westerhof et al., 2008a). These units were poorly studied due to their occurrence in isolated areas. In this article, we present structural, stratigraphic, and petrographic information supported by U-Pb and Lu-Hf detrital zircon data of four representative metasedimentary samples, the crystallization age of a *meta*-andesite of the Fíngoè Supergroup and the xenocrystic zircon grains of a dolerite in Cazula Group. The data obtained allowed to reassess the origin and tectonic significance of each association, as well as the role of these units in the evolution of the SIB and the implications for the ultimate assembly of Rodinia. On a broader scale, the integration with geochronological data from the SIB and SE Africa units exposed new perspectives about the regional tectonic evolution with identification of subduction processes and continental convergence and docking.

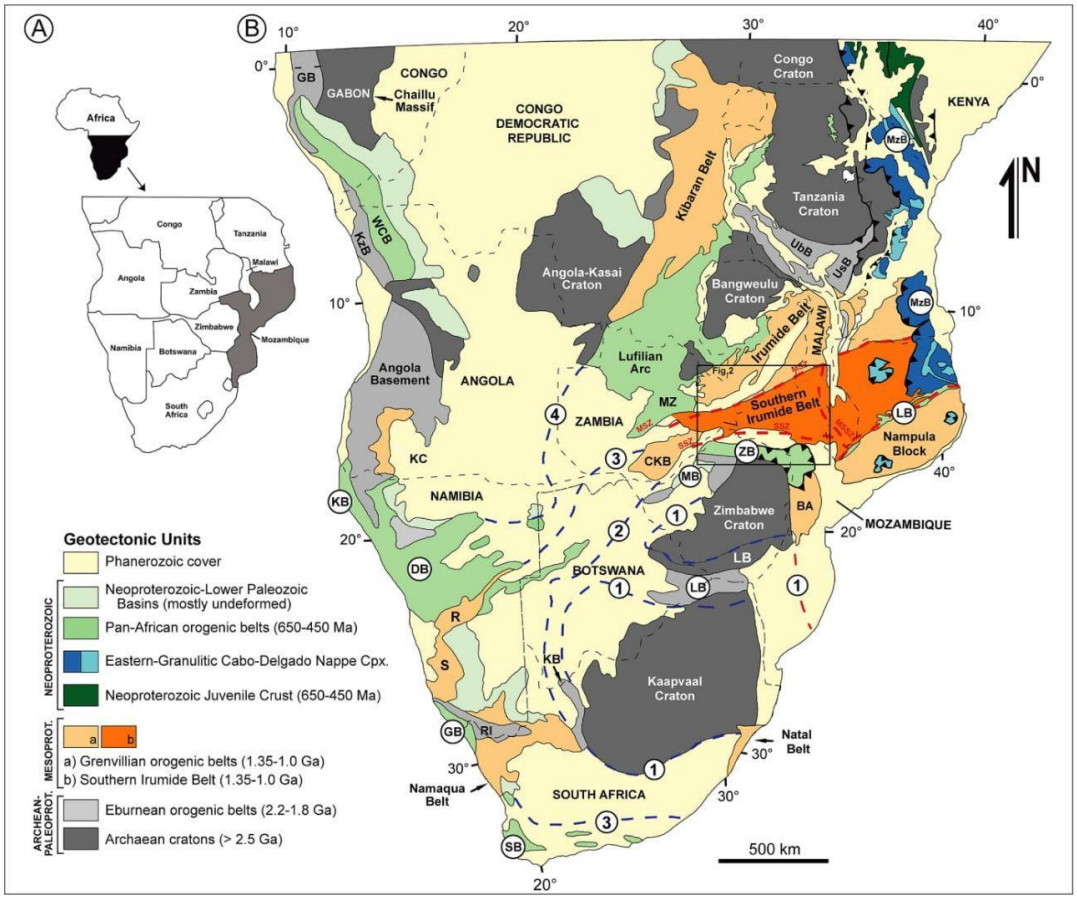

Fig. 1. Simplified tectonic map of southern Africa, adapted from Hanson (2003). A) Location of the map in Africa. B) Location of the Mozambique in Africa and of the tectonic map in the country. C) Geotectonic map with the main units of central and southern Africa. Black dashed lines indicate the political boundaries. Blue dashed lines in the Kalahari region indicate inferred positions of tectonic boundaries. Legend: 1: western edge of Archean cratons; 2: boundary between Eburnean and Grenvillian orogenic belts; 3: boundary between Grenvillian and Pan-African orogenic belts; 4: western edge of Pan-African orogenic belts. Legend of the stratigraphic and tectonic units: ATZ- Angònia Thrust Zone; BA- Bárue Arc, CK- Choma-Kalomo Block, LB- Limpopo Belt, MB- Magondi Belt, MzB- Mozambique Belt, R- Rehoboth Inlier, RI- Richtersveld Terrane, S- Sinclair Sequence, UB- Ubendian Belt, UsB- Usagaran Belt, ZB- Zambezi Belt. Shear Zones: ASZ- Angònia, MSZ- Mwembeshi, SSZ- Sanangoè. The black rectangle shows the location of the map of the Fig. 2. (For interpretation of the references to color in this figure legend, the reader is referred to the web version of this article.)

2. Geological context

The Precambrian basement of the Tete Province has a protracted tectonic evolution with the superposition of at least three orogenic events, preserved by the Mesoproterozoic Southern Irumide (NE-SW and NW-SE trend), and by the Neoproterozoic Mozambique (N—S trend) and Zambezi (E-W trend) belts (GTK Consortium, 2006; Westerhof et al., 2008a; Chaúque et al., 2017, 2019) (Fig. 1). The main crustal growth events exposed at the Tete Province are related to subduction and magmatic arc building processes (1328–1080 Ma) and the following continental collision that occurred in the Late Mesoproterozoic (1080–1060 Ma) (GTK Consortium, 2006; Westerhof et al., 2008a). These events characterize the Irumide Orogeny of the SIB. The belt was reworked and affected by thrust systems and high-angle transcurrent shear zones, with the imbrication of the Neoproterozoic units of the Zambezi and Mozambique belts surrounding the northeastern portion of the Zimbabwe Craton.

The SIB (also called Tete-Chipata Belt, GTK Consortium, 2006; Westerhof et al. 2008a) composes a Mesoproterozoic magmatic arc system extending through northernmost Zimbabwe, SE Zambia, and NW Mozambique (Fig. 2). Further east in Malawi, NE Mozambique and southern Tanzania, the Marrupa and Unango complexes are the continuation of the SIB (Bingen et al., 2009, Hauzenberger et al., 2014; Thomas et al., 2016). The belt is bounded by two major continental-scale shear zones. The Mwembeshi Shear Zone at the north shows a NE-SW trend and defines the boundary between the Southern Irumide and the Irumide belts representing a Mesoproterozoic suture zone (Johnson et al., 2006; Sarafian et al., 2018). The southern boundary of the SIB is characterized by the E-W trending Sanangoè Shear Zone, a south-verging oblique structure that thrusted the SIB units over the Zimbabwe Craton. The continuity of the belt to the east is affected by the NW-SE trending and southwest-verging Angonia Shear Zone (Grantham et al. 2007; Westerhof et al., 2008a; Bingen et al. 2009). In NW Mozambique, the SIB is exposed as a continuous belt between the Zambezi Belt to the south, and the Mozambique Belt to the east. The contact between the SIB and Zambezi Belt is overlain by the sedimentary and volcanic rocks of the Karoo Supergroup (Upper Carboniferous to Lower Jurassic) of the Mid-Zambezi Basin.

The voluminous Stenian (1.2–1.0 Ga) magmatism of the SIB is represented by an initial episode of juvenile magmatism and accretion, followed by collisional and post-collisional events involving limited reworking of an Archean-Paleoproterozoic crust. The former period characterizes the accretionary phase marked by oceanic crust subduction and the building of intra-oceanic and continental magmatic arcs (Johnson and Oliver, 2004; Johnson et al., 2005, 2006; Westerhof et al., 2008a, 2008b). This arc system was developed at the border of a continent, commonly assigned to a cryptic cratonic core, referred to as Niassa Craton (Andreoli, 1984; Daly, 1986; Sarafian et al., 2018; Celli

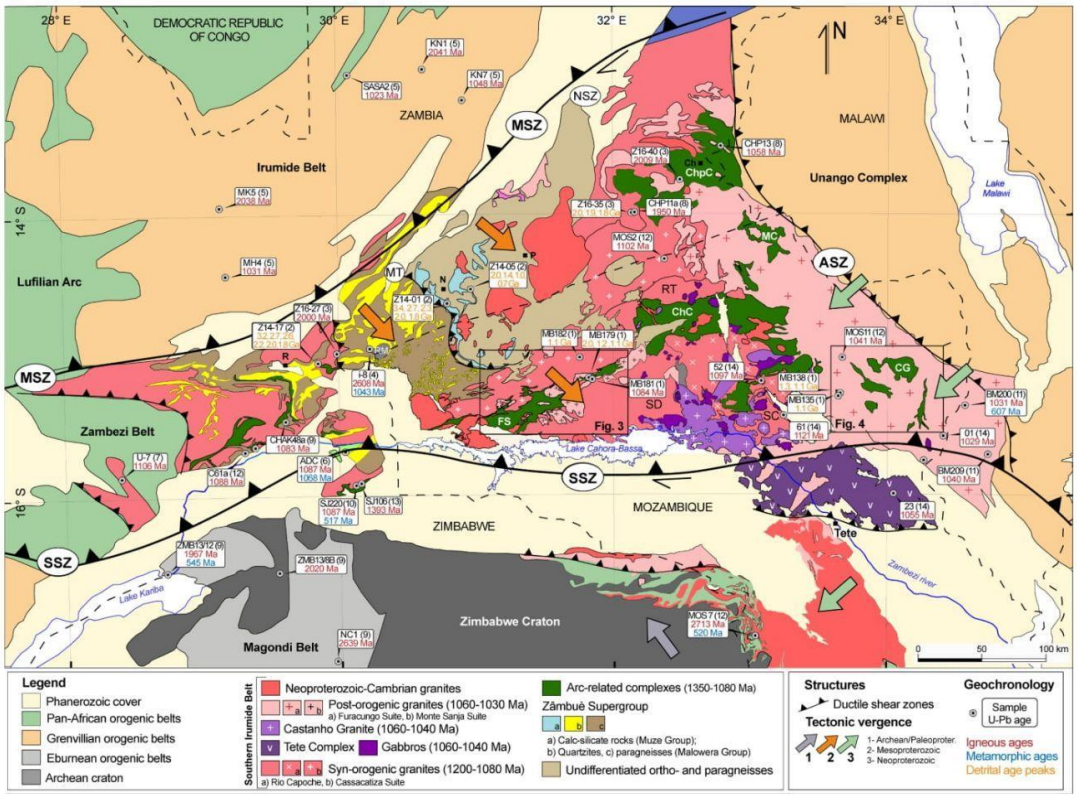

Fig. 2. Simplified tectonic map of the Southern Irumide Belt with lithological units adapted and modified from Johnson et al., (2006, 2007) and GTK Consortium (2006). In the boxes, the available geochronological data. Legend of the litostratigraphy: AS- Atchiza Suíte, CG- Cazula Group, ChC– Chidzolomondo Group, ChpC- Chipata Complex, FS- Fíngoè Supergroup, MC- Mualadzi Group, MLG- Malowera Group, RT- Rio Tsafuro Granite, RM- Rio Mepembe Complex, SC- Serra Chiúta Granite, SD- Serra Danvura Granite. Structural legend: ASZ- Angónia Thrust Zone, MSZ- Mwembeshi Shear Zone, MT- Mchimadzi Thrust, NSZ- Nyamadzi Shear Zone, SSZ- Sanangoè Shear Zone. Cities/Villages: Ch– Chipata, N- Niymba, R- Rufunsa, P- Petauke. The black rectangles show the location of the maps of the Figs. 3 and 4.

et al., 2020) or Rushinga Microcontinent (Begg et al., 2009; Alessio et al., 2019a), or also to the Central African Craton (Johnson and Oliver, 2004; Johnson et al., 2005; Alessio et al., 2019a, 2019b). The relics of the basement are diffused in the belt and their nature and extent remains poorly constrained (Johnson et al., 2006, 2007; Westerhof et al., 2008a; Alessio et al., 2019b). These arc associations were reworked by collisional processes involving the Zimbabwe, Bangweulu-Angola-Kasai, and Antarctica cratons during the Rodinia assembly (Dalziel, 1997; Dalziel et al., 2000; Meert, 2002; Li et al., 2008; Goscombe et al., 2020). Later, the SIB was affected by Neoproterozoic magmatic and metamorphic events related to the Pan-African orogenic cycle and the Gondwana assembly (GTK Consortium, 2006; Fritz et al., 2013; Chaúque et al., 2017, 2019).

The geological knowledge of the SIB remains fragmentary and most of published data is concentrated on the southern and eastern Zambia regions, where the belt was subdivided into thrust-stacked terranes. The SIB complex internal architecture and lithological diversity is a result of deformation, exhumation, and development of shear and thrust zones, due to the Irumide and Pan-African orogenies (Johnson et al., 2006). In the NW portion of Mozambique, the belt is constituted by supracrustal metamorphic complexes surrounded by *syn*-orogenic granitoids and intruded by voluminous late-orogenic magmatism comprising concordant plutons of high-K granites, charnockites, and gabbro-anorthosite complexes (GTK Consortium, 2006; Westerhof et al., 2008a).

2.1. Supracrustal complexes

The Zâmbuè (ZS) and the Fíngoè (FS) Supergroups constitute NE-SW trending elongated and continuous belts, while the Cazula, Chidzolomondo and Mualadzi, and Groups occur as roof pendants and xenoliths in the Stenian granites of the Irumide Suites (Fig. 2). The Zâmbuè Supergroup is disposed as a belt in the northwestern portion of the studied area and extends to the north into the Nyimba and Rufunsa regions of Zambia (Fig. 2). The ZS comprises the basal ortho- and paragneisses of the Rio Meze and Rio Mepembe formations (basement inliers?), and the dominant *meta*-arkoses, quartzites and pelitic gneisses of the Malowera Group. These units were covered by the marbles, calc-silicate gneisses and impure quartzites of the Muze Group (GTK Consortium, 2006). The Malowera Group units were considered as a passive margin sequence deposited over the basement rocks before the accretionary phase. The maximum depositional age was established at ca. 1300–1200 Ma (GTK Consortium, 2006; Westerhof et al., 2008a). The Muze Group units are disposed as a curvilinear NW-SE trending belt, tectonically overlying the above-mentioned units, and are probably a younger Neoproterozoic sequence, as stated by Johnson et al. (2006) for the correlated Sasare volcanic units in the Petauke region of Zambia.

The Fíngoè Supergroup (FS) is an N30°E trending deformed metavolcano-sedimentary sequence, mainly exposed as an elongated belt 180 km long and up to 25 km wide (Fig. 3A). The FS was subdivided into two groups (GTK Consortium, 2006). The lower Monte Messuco Group comprises the marbles, mica schists, metachert, banded ironstone and mafic to ultramafic metavolcanic rocks of the Monte Rupanjaze Formation, and the acidic metatuffites and other metapyroclastic rocks, with minor amphibolites (metabasalts) and *meta*-andesites of the Monte Muinga Formation. The metavolcanic rocks range between tholeiitic basalts, to calc-alkaline *meta*-andesites and metarhyolites (GTK Consortium, 2006). A *meta*-andesite yielded a U-Pb SHRIMP zircon age of 1327 ± 16 Ma (GTK Consortium, 2006, Mänttäri, 2008). The upper Monte Tchicombe Group comprises the Rio Mucamba Formation, constituted by felsic metavolcanic rocks, metaconglomerates, metasandstones and quartzites, and at the top, the Monte Puéque Formation exposes gneisses and calc-silicate schists. The metamorphic conditions vary from upper-greenschist to lower-amphibolite facies (GTK Consortium, 2006). The supracrustal rocks were strongly deformed and

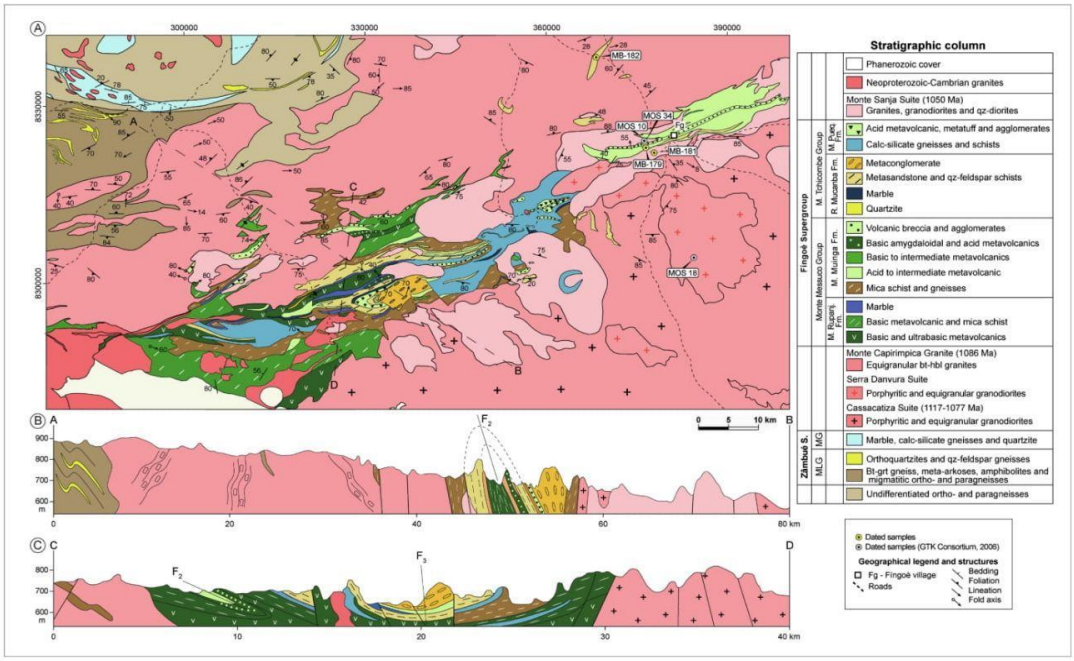

Fig. 3. A) Geological map of the Fíngoè Supergroup region (extracted and modified from GTK Consortium, 2006). Legend: MLG- Malowera Group, MG- Muze Group; B) Geological cross-section A-B; C) Geological cross-section C-D (modified from GTK Consortium, 2006).

generally show steep to vertical metamorphic NE-SW trending foliations (Fig. 3B, C). Early deformational events generated the S_1 and S_2 foliations, preserved as centimetric to metric, tight to isoclinal recumbent F_1 and F_2 folds, deformed by kilometer-scale open to close normal F_3 folds. The main deformational events defined the NE-SW structural trending of the Fíngoè Supergroup. The contact of the FS with the surrounding Cassacatiza Suite, Serra Danvura and Monte Capirimpica granitoids are concordant, as indicated by the magmatic and tectonic foliations. The FS was partially segmented by NW-SE and E-W trend normal faults associated with the deposition of the Karoo Supergroup during the Phanerozoic (Fig. 3C). Small occurrences of supracrustal rocks within the adjacent granitoids manifest a far wider extension than the relatively narrow Fíngoè fold and thrust belt. The FS was interpreted as a magmatic arc dating to ca. 1300 Ma, encompassed by the younger magmatism of the Cassacatiza Suite (1117 ± 12 Ma, 1077 ± 2 Ma), Monte Capirimpica (1086 ± 7 Ma) and Serra Danvura granitoids (Westerhof et al., 2008a, Mänttäri, 2008). The supracrustal rocks are intruded by the granitoids of the Monte Sanja Suite (1050 ± 8 Ma) and by the Neoproterozoic Monte Inchinga Granite.

The rocks of the Cazula Group (CG) are distributed in the eastern portion of the studied area as six irregular-shaped xenoliths up to 40 km long and 15 km wide, included in the Furacungo Suite granitoids (mainly in the Desaranhama Granite) (Fig. 2). The CG is constituted by quartz-feldspathic schists (metapsamites), calc-silicatic schists, quartzites and amphibolites, interpreted as metabasalts (GTK Consortium, 2006). The metasediments have a NW-SE trending schistosity, concordant with the magmatic and mylonitic foliation of the Desaranhama Granite. We studied the westernmost bodies of this group (Fig. 4). The late-orogenic Desaranhama Granite (ca. 1040 Ma) constraints the time of deformation of the Cazula Group.

2.2. Irumide intrusive suites

The supracrustal units are surrounded and supported by the granitoids of the Cassacatiza and Serra Danvura suites and by the Monte Capirimpica, Rio Capoche, and Serra da Chiúta granites. These lithodemic units are concordant with the metamorphic and deformational trend of the belt and represent the *syn*-orogenic plutonic arc magmatism of the Irumide Orogeny emplaced between 1201 and 1080 Ma (GTK Consortium, 2006; Westerhof et al., 2008a; Mäkitie et al. 2008). In contrast, the intrusive late-orogenic Mussata, Chacocoma and Furacungo Suite granitoids show crystallization ages between 1060 and 1020 Ma (GTK Consortium, 2006; Westerhof et al., 2008a; Mänttäri, 2008). The felsic magmatism is coeval with the charnockites of the Castanho Granite and with the mafic rocks of the Tete Suite, and with the Chipera, Rio Chiticula, Muenda and Ualádze gabbros. This younger bimodal magmatism represents the post-collisional phase of the Irumide Orogeny (Westerhof et al., 2008a, b). These intrusive suites occur predominantly to the north of the Tete Suite, comprising NW-SE trending elongated plutons with concordant magmatic foliation. The syeno- to monzogranites have porphyritic textures with variable contents of K-feldspar megacrysts, as well as biotite and hornblende (Mäkitie et al., 2008). The common presence of mafic enclaves and dioritic to gabbroic bodies demonstrates the mixing and mingling between granitic and mafic magmas. The granites show a high-K calc-alkaline composition while the mafic rocks have a tholeiitic (E-MORB) signature.

Besides the voluminous Stenian magmatism, there are records of Neoproterozoic magmatism in the Tete Province (Mäkitie et al., 2008; Westerhof et al., 2008a). The Tonian rocks (860–780 Ma) comprise the mafic-felsic Matunda, Atchiza and Guro Suites. This tholeiitic to calc-alkaline magmatism was conditioned by NE-SW to E-W extensional structures and is related to the Rodinia break-up (Westerhof et al., 2008a; Ibraimo and Larsen, 2015). The Late Ediacaran-Cambrian (550–470 Ma) granites occur as restricted plutons and represent the

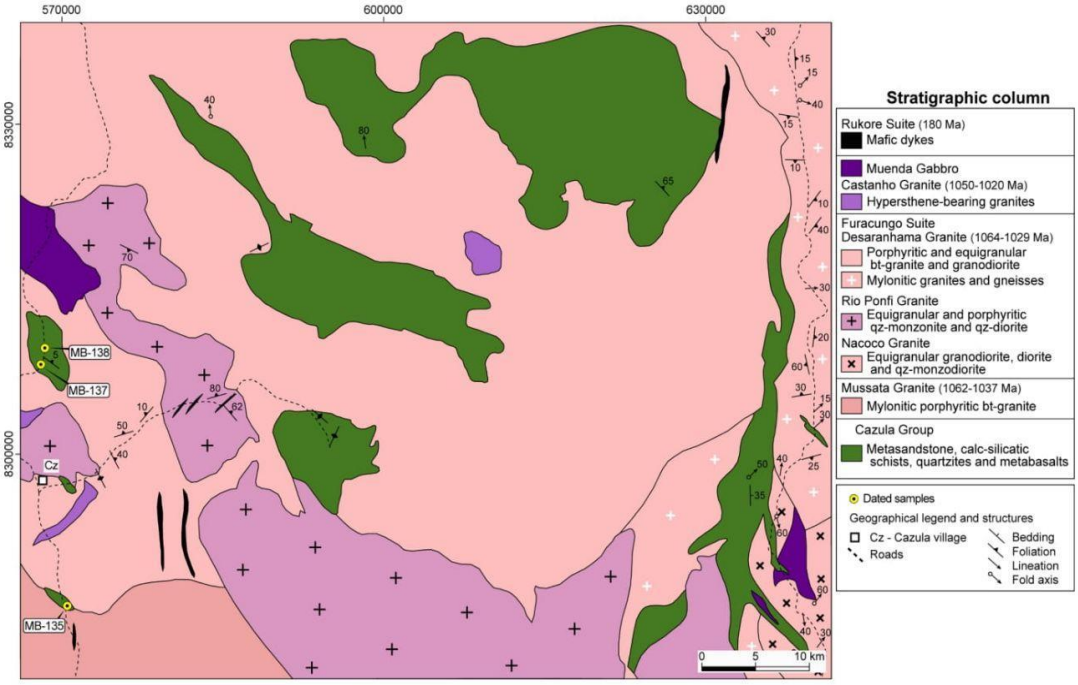

Fig. 4. Geological map of the Cazula Group (modified from GTK Consortium, 2006) with the location of the analyzed samples. Legend: Cz- Cazula village.

late- to post-collisional magmatism of the Pan-African Orogenic Cycle (Westerhof et al., 2008a; Goscombe et al., 2020).

3. Methods

To investigate the origin and tectonic setting of the supracrustal associations from Zâmbué and Fíngoè Supergroups and Cazula Group, were selected four samples of metasedimentary rocks to detrital zircon provenance, one dolerite sample and one sample of *meta*-andesite for U-Pb and Lu-Hf zircon isotopic determinations. To evaluate the results and support the interpretations we compiled geological, geochemical and isotopic data from the SIB regions of Zambia and Zimbabwe.

The zircon grains were extracted using conventional techniques of heavy mineral concentration, by means of jaw crushers, milling, manual panning and hand-picking under a binocular microscope. After separation, the zircon grains were mounted onto epoxy resin discs and polished to expose the grain centers. Prior to U-Pb analysis, the morphology and internal structure of zircons grains were characterized by SEM-cathodoluminescence (CL) in a JEOL 6510 Scanning Electron Microscope at DEGEO/UFOP. The CL images were used to examine morphological characteristics of zircon grains and to select areas for spot analyses. U-Pb analyses were carried out at the Isotopic Geochemistry Laboratory, the Universidade Federal de Ouro Preto, using a Thermo-Finnegan Neptune multi-collector ICP-MS coupled with a Photon-Machines 193 nm excimer laser system (LA-MC-ICP-MS). Data were acquired using peak jumping mode with background measurement during 20 *sec*, zircon ablation during 20 *sec* and 30 μm spot size. Analyses were conducted over several analytical sessions. The GJ-1 zircon standard (Jackson et al., 2004) was used as a primary standard for this study with the Plešovice zircon standard ($^{206}Pb/^{238}U$ = 337 Ma, $^{207}Pb/^{235}U$ = 337 Ma and $^{207}Pb/^{206}Pb$ = 339 Ma; Sláma et al., 2008) as a secondary standard. Data reduction was done in GLITTER® Software (Van Achterbergh et al., 2001), whereas the concordance, probability, radial and Concordia diagrams, and the weighted average ages were generated by the Excel Isoplot software (Ludwig, 2003) and the Isoplot-R Software (Vermeesch, 2018) according to procedures discussed and proposed by Spencer et al. (2016), Vermeesch (2018, 2021) and Barham et al. (2022). Probability density plots (PDP) and Kernel (KDP) plots, as well as, the weighted average ages, were calculated based on the $^{207}Pb/^{206}Pb$ ages, to present the most representative data of the analyzed zircons, since most of the ages obtained are ~ 1.2 Ga or older. The cut-off age varies somewhat within the literature (~between 1.0 and 1.5 Ga), with ages $^{206}Pb/^{238}U$ representing the youngest zircons (Gehrels et al., 2008, Spencer et al. 2016, Vermeesch, 2021). Maximum depositional ages (MDA) were calculated using the 'Maximum Likelihood Age' (MLA) method (Vermeesch, 2021) and the results were compared with all the Maximum Depositional Age (MDA) methods discussed and revised by Coutts et al. (2019). For comparison purposes, an average age of the main population of younger concordant grains was obtained by the Tera-Wasserburg Concordia method and a $^{207}Pb/^{206}Pb$ weighted average age. The complete U-Pb zircon data of two sessions of analysis and the reference material results are given in Supplementary Table S1.

The Lu-Hf isotopic analyses of the previously dated zircon grains were conducted in the Isotopic Geochemistry Laboratory of Ouro Preto Federal University (UFOP). The Lu-Hf data were acquired using a Thermo-Finnigan Neptune multicollector ICP-MS instrument coupled with a Photon-Machines 193 nm Excimer Laser System (LA-MC-ICP-MS) following the methods of Gerdes and Zeh (2006). The analysis used a bunch of standard zircons such as Temora (Black et al., 2003, Wu et al., 2006), GJ-1 (Jackson et al., 2004), Plešovice (Sláma et al., 2008), Mud Tank (Black and Gulson, 1978, Woodhead and Hergt, 2005), 91,500 (Goolaerts et al., 2004), which yielded $^{176}Hf/^{177}Hf$ of 0.282677 ± 0.000013 (n = 2), 0.282007 ± 0.000005 (n = 5), 0.282473 ± 0.000013 (n = 10), 0.282497 ± 0.000004 (n = 12), 0.282325 ± 0.000003 (n = 12), respectively (±2SD) (Supplementary Table S2).

For the calculation of εHf values, we used the ^{176}Lu decay constant of 1.867×10^{-11} (Söderlund et al., 2004) and the values of $^{176}Hf/^{177}Hf$ = 0.282785 and $^{176}Lu/^{177}Hf$ = 0.0336 for the present-day chondrites (Bouvier et al., 2008). For calculation of the depleted mantle evolution curve and the two-stage Hf model ages (T^2_{DM}), we adopted the values $^{176}Hf/^{177}Hf$ = 0.28325 and $^{176}Lu/^{177}Hf$ = 0.0388 of present-day depleted mantle (Griffin et al., 2000; updated by Andersen et al., 2009). The analytical data are available in Supplementary Table S2.

4. Results

4.1. U-Pb geochronology

We selected four metassedimentary samples including a metasandstone (MB-182) from the Zâmbuè Supergroup, a calc-silicate schist (MB-179) from the Fíngoè Supergroup, a metasandstone (MB-135) and a grt-bt-qz schist (MB-138) from Cazula Group, and two igneous samples including a *meta*-andesite (MB-181) from Fíngoè Supergroup and a dolerite (MB-137) from the Cazula Group. A total of 366 analyses were performed and 301 concordant or near concordant U-Pb zircon ages were obtained for the analyzed samples.

4.1.1. Zâmbuè Supergroup

The medium-grained metasandstone MB-182 sample was collected from a slab outcrop in a small window of Zâmbuè Supergroup within the Cassacatiza Suite granitoids (UTM: 36 L, 368,568 E/8338292 S). The feldspathic *meta*-arkose shows a light brown color and a weakly foliated structure associated to a medium-grained lepidoblastic texture with oriented muscovite aggregates. The main texture is polygonal to interlobate granoblastic, constituted by quartz and microcline, with subordinated plagioclase (Fig. 5A). We analyzed 96 zircon grains that resulted in 68 concordant ages. The zircon crystals have euhedral prismatic shapes with pyramidal terminations. The size ranges from 120 to 320 μm and aspect ratio from 3:1 to 2:1. In CL images all crystals show oscillatory zoning (Fig. 6A. Th/U ratios range between 0.36 and 1.02 and are indicative of igneous zircon. The probability density plot shows $^{207}Pb/^{206}Pb$ ages between 1208 and 1086 Ma, with a single grain of 1867 Ma (Fig. 7A). A main peak of 1110 ± 2 Ma (MSWD = 1.0, n = 34) was defined by a $^{207}Pb/^{206}Pb$ weighted average age, confirmed by a Concordia (Tera-Wasserburg) age of 1111 ± 2 Ma (MSWD = 0.65, n = 28) (Fig. 7A). The MLA (Maximum Likelihood Age) calculation of sample MB-182 yielded a maximum depositional age of 1110 ± 2 Ma (Fig. 7A).

4.1.2. Fíngoè Supergroup

The medium-grained calc-silicatic schist sample (MB-179) was collected from a boulder along the road close to the Fíngoè town (UTM: 36 L, 376,725 E/8322954 S). The calc-silicatic schist has a light green color and preserved primary compositional banding (S0) defined by the alternation of millimeter (5–20) thick layers rich in epidote, garnet and muscovite, and quartz-feldspathic-rich layers (Fig. 5B). The felsic levels are dominant and show polygonal granoblastic texture defined by a quartz, epidote, garnet and plagioclase arrangement (Fig. 5C, D). This banding was folded and transposed to a spaced S_1 schistosity characterized by a medium-grained lepidoblastic texture (Fig. 5E). We analyzed 51 zircon grains from the calc-silicatic schist of which 37 concordant ages were obtained. The zircon crystals have prismatic and equidimensional shapes, often fragments of larger grains, with rounded pyramidal and straight terminations. Grain size ranges from 108 to 220 μm and aspect ratio from 3:1 to 2:1. In CL images, the crystals reveal internal igneous textures, including oscillatory zoning (Fig. 6B). Th/U ratios of 0.26–1.10 are common in magmatic zircon grains (Belousova et al., 2002). The $^{207}Pb/^{206}Pb$ zircon ages range from 2635 Ma to 1106 Ma, with a main population between 1199 and 1106 Ma (Fig. 7B). The probability density plot shows a narrow spectrum of $^{207}Pb/^{206}Pb$ ages with graphical age peaks at 1096, 1230 and 1987 Ma. A $^{207}Pb/^{206}Pb$

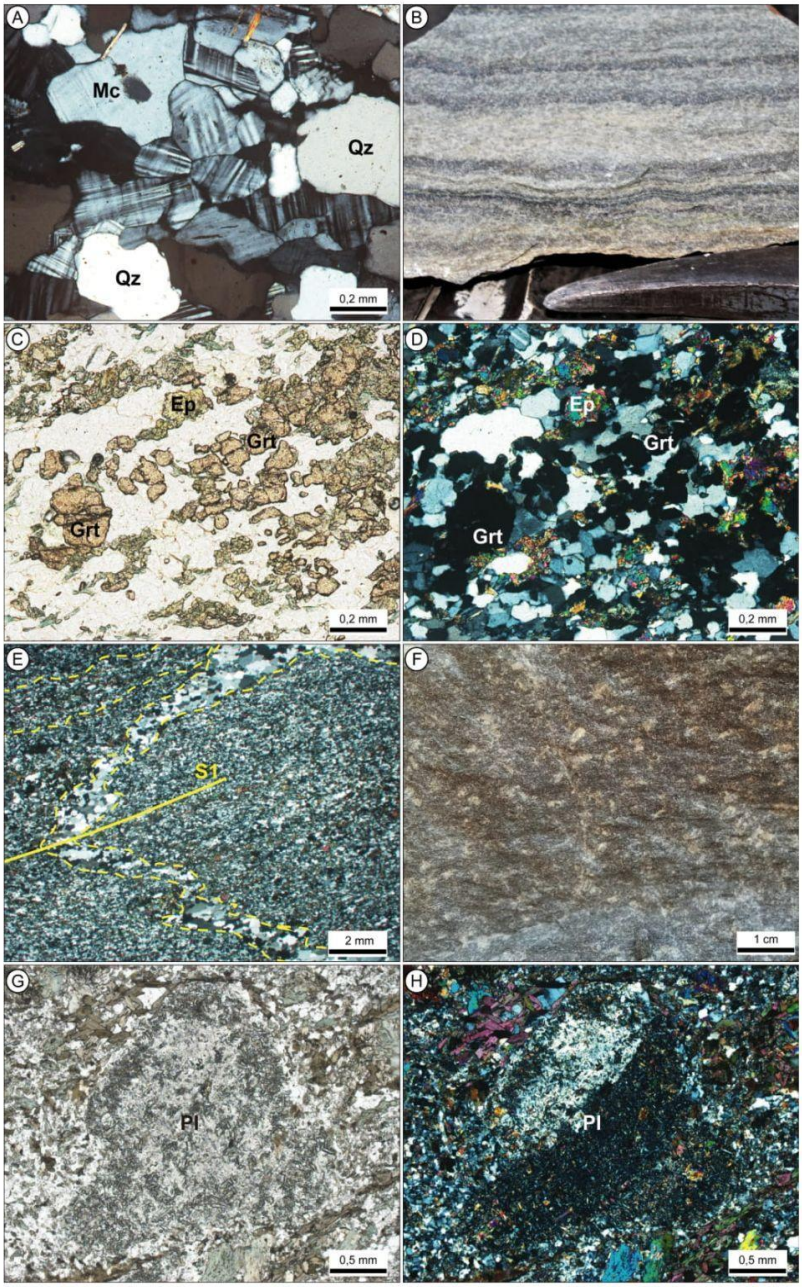

Fig. 5. A) meta-arkose of the Malowera Group (Zâmbuè Supergroup) with blastopsamitic texture defined by subrounded clast of microcline and quartz involving by granoblastic polygonal fabric (crossed polarizer), B) Compositional layering (S0) in calc-silicate schist (MB-179), C) Ep-hb-pl-qz-gros schist (MB-179) from the Fíngoè Supergroup. showing a discontinuous and spaced schistosity and epidote (Ep) and grossular (Gt) porphyroblasts (plane-polarized light), D) Same section with crossed polarizer, E) Detail of F1 fold with deformation of the compositional layering (S0) and formation of the S1 axial surface (plane-polarized light) (MB-179), F) Blastoporphyritic texture with relicts of plagioclase phenocrysts in the dated *meta*-andesite (MB-181); G) Same rock with relict of euhedral plagioclase (Pl) phenocrystal involved by medium-grained polygonal granoblastic texture with plagioclase and epidote, and lepidoblastic texture with biotite (Bt), chlorite and muscovite (plane-polarized light), H) Same section at crossed polarizer.

weighted average age of 1143 ± 6 Ma (MSWD = 0.52, n = 13) was defined by the main younger population (Fig. 7B) and a Concordia (Tera-Wasserburg) age of 1138 ± 4 Ma (MSWD = 1.0, n = 13). The MLA (Maximum Likelihood Age) calculation of the sample MB-179 yielded a maximum depositional age of 1110.97 ± 8.36 Ma (Fig. 7B).

The *meta*-andesite MB-181 sample was collected from an outcrop close to the Fíngoè village (UTM: 36 L, 378,525 E/8322077 S) and represents the intermediate volcanism of Monte Muinga Formation (GTK Consortium, 2006). The rock has a porphyritic texture defined by euhedral lath-type plagioclase porphyroclasts (0.5–1.5 mm) (Fig. 5F). The fine-grained matrix is constituted by plagioclase, hornblende, biotite and low contents of quartz, with nematoblastic texture characterized by oriented amphibole (Fig. 5G, H). The zircon crystals show euhedral prismatic shapes with straight terminations and sizes ranging between 120 and 220 μm, with aspect ratio from 3:1 to 2:1 (Fig. 8A). Th/U ratios between 0.69 and 1.18 confirm the magmatic origin. Were analyzed six

Fig. 6. CL images of the analyzed zircon grains. A) meta-arkose (MB-182) from Malowera Group (Zâmbuè Supergroup), B) Calc-silicate schist (MB-179) from Fíngoè Supergroup, C) Metasandstone (MB-135) from Cazula Group, D) Garnet-biotite-qz schist (MB-138) from Cazula Group and E) Intrusive dolerite (MB-137) in the Cazula Group. Yellow circles show the spot location of the U-Pb analysis, while the white circle show the spots of the U-Pb and Lu-Hf analysis. Legend of the spot results. First line: number of the analyzed spot in the table of data, Second line: U-Pb age, and Third line: epsilon Hf(t) value.

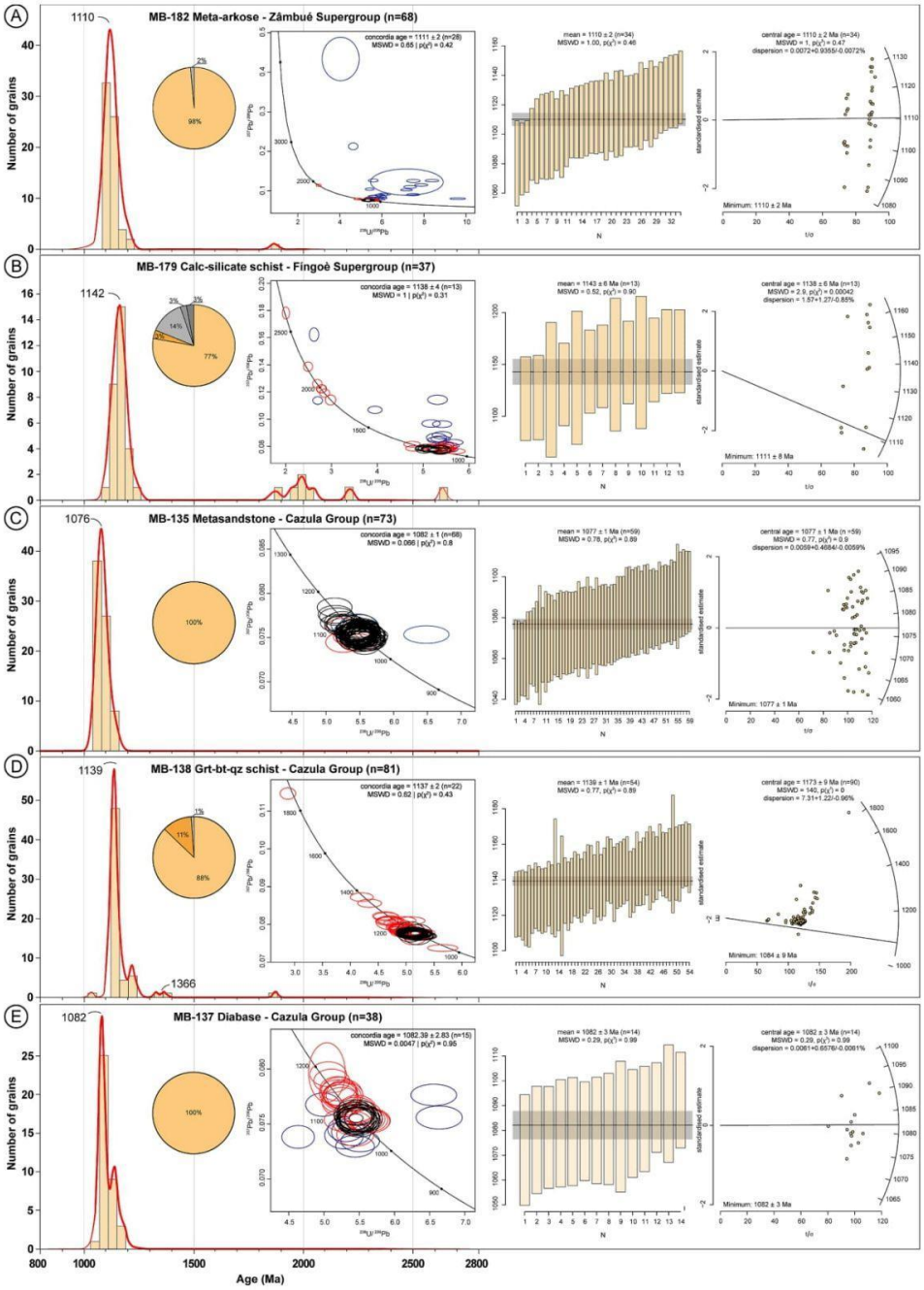

Fig. 7. Histogram and relative density plot of U-Pb detrital zircon ages of this work. A) meta-arkose (MB-182), B) Calc-silicate schist (MB-179), C) Metasandstone (MB-135), D) Garnet-biotite-qz schist (MB-138), and E) Intrusive dolerite (MB-137).

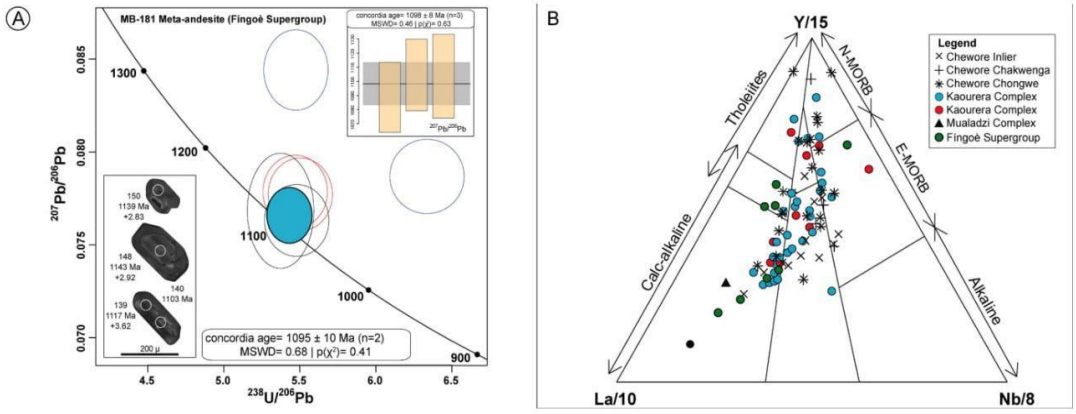

Fig. 8. A) Concordia age for the *meta*-andesite (MB-181) of the Fíngoè Supergroup, B) La/10 × Y/15 × Nb/8 diagram (Cabanis and Lacolle, 1989) for the meta-volcanic rocks from Fíngoè Supergroup and for the Chewore, Kaourera and Mualadzi complexes, showing an orogenic trend. Data from: Oliver et al. (1998), Johnson and Oliver (2004), GTK Consortium, 2006a; Johnson et al. (2007).

zircon grains from the *meta*-andesite and most of the analyzes show some degree of discordance, two were discarded. The values obtained considering the four grains and the two most concordant analyzes vary around ~ 5 Ma. Three more concordant analysis yielded a $^{207}Pb/^{206}Pb$ weighted average age of 1098 ± 8 Ma (MSWD = 0.46), while the two concordant zircons generated a Concordia (Tera-Wasserburg) age of 1095 ± 10 Ma (MSWD = 0.68) (Fig. 8A).

4.1.3. Cazula Group

The sample MB-135 corresponds to a fine- to medium-grained meta-asandstone collected from a road cut outcrop in a ten of meters-size xenolith of the Cazula supracrustals in the Desaranhama Granite, close to the contact with Mussata Granite (UTM: 36 L, 570,701 E/8285581 S). The metapsamite shows light gray color and a plane-parallel structure defining a compositional banding of centimetric thickness (Fig. 9A). Internally, a weakly foliated structure is defined by orientation of biotite. The main texture is fine-grained granoblastic polygonal with quartz, plagioclase and microcline. We analyzed 76 zircon grains and obtained 73 concordant ages. The zircon crystals are predominantly equidimensional, many fragments of larger grains, with subrounded terminations. The size ranges from 40 to 330 µm and aspect ratio from 3:1 to 1:1. In CL images, the crystals show oscillatory and sector zoning (Fig. 6C). Th/U ratios range between 0.23 e 1.01, indicating magmatic origin. The probability density plot shows a narrow spectrum and a single graphical age peak with $^{207}Pb/^{206}Pb$ ages ranging between 1157 and 1052 Ma (Fig. 7C). These zircons show a $^{207}Pb/^{206}Pb$ weighted average age of 1077 ± 1 Ma (MSWD = 0.78, n = 59) and a Concordia (Tera-Wasserburg) age of 1082 ± 1 Ma (MSWD = 0.08, n = 68) (Fig. 7C). The MLA (Maximum Likelihood Age) calculation of the sample MB-135 yielded a maximum depositional age of 1077 ± 1 Ma (MSWD = 0.77, n = 59) (Fig. 7C).

The grt-bt-qz schist sample (MB-138) was collected from a road cut outcrop in a large xenolith of Cazula Group close to Cazula town (UTM: 36 L, 568,291 E/8309001 S). The schist has dark grey color and spaced schistosity marked by medium-grained lepidoblastic texture defined by orientation of biotite (Fig. 9B). The garnet occurs as subhedral porphyroblasts with internal *syn*-kinematic fine trails preserved by inclusions of quartz and opaque minerals (Fig. 9C, D). Were analyzed 90 zircon grains and obtained 81 concordant ages. The zircon crystals have euhedral and elongated prismatic shapes with pyramidal terminations. The grain size ranges from 82 to 230 µm and aspect ratio from 4:1 to 1:1. In CL images, the grains exhibit igneous texture and oscillatory zoning (Fig. 6D). Th/U ratios range between 0.18 e 1.40. The probability density plot shows $^{207}Pb/^{206}Pb$ ages ranging from 1875 to 1034 Ma, with a main age peak defined by a narrow interval of ages between 1187 and 1114 Ma (Fig. 7D). This main interval of results yielded a $^{207}Pb/^{206}Pb$ weighted average age of 1139 ± 1 Ma (MSWD = 0.77, n = 54) and a Concordia (Tera-Wasserburg) age of 1137 ± 2 Ma (MSWD = 0.62, n = 22) (Fig. 7D). A maximum depositional age of 1084 ± 19 Ma (MSWD = 140, n = 90) was obtained by the MLA (Maximum Likelihood Age) method (Fig. 7D).

The dolerite sample (MB-137) is intrusive in the Cazula Group supracrustals and was collected from an outcrop in a small stream along the road close to the Cazula town (UTM: 36 L, 568,133 E/8307994 S). The diabase occurs as a sill and has dark grey color and a fine-grained massive texture. The rock is composed of plagioclase, pyroxene and opaque minerals arranged in an intergranular texture. (Fig. 9E, F). Were analyzed 47 zircon grains and obtained 38 concordant ages. The zircon crystals have euhedral and elongated prismatic shapes with pyramidal terminations. Most of the grains have incipient rounded faces, suggesting sedimentary reworking. We interpreted these zircon grains as inherited xenocrysts with the youngest cluster indicating the maximum emplacement age. The grain size ranges from 100 to 200 µm and aspect ratio from 3:1 to 2:1. In CL images, the grains exhibit igneous texture and oscillatory zoning (Fig. 6e). Th/U ratios range between 0.23 e 1.01. The probability density plot shows a single graphical age peak with $^{207}Pb/^{206}Pb$ ages ranging from 1189 to 1042 Ma (Fig. 7E). The $^{207}Pb/^{206}Pb$ weighted average ages shows three distinct ages intervals. The younger zircons yielded a weighted average age of 1082 ± 3 Ma (MSWD = 0.29, n = 14) and a Concordia (Tera-Wasserburg) age of 1082 ± 3 Ma (MSWD = 0.0047, n = 15) (Fig. 7E). The MLA (Maximum Likelihood Age) calculation of the sample MB-137 yielded an age of 1082 ± 3 Ma (MSWD = 0.29, n = 14) (Fig. 7E).

4.2. Lu-Hf isotopic data

The same zircon crystals investigated by U-Pb were analyzed to Lu-Hf compositions. The analyses were conducted in the same spots of the previous U-Pb investigation. A total of 118 Lu-Hf determinations were obtained. The results show a similar isotopic composition of juvenile mantle magmas with mixing of isotopically evolved continental crust.

4.2.1. Zâmbuè Supergroup

We determined the Lu-Hf isotopic compositions of twenty-four zircon grains from the metasandstone (MB-182). The analyzed crystals

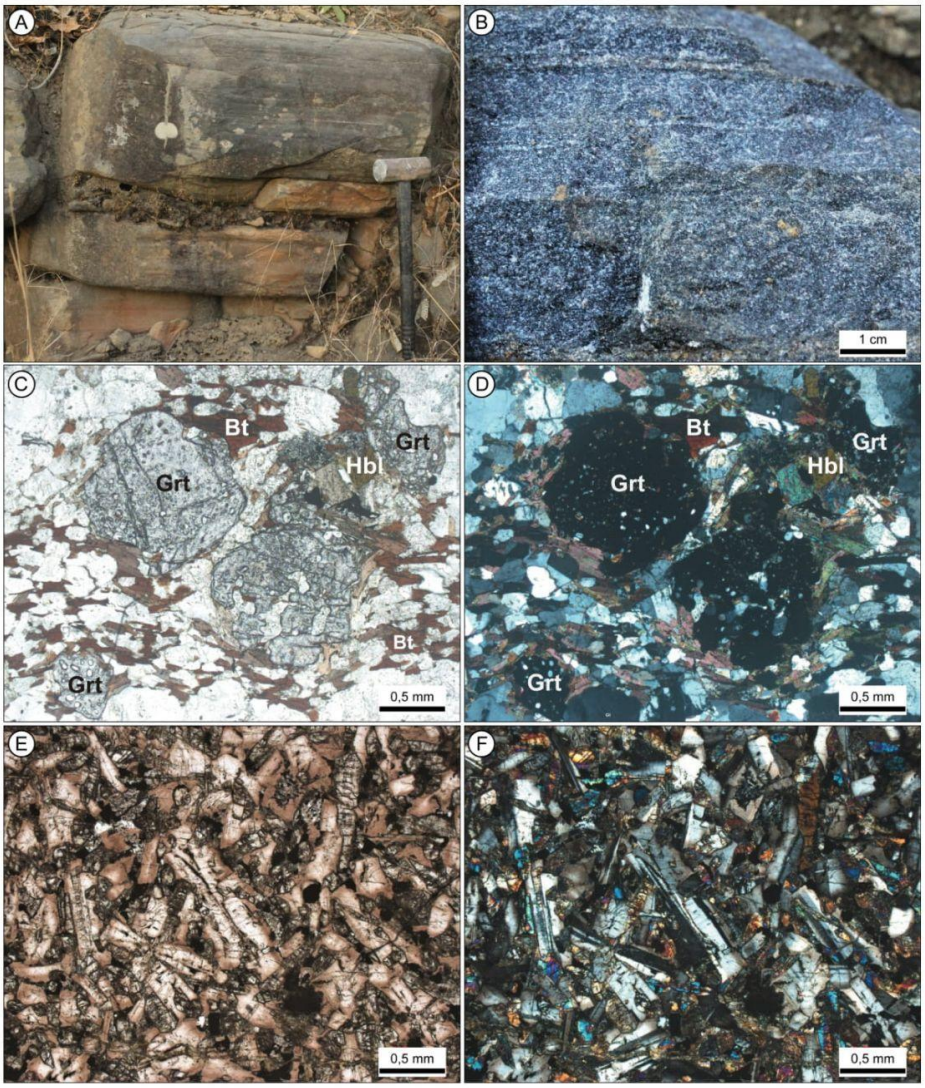

Fig. 9. Macroscopic and microscopic features of the Cazula Group rocks. A) Compositional layering (S0) in metasandstone (MB-138) alternating continuous and irregular felsic levels of qz-feldspathic-rich composition and biotite-rich mafic levels, B) Detail of the S0 in fresh rocks surface, C) Garnet-biotite schist (MB-138) with *syn*-S2 garnet porphyroblasts and lepidoblastic texture of biotite (plane-polarized light), D) Same section in crossed polarizer, E) Intergranular texture of the intrusive dolerite (MB-137), F) Same section in crossed polarizer.

have ages between 1180 and 1102 Ma and positive εHf(t) values between +9.88 and +2.03 (Fig. 10). These grains show T^2_{DM} ages between 1.70 and 1.26 Ga.

4.2.2. Fíngoè Supergroup

Fifteen zircon grains from the calc-silicate schist (MB-179) were analyzed. Twelve zircon grains with ages ranging between 1199 and 1119 Ma show εHf(t) values ranging from +9.04 and −0.67 (Fig. 10a). These grains show T^2_{DM} ages between 1.89 and 1.34 Ga. Two Paleoproterozoic grains dated at 2211 and 1991 Ma yielded εHf(t) values of −7.71 and −1.94 (Fig. 10) with T^2_{DM} ages of 2.80 and 2.94 Ga, respectively. The three analyzed zircon grains from the *meta*-andesite (MB-181) have ages of 1148–1117 Ma and positive εHf(t) values between +4.31 and +2.34 (Fig. 10). The T^2_{DM} ages vary between 1.69 and 1.60 Ga.

4.2.3. Cazula Group

We determined the Lu-Hf isotopic compositions of thirty-one zircon crystals from the metasandstone (MB-135). The analyzed crystals have ages between 1110 and 1060 Ma and εHf(t) values varying between +6.46 and −12.24 (Fig. 10). The T^2_{DM} ages range from 2.45 to 1.43 Ga. From the zircon crystals of the gt-bt-qz schist (MB-138), twenty-nine Lu-Hf isotopic compositions were obtained. The analyzed crystals have ages between 1328 and 1034 Ma and εHf(t) values between +9.73 and −0.64

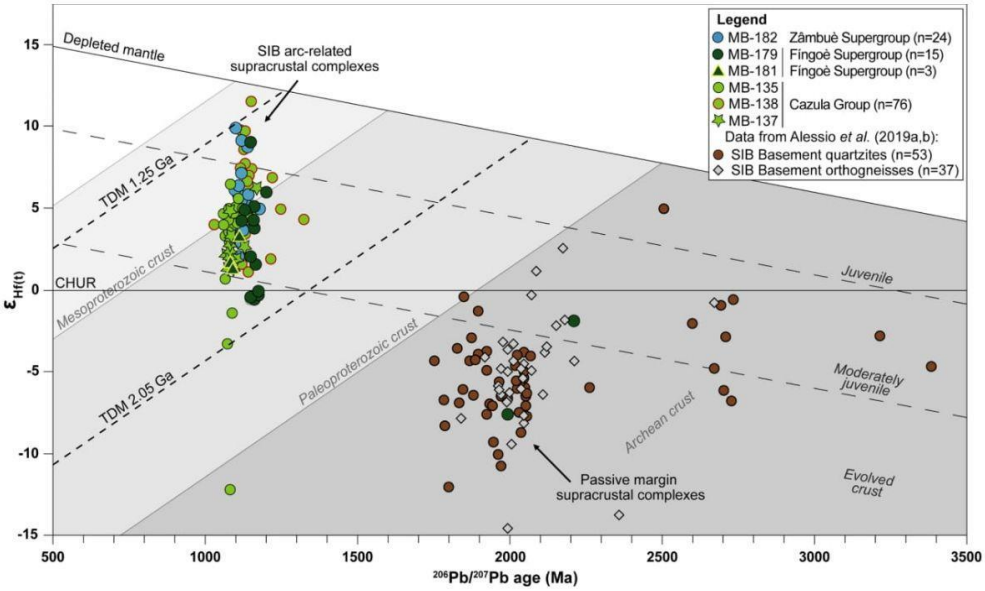

Fig. 10. A) εHf values versus U-Pb ages diagram. The average crust fields were calculated using the average continental crust $^{176}Lu/^{177}Hf$ ratio of 0.015 (Griffin et al., 2004) and the black dashed lines classify fields of juvenile material (0–5 Ɛ-units below DM), moderately juvenile (5–12 Ɛ-units below DM) and evolved (>12 Ɛ-units below DM) like proposed by Reimann et al. (2010).

(Fig. 10). The T^2_{DM} ages range from 1.87 to 1.21 Ga. The zircon grains from the intrusive dolerite (MB-137) have ages between 1170 and 1071 Ma and εHf(t) values varying between +6.20 and +1.19 (Fig. 10). The T^2_{DM} ages range from 1.73 to 1.52 Ga.

5. Discussions

The NW region of Mozambique and its border with the eastern portion of Zambia, northern Zimbabwe, and western Malawi host the various units of the Southern Irumide Belt. The Fíngoè Supergroup and the Cazula Group were the first metasediments from arc-related basins recognized in the SIB of NW Mozambique. These units were mapped and defined by the GTK Consortium (2006), but its stratigraphy, geochronology and tectonic significance has been poorly investigated. The detrital zircon grains from the rock associations of the Zâmbué, Fíngoè, and Cazula show euhedral prismatic shapes and well-preserved magmatic oscillatory zoning, indicating igneous sources and short sedimentary transport.

The supracrustal associations are the older units of the SIB and show a regional metamorphic foliation in the NE-SW direction. The schistosity to incipient gneiss banding records a complex and polyphasic evolution characterized by the development of the S_1 and S_2 foliations under low- to medium-grade metamorphic conditions. Both Zâmbuè and Fíngoè Supergroups are bounded by oblique and transcurrent ductile shear zones and are cut by late-orogenic bodies of porphyritic granitoids, charnockites, and gabbro-anorthosite complexes with emplacement ages between 1060 and 1020 Ma (GTK Consortium, 2006, Westerhof et al. 2008a). The Fíngoè Supergroup constitutes an elongated belt of N60°E direction, separated from the Zâmbuè units by the *syn*-orogenic granites of the Cassacatiza Suite and of the Serra Danvura and Monte Capirimpica, with ages between 1117 Ma and 1086 Ma (GTK Consortium, 2006, Westerhof et al. 2008a). The Fíngoè Supergroup comprises basic to acid metavolcanic rock associations with subordinate metapelites, metaconglomerates, calc-silicate schists and marbles. Geochemical data from the Fíngoè and other correlated metavolcanic rocks of NE Zambia, when plotted in the diagram of Cabanis and Lacolle (1989) (Fig. 8B), shows an orogenic trend and a composition like mantle magmas generated in subduction zones. Two samples of intermediate metavolcanic rocks showed crystallization ages of 1328 Ma (MOS-34, GTK Consortium, 2006) and 1098 Ma (MB-181).

The granites of the Cassacatiza suite, Serra Danvura and Monte Capirimpica constitute elongated bodies concordant with the NE-SW oriented ductile shear zones. The trace of the magmatic foliation of these granitoids can be observed on the map in Fig. 3, confirming the *syn*-tectonic character of the magmatism positioning and its contemporaneity with the D_1 and D_2 deformation events and in part, with the orogenic metamorphism at ca. 1080 Ma (GTK Consortium, 2006). The granites of the Monte Sanja and Castanho Granite suites are intrusive in the metamorphic rocks of the Zâmbuè and Fíngoè Supergroups, and in the *syn*-orogenic granite suites. These bodies show elongate shapes and crystallization ages between 1060 and 1020 Ma, suggesting the reactivation of ductile shear zones during the late-orogenic stages of the SIB (GTK Consortium, 2006, Westerhof et al. 2008a).

5.1. Isotopic data and source areas

The metasediments of the Zâmbuè and Fíngoè Supergroups and of the Cazula Group show dominance of Stenian (1200–1086 Ma) detrital zircon grains with minor Ectasian (1364–1203 Ma) and very subordinate Paleoproterozoic and one Archean age (Fig. 7). The detrital zircon patterns indicate that these supracrustal sequences received contributions mostly from the Mesoproterozoic units that characterize the Fíngoè magmatic arc of the SIB.

The bulk of the analyzed detrital zircon grains presented Stenian ages ranging between 1250 and 1080 Ma, broadly corresponding to the *syn*-orogenic arc magmatism of the SIB in the Tete Province (Fig. 11) (Mänttäri, 2008; Westerhof et al., 2008a). The vertical array of positive $\varepsilon Hf_{(t)}$ values (+2 to +10) and the T^2_{DM} ages ranging between 1.75 and 1.30 Ga indicate juvenile sources, with limited contributions of crustal reworking (Fig. 10). Some zircon grains show T^2_{DM} ages between 2.95

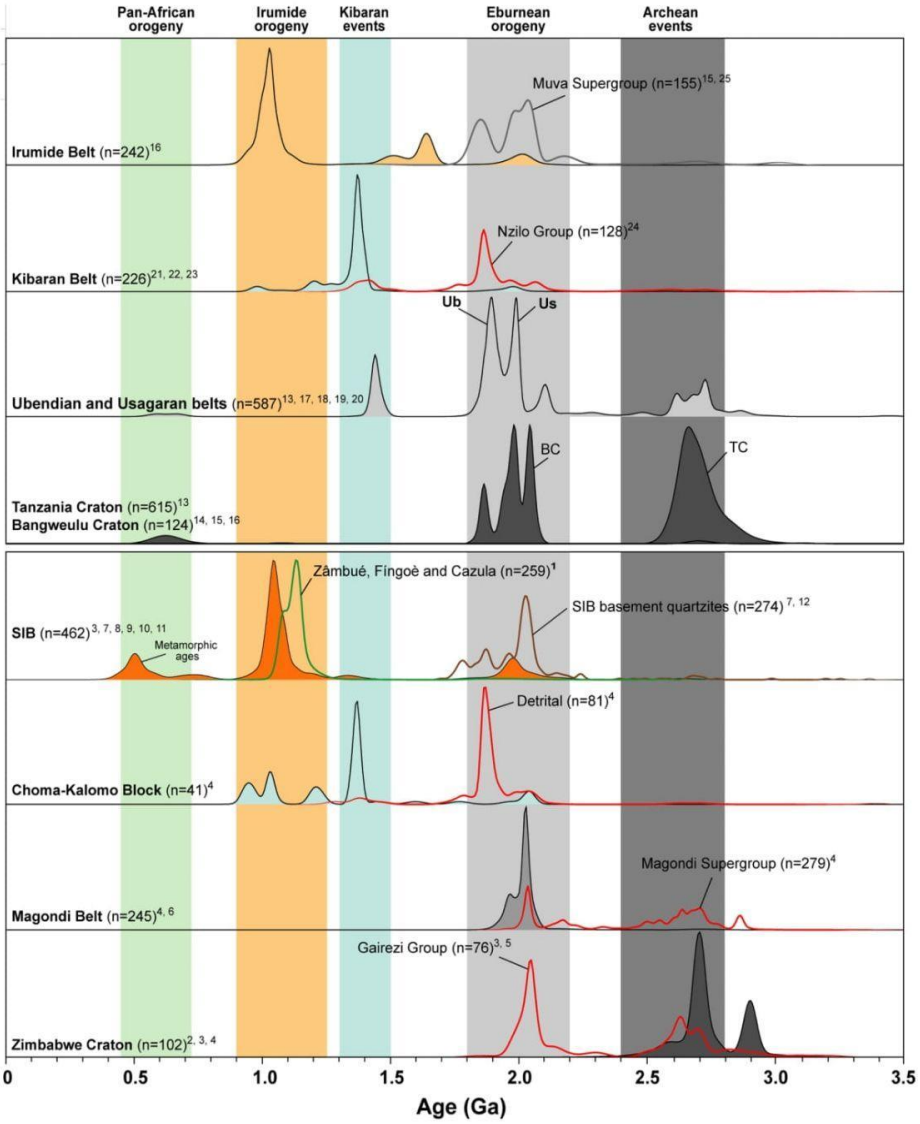

Fig. 11. Kernel Density Plots (KDP) from tectonic units of the SE Africa, including the Archean rocks from Zimbabwe, Bangweulu and Tanzania cratons, Paleoproterozoic units of Magondi, Ubendian and Usagaran belts, and Mesoproterozoic rocks from Choma-Kalomo Block, Kibaran, Irumide, and Southern Irumide belts. References: (1) This study; (2) Sumburane (2011); (3) Mänttäri (2008); (4) Glynn (2017); (5) Chaúque et al. (2017); (6) McCourt et al. (2001); (7) Alessio et al. (2019b); (8) Manda et al. (2019); (9) Oliver et al. (1998); (10) Jonhson et al. (2007b); (11) Johnson et al. (2006); (12) Alessio et al. (2019a); (13) Thomas et al. (2016); (14) Rainaud et al. (2005); (15) De Waele and Fitzsimons (2007); (16) De Waele et al. (2009); (17) Collins et al. (2004); (18) Thomas et al. (2013); (19) Lawley et al. (2013); (20) Thomas et al. (2019); (21) Kokonyangi et al. (2004); (22) Maier et al. (2007); (23) Tack et al. (2010); (24) Kokonyangi et al. (2007); (25) Rainaud et al. (2003).

and 1.70 Ga reflecting higher amounts of assimilation of isotopically evolved continental crust.

A single NeoArchean grain was identified in the calc-silicatic schist of the Fíngoè Supergroup, possibly indicating an Archean source of sediments or relics of Archean crust within the arc. In the Nyimba region of Zambia, a dioritic gneiss presented a LA-ICPMS U-Pb zircon age of 2608 ± 14 Ma, the oldest dated basement rock of the SIB (Cox et al., 2002). This orthogneiss is correlated to the Rio Mepembe Complex of the Zâmbué Supergroup. Two of these grains showed negative $\varepsilon Hf_{(t)}$ values similar to those presented by Alessio et al. (2019a, b) for basement orthogneisses and quartzites from the Chipata and Rufunsa regions at southeastern of Zambia (Fig. 2). Paleoproterozoic detrital zircon grains recorded in the Fíngoè Supergroup and Cazula Group were likely associated with similar orthogneisses inliers described by Alessio et al. (2019b) in the Chipata region (Fig. 2). The evolved isotopic signatures indicate that the Paleoproterozoic sources were formed by the reworking of Archean crust.

Early Ectasian detrital zircon grains were found in the MB-138 grt-bt-

qz schist from the Cazula Group, with an age peak of 1366 Ma (Fig. 7D). Ages from this period are subordinate in the SIB and correspond to the first magmatism phase in the Choma-Kalomo Block (Glynn et al., 2017), southernmost Zambia and in Kibaran Belt (Tack et al., 2013), at Congo and Tanzania (Fig. 11). The bulk of the analyzed detrital zircon grains presented ages ranging between 1164 and 1125 Ma, broadly corresponding to the *syn*-orogenic arc magmatism of the SIB in the Tete Province (Mänttäri, 2008; Westerhof et al., 2008a). The vertical array of predominantly positive $\varepsilon Hf_{(t)}$ values (+2 to +10) and the T^2_{DM} ages ranging between 1.75 and 1.30 Ga indicate isotopic signatures of juvenile sources, with limited contributions of crustal reworking (Fig. 10).

5.2. Tectonic setting and depositional age

The U-Pb and Lu-Hf detrital zircon data from the Zâmbué and Fíngoè Supergroups and Cazula Group reveal the same source rocks and analogous tectonic settings. A narrow provenance spectrum and an age peak close to the presumed depositional age are characteristic of arc-related basins (Cawood et al. 2012, Marschall et al., 2013, Barham et al. 2022) (Fig. 12B). The Zâmbuè Supergroup shows a distinct kind of sedimentary succession, with a thick *meta*-arkose package interlayered with quartzites and minor metapelites, marbles and calc-silicate gneisses, with minor volcanic contribution. The preserved sedimentary structures and facies associations are suggestive of a more mature succession, likely deposited in a continental passive margin environment or in a foreland basin. New zircon grains from the K-feldspar-rich metasandstone (MB-182) presented, however, a dominant range of ages between 1208 and 1086 Ma (Fig. 7), with positive εHf(t) values (+9.88 to +2.03) (Fig. 10). The T^2_{DM} ages range between 1.70 and 1.20 Ga. Previously, the SHRIMP dating of eighteen detrital zircons from a *meta*-arkose (MOS-33) from the Malowera Group recorded a heterogeneous population, including prismatic to oval, transparent to translucent, reddish-brown to colorless prismatic grains (GTK Consortium, 2006). The crystals have rounded or corroded cores, with internal oscillatory zonation. The igneous cores presented Archean (~2700–2500 Ma) and Paleoproterozoic (~2100–1900 Ma) ages. Four euhedral zircons yielded ages of 1300 and 1200 Ma, interpreted as the maximum depositional age. Homogeneous outer fringes around a rounded zoned core indicated ages around 1070 Ma were interpreted as related to a metamorphic event (Mänttäri, 2008). Also, the quartzite and metapelite samples analyzed by Alessio et al. (2019a) in the eastern portion of Zambia which are possibly correlated with Zâmbuè Supergroup show broad Archean and Paleoproterozoic sources (Fig. 11). The compositional and structural features of the Zâmbué Supergroup indicate that the rocks were deposited in a divergent setting. However, the contribution of the arc-related sources identified in the *meta*-arkose sample (MB-182) suggests the spatial and temporal relation with the arc, at least in the upper units of Malowera Group. Besides, the Zâmbué Supergroup may include distinct sedimentary sequences as passive margin and arc sequences and even foreland sediments, deformed during the Irumide Orogeny.

The Fíngoè Supergroup was previously interpreted as an intra-oceanic island arc around 1330 Ma (Fíngoè Arc), based on rock association, whole-rock geochemistry and in a U-Pb SHRIMP zircon age of 1327 ± 16 Ma from a felsic/intermediate metavolcanic rock (GTK Consortium, 2006, Westerhof et al. 2008A; Mänttäri, 2008). The new results of detrital zircon data for the calc-silicatic schist (MB-179) show a narrow spectrum of ages between 1164 and 1118 Ma and a maximum depositional age of 1110 Ma. The crystallization age of 1094 ± 10 Ma obtained in the *meta*-andesite (MB-181) may indicate that the rocks of the Fíngoè Supergroup can record two magmatic episodes related to distinct tectonic events.

The predominantly positive εHf(t) values between +9.04 and −0.67 and the T^2_{DM} ages ranging from 1.89 to 1.34 Ga corroborate the juvenile origin. The Fíngoè Supergroup is coeval to the active margin phase of the SIB and the stratigraphic sequence resembles those formed in basalt floored back-arc basins (GTK Consortium, 2006, Westerhof et al. 2008a). The lower volcanic sequence of the supergroup was interpreted by GTK Consortium (2006) as representative of the initial stage of the basin formation associated with active subduction and marked by the basaltic and andesitic to rhyolitic magmatism.

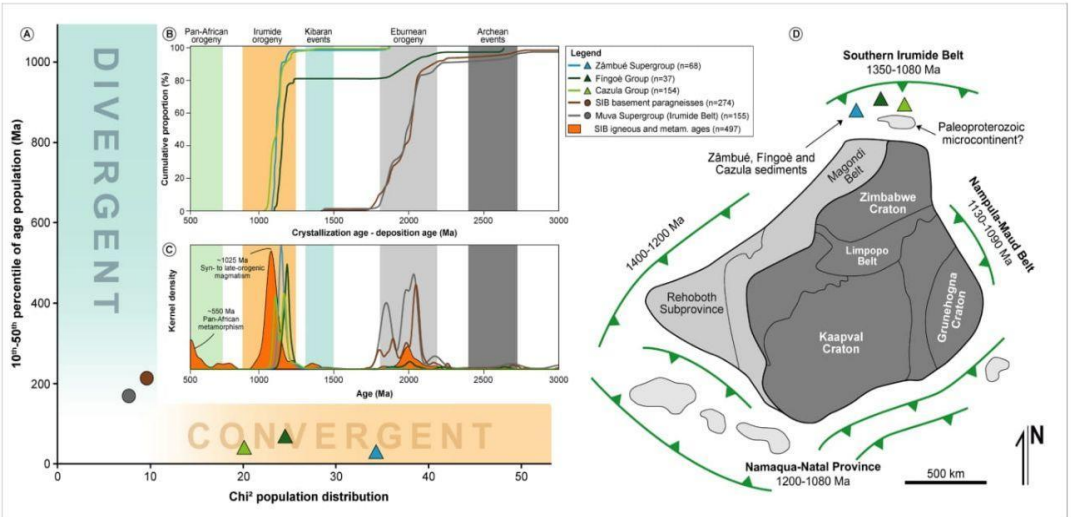

Fig. 12. Fig. 11. A) Bivariate discrimination plot of active convergent and divergent/passive margin tectonic settings (Barham et al. 2022) applied to the Southern Irumide Belt. Sample symbol and kernel density estimate age spectrum is color coded according to their combined detrital fingerprinting metric value in the legend. B) Disposition of the supracrustal complexes from SIB showing inferred convergent margin setting based on classification method of Cawood et al. (2012). C) Kernel density estimate age population for the analysed samples of the supracrustal complexes and from *syn*-to late-orogenic magmatism of the SIB. D) Paleogeographic reconstruction of the Kalahari Craton from the proposition of Jacobs et al. (2008), modified in the northern portion of the Zimbabwe Craton according to the results of investigations of supracrustal complexes of the SIB obtained in this work. Data for the figures C and D compiled from: Alessio et al. (2019a, b), De Waele and Fitzsimons (2007), Johnson et al. (2006, 2007), Johnson and Oliver (2004), Manttari (2008), Oliver et al. (1998), Rainaud et al. (2003).

Compared with the Fíngoè Supergroup, the metavolcano-sedimentary complexes of the Kaourera Arc in the Rufunsa region, NW Zimbabwe, are aligned in a NE-SW trend, indicating a possible spatial continuity (Fig. 2). The Kaourera complexes also presents mafic to felsic metavolcanic rocks with tholeiitic to low-K calc-alkaline composition and igneous crystallization ages of ca. 1080 Ma (Johnson and Oliver, 2004; Johnson et al., 2007). The Kaourera complexes rocks show LILE enrichment and negative Nb, P and Ti anomalies (Johnson et al., 2007). This chemical signature was interpreted as related to assimilation of continental crust by arc-setting mantle magmas generated in a subduction zone system (Fig. 8B). The predominantly negative εNd(t) values (-0.62 to −13.47) and the Nd_{TDM} ranging between 2500 and 1740 Ma demonstrate the assimilation of older continental crust. The acidic metavolcanic rocks show a similar REE pattern when compared to the andesitic and basaltic metavolcanic rocks. These features suggest poor crustal assimilation and strong influence of metasomatic processes related to the fluid released in an evolved subduction zone. Back-arc basalts generally show transitional composition between MORB and OIB and this trend was observed in the Kaourera Arc metabasalts. In this scenario, the development of the Fíngoè-Rufunsa arc system started at approximately between 1328 and 1100 Ma, as established by the early volcanism ages. The few published geologic data about the Cazula Group lithologies and the rock association are less indicative of the depositional setting. The U-Pb zircon data show a similar provenance pattern with a dominant age interval between 1157 and 1052 Ma and 1187–1114, and maximum depositional ages of 1084 ± 19 Ma and 1077 ± 3 Ma.

5.3. Tectonic implications

The characterization of the Zâmbué and Fíngoè Supergroups and the Cazula Group as arc-related basins reveals insights on the Irumide Orogeny and provides evidence about the origin and evolution of the SIB. Geochronologic and isotopic data from the tectonic units of SE Africa support three Proterozoic orogenic cycles: (i) Eburnean (2200–1800 Ma), (ii) Irumidian (1300–950 Ma) and Pan-African (850–500 Ma) (GTK Consortium, 2006). The immature character, the restricted zircon sources and the juvenile isotopic composition confirm the Fíngoè, Zâmbué and Cazula associations as arc-related sequences of the SIB in the NW region of Mozambique. The spatial relationship and the geochemical and isotopic characteristics of the supracrustal associations (Zâmbué, Fíngoè, Cazula, Rufunsa and Chipata) record the generation of magmatic arcs in the convergent tectonic setting during the Mesoproterozoic (Fig. 12A, B, C). The occurrence of these units in the northern portion of the Zimbabwe Craton supports the continuity of a subduction zone situated to the SW proposed by Jacobs et al. (2008) (Fig. 12D).

The Archean-Paleoproterozoic basement of the SIB was interpreted as an exotic cratonic fragment with respect to the adjacent Zimbabwe and Central African Craton (Angola-Kasai, Tanzania, and Bangweulu cratons) (Andreoli, 1984; Sarafian et al., 2018). However, the SIB basement orthogneisses show a strong chronological affinity with the Eburnean cycle belts that surround these cratons (Fig. 11). Goscombe et al. (2000) proposed that the SIB basement composes an extension of the Magondi Belt to the north of the Zimbabwe Craton. This belt records accretionary and collisional events of the Magondi Orogeny between 2100 and 1900 Ma. Furthermore, the evolution of this belt is like the Usagaran and Ubendian belts, located between the Tanzania and Bangweulu cratons. These orogenic belts record synchronous collisional events at ~ 2000 Ma. Similar orthogneisses were described as basement inliers by Alessio et al. (2019b), within supracrustal complexes in the southeast of Zambia.

The Mesoproterozoic belts of SE Africa present evidence of the breakup and dispersal of Columbia Supercontinent. Early Ectasian detrital zircon grains were found in the grt-bt-qtz schist from the Cazula Group, as well as in the Irumide and Kibaran belts and in the Choma-Kalomo Block. The oldest Mesoproterozoic age of the SIB is from a plagiogranite dyke of 1393 ± 22 Ma intruded in the Chewore Ophiolite of Rufunsa region, NW Zimbabwe (Fig. 2) (Oliver et al., 1998; Johnson and Oliver, 2004). The subordinate Ectasian magmatism was thought to record a protracted period of development and accretion of continental and island arcs at the southern margin of the Bangweulu Craton (Johnson and Oliver, 2004; Johnson et al., 2006, 2007; Westerhof et al., 2008a). In a regional context, the Late Calymmian to Early Ectasian events are commonly related to the Kibaran/Irumidian orogeny and linked to the global Grenville orogeny (e.g. Hanson et al., 2003; Kokonyangi et al., 2004). However, they occurred approximately 300 Ma before the Rodinia assembly and are indicative of extensional processes. We refer to "Kibaran events'' for the anorogenic, alkaline magmatism in the Usagaran Belt (Tanzania) (~1360 Ma, Vrana et al., 2003; ~1430–1400 Ma, Thomas et al., 2016, 2019), the oceanic crust formation in the Rufunsa region of the SIB (~1400 Ma; Oliver et al., 1998), the rift and passive margin sequences of the Democratic Republic of Congo and Burundi (~1420–1370 Ma, Kokonyangi et al., 2006, 2007; Fernandez-Alonso et al., 2012), and the mafic–ultramafic bimodal magmatism in the Kibaran Belt and the Choma-Kalomo Block in Zambia (~1370 Ma; Kokonyangi et al., 2004; Maier et al., 2007, 2008; Tack et al., 2010; Glynn et al., 2017). The regional extensional magmatism are related to the Columbia breakup and establish the minimum age for the formation of ocean basins at ca. 1400 Ma (Chaves, 2021).

In the SIB, the Chewore Ophiolite establishes the age of the ocean crust formation and hence the minimum depositional age for the passive margin sediments. Close to NW Mozambique border, detrital zircon from basement quartzites and metapelites from the Rufunsa and Chipata regions in SE Zambia showed sources with ages between 3400 Ma and 1700 Ma (Alessio et al. 2019a, 2019b). These samples are associated with basement inliers and compose passive margin sediments of the Irumide Orogeny. Their provenance patterns mimic those of the Muva Supergroup of the Irumide Belt in northern Zambia (Fig. 11), leading the authors to suggest a link between the SIB and the Irumide Belt in the Mesoproterozoic. Compared with our detrital zircon data, these samples do not represent arc sequences like Fíngoè and Cazula. The plate convergence and onset of subduction triggered the accretionary phase of the Irumide Orogeny in the SIB around ~ 1328 Ma (GTK Consortium, 2006).

The SIB records little magmatic activity during the Ectasian (1400–1200 Ma) and increases the magmatism from approximately 1200 Ma (Fig. 13). Compared to other regions of the SIB, the Tete and Fíngoè regions present older syn- and late-orogenic intrusive suites and a wider interval of magmatism between ca. 1201–1080 and 1060–1040 Ma. Detrital zircon signatures from the Zâmbué and Fíngoè Supergroups and Cazula Group provide evidence of the accretionary phase of Irumide Orogeny. The provenance data show that most of the older arc magmatic rocks were reworked or eroded and deposited in arc-related basins. The small difference between the crystallization age (CA) and the depositional age (DA) of the detrital zircon spectra support the hypothesis of sedimentary sequences associated with volcanic arcs generated in convergent tectonic settings associated with an orogenic belt (Fig. 12B) (Cawood et al. 2012). The geochemical and the isotopic juvenile character of the metavolcanic rocks also confirm the formation of the NE-SW arc-related basin systems, including the metavolcano-sedimentary sequences of the Fíngoè, Cazula and Chidzolomondo in the Tete Province and the Rufunsa and Chipata in Zambia.

The stratigraphic relationships concepts were developed based on preserved primary structures observed in outcrops, regional sections, and thin section microscopy data. In most of the area, the rock units were deformed and dismembered due to the shortening and thickening associated to the collisional processes of the Irumide Orogeny. The volcanic and sedimentary rocks associated with the arc magmatism, as well as the *syn*-orogenic granitic suites, were generated in the active convergent setting associated to subduction zones (Johnson et al., 2006, 2007; Westerhof et al., 2008a). The synchronicity of events throughout

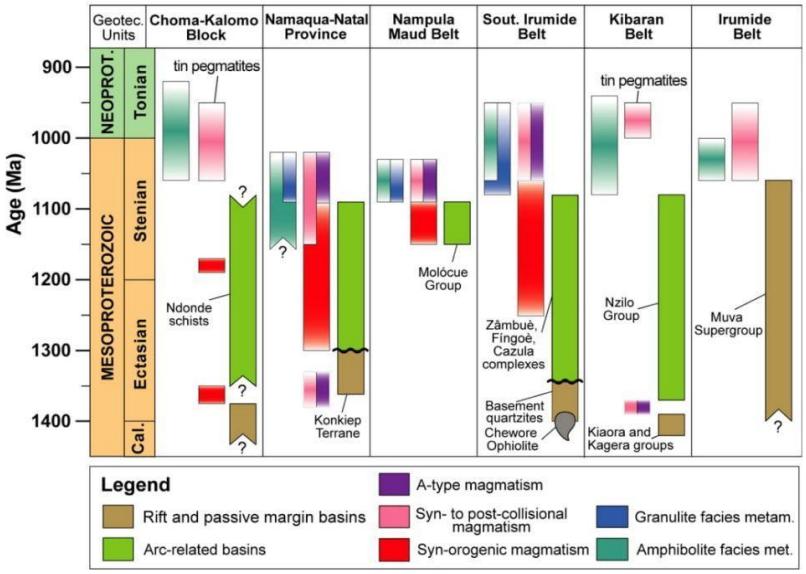

Fig. 13. Comparative evolution scheme of the main tectonic, magmatic and metamorphic events associated to evolution of the Mesoproterozoic belts of the southern and central portion of Africa. Legend: CKB- Choma-Kalomo Block, NNP- Namaqua-Natal Province, NMB- Nampula-Maud Belt, IB- Irumide Belt, KB- Kibaran Belt, SIB- Southern Irumide Belt. Data from: (1) Glynn et al. (2017); (2) Eglinton et al. (2006); (3) McCourt et al. (2006); (4) Cornell et al. (2015); (5) Mendonidis and Thomas (2019); (6) Bisnath et al. (2006); (7) Macey et al. (2010); (8) Macey et al (2013); (9) Johnson et al. (2006); (10) Westerhof et al. (2008a, 2008b); (11) Bingen et al. (2009); (12) Kokonyangi et al. (2007); (13) Fernandez-Alonso et al. (2012); (14) De Waele et al. (2009).

the SIB suggests a common tectonic evolution between approximately 1250–1080 Ma. The detrital zircon data from the analyzed samples of the SIB supracrustal associations set the maximum depositional ages from 1110 to 1080 Ma, slightly earlier to the continental collision metamorphism of the Irumide Orogeny.

The Zumbo and Fíngoè regions, and the SE portion of Zambia, comprise a wide Mesoproterozoic crustal area constituted by concordant belts of metamorphic supracrustal complexes, with different lithodemic assemblages and orogenic granitic belts. These units record the northern margin of the Zimbabwe Craton and the Fíngoè magmatic arc.

The SIB composes the network of Ectasian-Stenian orogenic belts that surround the central and southern of Africa cratons and were formed during the Rodinia assembly (Hanson, 2003), such as the Namaqua-Natal and Nampula-Maud belts (Bisnath et al., 2006; Eglinton, 2006; McCourt et al., 2006; Jacobs et al., 2008; Macey et al., 2010, Barham et al. 2022) (Fig. 12D). The tectonic evolution of these active continental margin and island arc terranes is broadly coeval (Fig. 13). Both the SIB and Namaqua-Natal belts record a complete Wilson Cycle (Cornell et al., 2015), with rifting and formation of oceanic basins between ~ 1400–1250 Ma, oceanic crust subduction and accretionary *syn*-orogenic magmatism between ~ 1250–1080 Ma, and late- to post-collisional magmatism around ~ 1060–950 Ma. The evolution of these orogenic belts as intra-oceanic and continental arcs was very similar, with few differences in the time span of the subduction and accretionary processes.

6. Conclusions

The Zâmbué and Fíngoè Supergroups and the Cazula Group show a dominance and a well-defined young age modes of the spectra of zircon U-Pb provenance, characteristics of convergent tectonic settings and associated with arc magmatism of the orogenic belts. The dominantly Stenian ages (1.20–1.08 Ga) indicate that the SIB arc magmatism was the main source of the detrital zircon. The dominantly positive εHf(t) values and the T^{2}_{DM} ages support a restricted contamination of the mantle magmas by variable amounts of older continental crust, a characteristic observed in active continental margin arcs or in intra-oceanic arcs close to the continent. These metavolcano-sedimentary sucessions compose the fragmented Fíngoè-Rufunsa arc basin system of the SIB.

The compositional features of the *syn*-orogenic mafic volcanic component, particularly in the Fíngoè Supergroup, set the final deposition of the arc-related basin systems around 1080 Ma. These basins were filled by sediments derived from the erosion of volcanic and plutonic rocks of the orogenic arc of 1200–1080 Ma. The restricted zircon provenance pattern and the predominantly juvenile Hf isotopic compositions confirm the local source of sediments and a maximum depositional age of 1111 and 1080 Ma.

The zircon provenance and the Hf isotopic compositional data, integrated with the geological mapping results, supported by stratigraphic and structural data, evidence the Mesoproterozoic Wilson Cycle of the SIB. The Zâmbué, Fíngoè and Cazula supracrustal associations represent fragments of an arc-related basin systems, tectonically interlayered with the other units of the SIB. We support the Southern Irumide Belt as a Grenvillian orogenic belt accreted to the continental margin of the Zimbabwe Craton in the Stenian period.

CRediT authorship contribution statement

T.S. Petry: Conceptualization, Data curation, Formal analysis, Investigation, Methodology, Validation, Visualization, Writing – original draft, Writing – review & editing. **R.P. Philipp:** Conceptualization, Data curation, Formal analysis, Investigation, Methodology, Validation, Visualization, Writing – original draft, Writing – review & editing, Funding acquisition. **D.L. Jamal:** Conceptualization, Investigation. **C. Lana:** Methodology, Data curation. **A.R. Alkmim:** Methodology, Data curation.

Declaration of Competing Interest

The authors declare that they have no known competing financial interests or personal relationships that could have appeared to influence the work reported in this paper.

Data availability

Data will be made available on request.

Acknowledgements

The authors acknowledge financial support from the Brazilian Research Council (CNPq), with PhD scholarship to T.S. Petry, productivity grant to R.P. Phillip and funding through Pró-Africa - 440126/2015-0. We appreciate the editor Wilson Teixeira and the reviewers Bruno Ribeiro and Simon P. Johnson for their constructive comments and suggestions that improved the quality of the manuscript. We appreciate the field support of the DNG and hope to keep working with our Mozambican friends Fátima Chaúque, Estevão Sumburane and Vicente Manjate. We thank the Geoscience Institute of the Universidade Federal do Rio Grande do Sul for facilities.

Appendix A. Supplementary material

Supplementary data to this article can be found online at https://doi.org/10.1016/j.precamres.2022.106860.

References

Alessio, B.L., Collins, A.S., Clark, C., Glorie, S., Siegfried, P.R., Taylor, R., 2019a. Age, origin and palaeogeography of the Southern Irumide Belt. Zambia. J. Geol. Soc. 176, 505–516. https://doi.org/10.1144/jgs2018-174.

Alessio, B.L., Collins, A.S., Siegfried, P., Glorie, S., De Waele, B., Payne, J.L., Archibald, D., 2019b. Neoproterozoic tectonic geography of the south-east Congo Craton in Zambia as deduced from the age and composition of detrital zircons. Geosci. Front. 10, 2045–2061. https://doi.org/10.1016/j.gsf.2018.07.005.

Andersen, T., Andersson, U.B., Graham, S., Åberg, G., Simonsen, S.L., 2009. Granitic magmatism by melting of juvenile continental crust: new constraints on the source of Palaeoproterozoic granitoids in Fennoscandia from Hf isotopes in zircon. J. Geol. Soc. 166, 233–247. https://doi.org/10.1144/0016-76492007-166.

Andreoli, M.A.G., 1984. Petrochemistry, tectonic evolution and metasomatic mineralisations of Mozambique belt granulites from S Malawi and Tete (Mozambique). Precambr. Res. 25, 161–186. https://doi.org/10.1016/0301-9268(84)90031-7.

Barham, M., Kirklanda, C.L., Handokob, A.D., 2022. Understanding ancient tectonic settings through detrital zircon analysis. Earth Planetary Sci. Lett. 583, 117425 https://doi.org/10.1016/j.epsl.2022.117425.

Begg, G., Griffin, W., Natapov, L., O'Reilly, S.Y., Grand, S., O'Neill, C., Hronsky, J., Djomani, Y.P., Swain, C., Deen, T., 2009. The lithospheric architecture of Africa: seismic tomography, mantle petrology, and tectonic evolution. Geosph 5, 23–50. https://doi.org/10.1130/GES00179.1.

Belousova, E.A., Griffin, W.L., O'Reilly, S.Y., Fisher, N.I., 2002. Igneous zircon: trace element composition as an indicator of source rock type. Contrib. Mineral. Petrol. 143, 602–622. https://doi.org/10.1007/s00410-002-0364-7.

Bingen, B., Jacobs, J., Viola, G., Henderson, I.H.C., Skår, Ø., Boyd, R., Thomas, R.J., Solli, A., Key, R.M., Daudi, E.X.F., 2009. Geochronology of the Precambrian crust in the Mozambique belt in NE Mozambique, and implications for Gondwana assembly. Precambr. Res. 170, 231–255. https://doi.org/10.1016/j.precamres.2009.01.005.

Bisnath, A., Frimmel, H.E., Armstrong, R.A., Board, W.S., 2006. Tectono-thermal evolution of the Maud Belt: New SHRIMP U-Pb zircon data from Gjelsvikfjella, Dronning Maud Land, East Antarctica. Precambr. Res. 150, 95–121. https://doi.org/10.1016/j.precamres.2006.06.009.

Black, L.P., Gulson, B.L., 1978. The age of the Mud Tank carbonatite, Strangways Range, Northern Territory. BMR J. Aust. Geol. Geophys. 3, 227–232.

Black, L.P., Kamo, S.L., Allen, C.M., Aleinikoff, J.N., Davis, D.W., Korsch, R.J., Foudoulis, C., 2003. TEMORA 1: A new zircon standard for Phanerozoic U-Pb geochronology. Chem. Geol. 200 (1-2), 155–170.

Bouvier, A., Vervoort, J.D., Patchett, P.J., 2008. The Lu–Hf and Sm-Nd isotopic composition of CHUR: constraints from unequilibrated chondrites and implications for the bulk composition of terrestrial planets. Earth Planet. Sci. Lett. 273, 48–57. https://doi.org/10.1016/j.epsl.2008.06.010.

Cabanis, B., Lecolle, M., 1989. Le diagramme La/10-Y/15-Nb/8: un outil pour la discrimination des series volcaniques et la mise en evidence des processus de melange et/ou de contamination crustale. C. R. Acad. Sci. Ser. II 309, 2023–2029.

Cawood, P.A., Hawkesworth, C.J., Dhuime, B., 2012. Detrital zircon record and tectonic setting. Geology 40, 875–878. https://doi.org/10.1130/G32945.1.

Celli, N.L., Lebedev, S., Schaeffer, A.J., Gaina, C., 2020. African cratonic lithosphere carved by mantle plumes. Nat. Commun. 11, 92. https://doi.org/10.1038/s41467-019-13871-2.

Chaúque, F.R., Cordani, U.G., Jamal, D.L., Onoe, A.T., 2017. The Zimbabwe Craton in Mozambique: a brief review of its geochronological pattern and its relation to the Mozambique Belt. J. Afr. Earth Sci. 129, 366–379. https://doi.org/10.1016/j.jafrearsci.2017.01.021.

Chaúque, F.R., Cordani, U.G., Jamal, D.L., 2019. Geochronological systematics for the Chimoio-Macossa frontal nappe in central Mozambique: implications for the tectonic evolution of the southern part of the Mozambique belt. J. Afr. Earth Sci. 150, 47–67. https://doi.org/10.1016/j.jafrearsci.2018.10.013.

Chaves, A.O., 2021. Columbia (Nuna) supercontinent with external subduction girdle and concentric accretionary, collisional and intracontinental orogens permeated by large igneous provinces and rifts. Precambr. Res. 352, 106017 https://doi.org/10.1016/j.precamres.2020.106017.

Collins, A.S., Reddy, S.M., Buchan, C., Mruma, A., 2004. Temporal constraints on Palaeoproterozoic eclogite formation and exhumation (Usagaran Orogen, Tanzania). Earth Plan. Sci. Let. 224, 175–192. https://doi.org/10.1016/j.epsl.2004.04.027.

Cornell, D.H., Van Schijndel, V., Simonsen, S.L., Frei, D., 2015. Geochronology of Mesoproterozoic hybrid intrusions in the Konkiep Terrane, Namibia, from passive to active continental margin in the Namaqua-Natal Wilson Cycle. Precambr. Res. 265, 166–188. https://doi.org/10.1016/j.precamres.2014.11.028.

Coutts, D.S., Matthews, W.A., Hubbard, S.M., 2019. Assessment of widely used methods to derive depositional ages from detrital zircon populations. Geosci. Front. 10 (4), 1421–1435.

Cox, R.A., Rivers, T., Mapani, B., Tembo, D., De Waele, B., 2002. New U–Pb data for the Irumide belt: LAM-ICP-MS results for Luangwa Terrane. Abstracts. In: 11th IAGOD Quadrennial Symposium and Geocongress Windhoek, p. 10.

Daly, M., 1986. The intracratonic Irumide belt of Zambia and its bearing on collision orogeny during the Proterozoic of Africa. Geol. Soc. London. Spec. Publ. 19, 321–328. https://doi.org/10.1144/GSL.SP.1986.019.01.18.

Dalziel, I.W.D., 1997. Neoproterozoic-Paleozoic geography and tectonics: Review, hypothesis, environmental speculation. Geol. Soc. of Am. Bull. 109, 16–42. https://doi.org/10.1130/0016-7606(1997)109%3C0016:ONPGAT%3E2.3.CO;2.

Dalziel, I.W.D., Mosher, S., Gahagan, L.M., 2000. Laurentia-Kalahari collision and the assembly of Rodinia. J. Geol. 108, 499–513. https://doi.org/10.1086/314418.

De Waele, B., Fitzsimons, I.C.W., 2007. The nature and timing of Palaeoproterozoic sedimentation at the southeastern margin of the Congo Craton; zircon U-Pb geochronology of plutonic, volcanic and clastic units in northern Zambia. Precambr. Res. 159, 95–116. https://doi.org/10.1016/j.precamres.2007.06.004.

De Waele, B., Fitzsimons, I., Wingate, M., Tembo, F., Mapani, B., Belousova, E., 2009. The geochronological framework of the Irumide Belt: a prolonged crustal history along the margin of the Bangweulu Craton. Am. J. Sci. 309, 132–187. https://doi.org/10.2475/02.2009.03.

Eglinton, B.M., 2006. Evolution of the Namaqua-Natal Belt, southern Africa – A geochronological and isotope geochemical review. J. Afr. Earth Sci. 46, 93–111. https://doi.org/10.1016/j.jafrearsci.2006.01.014.

Fernandez-Alonso, M., Cutten, H., De Waele, B., Tack, L., Tahon, A., Baudet, D., Barritt, S.D., 2012. The Mesoproterozoic Karagwe-Ankole Belt (formerly the NE Kibara Belt): The result of prolonged extensional intracratonic basin development punctuated by two short-lived far-field compressional events. Precambr. Res. 216–219, 63–86. https://doi.org/10.1016/j.precamres.2012.06.007.

Fritz, H., Abdelsalam, M., Ali, K.A., Bingen, B., Collins, A.S., Fowler, A.R., Ghebreab, W., Hauzenberger, C.A., Johnson, P.R., Kusky, T.M., Macey, P., Muhongo, S., Stern, R.J., Viola, G., 2013. Orogen styles in the East African Orogen: a review of the Neoproterozoic to Cambrian tectonic evolution. J. Afr. Earth Sci. 86, 65–106. https://doi.org/10.1016/j.jafrearsci.2013.06.004.

Gehrels, G.E., Valencia, V.A., Ruiz, J., 2008. Enhanced precision, accuracy, efficiency, and spatial resolution of U-Pb ages by laser ablation–multicollector–inductively coupled plasma–mass spectrometry. Geochem. Geophys. Geosyst. 9 (3), Q03017. https://doi.org/10.1029/2007GC001805.

Glynn, S.M., Master, S., Wiedenbeck, M., Davis, S.W., Kramers, J.D., Belyanin, G.A., Frei, D., Obertür, T., 2017. The Proterozoic Choma-Kalomo Block, SE Zambia: exotic terrane or a reworked segment of the Zimbabwe craton? Precambr. Res. 298, 421–438. https://doi.org/10.1016/j.precamres.2017.06.020.

Goolaerts, A., Mattieli, N., Jong, J., Weis, D., Scoates, J.S., 2004. Hf and Lu isotopic reference values for the zircon standard 91500 by MC-ICP-MS. Chem. Geol. 206, 1–9. https://doi.org/10.1016/j.chemgeo.2004.01.008.

Goscombe, B., Armstrong, R., Barton, J., 2000. Geology of the Chewore Inliers, Zimbabwe: constraining the mesoproterozoic to palaeozoic evolution of the Zambezi belt. J. Afr. Earth Sci. 30, 589–627. https://doi.org/10.1016/S0899-5362(00)00041-5.

Goscombe, B., Foster, D.A., Gray, D., Wade, B., 2020. Assembly of central Gondwana along the Zambezi Belt: Metamorphic response and basement reactivation during the Kuunga Orogeny. Gondwana Res. 80, 10–465. https://doi.org/10.1016/j.gr.2019.11.004.

Grantham, G.H., Ingram, B.A., Cronwright, M.C., Roberts, M.P., Macey, P.H., Manhica, V., Matola, R., Fernando, S., Cune, G., Correa, E., 2007. Explanatory notes of the 1: 250.000 geological maps of sheets Furacungo (1433) and Ulongue (1434). Unpubl. Report, National Directorate of Geology, Maputo, Mozambique, pp. 174.

Griffin, W.L., Pearson, N.J., Belousova, E., Jackson, S.E., Van Achterbergh, E., O'Reilly, S.Y., Shee, S.R., 2000. The Hf isotope composition of cratonic mantle: LAM-MC-ICPMS analysis of zircon megacrysts in kimberlites. Geochim. Cosmochim. Acta 64, 133–147. https://doi.org/10.1016/S0016-7037(99)00343-9.

GTK Consortium, 2006. Map Explanation, Volume 4, Sheets Inhamambo (1430), Maluwera (1431), Chifunde (1432), Zumbo (1530), Fíngoè-Mágoè (1531), Songo (1532), Cazula (1533) and Zóbuè (1534). Unpubl. Report, National Directorate of Geology, Maputo, Mozambique, pp. 457.

Hanson, R.E., 2003. Proterozoic geochronology and tectonic evolution of southern Africa. Geol. Soc. London Spec. Publ. 206, 427–463. https://doi.org/10.1144/GSL.SP.2003.206.01.20.

Hauzenberger, C.A., Tenczer, V., Bauernhofer, A., Fritz, H., Klötzli, U., Kosler, J., Wallbrecher, E., Muhongo, S., 2014. Termination of the Southern Irumide Belt in Tanzania: zircon U/Pb geochronology. Precambr. Res. 255, 44–162. https://doi.org/10.1016/j.precamres.2014.09.021.

Ibraimo, D.L., Larsen, R.B., 2015. Geological setting, emplacement mechanism and igneous evolution of the Atchiza mafic-ultramafic layered suite in north-west Mozambique. J. Afr. Earth Sci. 111, 421–433. https://doi.org/10.1016/j.jafrearsci.2015.07.020.

Jackson, S.E., Pearson, N.J., Griffin, W.L., Belousova, E.A., 2004. The application of laser ablation-inductively coupled plasma-mass spectrometry to in-situ U-Pb zircon geochronology. Chem. Geol. 211, 47–69. https://doi.org/10.1016/j.chemgeo.2004.06.017.

Jacobs, J., Pisarevsky, S., Thomas, R.J., Becker, T., 2008. The Kalahari Craton during the assembly and dispersal of Rodinia. Precambr. Res. 160, 142–158. https://doi.org/10.1016/j.precamres.2007.04.022.

Johnson, S.P., Oliver, G.J.H., 2004. Tectonothermal history of the Kaourera Arc, northern Zimbabwe: implications for the tectonic evolution of the Irumide and Zambezi Belts of South Central Africa. Precambr. Res. 130, 71–97. https://doi.org/10.1016/j.precamres.2003.10.016.

Johnson, S.P., Rivers, T., De Waele, B., 2005. A review of the Mesoproterozoic to early Palaeozoic magmatic and tectonothermal history of south-central Africa: implications for Rodinia and Gondwana. J. Geol. Soc. 162, 433–450. https://doi.org/10.1144/0016-764904-028.

Johnson, S.P., De Waele, B., Liyungu, A., 2006. U-Pb sensitive high-resolution ion microprobe (SHRIMP) zircon geochronology of granitoid rocks in eastern Zambia: terrane subdivision of the Mesoproterozoic Southern Irumide Belt. Tectonics 25 (6), TC6004. https://doi.org/10.1029/2006TC001977.

Johnson, S.P., De Waele, B., Tembo, F., Katongo, C., Tani, K., Chang, Q., Iizuka, T., Dunkley, D., 2007. Geochemistry, geochronology and isotopic evolution of the Chewore-Rufunsa terrane, southern Irumide belt: a Mesoproterozoic continental margin arc. J. Petrol. 48, 1411–1441. https://doi.org/10.1093/petrology/egm025.

Kokonyangi, J., Armstrong, R.A., Kampunzu, A.B., Yoshida, M., Okudaira, T., 2004. U-Pb zircon geochronology and petrology of granitoids from Mitwaba (Katanga, Congo): implications for the evolution of the Mesoproterozoic Kibaran belt. Precambr. Res. 132, 79–106. https://doi.org/10.1016/j.precamres.2004.02.007.

Kokonyangi, J., Kampunzu, A.B., Armstrong, R., Yoshida, M., Okudaira, T., Arima, M., Ngulube, D.A., 2006. The Mesoproterozoic Kibaride belt (Katanga, SE D.R. Congo). J. Afr. Earth Sci. 46, 1–35. https://doi.org/10.1016/j.jafrearsci.2006.01.017.

Kokonyangi, J., Kampunzu, A., Armstrong, R., Arima, M., Yoshida, M., Okudaira, T., 2007. U-Pb SHRIMP dating of detrital zircons from the Nzilo Group (Kibaran Belt): implications for the source of sediments and Mesoproterozoic evolution of Central Africa. J. Geol. 115, 99–113. https://doi.org/10.1086/509270.

Lawley, C.J., Selby, D., Condon, D.J., Horstwood, M., Millar, I., Crowley, Q., Imber, J., 2013. Lithogeochemistry, geochronology and geodynamic setting of the Lupa Terrane, Tanzania: implications for the extent of the Archean Tanzanian Craton. Precambr. Res. 231, 174–193. https://doi.org/10.1016/j.precamres.2013.02.012.

Li, Z.X., Bogdanova, S.V., Collins, A.S., Davidson, A., De Waele, B., Ernst, R.E., Fitzsimons, I.C.W., Fuck, R.A., Gladkochub, D.P., Jacobs, J., Karlstrom, K.E., Lu, S., Natapov, L.M., Pease, V., Pisarevsky, S.A., Thrane, K., Vernikovsky, V., 2008. Assembly, configuration, and break-up history of Rodinia: a synthesis. Precambr. Res. 160, 179–210. https://doi.org/10.1016/j.precamres.2007.04.021.

Ludwig, K.R., 2003. In: User's Manual for Isoplot 3.00. A Geochronological Toolkit for Microsoft Excel. Berkeley Geochronology Center, Special Publication, pp. 1–70.

Macey, P.H., Thomas, R.J., Grantham, G.H., Ingram, B.A., Jacobs, J., Armstrong, R.A., Roberts, M.P., Bingen, B., Hollick, L., de Kock, G.S., Viola, G., Bauer, W., Gonzales, E., Bjerkgård, T., Henderson, I.H.C., Sandstad, J.S., Cronwright, M.S., Harley, S., Solli, A., Nordgulen, Ø., Motuza, G., Daudi, E., Manhiça, V., 2010. Mesoproterozoic geology of the Nampula Block, northern Mozambique: tracing fragments of Mesoproterozoic crust in the heart of Gondwana. Precambr. Res. 182, 124–148. https://doi.org/10.1016/j.precamres.2010.07.005.

Macey, P.H., Miller, J.A., Rowe, C.D., Grantham, G.H., Siegfried, P., Armstrong, R.A., Kemp, J., Bacalau, J., 2013. Geology of the Monapo Klippe, NE Mozambique and its significance for assembly of central Gondwana. Precambr. Res. 233, 259–281. https://doi.org/10.1016/j.precamres.2013.03.012.

Maier, W.D., Peltonen, P., Livesey, T., 2007. The ages of the Kabanga North and Kapalagulu intrusions, Western Tanzania: a reconnaissance study. Econ. Geol. 102, 147–154. https://doi.org/10.2113/gsecongeo.102.1.147.

Mäkitie, H., Lehtonen, M.I., Manninen, T., Marques, J.M., Cune, G., Mavie, H., 2008. Petrography and geochemistry of granitoid rocks in the northern part of Tete Province, Mozambique. Geol. Surv. Finl. Spec. Paper 48, 167–189.

Manda, B.W.C., Cawood, P.A., Spencer, C.J., Prave, T., Robinson, R., Roberts, N.M.W., 2019. Evolution of the Mozambique Belt in Malawi constrained by granitoid U-Pb, Sm-Nd and Lu-Hf isotopic data. Gondwana Res. 68, 93–107. https://doi.org/10.1016/j.gr.2018.11.004.

Mänttäri, I., 2008. Mesoarchean to lower Jurassic U-Pb and Sm-Nd ages from NW Mozambique. Geol. Surv. Finl. Spec. Paper 48, 81–119.

Marschall, H.R., Hawkesworth, C.J., Leat, P.T., 2013. Mesoproterozoic subduction under the eastern edge of the Kalahari-Grunehogna Craton preceding Rodinia assembly: the Ritscherflya detrital zircon record, Ahlmannryggen (Dronning Maud Land, Antarctica). Precambrian Res. 236, 31–45. https://doi.org/10.1016/j.precamres.2013.07.006.

McCourt, S., Hilliard, P., Armstrong, R.A., Munyanyiwa, H., 2001. SHRIMP U-Pb zircon geochronology of the Hurungwe granite northwest Zimbabwe: Age constraints on the timing of the Magondi orogeny and implications for the correlation between the Kheis and Magondi Belts. S. Afr. Jour. Geol. 104, 39–46. https://doi.org/10.2113/104.1.39.

McCourt, S., Armstrong, R.A., Grantham, G.H., Thomas, R.J., 2006. Geology and evolution of the Natal belt, South Africa. J. Afr. Earth Sci. 46, 71–92. https://doi.org/10.1016/j.jafrearsci.2006.01.013.

Meert, J.G., 2002. A synopsis of events related to the assembly of eastern Gondwana. Tectonophysics 362, 1–40. https://doi.org/10.1016/S0040-1951(02)00629-7.

Mendonidis, P., Thomas, R.J., 2019. A review of the geochronology of the Margate Terrane reveals a history of diachronous terrane docking and arc accretion across the Mesoproterozoic Natal belt, southeastern Africa. J. Afr. Earth Sci. 150, 532–545. https://doi.org/10.1016/j.jafrearsci.2018.07.021.

Oliver, G., Johnson, S., Williams, I., Herd, D., 1998. Relict 1.4 Ga oceanic crust in the Zambezi Valley, northern Zimbabwe: evidence for Mesoproterozoic supercontinental fragmentation. Geology. 26, 571–573. https://doi.org/10.1130/0091-7613(1998)026%3C0571:RGOCIT%3E2.3.CO;2.

Rainaud, C., Master, S., Armstrong, R.A., Robb, L.J., 2003. A cryptic Mesoarchean terrane in the basement to the central African Copperbelt. J. Geol. Soc. Lond. 160, 11–14. https://doi.org/10.1144/0016-764902-087.

Rainaud, C., Master, S., Armstrong, R.A., Robb, L.J., 2005. Geochronology and nature of the Palaeoproterozoic basement in the Central African Copperbelt (Zambia and the Democratic Republic of Congo), with regional implications. J. Afr. Earth Sci. 42, 1–31. https://doi.org/10.1016/j.jafrearsci.2005.08.006.

Reimann, C.R., Bahlburg, H., Kooijman, E., Berndt, J., Gerdes, A., Carlotto, V., Lopez, S., 2010. Geodynamic evolution of the early Paleozoic Western Gondwana margin 14–17S reflected by the detritus of the Devonian and Ordovician basins of southern Peru and northern Bolivia. Gondwana Res. 18, 370–384. https://doi.org/10.1016/j.gr.2010.02.002.

Sarafian, E., Evans, R.L., Abdelsalam, M.G., Atekwana, E., Elsenbeck, J., Jones, A.G., Chikambwe, E., 2018. Imaging Precambrian lithospheric structure in Zambia using electromagnetic methods. Gondwana Res. 54, 38–49. https://doi.org/10.1016/j.gr.2017.09.007.

Sláma, J., Košler, J., Condon, D.J., Crowley, J.L., Gerdes, A., Hanchar, J.M., Horstwood, M.S.A., Morris, G.A., Nasdala, L., Norberg, N., Schaltegger, U., Schoene, B., Tubrett, M.N., Whitehouse, M.J., 2008. Plešovice zircon- a new natural reference material for U-Pb and Hf isotopic microanalysis. Chem. Geol. 249 (1-2), 1–35.

Söderlund, U., Patchett, P.J., Vervoort, J.D., Isachsen, C.E., 2004. The ^{176}Lu decay constant determined by Lu–Hf and U-Pb isotope systematics of Precambrian mafic intrusions. Earth Planet. Sci. Lett. 219, 311–324. https://doi.org/10.1016/S0012-821X(04)00012-3.

Spencer, C.J., Kirkland, C.L., Taylor, R.J.M., 2016. Strategies towards statistically robust interpretations of in situ U-Pb zircon geochronology. Geosci. Front. 7, 581–589. https://doi.org/10.1016/j.gsf.2015.11.006.

Sumburane, E.I., 2011. Evolução crustal dos terrenos granito-greenstone de Manica, região centro-oeste de Moçambique. University of São Paulo, p. 331. Unpubl. PhD Thesis.

Tack, L., Wingate, M.T.D., De Waele, B., Meert, J., Belousova, E., Griffin, B., Tahon, A., Fernandez-Alonso, M., 2010. The 1375 Ma Kibaran event in Central Africa: prominent emplacement of bimodal magmatism under extensional regime. Precambr. Res. 180, 63–84. https://doi.org/10.1016/j.precamres.2010.02.022.

Thomas, R.J., Roberts, N.M.W., Jacobs, J., Bushi, A.M., Horstwood, M.S.A., Mruma, A., 2013. Structural and geochronological constraints on the evolution of the eastern margin of the Tanzania Craton in the Mpwapwa area, central Tanzania. Precam. Res. 224, 671–689. https://doi.org/10.1016/j.precamres.2012.11.010.

Thomas, R.J., Spencer, C., Bushi, A.M., Baglow, N., Boniface, N., de Kock, G.S., Horstwood, M.S.A., Hollick, L., Jacobs, J., Kajara, S., Kamihanda, G., Key, R.M., Maganga, Z., Mbawala, F., McCourt, W.J., Momburi, P., Moses, F., Mruma, A., Myambilwa, Y., Roberts, N.M.W., Saidi, H., Nyanda, P., Nyoka, K., Millar, I., 2016. Geochronology of the central Tanzania Craton and its southern and eastern orogenic margins. Precambr. Res. 277, 47–67. https://doi.org/10.1016/j.precamres.2016.02.008.

Thomas, R.J., Jacobs, J., Elburg, M.A., Mruma, A., Kamihanda, G., Kankila, A., Masanja, A., Saidi, H., 2019. New U-Pb-Hf zircon isotope data for the Paleoproterozoic Ubendian belt in the Chimala area. SW Tanzania. Geosci. Front. 10 (6), 1993–2006. https://doi.org/10.1016/j.gsf.2018.05.010.

Van Achterberg, E., Ryan, C., Jackson, S., Griffin, W., 2001. Data reduction software for LA-ICP-MS. In: Sylvester, P. (Ed.), Laser Ablation ICP-MS in the Earth Science – Principles and Applications. Mineralogical Association of Canada, Newfoundland, pp. 239–243.

Vermeesch, P., 2018. IsoplotR: A free and open toolbox for geochronology. Geosci. Front. 9, 1479–1493. https://doi.org/10.1016/j.gsf.2018.04.001.

Vermeesch, P., 2021. Maximum depositional age estimation revisited. Geosci. Front. 12, 843–850. https://doi.org/10.1016/j.gsf.2020.08.008.

Westerhof, A.P., Lehtonen, M.I., Mäkitie, H., Manninen, T., Pekkala, Y., Gustafsson, B., Tahon, A., 2008a. The Tete-Chipata Belt: a new multiple terrane element from western Mozambique and southern Zambia. Geol. Surv. Finl. Spec. Paper 48, 145–166.

Westerhof, A.P., Tahon, A., Koistinen, T., Lehto, T., Akerman, C., 2008b. Igneous and tectonic setting of the allochtonous Tete Gabro-Anorthosite Suite, Mozambique. Geol. Surv. Finl. Spec. Paper 48, 191–210.

Woodhead, J.D., Hergt, J.M., 2005. A Preliminary appraisal of seven natural zircon reference materials for in situ Hf isotope determination. Geostand. Geoanal. Res. 29, 183–195. https://doi.org/10.1111/j.1751-908X.2005.tb00891.x.

Wu, F.-Y., Yang, Y.-H., Xie, L.-W., Yang, J.-H., Xu, P., 2006. Hf isotopic compositions of the standard zircons and baddeleyites used in U-Pb geochronology. Chem. Geol. 234, 105–126. https://doi.org/10.1016/j.chemgeo.2006.05.003.

Further reading

Anhaeusser, C., 2014. Archaean greenstone belts and associated granitic rocks – A review. J. Afr. Earth Sci. 100, 684–732. https://doi.org/10.1016/j.jafrearsci.2014.07.019.

Brown, M., 2007. Metamorphic Conditions in Orogenic Belts: a Record of Secular Change. Int. Geol. Rev. 49, 193–234. https://doi.org/10.2747/0020-6814.49.3.193.

Bulambo, M., de Waele, B., Kampunzu, A.B., Tembo, F., 2004. SHRIMP U-Pb geochronology of the Choma-Kalomo block (Zambia) and geological implications. Abstracts volume, 20th Colloquium of African Geology, Orléans, France.

Collins, W.J., 2002. Hot orogens, tectonic switching, and creation of continental crust. Geology 30, 535–538. https://doi.org/10.1130/0091-7613(2002)030%3C0535:HOTSAC%3E2.0.CO;2.

De Waele, B., Liegeois, J.P., Nemchin, A.A., Tembo, F., 2006. Isotopic and geochemical evidence of Proterozoic episodic crustal reworking within the Irumide Belt of south central Africa, the southern metacratonic boundary of an Archaean Bangweulu Craton. Precambr. Res. 148, 225–256. https://doi.org/10.1016/j.precamres.2006.05.006.

Dickinson, W.R., Gehrels, G.E., 2009. Use of U-Pb ages of detrital zircons to infer maximum depositional ages of strata: a test against a Colorado Plateau Mesozoic database. Earth Plan. Sci. Let. 288, 115–125. https://doi.org/10.1016/j.epsl.2009.09.013.

Dröllner, M., Barham, M., Kirkland, C.L., Ware, B., 2021. Every zircon deserves a date: selection bias in detrital geochronology. Geol. Mag. 158 (6), 1135–1142.

Faccenda, M., Minelli, G., Gerya, T.V., 2009. Coupled and decoupled regimes of continental collision: numerical modeling. Earth Plan. Sci. Let. 278, 337–349. https://doi.org/10.1016/j.epsl.2008.12.021.

Göğüş, O.H., Ueda, K., 2018. Peeling back the lithosphere: Controlling parameters, surface expressions and the future directions in delamination modeling. J. Geodyn. 117, 21–40. https://doi.org/10.1016/j.jog.2018.03.003.

Goscombe, B., Armstrong, R., Barton, J.M., 1998. Tectonometamorphic evolution of the Chewore Inliers: Partial re-equilibration of high-grade basement during the Pan-African Orogeny. J. Petrol. 39 (7), 1347–1384. https://doi.org/10.1093/petroj/39.7.1347.

Hanson, R.E., Wilson, T.J., Brueckner, H.K., Onstott, T.C., Wardlaw, M.S., Johns, C.C., Hardcastle, K.C., 1988. Reconnaissance geochronology, tectonothermal evolution, and regional significance of the middle Proterozoic Choma-Kalomo Block, Southern Zambia. Precambr. Res. 42, 39–61. https://doi.org/10.1016/0301-9268(88)90009-5.

Hawkesworth, C.J., Dhuime, B., Pietranik, A.B., Cawood, P.A., Kemp, A.I.S., Storey, C.D., 2010. The generation and evolution of the continental crust. J. Geol. Soc. 167, 229–248. https://doi.org/10.1144/0016-76492009-072.

Hunting Geology and Geophysics Limited, 1984. Mineral Inventory Project. Unpubl. Rept., National Directorate of Geology, Maputo, Mozambique, pp. 329.

Karmakar, S., Schenk, V., 2016. Mesoproterozoic UHT metamorphism in the southern irumide belt, Chipata, Zambia: petrology and in situ monazite dating. Precambr. Res. 275, 332–356. https://doi.org/10.1016/j.precamres.2016.01.018.

Katongo, C., Koller, F., Kloetzli, U., Koeberl, C., Tembo, F., De Waele, B., 2004. Petrography, geochemistry, and geochronology of granitoid rocks in the Neoproterozoic-Paleozoic Lufilian-Zambezi belt, Zambia: Implications for tectonic setting and regional correlation. J. Afr. Earth Sci. 40, 219–244. https://doi.org/10.1016/j.jafrearsci.2004.12.007.

Kroner, A., Willner, A.P., Hegner, E., Jaeckel, P., Nemchin, A., 2001. Single zircon ages, PT evolution and Nd isotopic systematics of high-grade gneisses in southern Malawi and their bearing on the evolution of the Mozambique belt in southeastern Africa. Precambr. Res. 109, 257–291. https://doi.org/10.1016/S0301-9268(01)00150-4.

McFarlane, H.B., Thébauld, N., Parra-Avila, L.A., Armit, R., Spencer, C., Ganne, J., Aillères, L., Baratoux, L., Betts, P.G., Jessel, M.W., 2019. Onset of the supercontinent cycle: evidence for multiple oceanic arc accretion events in the Paleoproterozoic Sefwi Greenstone Belt of the West African Craton. Precambr. Res. 335, 105450 https://doi.org/10.1016/j.precamres.2019.105450.

Mtabazi, E.G., Boniface, N., Andresen, A., 2019. Geochronological characterization of a transition zone between the Mozambique Belt and Unango-Marrupa Complex in SE Tanzania. Precambr. Res. 321, 134–153. https://doi.org/10.1016/j.precamres.2018.11.017.

Pinna, P., Jourde, G., Calvez, J.Y., Mroz, J.P., Marques, J.M., 1993. The Mozambique Belt in northern Mozambique: Neoproterozoic (1100–850 Ma) crustal growth and tectogenesis, and superimposed Pan-African (800–550 Ma) tectonism. Precambr. Res. 62, 1–59. https://doi.org/10.1016/0301-9268(93)90093-H.

Puetz, S.J., Spencer, C.J., Ganade, C.E., 2021. Analyses from a validated global U-Pb detrital zircon database: Enhanced methods for filtering discordant U–Pb zircon analyses and optimizing crystallization age estimates. Earth-Sci. Rev. 220, 103745 https://doi.org/10.1016/j.earscirev.2021.103745.

Ueda, K., Gerya, T.V., Burg, J.-P., 2012. Delamination in collisional orogens: thermomechanical modeling. J. Geoph. Res. Solid Earth 117 (B8), n/a–n/a.

Vrána, S., Kachlík, V., Kröner, A., Marheine, D., Seifert, A.V., Zacek, V., Baburek, J., 2004. Ubendian basement and its late Mesoproterozoic and early Neoproterozoic structural and metamorphic overprint in northeastern Zambia. J. Afr. Earth Sci. 38, 1–21. https://doi.org/10.1016/j.jafrearsci.2003.09.001.

Whitney, D.L., Evans, B.W., 2010. Abbreviations for names of rock-forming minerals. Am. Mineral. 95 (1), 185–187. https://doi.org/10.2138/am.2010.3371.

6.2. ***The timing of Irumide Orogeny collisional events constrained by U-Pb-Hf zircon data from granulites and charnockites of the Southern Irumide Belt, NW Mozambique.***

Submetido a revista Precambrian Research.

Gmail

Thales Petry <thalesspetry@gmail.com>

PRECAM-D-23-00043 - Confirming your submission to Precambrian Research

1 mensagem

Precambrian Research <em@editorialmanager.com> 1 de fevereiro de 2023 às 02:21
Responder a: Precambrian Research <support@elsevier.com>
Para: Thales Sebben Petry <thalesspetry@gmail.com>

ELSEVIER

This is an automated message.

The timing of Irumide Orogeny collisional events constrained by U-Pb-Hf zircon data from granulites and charnockites of the Southern Irumide Belt, NW Mozambique.

Dear Mr Petry,

We have received the above referenced manuscript you submitted to Precambrian Research. It has been assigned the following manuscript number: PRECAM-D-23-00043.

To track the status of your manuscript, please log in as an author at https://www.editorialmanager.com/precam/, and navigate to the "Submissions Being Processed" folder.

Thank you for submitting your work to this journal.

Kind regards,
Precambrian Research

More information and support

You will find information relevant for you as an author on Elsevier's Author Hub: https://www.elsevier.com/authors

FAQ: How can I reset a forgotten password?
https://service.elsevier.com/app/answers/detail/a_id/28452/supporthub/publishing/kw/editorial+manager/

For further assistance, please visit our customer service site: https://service.elsevier.com/app/home/supporthub/publishing/. Here you can search for solutions on a range of topics, find answers to frequently asked questions, and learn more about Editorial Manager via interactive tutorials. You can also talk 24/7 to our customer support team by phone and 24/7 by live chat and email.

This journal uses the Elsevier Article Transfer Service. This means that if an editor feels your manuscript is more suitable for an alternative journal, then you might be asked to consider transferring the manuscript to such a journal. The recommendation might be provided by a Journal Editor, a dedicated Scientific Managing Editor, a tool assisted recommendation, or a combination. For more details see the journal guide for authors.

#AU_PRECAM#

To ensure this email reaches the intended recipient, please do not delete the above code

ELSEVIER

RELX™

Precambrian Research

The timing of Irumide Orogeny collisional events constrained by U-Pb-Hf zircon data from granulites and charnockites of the Southern Irumide Belt, NW Mozambique.

--Manuscript Draft--

Manuscript Number:	
Article Type:	Research Paper
Keywords:	Rodinia assembly; Irumide Orogeny; continental collision; high-temperature metamorphism; charnockitic magmatism
Corresponding Author:	Thales Sebben Petry, Msc BRAZIL
First Author:	Thales Sebben Petry, Msc
Order of Authors:	Thales Sebben Petry, Msc
	Petry
	T.S.1*
	Philipp
	R.P.1
	Cabrita
	D.I.G.2
	Jamal
	D.L.3
	Rômulo Machado
	Cristiano Lana
Abstract:	To define and characterize the tectonic evolution of an orogenic belt, it required a wide database including types and compositions of the magmatism, settings of sedimentation and metamorphic conditions, supported by precise geochronological and isotopic data. In the Mesoproterozoic Southern Irumide Belt of the Tete Province, NW Mozambique, the high-grade gneisses from the Chidzolomondo Complex, provide constraints about the transition from accretionary to collisional stage of the Irumide Orogeny. The granulitic complex comprises a volcano-sedimentary succession intruded by syn-orogenic granitoids, metagabbros and charnockitic gneisses. Detrital zircon from a pelitic gneiss showed ages between 1344-1098 Ma and minor Paleoproterozoic and Archean contributions. The maximum depositional age was established at 1121 ± 2 Ma. The variable εHf(t) values (-10 to +7) and the TDM2 ages ranging 1.41-2.44 Ga indicated source areas with juvenile to evolved signatures. The crystallization age of a metagabbro (1133 ± 15 Ma) and a charnockitic gneiss (1097 ± 3 Ma) represent the syn-orogenic magmatism. The positive εHf(t) values (+1.5 to +4.5) indicate a juvenile signature, and the TDM2 ages ranging between 1.6-1.8 Ga support the limited contribution of continental crust for the magmatism. Phase equilibria modeling indicates that the granulite facies conditions were reached between 785–795 °C and 3.7–4.2 kbar. Dating of zircon overgrowths from the high-grade gneisses characterizes three distinct metamorphic events. The M1 event at 1092 ±5 Ma was identified in the pelitic gneiss and is coeval to the syn-orogenic magmatism. The M2 event was identified in all samples and is thought to record the peak of the collisional metamorphism at ca. 1060 Ma. The M3 event at 1023 ±12 Ma records the contact metamorphism identified in the metagabbro sample near a charnockite intrusion. A charnockite and a gabbro record the post-collisional magmatism with ages of 1026±4 Ma and 1026±12 Ma. The results allowed to establish the timing of the last events of the Irumide Orogeny: (i) maximum depositional age of the Chidzolomondo Complex and correlated arc-related basins at 1120 Ma; (ii) syn-orogenic magmatism until ca. 1080 Ma; (iii) peak-collisional metamorphism at ca. 1060 Ma; (iv) post-collisional magmatism between 1050-1000 Ma.

Suggested Reviewers:	Simon Paul Johnson simonpaul.johnson@dmp.wa.gov.au
	Ben Goscombe ben.goscombe@gmail.com
	Bruno Ribeiro bruno.vieiraribeiro@curtin.edu.au
	Bernard Bingen bernard.bingen@ngu.no
	Bert De Waele bdewaele@srk.com.au

January 31, 2022

Dear Editor(s)

We submit the manuscript entitled "**THE TIMING OF IRUMIDE OROGENY COLLISIONAL EVENTS CONSTRAINED BY U-PB-HF ZIRCON DATA FROM GRANULITES AND CHARNOCKITES OF THE SOUTHERN IRUMIDE BELT, NW MOZAMBIQUE**" by Thales Sebben Petry, Ruy Paulo Philipp, Dina Cabrita Daud Liace Jamal, Cristiano Lana, Romulo Machado. We would like to have it considered for publication in the journal *Precambrian Research.*

This article is suitable for *Precambrian Research* because it involves advances for understanding the Precambrian evolution of the Southern Irumide Belt (SIB). The SIB composes a Mesoproterozoic magmatic arc system located between the Zimbabwe and the Bangweulu cratons in a key area for the understanding of the regional tectonic evolution during the Rodinia assembly. A few published studies discuss their tectono-metamorphic evolution.

This paper provides substantial advances on the timing of transition from accretionary to collisional orogen in the SIB. This is the first detailed geochronological study performed in the high-grade gneisses of Chidzolomondo Complex and the post-collisional charnockitic and gabbroic magmatism of the belt. The study integrates petrological data including P-T estimations, whole rock geochemistry and U-Pb and Lu-Hf zircon data from igneous, detrital and metamorphic zircon. The obtained data allowed to set: (i) the maximum depositional age of the Chidzolomondo Complex and correlated arc-related basins at 1120 Ma; (ii) the syn-orogenic magmatism until ca. 1080 Ma; (iii) peak-collisional metamorphism at ca. 1060 Ma; (iv) post-collisional granitic and mafic magmatism between 1050-1000 Ma.

Based on detrital zircon provenance and whole-rock geochemistry we interpret the

Chidzolomondo Complex as a Mesoproterozoic arc-related basin of the SIB. The main source of sediments were the juvenile arc rocks with minor Archean and Paleoproterozoic sources. The maximum depositional age was established at 1121 ± 2 Ma. The volcano-sedimentary sequence was intruded by syn-orogenic gabbro at 1133 ± 15 Ma and charnockite at 1097 ± 3 Ma. The metamorphic zircon overgrowths evidenced the polyphasic evolution of the complex and provided evidence of three metamorphic events. The phase equilibria modeling indicated peak metamorphic conditions between 785–795 ºC and 3.7–4.2 kbar. The first metamorphic event at 1092 ± 5 Ma was coeval do the emplacement of the syn-orogenic charnockite. The second metamorphic event records the peak-collisional metamorphism at ca. 1060 Ma. The third metamorphic at 1023 ± 12 Ma records the contact metamorphism related to the emplacement of post-collisional charnockite and gabbro at 1026 ± 4 Ma and 1026 ± 12 Ma. We envision that our paper will contribute to the understanding of the final Mesoproterozoic evolution of the SIB.

We suggest the following referees (in no particular order) because they developed relevant studies about the Precambrian evolution of the Southern Irumide belt and the SE Africa units.

- PhD Simon Paul Johnson - email address: simonpaul.johnson@dmp.wa.gov.au
- PhD Ben Goscombe - email address: ben.goscombe@gmail.com
- PhD Bruno Ribeiro - email address: bruno.vieiraribeiro@curtin.edu.au
- PhD Bernard Bingen - email address: bernard.bingen@ngu.no

We greatly appreciate your consideration of this manuscript. Please do not hesitate to contact the primary author if you have any questions.

Sincerely,

Thales Sebben Petry

Thales Sebben Petry (*corresponding author)

Universidade Federal do Rio Grande do Sul

Av. Bento Gonçalves, 9500, Porto Alegre, 91500-000, RS, Brazil

thalesspetry@gmail.com

+55 51 998641539

Ruy Paulo Philipp

Universidade Federal do Rio Grande do Sul

Dina Cabrita

Universidade de São Paulo

Daud Liace Jamal

Universidade Eduardo Mondlane

Cristiano de Carvalho Lana

Universidade Federal de Ouro Preto

Romulo Machado

Universidade de São Paulo

- U-Pb and Lu-Hf zircon data from granulite of Chidzolomondo Complex.
- Provenance spectra and Hf signatures indicate deposition in arc-related basin.
- Polyphasic metamorphic evolution recording transition from accretionary to collisional orogen.
- Post-collisional metamorphism due to charnockite intrusion.

The timing of Irumide Orogeny collisional events constrained by U-Pb-Hf zircon data from granulites and charnockites of the Southern Irumide Belt, NW Mozambique.

Petry, T.S.[1*], Philipp, R.P.[1], Cabrita, D.I.G.[2], Jamal, D.L.[3], Machado, R.[2], Lana, C.[3]

[1] Programa de Pós-Graduação em Geociências, Instituto de Geociências, Universidade Federal do Rio Grande do Sul, Av. Bento Gonçalves, 9500, Porto Alegre, 91500-000, RS, Brazil
[2] Instituto de Geociências, Universidade de São Paulo, Rua do Lago 562, CEP 05508-080, São Paulo, SP, Brazil
[3] Departamento de Geologia, Universidade Eduardo Mondlane, Av. Moçambique km 1.5, Caixa Postal 257, Maputo, Mozambique.
[4] Departamento de Geologia, Universidade Federal de Ouro Preto (UFOP), Morro do Cruzeiro, Ouro Preto, Minas Gerais, 35400-000, Brazil
*Corresponding author, E-mail: thalesspetry@gmail.com

Abstract

To define and characterize the tectonic evolution of an orogenic belt, it required a wide database including types and compositions of the magmatism, settings of sedimentation and metamorphic conditions, supported by precise geochronological and isotopic data. In the Mesoproterozoic Southern Irumide Belt of the Tete Province, NW Mozambique, the high-grade gneisses from the Chidzolomondo Complex, provide constraints about the transition from accretionary to collisional stage of the Irumide Orogeny. The granulitic complex comprises a volcano-sedimentary succession intruded by syn-orogenic granitoids, metagabbros and charnockitic gneisses. Detrital zircon from a pelitic gneiss showed ages between 1344-1098 Ma and minor Paleoproterozoic and Archean contributions. The maximum depositional age was established at 1121 ± 2 Ma. The variable εHf(t) values (-10 to +7) and the T_{DM}^2 ages ranging 1.41-2.44 Ga indicated source areas with juvenile to evolved signatures. The crystallization age of a metagabbro (1133 ± 15 Ma) and a charnockitic gneiss (1097 ± 3 Ma) represent the syn-orogenic magmatism. The positive εHf(t) values (+1.5 to +4.5) indicate a juvenile signature, and the T_{DM}^2 ages ranging between 1.6-1.8 Ga support the limited contribution of continental crust for the magmatism. Phase

equilibria modeling indicates that the granulite facies conditions were reached between 785–795 ºC and 3.7–4.2 kbar. Dating of zircon overgrowths from the high-grade gneisses characterizes three distinct metamorphic events. The M_1 event at 1092 ±5 Ma was identified in the pelitic gneiss and is coeval to the syn-orogenic magmatism. The M_2 event was identified in all samples and is thought to record the peak of the collisional metamorphism at ca. 1060 Ma. The M_3 event at 1023 ±12 Ma records the contact metamorphism identified in the metagabbro sample near a charnockite intrusion. A charnockite and a gabbro record the post-collisional magmatism with ages of 1026±4 Ma and 1026±12 Ma. The results allowed to establish the timing of the last events of the Irumide Orogeny: (i) maximum depositional age of the Chidzolomondo Complex and correlated arc-related basins at 1120 Ma; (ii) syn-orogenic magmatism until ca. 1080 Ma; (iii) peak-collisional metamorphism at ca. 1060 Ma; (iv) post-collisional magmatism between 1050-1000 Ma.

Keywords: Rodinia assembly, Irumide Orogeny, continental collision, high-temperature metamorphism, charnockitic magmatism.

1. Introduction

The high-grade metamorphic rocks provide constraints of the geodynamic evolution of accretionary and collisional orogens (Harley, 1998; Brown, 2007, 2009; Brown and Johnson, 2018, 2019a,b; Kelsey, 2015). The U-Pb geochronology of metamorphic zircon and monazite to P-T points or path segments promoted great improvement in the metamorphic petrology and in the geodynamic modeling studies (Harley et al. 2007; Kelsey et al. 2015). Most of the geodynamic models suggest that regional high temperature and UHT metamorphism is, principally, related to subduction, coupled with elevated crustal radiogenic heat generation rates or associated to deep portions of collisional belts (Harley et al. 2007, 2008; Kelsey et al. 2015;). In association with the stratigraphic and structural data, the time relations between the orogenic metamorphism and the generation of the granitic magmatism provides the necessary

elements to define an accretionary-, collisional- or intracontinental-type orogen (Cawood et al. 2022).

The Southern Irumide Belt (SIB) records the transition of the Grenvillian Cycle in the SE Africa. The SIB is located between the Zimbabwe and the Bangweulu cratons and record the ocean closure and continental collision between these plates during Rodinia assembly. The initial subsidence processes associated to an extensional event, and the evolution of the accretionary to collisional-type orogen characterize the Irumide Orogeny (1400-1000 Ma), the registry of a complete Wilson Cycle in the SIB. A large range of magmatic and restricted metamorphic ages were reported defining the main activity of the belt between 1200 and 1000 Ma (GTK Consortium, 2006; Johnson et al. 2006, 2007; Westerhof et al. 2008; Mänttäri, 2008; Bingen et al. 2009; Alessio et al. 2019a, b; Petry et al. 2022; Philipp et al. 2023). However, the timing of transition from accretionary to collisional orogen remains controversial.

We investigated the stratigraphic and temporal relationship of the high-grade supracrustal rocks of the Chidzolomondo Complex and the intrusive charnockitic to gabbroic post-collisional magmatism. To understand the tectonometamorphic evolution of the paragneisses of the complex we present petrological data including P-T estimations, whole rock geochemistry and U-Pb and Lu-Hf zircon data from igneous, detrital and metamorphic zircon. The results, integrated with published data, indicate the timing of the Irumide Orogeny last events: (1) maximum depositional age of Chidzolomondo Complex arc-related basin at 1121 ± 2 Ma; (2) accretionary phase extending until ca. 1080 Ma with associated magmatism and metamorphism; (3) granulite-facies metamorphism and collisional peak at 1060 Ma; (4) intrusive post-collisional granitic and mafic magmatism between 1050-1000 Ma. The juvenile Hf signatures of the syn- to late-orogenic magmatism and the post-collisional magmatism suggest the continuous contribution of mantle magmas during the

80 evolution of the SIB.

81 **2. Geological setting**

82 The Precambrian basement of the Tete Province has a polycyclic evolution preserved
83 by the Mesoproterozoic Southern Irumide (NE-SW and NW-SE trend), and by the
84 Neoproterozoic Mozambique (N–S trend) and Zambezi (E-W trend) belts (GTK Consortium,
85 2006; Westerhof et al., 2008; Chaúque et al., 2017, 2019, Petry et al., 2022) (Fig. 1). The
86 main crustal growth events are related to subduction and arc accretion followed by the
87 continental collision in the Late Mesoproterozoic. These events characterize the Irumide
88 Orogeny in the SIB.

89 The SIB composes a Mesoproterozoic magmatic arc system extending through the SE
90 portion of Africa from SE Zambia and N Zimbabwe to NW Mozambique and W Malawi
91 (**Fig. 1**). The belt is located between the Zimbabwe and Central Africa cratons bounded by
92 two E-W to NE-SW continental-scale shear zones, the Mwembeshi Shear Zone (MSZ) at the
93 north, representing a Mesoproterozoic suture zone (Johnson et al., 2006; Sarafian et al.,
94 2018), and the Sanangoé Shear Zone (SSZ) at the south. To the east, the NW-SE trending and
95 SW-verging Angonia Shear Zone separate it from the Marrupa and Unango complexes, the
96 eastern continuation of the SIB (Bingen et al., 2009, Hauzenberger et al., 2014; Thomas et al.,
97 2016). The belt comprises metamorphosed supracrustal complexes surrounded by syn-
98 orogenic granitoids and intruded by late- to post-collisional high-K calc-alkaline granites,
99 charnockites, and gabbro-anorthosite complexes with relics of Paleoproterozoic to Archean
100 high-grade gneissic rocks (GTK Consortium, 2006; Johnson et al., 2006; Alessio et al.,
101 2019a, b; Westerhof et al., 2008a) (**Fig. 2**). The prevailing tectonothermal events in the SIB
102 are the late Mesoproterozoic metamorphism, corresponding to the syn-orogenic to post-
103 collisional magmatism of the SIB. The rocks associations were locally affected by the
104 deformation, metamorphism and magmatism of the Pan-African orogenic cycle and

105 Gondwana assembly between 880-500 Ma (GTK Consortium, 2006; Fritz et al., 2013;
106 Chaúque et al., 2017, 2019).

107 **INSERT FIGURE 1**

108 The supracrustal complexes were interpreted as deformed and metamorphosed passive
109 margin and arc basins deposited between ca. 1350-1080 Ma (Johnson et al., 2007; Westerhof
110 et al., 2008; Petry et al., 2022). They include metavolcanic rocks ranging from basalts to
111 rhyolites, and metassedimentary rocks including calc-silicate schists and gneisses, quartzites,
112 metasandstones and metapelites. The metamorphic conditions vary from greenschist to
113 granulite facies. In the Tete Province, the Chidzolomondo, Fíngoè, Cazula, Mualadzi and
114 Zâmbué supracrustal complexes were individualized by GTK Consortium (2006) and
115 previous workers due to their lithological, metamorphic and structural specificity. Detailed
116 descriptions of the supracrustal complexes of the Tete Province can be found in GTK
117 Consortium (2006), Westerhof et al. (2008) and Petry et al. (2022).

118 **INSERT FIGURE 2**

119 The Chidzolomondo Complex (ChC) occurs as two distinct NE-SW elongated and
120 discontinuous belts (**Fig. 2**). The northern exposure is a belt of 120 km length and 10 to 20
121 km width comprising basic to intermediate gneisses of volcanic origin interlayered with
122 subordinate calc-silicate gneisses. The orthogneisses are dark gray to greenish gray, fine- to
123 medium-grained equigranular, massive or banded pyroxene and two-pyroxene gneisses (GTK
124 Consortium, 2008). Lithological classification diagrams plot as basalt and andesite with
125 minor felsic members and a subalkaline tholeiitic to slightly calc-alkaline affinity (GTK
126 Consortium 2006). The southern exposure consists of five contiguous bodies with ca. 20 km
127 length and 15 km width, comprising migmatitic quartz-feldspathic and calc-silicate gneisses,
128 metavolcanic rocks, with minor metapelitic lenses and metagabbro intrusions (GTK
129 Consortium, 2006). The mineral assemblages and geothermobarometry of orthopyroxene-

130 garnet-bearing granulites and two-pyroxene gneisses indicated peak metamorphism with P-T
131 conditions of 700-800 °C and 3.5-4.8 kbar for the basic granulites of the northern exposure of
132 the ChC (Westerhof et al., 2008). The intrusion of late- to post-collisional granites and
133 gabbros causes intense retrograde assemblages related to contact metamorphism superposed
134 over the orogenic metamorphism (GTK Consortium, 2006).

135 **INSERT FIGURE 3**

136 The supracrustal complexes are encompassed by the voluminous late-Mesoproterozoic
137 magmatism comprising syn-orogenic and late- to post-collisional suites (**Fig. 3**). In the Tete
138 Province the syn-orogenic Rio Capoche, Serra da Chiuta, Rio Tsafuro, Monte Capirimpica
139 granites and the Cassacatiza and Serra Danvura granitic suites have ages between ~1200-
140 1080 Ma (GTK Consortium, 2006; Manttari, 2008; Philipp et al. 2023). They compose NE-
141 SW elongated batholiths with concordant magmatic foliation, locally deformed and
142 metamorphosed (GTK Consortium, 2006). The average rock types are medium to coarse-
143 grained porphyritic biotite (±hornblende) granites and granodiorites. The presence of variable
144 size (cm to km) xenoliths of metasediments and amphibolites of the supracrustal complexes
145 are common.

146 The younger intrusive suites (<1080 Ma) reflect the partial melting of the continental
147 crust and the ascension of the asthenosphere in the post-collisional extensional environment
148 (Westerhof et al., 2008). The Mussata and Chacocoma granites and the Furacungo Suite
149 (Desaranhama, Nacoco, Rio Ponfi and Monte Dezenza gneisses) characterize the late- to
150 post-collisional granitic magmatism in the Tete Province, with U-Pb zircon ages between
151 1060-1000 Ma (GTK Consortium, 2006; Westerhof et al., 2008; Philipp et al. 2023). The
152 most common rock type are K-felspar porphyritic granitoids, locally mylonitized and
153 deformed. Concurrently, the charnockitic magmatism of the Castanho Suite and the basic
154 stratiform rocks of the Tete Suite and the Chipera, Rio Chiticula, Muenda and Ualadze

gabbros show ages between 1060-1000 (GTK Consortium, 2006; Philipp et al. 2023). The Castanho Suite charnockites and layered gabbro-anorthosite bodies are restricted to the ChC domain and were thought to have formed by melting of the (dehydrated) lower crust (Westerhof et al., 2008).

3. Methods

3.1. Geochemistry analysis

We selected seven samples of ortho and paragneisses of the ChC and twelve samples of the Castanho Suite charnockites for whole-rock chemical analysis. The geochemical analyses were conducted at the ACME Analytical Laboratories, Canada, by the ICP technique (Inductively Coupled Plasma – Emission Spectrometry) for major elements, with 0.01% detection limit, and for Sc, Be, V, Ba, Sr, Y, and Zr, with the detection limit between 1 and 5 ppm. For the remaining trace elements and rare earth elements (REEs), the ICP-MS technique (Inductive Coupled Plasma – Emission Spectrometry Mass) was used, with a detection limit of 0.005–2 ppm. The whole-rock geochemical data, including major, minor, trace, and rare earth elements, are given in **Supplementary Data - Table 1**.

3.2. Mineral Chemistry

The chemical analysis of garnet and biotite in one sample of pelitic gneiss was made with the Electron Probe Micro Analyzer (EPMA), Cameca SX Five model, directly into the thin sections coated with carbon at the Laboratory of Electronic Microprobe in the CPGq/UFRGS. The energy conditions of the analysis by EPMA were of 15 kV and 15 nA, with a beam of 5 μm diameter. The chemical composition of the garnet and biotite is available in the **Supplementary Data - Table 2**.

3.3. Phase equilibria modeling

Isochemical phase equilibria diagram was constructed for bulk composition

179 representative of an pelitic gneiss from the Chidzolomondo Complex Group using the
180 Perple_X software (Connolly, 2005) and the internally consistent thermodynamic database of
181 Holland and Powell (2011) (hp11ver.dat, tc-ds61in Perple_X). The bulk rock composition of
182 the sample was obtained from X-ray fluorescence analyses. The minerals involved in phase
183 diagram construction include: garnet, clinopyroxene, orthopyroxene, white mica, staurolite,
184 biotite, cordierite, feldspar, magnetite, ilmenite and silicate liquid (melt). The following
185 solution models were used: Gt(W), Bi(W), Mica(W), St(W), Crd(W), Opx(W) melt(W)
186 (White et al., 2014), Cpx(HP) (Holland and Powell, 1996), feldspar (Fuhrman and Lindsley,
187 1988) and IlHm(A) (Andersen and Lindsley, 1988). The H_2O content was estimated so that
188 the modelled rock composition was saturated in H_2O immediately below the solidus (cf.,
189 White et al., 2001) and the contents of P_2O_5 was neglected due to the its low concentration.
190 The calculations were undertaken in the NCKFMASHTO chemical model (Na_2O-CaO-K_2O-
191 FeO-MgO-Al_2O_3-SiO_2-H_2O-TiO_2-O_2).

192 To obtain the bulk rock composition prior to melt loss, the modeled bulk composition
193 was recalculated above the solidus using the single-step melt-reintegration method (Bartoli,
194 2017; White et al., 2004). The modeled bulk composition was recalculated by adding the
195 corresponding amount of 8 vol.% of melt, taking the melt composition produced in
196 experimental melting of a metapelite sample under conditions of 775 ºC, 6 kbar and 2 wt.%
197 of added water (Patiño Douce and Harris, 1998). The definition of the P and T conditions of
198 the orogenic metamorphism were obtained from the XMg of garnet and biotite.

199 **3.4 U-Pb zircon geochronology and Hf isotopic composition**

200 To carry out LA-ICP-MS U-Pb zircon analysis, we selected three samples from the
201 ChC including a high-grade pelitic gneiss (MB-146, mc-crd-bt-grt-qz-pl-opx gneiss), a
202 metagabbro (MB-144), and an opx-bearing qz-monzonite gneiss (MB-148), and two samples
203 of the surrounding and intrusive rocks, including a opx-bearing qz-monzonite (MB-141) of

204 the Castanho Suite and a gabbro (MB-147) of the Rio Chiticula Gabbro. All these samples
205 are located in the same geological section that cuts through the village of Chidzolomondo.
206 The zircon grains from the selected samples were extracted using conventional
207 techniques of heavy mineral concentration, by means of jaw crushers, milling, manual
208 panning and hand-picking under a binocular microscope. After separation, the zircon grains
209 were mounted onto epoxy resin discs and polished to expose the grain centers. Prior to U-Pb
210 analysis, the morphology and internal structure of zircon grains were characterized by SEM-
211 cathodoluminescence (CL) in a JEOL 6510 Scanning Electron Microscope at
212 DEGEO/UFOP. The CL images were used to examine morphological characteristics of
213 zircon grains and to select areas for spot analyses. U-Pb analyses were carried out at the
214 Isotopic Geochemistry Laboratory, the Universidade Federal de Ouro Preto, using a Thermo-
215 Finnegan Neptune multi-collector ICP-MS coupled with a Photon-Machines 193 nm excimer
216 laser system (LA-MC-ICP-MS). Data were acquired using peak jumping mode with
217 background measurement during 20 sec, zircon ablation during 20 sec and 30 µmspot size.
218 Analyses were conducted over two analytical sessions. The GJ-1 (Jackson et al., 2004),
219 Plešovice (Sláma et al., 2008) and BB (Santos et al., 2017) zircon standards were used for
220 this study. Data reduction was done in GLITTER® Software (Van Achterbergh et al., 2001),
221 whereas the concordance, probability, radial and Concordia diagrams, and the weighted
222 average ages were generated by the Isoplot-R Software (Vermeesch, 2018). The maximum
223 depositional age (MDA) of the paragneiss were calculated using the 'Maximum Likelihood
224 Age' (MLA) method (Vermeesch, 2021) and the results were compared with all the
225 Maximum Depositional Age (MDA) methods discussed and revised by Coutts et al. (2019).
226 The complete U-Pb zircon data of two sessions of analysis and the reference material results
227 are given in **Supplementary Data - Table 3**.
228 The Lu-Hf isotopic analyses of dated zircon grains were conducted in the Isotopic

229 Geochemistry Laboratory of Ouro Preto Federal University (UFOP). The Lu-Hf data were
230 acquired using a Thermo-Finnigan Neptune multicollector ICP-MS instrument coupled with a
231 Photon-Machines 193 nm Excimer Laser System (LA-MC-ICP-MS) following the methods
232 of Gerdes and Zeh (2006). The analysis used a bunch of standard zircons such as GJ-1
233 (Jackson et al., 2004), Plešovice (Sláma et al., 2008), Mud Tank (Black and Gulson, 1978,
234 Woodhead and Hergt, 2005), BB (Santos et al., 2017), which yielded $^{176}Hf/^{177}Hf$ of
235 0.282482±0.000013 (n=7), 0.282000±0.0000005 (n=10), 0.282504±0.0000044 (n=11),
236 0.281671±0.0000028 (n=8), respectively (±2SD).
237 For the calculation of εHf values, we used the ^{176}Lu decay constant of 1.867 x 10^{-11}
238 (Söderlund et al., 2004) and the values of $^{176}Hf/^{177}Hf = 0.282785$ and $^{176}Lu/^{177}Hf = 0.0336$ for
239 the present-day chondrites (Bouvier et al., 2008). For calculation of the depleted mantle
240 evolution curve and the two-stage Hf model ages (T_{DM}^2), we adopted the values $^{176}Hf/^{177}Hf =$
241 0.28325 and $^{176}Lu/^{177}Hf = 0.0388$ of present-day depleted mantle (Griffin et al., 2000;
242 updated by Andersen et al., 2009). The analytical data are available in **Supplementary Data**
243 **- Table 4**.

244 **4. Results**

245 **4.1. Mineralogy and microstructures**

246 The summarized petrographic features of representative samples are described below.
247 The rock samples were selected to investigate the metamorphic conditions that affected the
248 ChC and include three metapelitic rocks, a calc-silicate gneiss and a metagabbro.
249 Representative photomicrographs of the rocks are shown in **Figures 4 and 5**. The pelitic
250 gneisses are dark brown, fine grained with irregular and continuous banding, locally
251 presenting lenses of garnet porphyroblasts aggregates. The calc-silicate gneiss is greenish to
252 greenish brown, fine grained with regular compositional banding and subordinate lenses of

253 metapelitic gneiss. They are rich in plagioclase and diopside, with variable amounts of quartz,
254 biotite, cordierite and titanite, indicating carbonatic protoliths in the primary sedimentary
255 sequence. The mineral abbreviations are based on Whitney and Evans (2010).

256 **4.1.1 Pelitic gneisses**

257 The high-grade pelitic gneisses consists of bt-mc-qz-pl-opx gneiss (MB-143A), crd-qz-
258 bt-pl-opx migmatitic gneiss (MB-145) and mc-crd-bt-grt-qz-pl-opx gneiss (MB-146). The
259 irregular mafic and felsic banding partially preserved the primary bedding. The felsic levels
260 are continuous (2-6 mm) and show polygonal granoblastic texture comprising recrystallized
261 polygonal-type plagioclase, microcline and quartz crystals, with variable amounts of
262 interstitial cordierite and orthopyroxene. The mafic bands comprise aggregates of
263 orthopyroxene (0.2-1 mm) and fox-red biotite (0.3-1 mm) with variable amounts of garnet.
264 Subidioblastic garnet porphyroblasts (1-4 mm) contain numerous biotite, quartz, zircon,
265 monazite and opaque minerals inclusions. The cordierite forms xenoblastic to subidioblastic
266 prismatic and poikiloblastic crystals (0.3-1 mm). Orthopyroxene occur as subidioblastic
267 polygonal or prismatic crystals. The biotite shows reddish-brown pleochroism and partial
268 melting features with thin quartz films surrounding the grains.

269 Concordantly to the banding, injections of quartz-feldspathic composition (5-30 mm)
270 show massive structure and medium-grained equigranular texture constituted by plagioclase,
271 quartz and cordierite. Thin quartz films surround the biotite and quartz grains of the pelitic
272 gneisses close to these injections showing the partial melting of these minerals. Very fine
273 biotite fringes were observed close to the larger biotite crystals. The symplectic intergrowth
274 of cordierite and diopside are subordinate in the gneisses. The cordierite occur as fine and
275 vermiform films associated with the plagioclase or constituting larger crystals associated with
276 vermiform aggregates of diopside. These disequilibrium textures were interpreted as a
277 product of the reaction of plagioclase and garnet during abrupt decompression.

INSERT FIGURE 4

INSERT FIGURE 5

4.1.2 Calc-silicatic gneiss

The ti-qz-pl-opx-di gneiss (MB-143B) have poorly defined compositional mafic and felsic banding and medium-grained polygonal granoblastic texture. The felsic levels are continuous (2-6 mm) composed of plagioclase and quartz, with subordinate microcline and interstitial orthopyroxene and clinopyroxene. The mafic levels are discontinuous (0.5-3 mm) composed by diopside and low contents of phlogopite, titanite and opaque minerals with interstitial plagioclase, quartz and microcline. The pyroxenes form nematoblastic to polygonal granoblastic aggregates of short prismatic crystals or xenoblastic porphyroblasts. Phlogopite crystals show reddish- to orange-brown pleochroism and occur as interstitial aggregates associated with the clinopyroxene. The plagioclase is polygonal, subidioblastic to idioblastic, and the microcline are equigranular and subidioblastic. Quartz is interstitial, constituted by polygonal-shape recrystallized grains and deformed subgrains with regular extinction.

The primary bedding is partially preserved by four compositional levels: (i) pelitic levels rich in garnet and orthopyroxene (±biotite); (ii) aluminous calci-silicatic levels rich in diopside and phlogopite; (iii) psammitic levels with quartz, plagioclase and variable K-feldspar amounts; (iv) siliceous calci-silicatic levels with plagioclase, quartz, cordierite and few diopside and orthopyroxene.

4.1.3 Metagabbro

The metagabbro (MB-144) have dark green color, medium- to coarse granulometry with an incipient banding. The rock is predominantly composed of reliquiar prismatic to plagioclase crystals (1-2 mm) with apatite inclusions and ophitic texture with augite and

orthopyroxene as interstitial aggregates. The main texture is blastointergranular, constituted by relics of plagioclase aggregates and interstitial clinopyroxene and orthopyroxene. The main mafic mineral is the augite with short prismatic habit (0.5-2 mm). Rare globular olivine crystals (0.5-1 mm) with fine orthopyroxene and augite coronas surrounded by hornblende were observed. The mafic minerals are partially included in the plagioclase characterizing the subophitic texture. The igneous fabrics were partially recrystallized and involved by fine bands of medium-grained granoblastic polygonal-type plagioclase, diopside and orthopiroxene grains.

4.1.4 Charnockitic gneiss

The charnockitic gneiss (MB-148) shows medium- to coarse-grained and inequigranular texture with mafic and felsic compositional banding. The mafic bands (1-3 mm) are discontinuous and constituted by orthopyroxene, hornblende, biotite and opaque minerals aggregates. The felsic bands comprise microcline and plagioclase aggregates with interlobate to polygonal granoblastic textures. Idioblastic interstitial orthopyroxene (0.1-0.3 mm) are disseminated in the felsic bands. Large porphyroclasts of microcline, plagioclase and quartz (1-3 mm) are involved by metamorphic fabric characterizing the blastoinequigranular texture. Hornblende and opaque minerals replacing the orthopyroxene suggest the re-equilibrium of the orthopyroxene. The myrmekitic texture developed along the main foliation indicates medium amphibolite facies conditions. The recrystallization of the protolith, an opx-bearing monzogranite, and development of polygonal granoblastic texture with Mc + Pl + Opx + Hb mineral assemblage indicate at least conditions of upper amphibolite facies.

4.1.5. Castanho Suite charnockites

The Castanho Suite includes several intrusive plutons of charnockites of typical brown color (the castanho in Portuguese). These rocks don't have incipient evidence of deformation

and metamorphism. The syenite and monzonites from Castanho Suite show massive structure or an incipient igneous foliation defined by the alignment of ortopyroxene and hornblende aggregates. The main texture is medium- to coarse-grained equigranular constituted by prismatic crystals of K-feldspar (or and mc) and plagioclase, with ameboid quartz, and interstitial aggregates of clinopyroxene (aug) and subordinate orthopyroxene (hy), biotite and magnetite.

4.2. Whole-rock geochemistry

Major and trace elements compositions of the studied rocks are presented in **Figures 6, 7 and 8**. The gneisses from Chidzolomondo Complex are represented by subalkaline metavolcanic and metavolcanoclastic rocks of expanded composition including metabasalts, meta-andesites and metarhyolites as exposed in the TAS and Q-P (DeBon and Le Fort, 1983) diagrams (**Fig. 6A, B, C**). However, the protoliths of the studied samples of the southern segment of the ChC were interpreted as meta-epiclastic volcanogenic rocks as pelites and calc-silicatic rocks metamorphosed in high-grade conditions. The Al-alkalis relations observed in the Shand (1943) and A-B (DeBon and Le Fort, 1983) diagrams shows a metaluminous to slightly peraluminous trend (**Figs. 6d, e**). In the Fe-index and MALI diagrams (Frost and Frost, 2008, 2011) the metavolcanic association shows composition equivalent to magnesian granites from calcic-alkalic to calcic series (**Fig. 6f, g**). In the tectonic diagrams as Rb vs. Y+Nb (Pearce, 1996)(**Fig. 8a**), R1-R2 (De la Roche et al. 1980) the samples plot in the active continental margins volcanic arc or pre-plate collision field (**Fig. 8B**). In the diagrams of Th/Yb vs. Ta/Yb (Pearce, 1982), Th vbs. Ta, Th/Hf vs. Ta/Hf and Th/Ta vs. Yb (Gorton and Schandl, 2002) the samples of ChC plot in the oceanic arc or in the active continental margin (**Fig. 8C, D, F, G**). The evaluation of the source rocks in the diagram of Laurent et al. (2014) shows the metavolcanic and metavolcaniclastic rocks of the ChC were derived from low-K to high-K mafic rocks, suggesting a partial melting of the E-

MORB and/or OIB sources.

INSERT FIGURE 6

INSERT FIGURE 7

The Castanho Suite comprise two groups of rocks, the main association is constituted by opx-bearing granitic rocks from subalkaline and monzonitic trend, including monzonite and qz-monzonite, syenite and granite, while the subordinate association of the mafic microgranular enclaves, is constituted by tholeiitic gabbros, as exposed in the TAS (Le Bas et al. 1986) and Q-P (DeBon and Le Fort, 1983) diagrams (**Fig. 6A, B, C**). The Al-alkalis relations observed in the Shand (1943) and A-B (Debon and Le Fort, 1983) diagrams shows a well-defined and distinct metaluminous trend for the granites and mafic enclaves (**Fig. 6D, E**). In the Fe-index and MALI diagrams (Frost et al. 2001, Frost and Frost, 2011) the charnockites show composition of ferroan granites from alkali-calcic series, while the mafic enclaves are magnesian (**Fig. 6F, G**). The alkaline composition and the whitin-plate tectonic setting was confirmed in the tectonic diagrams as Rb vs. Y+Nb (Pearce, 1996) (**Fig. 8A**), R1-R2 (De la Roche et al. 1980) (**Fig. 8B**), Th/Yb vs. Ta/Yb (Pearce, 1982), Th vs. Ta, Th/Hf vs. Ta/Hf and Th/Ta vs. Yb (Schandl and Gorton, 2002) (**Fig. 8C, D, F, G**), and in the A-type diagrams of Whalen et al. (1987) (**Fig. 8I, J, K**). In the diagram of Laurent et al. (2014) to evaluate the magma sources, the charnockites show a derivation from high-K mafic rocks, suggesting the partial melting of E-MORB.

INSERT FIGURE 8

The trace element patterns of the ChC gneisses and the Castanho Suite charnockites are similar. In the NMORB normalized trace element plots (**Fig. 7A, C**), the samples are characterized by enrichment of large lithophile elements (LILEs) such as Rb, Ba and K, suggesting fractional crystallization. The rocks show negative Nb, Ta, P and Ti and rather constant high field strength elements (HFSE). In the chondrite normalized REE plot (**Fig. 7B,**

D), the samples are characterized by enrichment of light REE and flat heavy REE, suggesting fractional crystallization. Most samples present negative Eu anomaly and some present positive Eu anomaly, suggesting the plagioclase fractionation and accumulation, respectively.

4.3. Phase equilibria modeling

A sample of high-grade pelitic gneiss (MB-146, mc-crd-bt-grt-qz-pl-opx gneiss) from Chidzolomondo Complex was selected for phase equilibria modeling. The calculated phase equilibria diagram shows the subsolidus fields dominated by assemblages containing garnet, biotite Al-rich phase, quartz and feldspar. The solidus occurs between 700 and 750 ºC and has a steep negative slope in low pressure Al-free fields. The peak metamorphic assemblage is represented by the field biotite + garnet + plagioclase + orthopyroxene + cordierite + quartz + rutile + magnetite + melt and is stable between 778 to 813 ºC and 3.1 to 5.8 kbar. The peak assemblage field was contoured with compositional isopleths of XMg in garnet and biotite and the measured compositions indicate conditions of 785–795 ºC and 3.7–4.2 kbar (**Fig. 9A**, blue field).

Garnet occurs as syn-tectonic porphyroblasts to the gneiss banding, with subidioblastic globular shapes and poikiloblastic relationships defined by inclusions of quartz, biotite and opaque minerals (**Fig. 4**). The analysis profiles to evaluate the variation of the composition of garnet consisted of 20 to 25 points disposed in a continuous way from one extremity to the other of the grain (**Fig. 9B**). These crystals are associated with more mafic levels, where garnet is accompanied by orthopyroxene and biotite (**Fig. 4**). The felsic levels are also aluminous and consist of cordierite-rich aggregates, with subordinate contents of plagioclase, K-feldspar and quartz (**Fig. 4**). The result of the microprobe analysis of the garnet along of the investigated profiles showed a homogeneous composition with no variation in contents of Mg, Fe, Ca and Al.

400 **4.4. U-Pb geochronology**

401 We selected three samples of high-grade gneisses from the Chidzolomondo Group
402 including the metagabbro (MB-144), the mc-crd-bt-grt-qz-pl-opx gneiss (MB-146) and the
403 charnockitic gneiss (MB-148), one sample of charnockite from the Castanho Suite (MB-141)
404 and one sample from the Rio Chiticula gabbro (MB-147). A total of 251 analyses were
405 performed and 203 concordant U-Pb zircon ages were obtained for the analyzed samples (see
406 **Supplementary Data - Table 3**). The spots were selected based on the zircon internal
407 textures to determine the ages of detrital and igneous cores and the metamorphic rims. The
408 **figure 10** presents CL images of representative zircon grains. The cut-off age is 1.3 Ga, so
409 most of the ages obtained are expressed as $^{206}Pb/^{238}U$ age.

410 **INSERT FIGURE 10**

411 The zircon grains from the mc-crd-bt-grt-qz-pl-opx gneiss (MB-146B) are translucent,
412 colorless or light brownish, prismatic with rounded terminations to oval. They have a size
413 range of 90-250 μm and an aspect ratio of 3:1 to 1:1. The CL images show prominent
414 irregular shape detrital cores surrounded by three types of metamorphic rims (**Fig. 10A**). The
415 most internal rims are discontinuous and thin (<10 μm of width) with cloudy texture and
416 bright in CL. The intermediary rims comprise continuous and oscillatory zoning overgrowths
417 with dark gray CL appearance. The external overgrowths are homogeneous and light gray in
418 CL. We analyzed 108 spots and data from eighty-four spots yielded concordant ages (<5%
419 discordance). These concordant or near-concordant ages vary from 2649 to 1061 Ma (**Fig.**
420 **11A**) and characterizes detrital and metamorphic domains in the zircon grains. Their U
421 content and Th/U ratios are in the range of 60-891 ppm and 0.05-4.31, respectively. The first
422 domain comprises 70 detrital cores varying from 2649 to 1093 Ma and Th/U ratios between
423 0.06-4.31. The main age peak is around 1130 Ma and the maximum depositional age (MDA)
424 calculated with the youngest zircon population yielded an age of 1100±6 Ma (n=11,

425 MSWD=0.15) **(Fig. 11B)** slightly younger than the Maximum Likelihood Age (MLA)
426 (Vermeesch, 2021) of 1121±2 Ma **(Fig. 11C)**. The second analyzed domain comprises 15 Cl-
427 gray rims with ages of 1113-1072 Ma and Th/U ratios between 0.05-2.32. The analyses
428 yielded a concordia age of 1092±5 Ma (MSWD=0.042) and a weighted mean average of
429 1092±5 Ma (MSWD=1.8). The third domain comprises three CL-bright rims with ages of
430 1066-1061 Ma and Th/U ratios between 0.37-1.18. The concordia age of 1064±10 Ma
431 (MSWD=0.005) and the weighted mean average of 1064±5 Ma (MSWD=0.074) were
432 obtained for these analyses.

433 **INSERT FIGURE 11**

434 Zircon grains from the metagabbro (MB-144) are translucent, colorless or light
435 brownish, idioblastic with common inclusions, and partly rounded. They have a size range of
436 180-300 μm and an aspect ratio of 4:1 to 2:1. Most of the crystals show a recrystallized core
437 with fir-tree, polygonal and sector zoning surrounded by concentric or homogenous gray rims
438 (**Fig. 10B**). The external overgrowths are bright in CL with features of dissolution in the
439 internal zones. Forty-six spots were analyzed and data from 38 spots yielded concordant ages
440 (<5% discordance). These concordant or near-concordant ages vary from 1140 to 1021 Ma
441 **(Fig. 12A)** characterizing three domains in the zircon grains. Their U content and Th/U ratios
442 are in the range of 55–797 ppm and 0.18–4.14, respectively. The first domain comprises three
443 igneous cores of 1140-1115 Ma and Th/U ratios of 3.9 and 1.6, respectively. Two of them
444 yielded a concordia age of 1133±15 Ma (MSWD=0.06) **(Fig. 12A)** and a weighted mean
445 average of 1133±7 Ma (MSWD=0.99) **(Fig. 12B)**. The second domain comprises the
446 metamorphic cores and the CL-gray rims and includes 33 concordant spots varying in age
447 from 1085 to 1038 Ma with Th/U ratios between 0.18-4.14. This group yielded a concordia
448 age of 1061±3 Ma (MSWD=0.01) and a weighted mean average of 1061±3 Ma
449 (MSWD=1.7). The third domain includes two analyses of the CL-bright rims with 1030 and

450 1019 Ma and Th/U ratios of 2.57 and 2.12, respectively. This domain yielded a concordia age
451 of 1023±13 Ma (MSWD=0.01) and a weighted mean average of 1023±12 (MSWD=0.28).
452 **INSERT FIGURE 12**
453 The zircon grains from the charnockitic gneiss (MB-148) are translucent, colorless and
454 prismatic, commonly fractured. The CL images show the predominant oscillatory zoning
455 surrounded and reabsorbed by homogeneous light gray metamorphic rims (**Fig. 10C**). We
456 analyzed 47 spots and data from 42 yielded concordant ages (<5% discordance). These ages
457 vary from 1495 to 1047 Ma and characterizes two domains in the zircon crystals. Their U
458 content and Th/U ratios are in the range of 38-838 ppm and 0.92-3.30, respectively. The older
459 age was obtained from inherited zircon grain of 1495 Ma. The bulk of the analysis comprises
460 38 igneous cores with ages from 1134-1071 Ma and Th/U ratios between 1.04-2.91. They
461 yielded a concordia age of 1097±3 Ma (MSWD=0.16) (**Fig. 12C**) and a weighted mean
462 average of 1097±3 Ma (MSWD=3.4) (**Fig. 12D**). The second domain comprises four CL-
463 gray rims with ages of 1070-1047 Ma and Th/U ratios between 0.92-3.30. The concordia age
464 of 1060±10 Ma (MSWD=0.058) and the weighted mean average of 1060±10 Ma
465 (MSWD=1.7) were obtained for this domain.
466 The zircon grains from the charnockite sample (MB-141) are prismatic with irregular
467 and corroded edges, size ranging between 380-180 μm and aspect ratios of 5:1 to 2:1.
468 Oscillatory zoning is the main texture and the CL images reveal resorption features including
469 the external bright rims (**Fig. 10D**). We analyzed 35 spots and data from 25 yielded
470 concordant or near concordant ages (<5% discordance) between 1063-980 Ma. The U content
471 and Th/U ratios are in the range of 37-209 ppm and 0.10-1.01, respectively. We obtained 21
472 ages in the igneous cores varying from 1063 to 1012 Ma which yielded a concordia age of
473 1026±4 Ma (MSWD=2.3) **(Fig. 13A)**. Four CL-bright rims yielded a concordia age of
474 1002±12 Ma (MSWD=2.9).

The zircon grains from the gabbro sample (MB-147) are prismatic with size ranging from 250 to 150 μm with aspect ratios of 3:1 to 2:1. The crystals present broad oscillatory zoning. We analyzed 15 spots and data from 9 yielded concordant ages (<5% discordance). Their U content and Th/U ratios are in the range of 46-503 ppm and 0.15-1.05, respectively. The ages vary from 1048 to 998 Ma and yielded a concordia age of 1026±9 Ma (MSWD=0.1) interpreted as crystallization age of the gabbro (**Fig. 13B**).

INSERT FIGURE 13

4.5. Lu-Hf isotopic data

The same zircon spots of U-Pb analysis were investigated for determination of 36 Lu-Hf isotopic compositions (see **Supplementary Data - Table 4**). For the Mc-cord-flog-grt-qz-plg-diop gnaisse (MB-146B) we determined nine Lu-Hf compositions. We analyzed the detrital cores domain with ages between 1716-1104 Ma and the εHf(t) values range between +8.15 and -10.46 (**Fig. 14**). These grains show T_{DM}^2 ages between 2.44 and 1.41 Ga. Twelve zircon grains from the metagabbro sample (MB-144) were analyzed. The analyses were performed in the recrystallized cores with ages from 1083-1046 Ma yielding positive εHf(t) values between +4.56 and +2.17. The T_{DM}^2 ages vary from 1.65 and 1.54 Ga. From the syenogranitic gneiss (MB-148) fifteen Lu-Hf isotopic compositions were determined. We analyzed the igneous cores of the zircon grains in the range of 1495-1043 Ma with positive εHf(t) values between +11.59 and +1.44. The T_{DM}^2 ages range between 1.70 and 1.48 Ga.

INSERT FIGURE 14

5. Discussions

For this study we integrated the geological mapping and structural information with petrological data, and laboratory analysis including the chemical composition of rocks and minerals, and U-Pb-Hf zircon geochronology and isotopic composition. The geological

499 mapping, stratigraphic and contact relationships between the units of the Chidzolomondo
500 Complex and the adjacent intrusive gabbros of the Rio Chiticula Gabbro and the charnockites
501 of the Castanho Suite were evaluated based on the survey conducted by GTK Consortium
502 (2006). New field work was carried out for detailed description of lithotypes and sampling.
503 The Chidzolomondo Complex gneisses occurs as six nearly continuous xenoliths within
504 the syn-orogenic to post-collisional magmatic rocks of the SIB. The aerogeophysical images
505 indicate two compositionally distinct segments of the ChC (GTK Consortium, 2006a). The
506 northern segment shows strong magnetic and low radiometric signatures delineating the well-
507 developed ENE-WSW to E-W linear structures. The geophysical signature contrasts with the
508 surrounding granitoids evidence the basic to intermediate composition of these rocks. The
509 rocks of northern segment comprises banded pyroxene and two-pyroxene gneisses with
510 subordinate plagioclase, garnet, biotite and quartz. The regular compositional banding and the
511 prismatic porphyroclasts of plagioclase and clinopyroxene support the volcanic and
512 volcaniclastic nature of the protoliths. The P-T conditions were estimated around 700-800 °C
513 and 3.5-4.8 kbar (Westerhof et al., 2008).
514 The southern segment is characterized by the absence of magnetic signal,
515 distinguishing it from the adjacent granites. On the other hand, their radiometric signatures
516 (Th-K) are similar, suggesting that granitic intrusions may be abundant in the southern
517 segment of the ChC, or strongly affected it (GTK Consortium, 2006). The complex mostly
518 comprises paragneisses with minor mafic metavolcanic and metaplutonic rocks, locally
519 deformed by ductile shear zones. We conducted the field work in a NE-SW geological
520 section crossing the southeastern xenolith of the Chidzolomondo Complex extending from
521 Chiuta Hills, Chidzolomondo village until Furacungo locality. The continuity of the
522 expositions and the coherence of the structural data allowed the interpretation of the ChC as a
523 roof pendant inside the intrusive granites and gabbro suites. The main sequence of this body

524 comprises intercalated pelitic migamtitic gneisses and calci-silicatic gneisses, with syn-
525 orogenic (meta)gabbro and (meta)charnockite intrusions.

526 **5.1. Petrogenesis**

527 The observed paragneisses show regular compositional and textural banding composed
528 of continuous felsic levels and discontinuous mafic lenses, partially preserving the primary
529 bedding. Discontinuos mafic layers constituted by orthopyroxene, garnet and biotite were
530 developed in aluminous-rich pelitic lenses, with the quartz-feldspathic levels representing
531 psammitic layers. The calci-silicatic layers are rich in diopside and phlogopite and represent
532 the mixed pelitic and carbonatic layers evidencing the original carbonate-siliciclastic
533 sedimentary sequence (metamarls). The ChC samples show a wide range of composition
534 from basic to acidic gneisses with calcic to calc-alkaline affinity and were interpreted as
535 metavolcanic and metavolcaniclastic rocks by GTK Consortium (2006). In the southern
536 segment of the ChC the paragneisses were interpreted as meta-epiclastic rocks generated by
537 erosion and short transport of the arc-related volcanic rocks. These rocks plot in the volcanic
538 arc and active continental margin settings in the geotectonic diagrams (**Fig. 8**). The syn-
539 orogenic nature of the sedimentary and volcanic protoliths are well characterized and in
540 agreement with the observed in other supracrustal complexes of the SIB (Johnson et al.,
541 2007, Westerhof et al., 2008; Petry et al., 2022).

542 The well-developed medium grained polygonal granoblastic texture and the mineral
543 assemblage with crd + gt + opx + bt in metapelitic and pl + mc + qz + di ± phl ± opx in calc-
544 silicatic gnaisses are indicative of granulite facies metamorphic conditions (~700-800º and 2-
545 6 kbar). More precisely, the phase equilibria modeling revealed high-temperature and low-
546 pressure peak metamorphic conditions (785–795 ºC and 3.7–4.2 kbar) in the central zone of
547 the southern segment. Similar P-T conditions were estimated for basic orthogneisses of the
548 northern segment of the ChC (Westerhof et al., 2008). The increasing abundance of cordierite

549 and the degree of migmatization indicate the raising of metamorphic grade to SW in the
550 studied section. The partial melting features include concordant quartz-feldspathic injections
551 along the gneissic banding and thin films of quartz and feldspar around the biotite, quartz and
552 cordierite. The growth of cordierite and orthopyroxene at the expense of garnet and
553 plagioclase indicate post-peak isothermal (high-T) decompression, as previously indicated by
554 the GTK Consortium (2006) for the northern segments of the ChC.
555 Syn-orogenic gabbroic (MB-144) and charnockitic (MB-148) intrusions of variable size
556 (up to 50 m) were identified within the ChC supracrustals. They partially preserve the
557 magmatic fabrics and mineralogy and intrude the sedimentary sequence prior to the high-
558 grade metamorphism. The metagabbro metamorphic assemblage of Pl + Di + Hy is indicative
559 of granulite facies (>800° C) and low-pressure conditions (4-6 kbar) (Bucher and Grapes,
560 2011). The charnockitic gneiss shows evidence of ductile deformation and recrystallization in
561 conditions of upper amphibolite to granulite facies. The charnockitic gneiss identified within
562 the ChC doesn't belong to the Castanho Suite.
563 Several plutpons of charnockites from Castanho Suite charnockites and gabbros from
564 Rio Chiticula Gabbro intrude the granulitic gnaisses of the Chidzolomondo Complex. The
565 charnockitic rocks are intimately associated with the ChC granulites forming a
566 granulite/charnockite domain in the Tete Province. The plutons of Castanho Suite were
567 thought to be formed by melting of the dehydrated and high-grade lower continental crust
568 under thermal influence of underplated magmas (GTK Consortium, 2006; Westerhof et al.,
569 2008). The charnockites in general sense is used to refer to the opx-bearing granitoids,
570 including opx-qz monzonite and opx-monzogranites terms. The bulk chemistry is a
571 significant compositional parameter and would reflect the mechanisms that produce
572 charnockitic magmas (Frost and Frost, 2008). The main composition of the analyzed
573 charnockites is alkali-calcic and ferroan plotting as within-plate and A-type magmas, which

574 suggests the derivation of E-MORB sources with minor crustal components. In this scenario,
575 the charnockitic magmatism of the Tete Province was probably originated by the
576 differentiation of underplated magmas in the post-collisional extensional setting, hence is a
577 thermal source for the HT to UHT metamorphism and not its consequence. This hypothesis is
578 supported by contemporary igneous and metamorphic U-Pb zircon ages.

579 **5.2. Zircon geochronology**

580 New metamorphic zircon can grow, overgrow and recrystallize the original zircon from
581 the protolith zircon under high-grade conditions or in lower T but under high PH_2O and O_2,
582 frequently resulting in a complex textural pattern of zircon growths (Rubatto, 2017, Kunz et
583 al., 2018). In this case, if little or not disturbed, the zircon crystals keep a polyphasic
584 chronological story. Lower Th/U ratios (<0.1) were usually adopted as an indicator of
585 metamorphic zircon. However, many studies show higher and scattered Th/U values (>0.1),
586 especially under high-grade metamorphic conditions (Hoskin and Black, 2000; Kunz et al.,
587 2018; Laurent et al., 2018). Zircon grown near the peak of metamorphism is expected to have
588 elevated Th/U ratios (Yakymchuck et al., 2018). In this case, the textural features show
589 imperative evidence of the zircon growth record to guide the analysis site selection (Vavra et
590 al., 1996, 1999). The U-Pb analysis of metamorphic zircon often exhibits a spectrum of ages
591 due to concealed Pb-loss, partial recrystallization and dissolution-reprecipitation, or mixed
592 analyses domains. Detailed investigation of zircon crystals from the granulite samples
593 revealed distinct core-rim proportions, types and internal textures (Rubatto, 2017). In the
594 high-grade gneisses of ChC, the different crystal domains show a coherent range of ages
595 indicating three metamorphic events: i) M_1 - 1092±5 Ma; ii) M_2 - 1061±3 Ma; iii) M_3 -
596 1023±13 Ma. We interpreted the M_1 and M_2 as related to orogenic metamorphis, and a M_3
597 event associated to a new metamorphic conditions related to development of the transcurrent
598 ductile shear zone

599 The results obtained in the 70 detrital zircon cores from the mc-crd-bt-grt-qz-pl-opx
600 gneiss (MB-146) show dominance of Mid- to Late-Mesoproterozoic ages (1332–1093 Ma)
601 with subordinate Paleoproterozoic and Archean contributions. The main source areas are
602 related to the syn-orogenic magmatism of the SIB and maximum depositional age was
603 established at 1121±2 Ma (**Fig. 11C**). The detrital cores are surrounded by three types of
604 rims. The innermost rim is bright in cathodoluminescence, cloudy and discontinuous, too thin
605 to analyze (**Fig. 10A**). This overgrowth appears to be related with corrosion along the contact
606 between the nucleus of the zircon and have textural features of zircon grown by dissolution–
607 precipitation processes under low-grade conditions (Rubatto, 2017; Kunz et al., 2018). The
608 second rim is a gray isometric overgrowth with homogeneous or weak oscillatory zoning and
609 up to 50 μm. The concordia age of 1092±5 Ma was determined in this domain, representing
610 the older M_1 metamorphic event identified in the ChC related to the accretionary phase. The
611 outer CL-bright rims are strongly luminescent and with resorption features. This type of rim
612 was described by Vavra et al. (1999) as surface-controlled alteration and is often related to
613 fluid-induced recrystallization from the outside inward to the interior of the crystal. This
614 domain was assigned to the M_2 event and defined by a Concordia age of 1064±5 Ma.
615 The bodies of metagabbro amd charnockitic gneiss are intrusive in the granulitic
616 gneisses of the complex and their crystallizations ages characterize the syn-orogenic
617 magmatism of the SIB. The metagabbro (MB-144) have xenocrystal zircon grains with broad
618 oscillatory zoning, which yielded a Concordia age of 1133±15 Ma interpreted as the age of
619 the igneous crystallization. They also occur as tiny xenocrysts within metamorphic zircon
620 (**Fig. 10B**), suggesting the dissolution of smaller zircon grains by the Ostwald ripening
621 process (Rubatto, 2017). The metamorphic cores comprise oval to slightly prismatic and
622 multifaceted CL-gray nucleus with polygonal and fir-tree textures surrounded by isometric
623 darker overgrowths up to 70 μm. This textural feature is common in prograde paths and

624 indicates the shift from the amphibolite (prismatic and multifaceted) to the granulite facies
625 (rounded and isometric) (Vavra et al., 1999; Rubatto, 2017). These domains don't differ in
626 age and compose the metamorphic cores yielding an age of 1061±3 Ma, characterizing the
627 peak-collisional metamorphic event (M_2). The outer CL-bright rims present resorption
628 features and yielded a Concordia age of 1023±12 Ma interpreted as the age of the M_3
629 metamorphic event coeval with the movement of the main ductile shear zones and associated
630 to the the nearby charnockite intrusion (MB-141), the most probable heat and/or fluid source.
631 The igneous zircon of the intrusive charnockitic gneiss (MB-148) shows well-preserved
632 igneous prismatic shapes and well-developed oscillatory zoning (**Fig. 10C**). The zircon
633 crystals are rather fractured, the probable cause for the slight discordance of some analysis
634 and the greater age dispersion. The Concordia age of 1097±3 Ma, interpreted as the igneous
635 crystallization age of the charnockite and coeval with the M_1 metamorphic event. The thin
636 outer CL-bright rims present in some zircon grains show resorption features. The analysis
637 performed in the rims yielded a Concordia age of 1060±10 Ma, interpreted as the age of the
638 M_2 metamorphic event.
639 The igneous zircon grains of the charnockite from Castanho Suite and the gabbro
640 sample from the Rio Chiticula Gabbro yielded identical crystallization ages of 1026±4 Ma
641 and 1026±9 Ma, respectively. Both plutons present a local igneous foliation and show
642 intrusive contact relationships with the granulitic gneisses and orthogneisses of the ChC.
643 These obtained ages are contemporary with the post-peak metamorphic event M_3 identified in
644 the outer rims of the zircon crystals from metagabbro sample, reinforcing the hypothesis of
645 contact metamorphism. The charnockite zircons grains present CL-bright rims with
646 resorption features that yielded a younger metamorphic age of 1002±12 Ma, which is also in
647 the range of the M_3 metamorphic event.

5.3. SIB granulite domains

The lithological diversity and the complex structural/metamorphic architecture of the SIB led some authors to support the collage of exotic terranes (Johnson et al., 2006; Westerhof et al., 2008), consequently dissociating their origin. In this scenario, the granulite terranes were thought to compose older crustal fragments (Westerhof et al., 2008). However, the geochronological and isotopic data evidence a common tectonic evolution for the SIB in the late-Mesoproterozoic. Rather than an exotic terranes the belt shows structural/metamorphic domains bounded by internal shear and thrust zones (Petry et al., 2022). From this perspective we briefly compare the tectonometamorphic events of the granulite domains of the SIB, the Chidzolomondo Complex, the Chipata Complex and the Granulite Terrane of Chewore Complex in the Rufunsa region (**Fig. 2**).

To the west of the SIB, in northern Zimbabwe, the Granulite Terrane (GT) of the Chewore Complex comprises anhydrous sillimanite or orthopyroxene-bearing quartz-feldspathic gneisses and granitic orthogneisses with minor metapelite and mafic granulites (Goscombe et al., 1994, 2000). The maximum depositional age of the Chewore Complex is constrained by the U-Pb zircon age of a dacite of 1082±7 Ma (Johnson and Oliver, 2004). A granitic orthogneiss yielded U-Pb zircon crystallization age of 1087±9 Ma and metamorphic ages of 1068±21 Ma and 526±17 Ma (Goscombe et al., 2000). The stratigraphic relationships and these ages unveil the same framework identified in the ChC, with syn-orogenic granitic bodies intruding the host volcano-sedimentary sequence prior to the collisional metamorphism at ca. 1060 Ma. The peak metamorphic assemblages such spinel-garnet-sillimanite migmatitic metapelite, two-pyroxene gneisses and opx-gt qz-feldspathic gneisses indicate P-T conditions of >800°C and 4-5 kbar. The GT lithologies experienced peak metamorphic conditions of 690-810°C and 3.3-5.5 kbar (Goscombe et al., 1998), the same range of the ChC granulites. The HT-LP metamorphism was accompanied by two isoclinal

673 folding events supporting their syn-tectonic nature. The younger metamorphic age records the
674 partial re-equilibration under mid-amphibolite conditions restricted to the proximity of the
675 south verging shear zones related to the Zambezi Belt.

676 In the northern portion of the SIB, in Zambia, the Chipata Complex (CpC) comprises
677 mafic, felsic and pelitic granulites, metagabbros, hornblende-biotite gneisses. The complex is
678 intruded and surrounded by K-feldspar porphyritic granites and charnockites. The
679 lithostratigraphic framework resembles those identified in the ChC region. The metapelitic
680 granulites of the CpC experienced HT-UHT peak metamorphic conditions at mid crustal
681 depths conditions of 870-1000°C and ~6 kbar, followed by the isobaric cooling (Karmakar
682 and Schenk, 2016). The in situ monazite revealed that the peak metamorphic conditions must
683 have occurred between 1031-1013 Ma, with a slightly older metamorphic age at 1067±15
684 Ma. Karmakar and Schenk (2016) postulated the relationship between the charnockitic
685 magmatism and the UHT metamorphism in the Chipata Complex, which is now confirmed in
686 the ChC. Two charnockites from Chipata yielded crystallization ages of 1040±5 Ma and
687 1039±6 Ma (Alessio et al., 2019a), not in the range of monazite ages, but in the context of the
688 post-collisional metamorphic event (M3). The granulite/charnockite domain of the Chipata
689 Complex is bounded and crosscut by N-S to NW-SE high-strain shear and thrust zones
690 (Johnson et al., 2006). It must compose the northwestern extension of the same structural
691 granulite/charnockite domain of the Tete Province (**Fig. 2**).

692 The metavolcano-sedimentary complexes of Rufunsa region, the Fíngoè Supergroup
693 and the Chidzolomondo Complex are aligned in a NE-SW trend, indicating a possible spatial
694 continuity (Petry et al., 2022). In short, we support that granulite domains of the SIB
695 comprise arc-related volcano-sedimentary sequences, possibly passive margin too, intruded
696 by syn-orogenic granites, deep buried and metamorphosed under HT-LP conditions during
697 the collisional events of the Irumide Orogeny. The granulite domains were locally reworked

during the Pan-African orogenies. The final uplift and exhumation placed the high-grade metamorphic rocks side-by-side with their lower grade correlates, like the Chidzolomondo Complex and the Fíngoè Supergroup in the Tete Province.

5.4. Tectonic implications

The SIB is a wide Mesoproterozoic crustal area constituted by concordant belts of metamorphosed supracrustal complexes, with different lithodemic assemblages, and orogenic granitic suites. The magmatic arcs of the SIB are represented by metavolcano-sedimentary associations and granitic to gabbroic syn-orogenic suites recording the volcanic arc (island and/or continental) formation and evolution behind a subduction zone bordering the northern margin of Zimbabwe Craton (1350-1080 Ma). The protoliths of the dated granulite samples originated in the accretionary phase of the SIB. The final accretion and collision with the southern margin of the Bangweulu Craton, the passive margin sequences of the Irumide Belt, occurred at ca. 1080 Ma. The peak of metamorphism, estimated around 1060 Ma, was followed by the emplacement of voluminous late- to post-collisional granitoids and massive bimodal magmatism from 1060 to 1020 Ma (Westerhof et al., 2008). The Chidzolomondo Complex provided time constraints of the final evolution of the Irumide Orogeny, especially the metamorphic events, whilst the charnockites and gabbros mark the post-collisional stage. The compiled detrital, magmatic and metamorphic data presented in **Figure 14** support the timing of events.

5.3.1 Accretionary phase

The arc-related rocks of the SIB comprise metavolcano-sedimentary sequences and granitic to gabbroic syn-orogenic suites. Supposedly, the oldest Mesoproterozoic rocks of the belt are the layered basic to acidic metavolcanic rocks with subordinate, metavolcanoclastic, metaconglomerates, metapelites and calc-silicatic schists and gneisses (GTK Consortium,

2006; Westerhof et al., 2008; Petry et al., 2022). A plagiogranite dyke of 1393±22 Ma from the Chewore Complex (Oliver et al., 1998) and a felsic metavolcanic rock of 1327±6 Ma from the Fíngoè Complex (GTK Consortium, 2006) mark the time of ocean crust formation and the onset of subduction, respectively. The early volcanism probably occurred in juvenile island-arcs with limited crustal influence and precedes 100 Ma of apparent tectonic quiescence.

The detrital zircon from the ChC paragneiss sample mainly presented Mesoproterozoic ages broadly corresponding to the arc rocks of the SIB and setting the maximum depositional age at 1121±2 Ma. The narrow provenance spectrum and the age peak close to the presumed depositional age are characteristic of arc-related basins (Cawood et al. 2012). The granulitic paragneiss provenance pattern mimics those from the Zâmbuè, Fíngoè and Cazula complexes reported by Petry et al. (2022), indicating their association as arc-related basins. The Mesoproterozoic detrital zircons show positive εHf(t) signatures (+2 to +10) with limited influence of crustal material, favoring the proposed intra-oceanic arc setting and the accretionary phase.

With time, the volcanic arc edifice has grown and matured and its roots thoroughly invaded by syn-orogenic granitic batholiths and gabbroic intrusions with crystallization ages between 1201 and 1077 Ma (GTK Consortium, 2006, Manttari, 2008). The structural continuity of the metamorphic complexes and their concordant fabrics with the main magmatic foliations support the contemporaneity of the development of arc-related volcano-sedimentary complexes and the syn-orogenic magmatism. These stratigraphic relationships are well preserved and described in the Rufunsa region of the SIB (Goscombe et al., 2000; Johnson and Oliver, 2004; Johnson et al., 2007). We reported two new igneous ages in this range, metagabbro (1133±15 Ma) and the charnockitic gneiss (1097±3 Ma). The crystallization age of the metagabbro suggest a slightly older MDA for the ChC supracrustals.

747 The crystallization age of the charnockitic gneiss intruded in the ChC is coeval with the M_1
748 event dated in the paragneiss sample (1092±5 Ma). This metamorphic event must be related
749 with magma loading in the upper and mid crustal levels in the active arc setting.

750 **5.3.2. Continental collision**

751 Following arc-accretion, the final phase of Mesoproterozoic orogenic activity
752 corresponds to deformation of the arc edifice and regional orogenic collisional
753 metamorphism. Previous studies argued that the ocean closure and collision with the passive
754 margin sediments (Irumide Belt) of the southern border of Central Africa Craton occurred at
755 ca. 1040 Ma (De Waele et al., 2006; Johnson et al., 2006, 2007; Karmakar and Schenk,
756 2016). This assumption was based on the peak of tectonic activity in the SIB between ~1090-
757 1040 Ma (in Zambia regions), supposedly syn-orogenic, and the "migration" of the
758 magmatism toward the Irumide Belt between 1040-1020 Ma, soon after the continental
759 collision. In this scenario, the main peak of magmatism and metamorphism were related to
760 the ending of the accretionary phase in an evolved island arc, as evidenced by the mixed
761 juvenile and more evolved isotopic signatures. On the other hand, Westerhof et al. (2008) set
762 the collision around 1070 Ma, based on the post-collisional nature of the bimodal magmatism
763 in the Tete Province dated between ~1050-1020 Ma.

764 The set of U-Pb zircon ages of the SIB (igneous, metamorphic and detrital), support the
765 second hypothesis and set the collision even earlier, at ca. 1080 Ma. The metamorphic zircon
766 from the granulite samples yielded ages close to 1060 Ma, the inferred age for the peak
767 collisional metamorphism. The noticeable decrease in the magmatic activity between 1080-
768 1060 Ma marks the probable period of major crustal thickening. The HT-LP peak
769 metamorphic conditions of the SIB granulites suggests a hot collisional orogen like the
770 Himalayan orogen. The inherited thermal structure of the prolonged oceanic crust subduction
771 and the slab breakoff processes can be envisaged as a cause to the elevated thermal gradients

772 (Zhang et al., 2022).

773 **5.3.3. Late to post-collisional magmatism**

774 The late to post-collisional granitic magmatism shows ages between ca. 1060-1000 Ma
775 (GTK Consortium et al., 2006). Concurrently, the bimodal magmatism of the SIB initiated at
776 1050 Ma with the emplacement of the gabbro-anorthositic stratiform complex of the Tete
777 Suite and the charnockitic magmatism (Westerhof et al., 2008). The charnockitic magmatism
778 is prolonged with ages between 1050 to 1000 Ma (GTK Consortium, 2006; Alessio et al.,
779 2019b; Manda et al., 2019; Tsunogae et al., 2021), possibly extending until 949±13 Ma
780 (Bingen et al., 2009). We reported two new igneous ages in this range, a charnockite from
781 Castanho Suite (1026±4 Ma) and a gabbro from Rio Chiticula Gabbro (1026±9 Ma). The
782 Castanho Suite show A-type geochemical characteristics, interpreted to have been generated
783 in a late to post-orogenic extensional setting from 1050 Ma. The massive magma
784 underplating and the intrusion of high-T charnockitic melts caused the contact metamorphism
785 in the ChC (M3 metamorphic event).

786 The high thermal gradient in the collisional orogen triggered the crustal melting in the
787 Irumide Belt resulting in extensive S-type granitic magmatism and HT-LP metamorphism
788 from 1040 Ma (De Waele, 2006). The alleged diachronism in the magmatism of the Southern
789 Irumide Belt and Irumide Belt is not supported by the geochronological data. Instead, the
790 major peak of magmatism and metamorphism of both is simultaneous and evidently post-
791 collisional (**Fig. 15**), supporting the continental collision of Zimbabwe and Bangweulu
792 cratons around 1080-1070 Ma.

793 **6. Conclusions**

794 The U-Pb-Hf zircon data from the Chidzolomondo Complex granulites and Castanho
795 Suite charnockites and Rio Chiticula gabbro revealed insights on the evolution of the arc-

796 related basins, recording the accretionary related orogenic metmorphism and the transition to
797 syn-collisional metamorphism, succeeded by a broad post-collisional magmatism and
798 metamorphism of the SIB. The complex textural patterns of metamorphic overgrowths above
799 igneous and detrital zircon cores allowed to characterize the polyphasic metamorphic
800 evolution of the granulite belt. The well-defined young age mode of detrital zircon spectra
801 from the ChC paragneiss is characteristic of convergent tectonic settings and associated with
802 the accretionary magmatism. The dominant Late-Mesoproterozoic ages (1250-1100 Ma) and
803 the positive εHf(t) signatures confirm the predominance of arc sources and set the maximum
804 depositional age of the arc-related basin at 1121 Ma.
805 The syn-orogenic magmatism is related with the first metamorphic imprints in the
806 volcano-sedimentary sequence at ca. 1095 Ma (M_1 metamorphic event). In the light of the
807 new geochronological data, integrated with the published ages, we support that the Irumide
808 Orogeny continental collision occurred around 1080 Ma. This is a period of crustal
809 thickening, deformation and metamorphism of the supracrustal complexes under greenschist
810 to granulite conditions with apparent quiescence of the magmatism in the SIB. The zircon
811 grains from the granulite samples showed a concise range of metamorphic ages with peak at
812 ca. 1060 Ma (M_2 metamorphic event), characterizing the climax of the collisional
813 metamorphism or early post-collisional phase.
814 The major peak of magmatism in the SIB is characterized by high-K granitic
815 magmatism and bimodal basic and charnockitic magmatism. They reflect the partial melting
816 of crustal sources and the charnockitic magmatism over 50 Ma in the post-collisional
817 extensional setting. The emplacement of basic intrusions and high-T charnockitic melts at
818 1026 Ma is concurrent with the contact metamorphism in the ChC (M_3 metamorphic event).
819 The Chidzolomondo Complex comprises a deeply buried arc-related basin of the Southern
820 Irumide Belt in the Tete Province. Intimately associated with Castanho Suite charnockites,

they form a structurally bounded granulite/charnockite domain.

Acknowledgements

The authors acknowledge financial support from the Brazilian Research Council (CNPq), with PhD scholarship to T.S. Petry, productivity grant to R.P. Philipp and funding through Pró-Africa - 440126/2015-0. We appreciate the field support of the DNG and hope to keep working with our Mozambican friends Fátima Chaúque, Estevão Sumburane and Vicente Manjate. We thank the Geoscience Institute of the Universidade Federal do Rio Grande do Sul for facilities.

References

Alessio, B.L., Collins, A.S., Clark, C., Glorie, S., Siegfried, P.R., Taylor, R., 2019a. Age, origin and palaeogeography of the Southern Irumide Belt. Zambia. J. Geol. Soc. 176, 505–516. https://doi.org/10.1144/jgs2018-174.

Alessio, B. L., Collins, A. S., Siegfried, P., Glorie, S., De Waele, B., Payne, J. L., Archibald, D., 2019b. Neoproterozoic tectonic geography of the south-east Congo Craton in Zambia as deduced from the age and composition of detrital zircons. Geosci. Front. 10, 2045-2061. https://doi.org/10.1016/j.gsf.2018.07.005.

Andersen, D.J., Lindsley, D.H., 1988. Internally consistent solution models for Fe-Mg-Mn-Ti oxides; Fe-Ti oxides. Am. Mineral. 73, 714–726.

Andersen, T., Andersson, U.B., Graham, S., Åberg, G., Simonsen, S.L., 2009. Granitic magmatism by melting of juvenile continental crust: new constraints on the source of Palaeoproterozoic granitoids in Fennoscandia from Hf isotopes in zircon. J. Geol. Soc. 166, 233–247. https://doi.org/10.1144/0016-76492007-166.

Bartoli, O., 2017. Phase equilibria modelling of residual migmatites and granulites: An evaluation of the melt-reintegration approach. J. Metamorph. Geol. 35, 919–942.

https://doi.org/10.1111/jmg.12261.

Bingen, B., Jacobs, J., Viola, G., Henderson, I.H.C., Skår, Ø., Boyd, R., Thomas, R.J., Solli, A., Key, R.M., Daudi, E.X.F., 2009. Geochronology of the Precambrian crust in the Mozambique belt in NE Mozambique, and implications for Gondwana assembly. Precambr. Res. 170, 231–255. https://doi.org/10.1016/j.precamres.2009.01.005.

Bouvier, A., Vervoort, J.D., Patchett, P.J., 2008. The Lu–Hf and Sm-Nd isotopic composition of CHUR: constraints from unequilibrated chondrites and implications for the bulk composition of terrestrial planets. Earth Planet. Sci. Lett. 273, 48–57. https://doi.org/10.1016/j.epsl.2008.06.010.

Brown M. 2007. Metamorphic conditions in orogenic belts: A record of secular change. International Geology Review, 49, 193–234.

Brown, M. 2009. Metamorphic patterns in orogenic systems and the geological record. Cawood, P.A. & Kröner, A. (eds). Earth Accretionary Systems in Space and Time. The Geological Society, London, Special Publications, 318, 37-74.

Brown, M. 2010. Melting of the continental crust during orogenesis: the thermal, rheological, and compositional consequences of melt transport from lower to upper continental crust. Canadian J. Earth Sci., 47, 655-694.

Brown, M., Johnson, T. 2018. Invited Centennial Article: Secular change in metamorphism and the onset of global plate tectonics. American Mineralogist, 103, 181-196.

Brown, M., Johnson, T. 2019a. Metamorphism and the evolution of subduction on Earth. American Mineralogist, 104, 1065-1082.

Brown, M., Johnson, T. 2019b. Time's arrow, time's cycle: Granulite metamorphism and geodynamics. Mineralogical Magazine, 83, 323–338.

Black, L.P., Gulson, B.L., 1978. The age of the Mud Tank carbonatite, Strangways Range, Northern Territory. BMR J. Aust. Geol. Geophys. 3, 227-232.

870 Cawood, P.A., Chowdhury, P., Mulder, J.A., Hawkesworth, C.J., Capitanio, F.A.
871 Gunawardana, P.M., Nebel, O. 2022. Secular evolution of continents and the Earth
872 System. Rev. of Geophys. 60, e2022RG000789. https://doi.org/10.1029/2022RG000789
873 Cawood, P.A., Hawkesworth, C.J., Dhuime, B., 2012. Detrital zircon record and tectonic
874 setting. Geology 40, 875–878. https://doi.org/10.1130/G32945.1.
875 Chaúque, F.R., Cordani, U.G., Jamal, D.L., Onoe, A.T., 2017. The Zimbabwe Craton in
876 Mozambique: A brief review of its geochronological pattern and its relation to the
877 Mozambique Belt. J. Afr. Earth Sci. 129, 366-379.
878 https://doi.org/10.1016/j.jafrearsci.2017.01.021.
879 Chaúque, F.R., Cordani, U.G., Jamal, D.L., 2019. Geochronological systematics for the
880 Chimoio-Macossa frontal nappe in central Mozambique: Implications for the tectonic
881 evolution of the southern part of the Mozambique belt. J. Afr. Earth Sci. 150, 47-67.
882 https://doi.org/10.1016/j.jafrearsci.2018.10.013.
883 Connolly, J.A.D., 2005. Computation of phase equilibria by linear programming: A tool for
884 geodynamic modeling and its application to subduction zone decarbonation. Earth Planet.
885 Sci. Lett. 236, 524–541. https://doi.org/10.1016/j.epsl.2005.04.033
886 Coutts, D.S., Matthews, W.A., Hubbard, S.M., 2019. Assessment of widely used methods to
887 derive depositional ages from detrital zircon populations. Geosci. Front. 10(4), 1421–
888 1435.
889 Debon, F., Le Fort, P. 1983. A Chemical-Mineralogical Classification of Common Plutonic
890 Rocks and Associations. Transactions of the Royal Society of Edinburgh: Earth Sciences
891 73, 135-149. http://dx.doi.org/10.1017/S0263593300010117
892 De la Roche, H., Leterrier, J., Grandclaude, P., Marchal, M. 1980. A Classification of
893 Volcanic and Plutonic Rocks Using R1-R2 Diagrams and Major Element Analyses—Its
894 Relationships with Current Nomenclature. Chem. Geol. 29, 183-210.

http://dx.doi.org/10.1016/0009-2541(80)90020-0

De Waele, B., Liegeois, J.P., Nemchin, A.A., Tembo, F., 2006. Isotopic and geochemical evidence of Proterozoic episodic crustal reworking within the Irumide Belt of south central Africa, the southern metacratonic boundary of an Archaean Bangweulu Craton. Precambr. Res. 148, 225–256. https://doi.org/10.1016/j.precamres.2006.05.006.

Fuhrman, M.L., Lindsley, D.H., 1988. Ternary-Feldspar modeling and thermometry. Am. Mineral. 73, 201–215.

Fritz, H., Abdelsalam, M., Ali, K.A., Bingen, B., Collins, A.S., Fowler, A.R., Ghebreab, W., Hauzenberger, C.A., Johnson, P.R., Kusky, T.M., Macey, P., Muhongo, S., Stern, R.J., Viola, G., 2013. Orogen styles in the East African Orogen: A review of the Neoproterozoic to Cambrian tectonic evolution. J. Afr. Earth Sci. 86, pp. 65-106. https://doi.org/10.1016/j.jafrearsci.2013.06.004.

Frost, B. R., Frost, C.D. 2008. A geochemical classification for feldspathic igneous rocks. J. of Petrol. 49, 1955-1969. https://doi.org/10.1093/petrology/egn054

Frost, B. R., Frost, C.D. 2008. On Ferroan (A-type) Granitoids: their Compositional Variability and Modes of Origin. J. of Petrol. 52, 39-53. https://doi:10.1093/petrology/egq070

Gerdes, A., Zeh, A. 2006. Combined U–Pb and Hf isotope LA-(MC-)ICP-MS analyses of detrital zircons: Comparison with SHRIMP and new constraints for the provenance and age of an Armorican metasediment in Central Germany. Earth Plan. Sci. Lett. 249, 47-61. https://doi.org/10.1016/j.epsl.2006.06.039.

Gorton, M.P., Schandl, E.S. 2002. From Continents to Island Arc: A Geochemical Index of Tectonic Setting for Arc-Related and within Plate Felsic to Intermediate Volcanic Rocks. Canad. Mineralog. 38, 1065-1073. http://dx.doi.org/10.2113/gscanmin.38.5.1065

Goscombe, B., Fey, P., Both, F. Structural evolution of the Chewore Inliers, Zambezi Mobile

920 Belt, Zimbabwe. J. Afr. Earth Sci. 19(3), 199-224. https://doi.org/10.1016/0899-
921 5362(94)90061-2
922 Goscombe, B., Armstrong, R., Barton, J.M., 1998. Tectonometamorphic evolution of the
923 Chewore Inliers: Partial re-equilibration of high-grade basement during the Pan-African
924 Orogeny. J. Petrol. 39(7), 1347-1384. https://doi.org/10.1093/petroj/39.7.1347.
925 Goscombe, B., Armstrong, R., Barton, J., 2000. Geology of the Chewore Inliers, Zimbabwe:
926 constraining the mesoproterozoic to palaeozoic evolution of the Zambezi belt. J. of Afr.
927 Earth Sci. 30, 589-627. https://doi.org/10.1016/S0899-5362(00)00041-5.
928 Grantham, G.H., Ingram, B.A., Cronwright, M.C., Roberts, M.P., Macey, P.H., Manhica, V.,
929 Matola, R., Fernando, S., Cune, G., Correa, E., 2007. Explanatory notes of the 1:250.000
930 geological maps of sheets Furacungo (1433) and Ulongue (1434). Unpubl. Report,
931 National Directorate of Geology, Maputo, Mozambique, pp. 174.
932 Griffin, W.L., Pearson, N.J., Belousova, E., Jackson, S.E., Van Achterbergh, E., O'Reilly,
933 S.Y., Shee, S.R., 2000. The Hf isotope composition of cratonic mantle: LAM-MC-ICPMS
934 analysis of zircon megacrysts in kimberlites. Geochim. Cosmochim. Acta 64, 133–147.
935 https://doi.org/10.1016/S0016-7037(99)00343-9.
936 GTK Consortium, 2006. Map Explanation, Volume 4, Sheets Inhamambo (1430), Maluwera
937 (1431), Chifunde (1432), Zumbo (1530), Fíngoè-Mágoè (1531), Songo (1532), Cazula
938 (1533) and Zóbuè (1534). Unpubl. Report, National Directorate of Geology, Maputo,
939 Mozambique, pp. 457.
940 Hoskin, P.W.O., Black, L.P. 2000. Metamorphic zircon formation by solid-state
941 recrystallization of protolith igneous zircon. J. Metamorphic Geol. 18, 423–439.
942 https://doi.org/10.1046/j.1525-1314.2000.00266.x
943 Hauzenberger, C.A., Tenczer, V., Bauernhofer, A., Fritz, H., Klötzli, U., Kosler, J.,
944 Wallbrecher, E., Muhongo, S., 2014. Termination of the Southern Irumide Belt in

945 Tanzania: Zircon U/Pb geochronology. Precambr. Res. 255, 44–162.
946 https://doi.org/10.1016/j.precamres.2014.09.021.
947 Harley, S.L. 1998. Ultrahigh-temperature crustal metamorphism. Geological Society,
948 London, Special Publications, 138, 81-107.
949 Harley, S.L. 2008. Refining the P–T records of UHT crustal metamorphism. J. Metamorph.
950 Geol. 26, 125-154. https://doi.org/10.1111/j.1525-1314.2008.00765.x
951 Harley, S.L., Kelly, N.M., Möller, A. 2007. Zircon behaviour and the thermal histories of
952 mountain chains. Elements 3, 25-30. https://doi.org/10.2113/gselements.3.1.25
953 Holland, T., Powell, R., 1996. Thermodynamics of order-disorder in minerals: I. Symmetric
954 formalism applied to minerals of fixed composition. Am. Mineral. 81, 1413–1424.
955 https://doi.org/10.2138/am-1996-11-1214
956 Holland, T.J.B., Powell, R., 2011. An improved and extended internally consistent
957 thermodynamic dataset for phases of petrological interest, involving a new equation of
958 state for solids. J. Metamorphic Geology 29, 333–383. https://doi.org/10.1111/j.1525-
959 1314.2010.00923.x
960 Jackson, S.E., Pearson, N.J., Griffin, W.L., Belousova, E.A., 2004. The application of laser
961 ablation-inductively coupled plasma-mass spectrometry to in-situ U-Pb zircon
962 geochronology. Chem. Geol. 211, 47-69. https://doi.org/10.1016/j.chemgeo.2004.06.017.
963 Johnson, S.P., Oliver, G.J.H., 2004. Tectonothermal history of the Kaourera Arc, northern
964 Zimbabwe: implications for the tectonic evolution of the Irumide and Zambezi Belts of
965 South Central Africa. Precambr. Res. 130, 71–97.
966 https://doi.org/10.1016/j.precamres.2003.10.016.
967 Johnson, S.P., De Waele, B., Liyungu, A., 2006. U-Pb sensitive high-resolution ion
968 microprobe (SHRIMP) zircon geochronology of granitoid rocks in eastern Zambia: terrane
969 subdivision of the Mesoproterozoic Southern Irumide Belt. Tectonics 25 (6), TC6004.

970 https://doi.org/10.1029/2006TC001977.
971 Johnson, S.P., De Waele, B., Tembo, F., Katongo, C., Tani, K., Chang, Q., Iizuka, T.,
972 Dunkley, D., 2007. Geochemistry, geochronology and isotopic evolution of the Chewore-
973 Rufunsa terrane, southern Irumide belt: a Mesoproterozoic continental margin arc. J.
974 Petrol. 48, 1411–1441. https://doi.org/10.1093/petrology/egm025.
975 Karmakar, S., Schenk, V., 2016. Mesoproterozoic UHT metamorphism in the southern
976 irumide belt, Chipata, Zambia: petrology and in situ monazite dating. Precambr. Res. 275,
977 332-356. https://doi.org/10.1016/j.precamres.2016.01.018.
978 Kelsey, D.E., Hand, M. 2015. On ultrahigh temperature crustal metamorphism: Phase
979 equilibria, trace element thermometry, bulk composition, heat sources, timescales and
980 tectonic settings. Geoscience Frontiers, 6, 311-356.
981 Kunz, B., Regis, D., Engi, M. 2018. Zircon ages in granulite facies rocks: decoupling from
982 geochemistry above 850 C? Contrib. to Mineral. and Petrol. 173, 1–21.
983 http://dx.doi.org/doi:10.1007/s00410-018-1454-5
984 Laurent, A., Janousek, V., Magna, T., Schulmann, K., Mikova, J. 2014. Petrogenesis and
985 geochronology of a post-orogenic calc-alkaline magmatic association: the Žulová Pluton,
986 Bohemian Massif. J. of Geosci. 59, 415-440. http://doi.org/10.3190/jgeosci.176.
987 Laurent, A.T., Bingen, B., Duchene, S., Whitehouse, M.J., Seydoux-Guillaume, A. 2018.
988 Decoding a protracted zircon geochronological record in ultrahigh temperature granulite,
989 and persistence of partial melting in the crust, Rogaland, Norway. Contrib. to Mineral. and
990 Petrol. 173(4), 29. https://doi.org/10.1007/s00410-018-1455-4
991 Macey, P.H., Thomas, R.J., Grantham, G.H., Ingram, B.A., Jacobs, J., Armstrong, R.A.,
992 Roberts, M.P., Bingen, B., Hollick, L., de Kock, G.S., Viola, G., Bauer, W., Gonzales, E.,
993 Bjerkgård, T., Henderson, I.H.C., Sandstad, J.S., Cronwright, M.S., Harley, S., Solli, A.,
994 Nordgulen, Ø., Motuza, G., Daudi, E., Manhiça, V., 2010. Mesoproterozoic geology of the

995 Nampula Block, northern Mozambique: tracing fragments of Mesoproterozoic crust in the
996 heart of Gondwana. Precambr. Res. 182, 124–148.
997 https://doi.org/10.1016/j.precamres.2010.07.005.
998 Manda, B.W.C., Cawood, P.A., Spencer, C.J., Prave, T., Robinson, R., Roberts, N.M.W.,
999 2019. Evolution of the Mozambique Belt in Malawi constrained by granitoid U-Pb, Sm-
1000 Nd and Lu-Hf isotopic data. Gondwana Res. 68, 93-107.
1001 https://doi.org/10.1016/j.gr.2018.11.004.
1002 Mänttäri, I., 2008. Mesoarchean to lower Jurassic U-Pb and Sm-Nd ages from NW
1003 Mozambique. Geol. Surv. Finl. Spec. Paper 48, 81–119.
1004 Oliver, G., Johnson, S., Williams, I., Herd, D., 1998. Relict 1.4 Ga oceanic crust in the
1005 Zambezi Valley, northern Zimbabwe: evidence for Mesoproterozoic supercontinental
1006 fragmentation. Geology. 26, 571-573. https://doi.org/10.1130/0091-
1007 7613(1998)026%3C0571:RGOCIT%3E2.3.CO;2.
1008 Patiño Douce, A.E., Harris, N., 1998. Experimental constraints on Himalayan anatexis. J.
1009 Petrol. 39, 689–710. https://doi.org/10.1093/petroj/39.4.689.
1010 Pearce, J.A. 1982. Trace element characteristics of lavas from destructive plate boundaries.
1011 Trace element characteristics of lavas from destructive plate boundaries. Andesites., 8
1012 (1982), pp. 528-548
1013 Pearce, J.A 1996. Sources and settings of granitic rocks. Episodes 19 (4), 120-125.
1014 https://doi.org/10.18814/epiiugs/1996/v19i4/005
1015 Petry, T.S., Philipp, R.P., Jamal, D.L., Lana, C., Alckmin, A.R. U-Pb and Lu-Hf zircon data
1016 of the Grenvilian arc-related Zâmbué, Fíngoè and Cazula supracrustal complexes,
1017 Southern Irumide Belt, NW Mozambique. Precambr. Res. 381, 106860.
1018 https://doi.org/10.1016/j.precamres.2022.106860.
1019 Rubatto, D. 2017. Zircon: The Metamorphic Mineral. Rev. Mineral. and Geochem. 83, 261-

295. https://doi.org/10.2138/rmg.2017.83.9

Santos, M.M., Lana, C., Scholz, R., Buick, I., Schmitz, M.D., Kamo, S.L., Gerdes, A., Corfu, F., Tapster, S., Lancaster, P., Storey, C.D., Basei, M.A.S., Tohver, E., Alkmim, A., Nalini, H., Krambrock, K., Fantini, C., Wiedenbeck, M., 2017. A new appraisal of Sri Lankan BB Zircon as reference material for LA- ICP-MS U-Pb geochronology and Lu-Hf isotope tracing. Geostand. Geoanal. Res. 41(3), 35-358. https://doi.org/10.1111/ggr.12167

Sarafian, E., Evans, R.L., Abdelsalam, M.G., Atekwana, E., Elsenbeck, J. Jones, A.G., Chikambwe,E. 2018. Imaging Precambrian lithospheric structure in Zambia using electromagnetic methods. Gondwana Res. 54, pp. 38–49. https://doi.org/10.1016/j.gr.2017.09.007.

Sláma, J., Kosler, J., Condon, D.J., Crowley, J.L., Gerdes, A., Hanchar, J.M., Horstwood, M.S., Morris, G.A., Nasdala, L., Norberg, N., Schaltegger, U., 2008. Plešovice zircon- a new natural reference material for U-Pb and Hf isotopic microanalysis. Chem. Geol. 249, 1-35. https://doi.org/10.1016/j.chemgeo.2007.11.005.

Thomas, R.J., Spencer, C., Bushi, A.M., Baglow, N., Boniface, N., de Kock, G.S., Horstwood, M.S.A., Hollick, L., Jacobs, J., Kajara, S., Kamihanda, G., Key, R.M., Maganga, Z., Mbawala, F., McCourt, W.J., Momburi, P., Moses, F., Mruma, A., Myambilwa, Y., Roberts, N.M.W., Saidi, H., Nyanda, P., Nyoka, K., Millar, I., 2016. Geochronology of the central Tanzania Craton and its southern and eastern orogenic margins. Precambr. Res. 277, pp. 47-67. https://doi.org/10.1016/j.precamres.2016.02.008.

Tsunogae, T., Uthup, S., Nyirongo, M.W., Takahashi, K., Rahman, M.S., Liu, Q., Takamura, Y., Tsutsumi, Y. 2021. Neoproterozoic crustal growth in southern Malawi: new insights from petrology, geochemistry, and U–Pb zircon geochronology, and implications for the Kalahari Craton–Congo Craton amalgamation. Precam. Res. 352, 106007. https://doi.org/10.1016/j.precamres.2020.106007

1045 Van Achterberg, E. Ryan, C., Jackson, S., Griffin, W., 2001. Data reduction software for LA-
1046 ICP-MS. P. Sylvester (Ed.), Laser Ablation ICP-MS in the Earth Science – Principles and
1047 Applications, Mineralogical Association of Canada, Newfoundland, pp. 239-243.
1048 Vavra, G., Gebauer, D., Schmid, R., Compston. W. 1996. Multiple zircon growth and
1049 recrystallization during polyphase Late Carboniferous to Triassic metamorphism in
1050 granulites of the Ivrea Zone (Southern Alps): an ion microprobe (SHRIMP) study.
1051 Contrib. Mineral. Petrol. 122, 337-358. https://doi.org/10.1007/s004100050132
1052 Vavra, G., Schmid, R., Gebauer, D. 1999. Internal morphology, habit and U-Th-Pb
1053 microanalysis of amphibolite-to-granulite facies zircons: geochronology of the Ivrea Zone
1054 (Southern Alps). Contrib. Mineral. Petrol. 134, 380-404.
1055 https://doi.org/10.1007/s004100050492
1056 Vermeesch, P., 2018. IsoplotR: A free and open toolbox for geochronology. Geoscience
1057 Frontiers 9, 1479-1493. https://doi.org/10.1016/j.gsf.2018.04.001
1058 Vermeesch, P., 2021. Maximum depositional age estimation revisited. Geosciences Frontiers
1059 12, 843–850. https://doi.org/10.1016/j.gsf.2020.08.008
1060 Yakymchuck, C., Kirkland, C.L., Clark, C. 2018. Th/U ratios in metamorphic zircon. J.
1061 Metamor. Geol. 36, 715-737. https://doi.org/10.1111/jmg.12307
1062 Westerhof, A.P., Lehtonen, M.I., Mäkitie, H., Manninen, T., Pekkala, Y., Gustafsson, B.,
1063 Tahon, A., 2008. The Tete-Chipata Belt: a new multiple terrane element from western
1064 Mozambique and southern Zambia. Geol. Surv. Finl. Spec. Paper 48, 145–166.
1065 Whitney, D.L., Evans B.W. 2010. Abbreviations for names of rock-forming minerals.
1066 American Mineralogist, 95, 185-187. DOI: 10.2138/am.2010.3371.
1067 White, R.W., Powell, R., Halpin, J.A., 2004. Spatially focussed melt formation in aluminous
1068 metapelites from Broken Hill, Australia. J. Metamorphic Geololgy 22, 825–845.
1069 https://doi.org/10.1111/j.1525-1314.2004.00553.x

White, R.W., Powell, R., Holland, T.J.B., 2001. Calculation of partial melting equilibria in the system Na2O-CaO-K2O-FeO-MgO-Al2O3-SiO2-H2O (NCKFMASH). J. Metamorphic Geology 19, 139–153. https://doi.org/10.1046/j.0263-4929.2000.00303.x

White, R.W., Powell, R., Johnson, T.E., 2014. The effect of Mn on mineral stability in metapelites revisited: new a-x relations for manganese-bearing minerals. J. Metamorphic Geology. 32, 809–828. https://doi.org/10.1111/jmg.12095

Whitney, D.L., Evans, B.W., 2010. Abbreviations for Names of Rock-Forming Minerals. American Mineralogist 95(1), 185-187. https://doi.org/10.2138/am.2010.3371

Zhang, H., Zengqian, H., Rolland, Y., Santosh, M., 2022. The cold and hot collisional orogens: Thermal regimes and metallogeny of the Alpine versus Himalayan-Tibetan belts. Ore Geol. Rev. 141, 104671. https://doi.org/10.1016/j.oregeorev.2021.104671

Figures captions

Figure 1. A) Location in the African continent. B) Location of Mozambique in southern Africa. C) Simplified tectonic map of southern Africa, adapted from Hanson (2003). Red dashed lines in the Kalahari Craton region show inferred position of the tectonic boundaries. Legend: 1: western edges of the Archean cratons; 2: boundaries between Eburnean and Grenvillian orogenic belts; 3: boundaries between Grenvillian and Pan-African orogenic belts; 4: western edge of the Pan-African orogenic belts. Legend of tectonic and stratigraphic units: ATZ- Angònia Thrust Zone; BA- Bárue Arc, CK- Choma-Kalomo Block, LB- Limpopo Belt, MB- Magondi Belt, MzB- Mozambique Belt, R- Rehoboth Inlier, RI- Richtersveld Terrane, S- Sinclair Sequence, UB- Ubendian Belt, UsB- Usagaran Belt, ZB- Zambezi Belt. Shear Zones: ASZ- Angônia, MSZ- Mwembeshi, SSZ- Sanangoè. The black rectangle shows the location of the map of the figure 2.

Figure 2. Simplified tectonic map of the Southern Irumide Belt with lithological units adapted and modified from Johnson et al., (2006, 2007) and GTK Consortium (2006). In the

1095 boxes, compiled U-Pb ages (references available in Supplementary Data - Table 5). Legend
1096 of the lithostratigraphic units: CC- Chewore Complex, CG- Cazula Group, ChC-
1097 Chidzolomondo Complex, CpC- Chipata Complex, FS- Fíngoè Supergroup, MC- Mualadzi
1098 Complex, RT- Rio Tsafuro Granite, SC- Serra da Chiúta Granite, SD- Serra Danvura Granite.
1099 Structural legend: ASZ- Angónia Thrust Zone, MSZ- Mwembeshi Shear Zone, MT-
1100 Mchimadzi Thrust, NSZ- Nyamadzi Shear Zone, SSZ- Sanangoè Shear Zone. The black
1101 rectangle shows the location of the map of the figure 3.

1102 **Figure 3.** Geological map of the Chidzolomondo Complex region. Extracted and modified
1103 from GTK Consortium (2006).

1104 **Figure 4**. Photomicrographs of the MB-146 mc-crd-bt-grt-qz-pl-opx gneiss sample. A)
1105 Interleaving of felsic bands with granoblastic texture constituted by pl+qz+mc and
1106 crd+qz+pl+opx, interspersed with mafic-rich levels with opx+grt+bt., B) and C) Detail of the
1107 compositional banding of metapelitic gneisses, D), E) Detail of relict compositional banding
1108 (S 0), F), G) H) Detail of felsic levels with polygonal granoblastic texture and garnet
1109 porphyroblasts. The yellow arrows show thin quartz lamellae indicative of partial melting, I)
1110 Cordierite (crd) grain detail, J) Opx detail, K) Partial melting features of biotite defined by
1111 thin quartz lamellae, L) Opx+crd+plag assembly. Yellow arrows indicate thin films of albite
1112 suggesting partial melting of plagioclase.

1113 **Figure 5**. Photomicrographs of the MB-144 metagabbro sample. A), B) Granoblastic texture
1114 with plagioclase+opx+diopside, C) Relict crystal of augite surrounding by granoblastic
1115 plagioclase, D) Relict of euhedral olivine involving by augite and hornblende in a coronitic
1116 texture, E), F), G), H) Photomicrographs of the MB-148 charnockitic gneiss sample.
1117 Metapelitic gneiss cutting by injection of deformed charnockite.

1118 **Figure 6**. Classification diagrams of Chidzolomondo Complex gneisses and Castanho Suite
1119 charnockites.

1120 **Figure 7**. Trace elements and REE spider diagrams of Chidzolomondo Complex gneisses and
1121 Castanho Suite charnockites.

1122 **Figure 8**. Geotectonic diagrams of Chizolomondo Complex gneisses and Castanho Suite
1123 charnockites.

1124 **Figure 9**. A) Isochemical phase diagram of mc-crd-bt-grt-qz-pl-opx gneiss (sample MB-146)
1125 with metamorphic peak assemblage defined by garnet + melt + opx + biotite + cordierite +
1126 feldspar + mf + quartz + rutile. B) Chemical composition profile of the analyzed garnet and
1127 the BSE image.

1128 **Figure 10**. CL images of representative zircon grains from the analyzed samples. A) Mc-crd-
1129 bt-grt-qz-pl-opx gneiss (MB-146); B) Metagabbro sample (MB-144); C) Charnockitic gneiss
1130 (MB-148); D) Charnockite (MB-141). The circles show the spot location of the U-Pb and Lu-
1131 Hf analysis. Legend of the spot results. First line: number of the analyzed spot in the data
1132 table; Second line: U-Pb age; Third line: epsilon Hf(t) value.

1133 **Figure 11**. A) Wetherhill concordia diagram of the U-Pb analysis (concordant and
1134 discordant) from sample MB-146 and the concordia ages; B) Weighted mean average
1135 diagram of the concordant ages with zircon grains showing the analysis domains; C)
1136 Histogram and radial plots of the detrital ages.

1137 **Figure 12**. A) Wetherill concordia diagram of the U-Pb analysis (concordant and discordant)
1138 from sample MB-144 and the concordia ages; B) Weighted mean average diagram of the
1139 concordant ages of sample MB-144 with zircon grains showing the analysis domains; C)
1140 Wetherill concordia diagram of the U-Pb analysis (concordant and discordant) from sample
1141 MB-148 and the concordia ages; B) Weighted mean average diagram of the concordant ages

1142 of sample MB-148 with zircon grains showing the analysis domains.

1143 **Figure 13**. A) Wetherill concordia diagram of the U-Pb analysis (concordant and discordant)
1144 from sample MB-141 and the concordia age; B) Wetherill concordia diagram of the U-Pb
1145 analysis (concordant and discordant) from sample MB-141 and the concordia age of the most
1146 concordant data.

1147 **Figure 14**. Diagram εHf versus U-Pb ages. The average crust fields were calculated using the
1148 average continental crust $^{176}Lu/^{177}Hf$ ratio of 0.015 (Griffin et al., 2004) and the black dashed
1149 lines classify fields of juvenile material (0–5 Ɛ-units below DM), moderately juvenile (5–12
1150 Ɛ-units below DM) and evolved (> 12 Ɛ-units below DM) like proposed by Reimann et al.
1151 (2010).

1152 **Figure 15**. Kernel Density Plots (KDP) of compiled detrital, igneous and metamorphic U-Pb
1153 age data of the SIB. The symbologies represent the absolute ages of the samples and the
1154 references are available in Supplementary Data - Table 5.

1155

1156

1157

Figure 1

Click here to access/download;Figure;Figure 1.tif

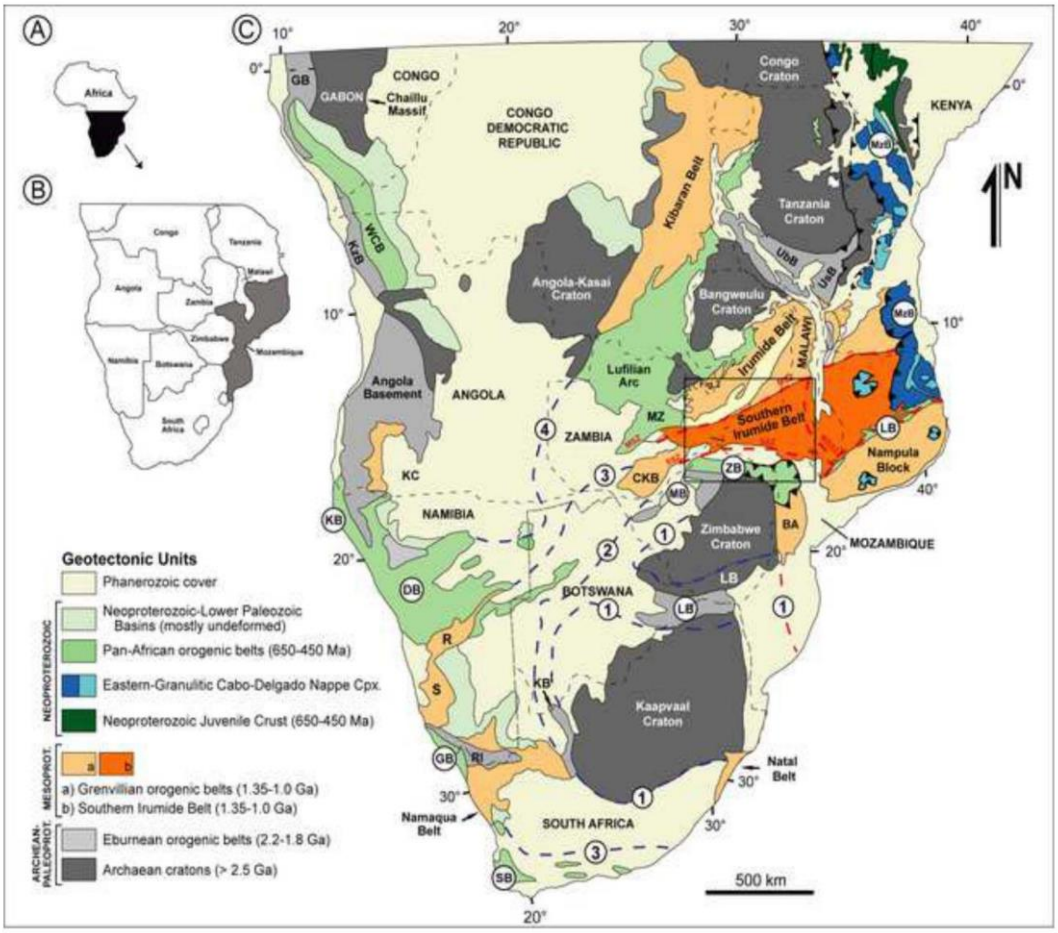

Figure 2

Click here to access/download;Figure;Figure 2.tif

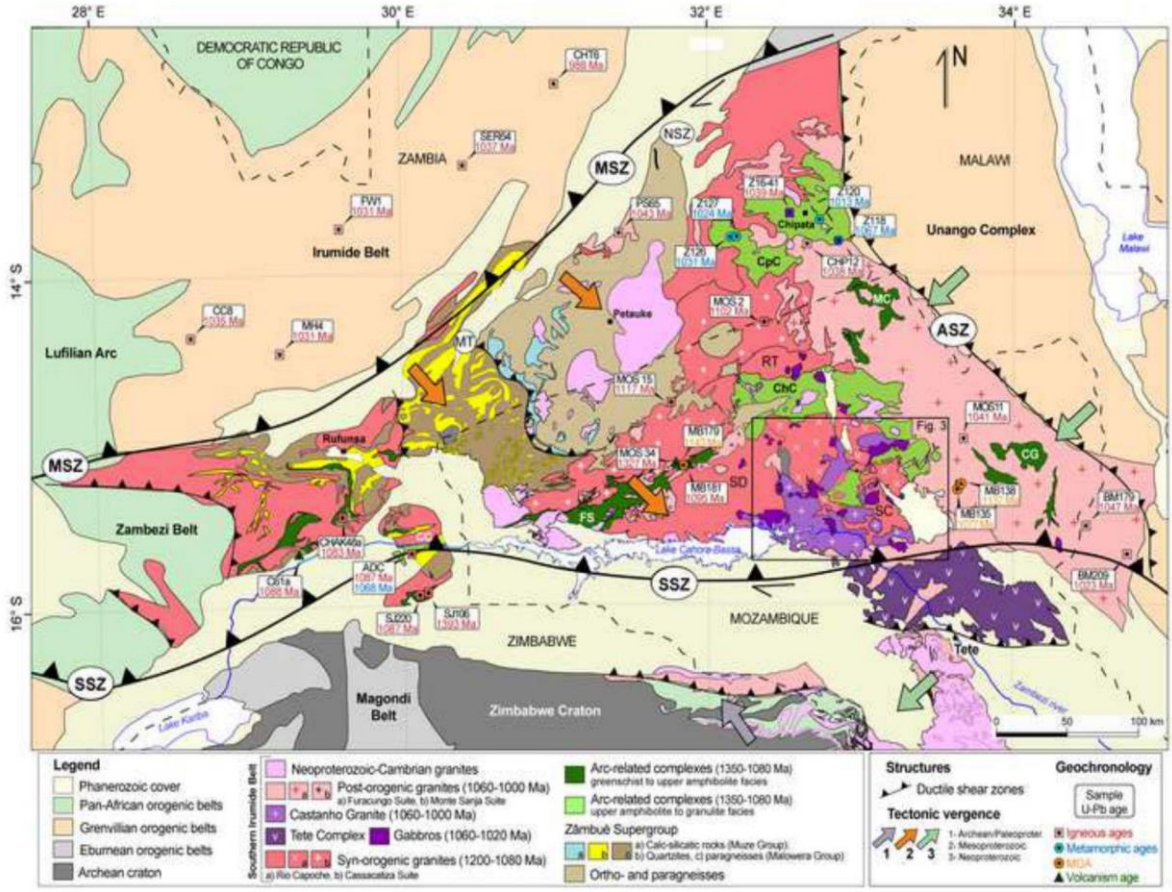

Figure 3

Click here to access/download;Figure;Figure 3.tif

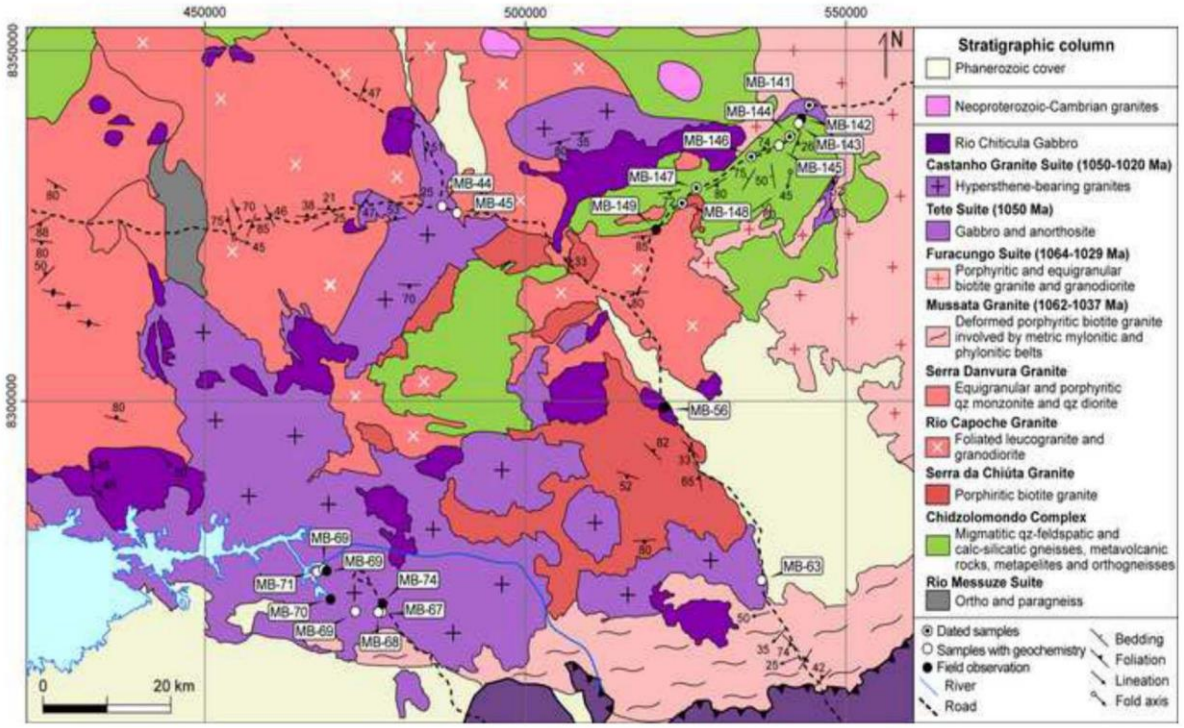

Figure 4

Click here to access/download;Figure;Figure 4.tif

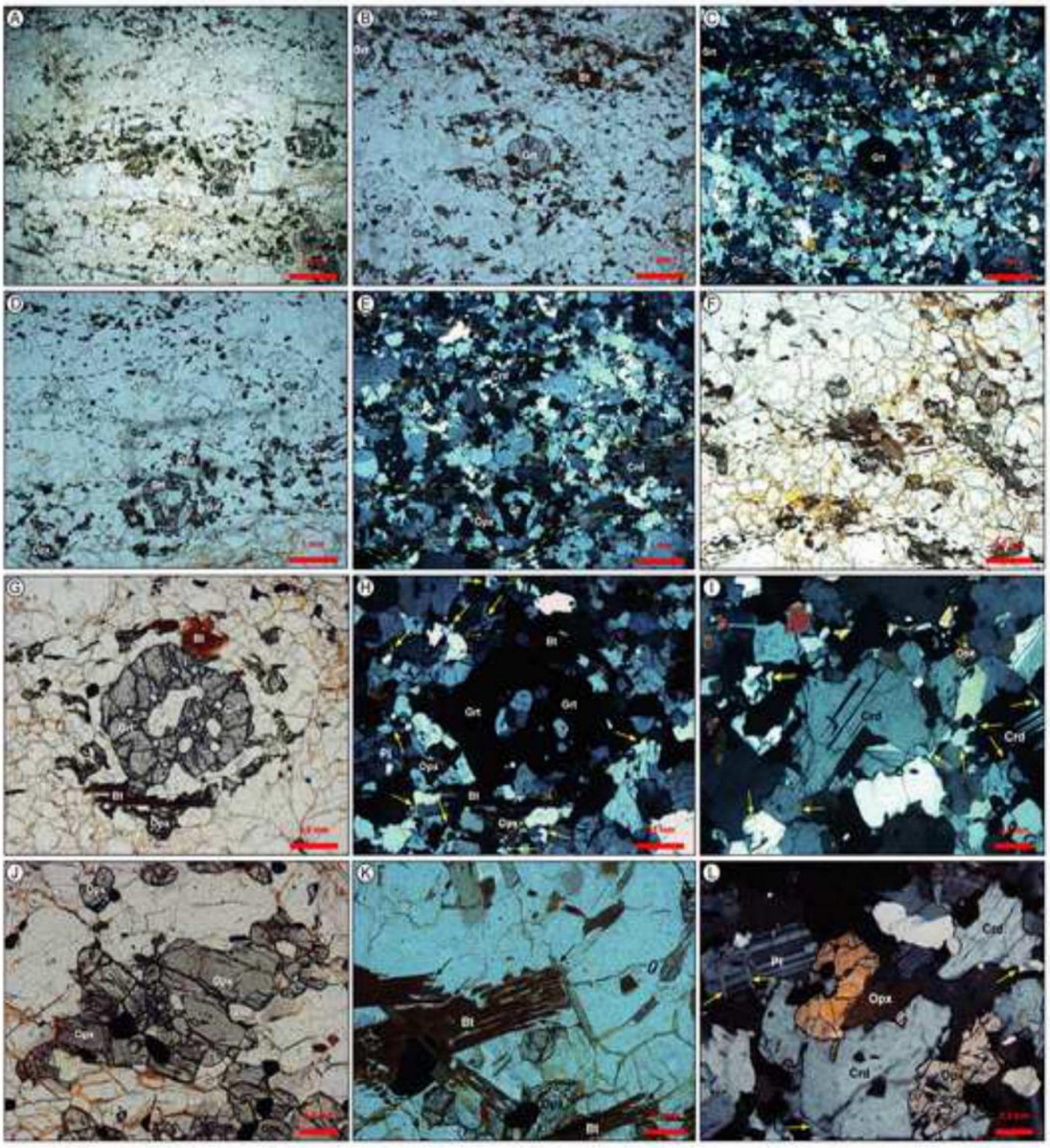

Figure 5

Click here to access/download;Figure;Figure 5.tif

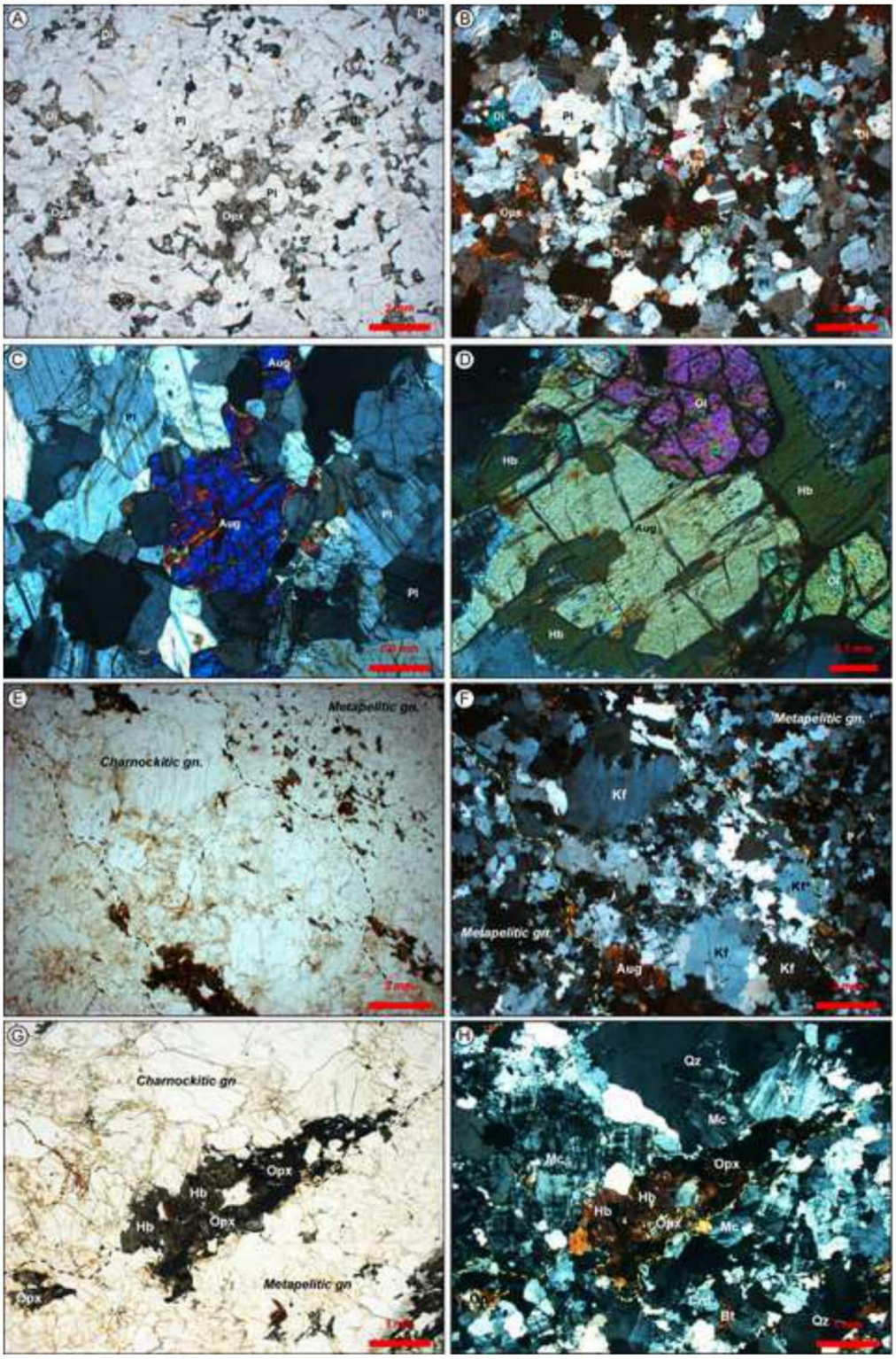

Figure 6

Click here to access/download;Figure;Figure 6.tif

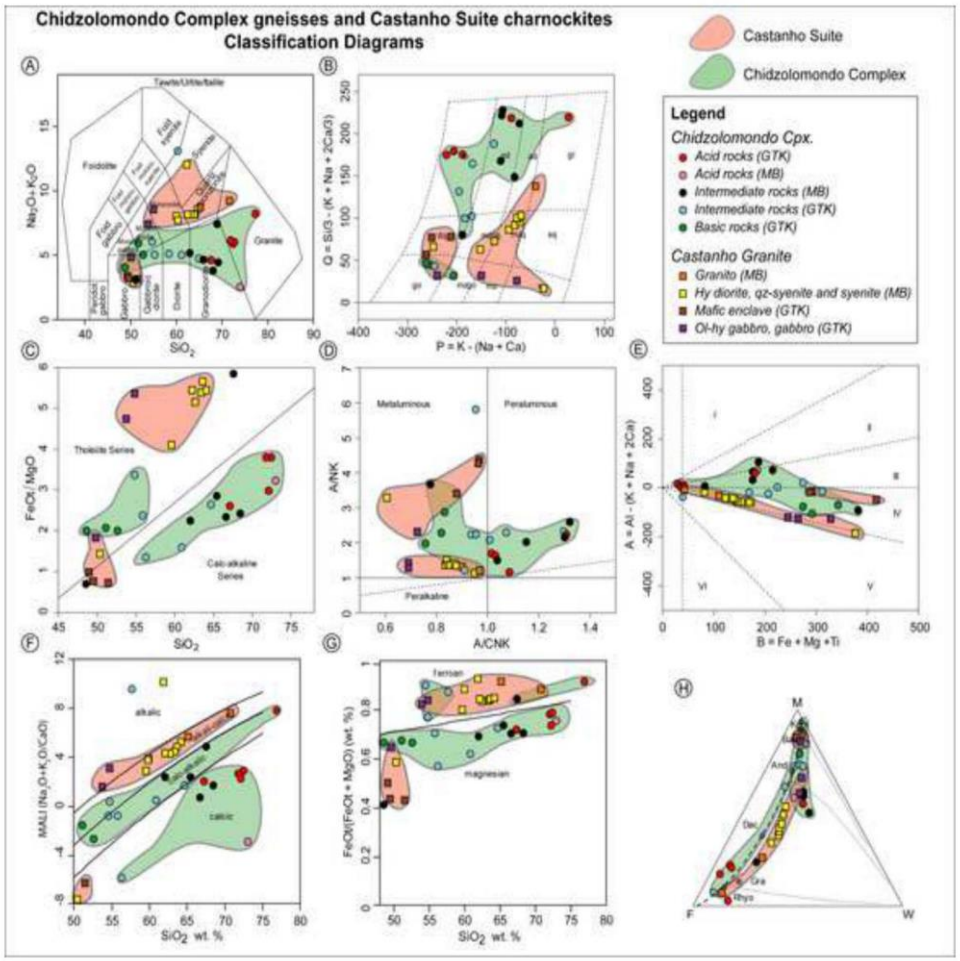

Figure 7

Click here to access/download;Figure;Figure 7.tif

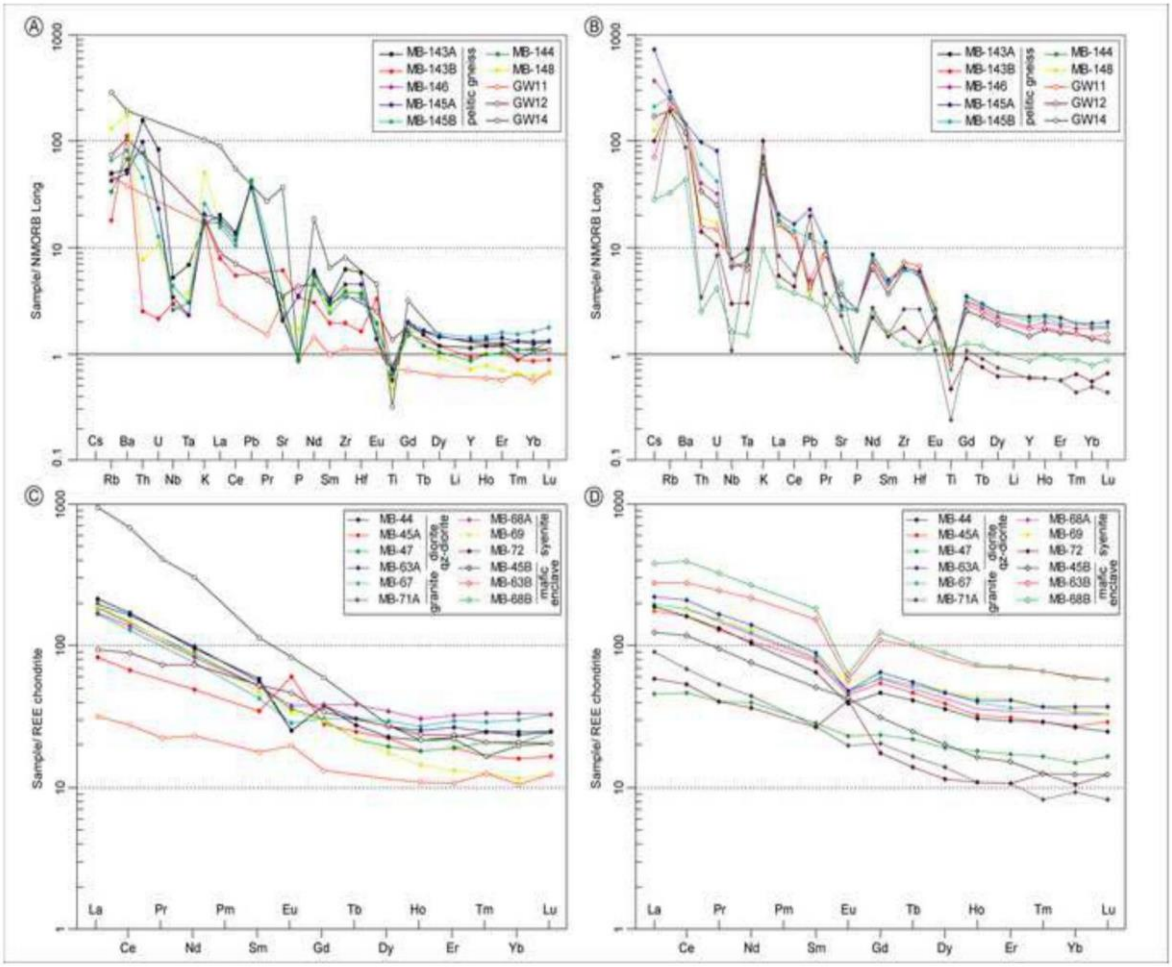

Figure 8

Click here to access/download;Figure;Figure 8.tif

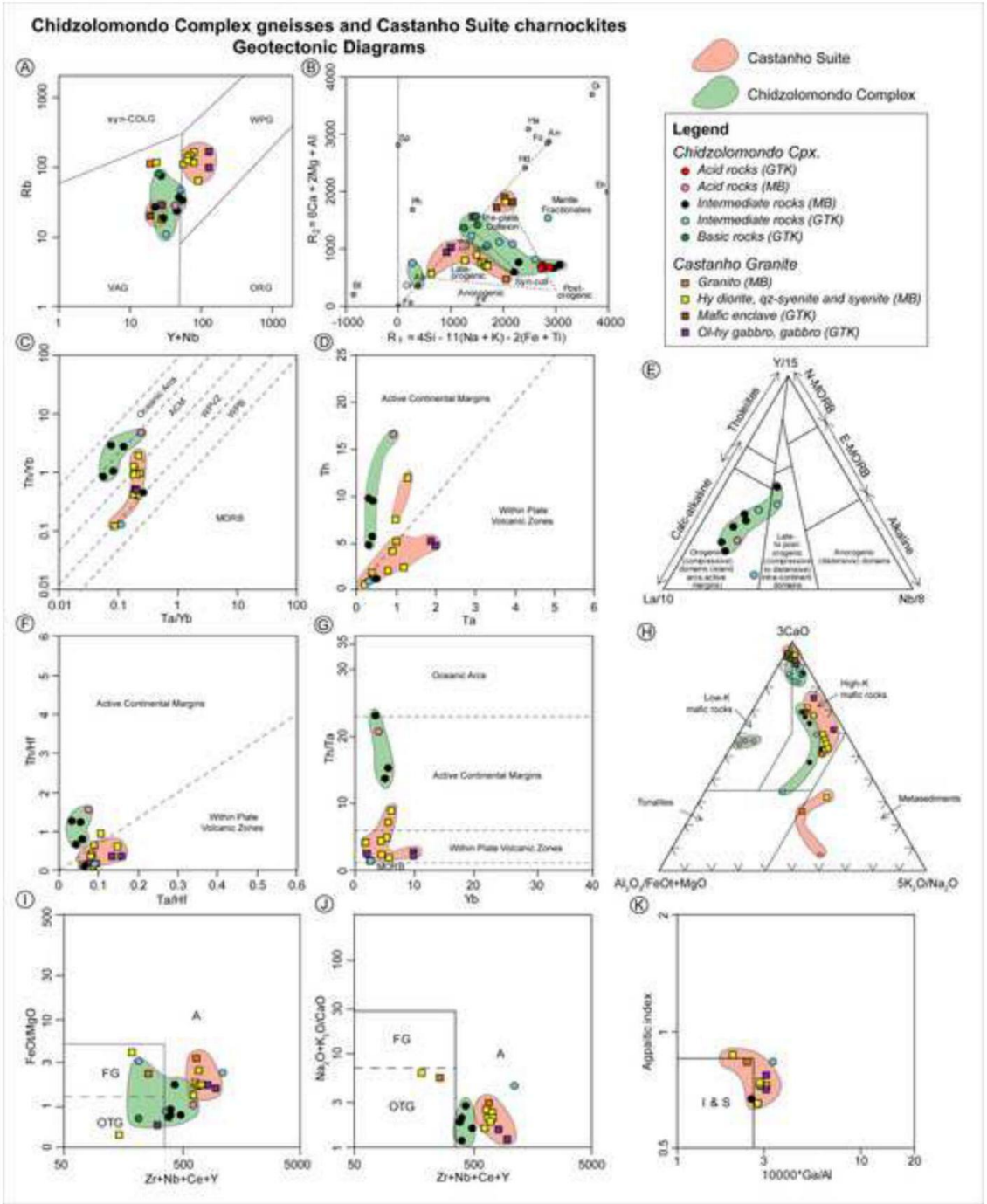

Figure 9

Click here to access/download;Figure;Figure 9.tif

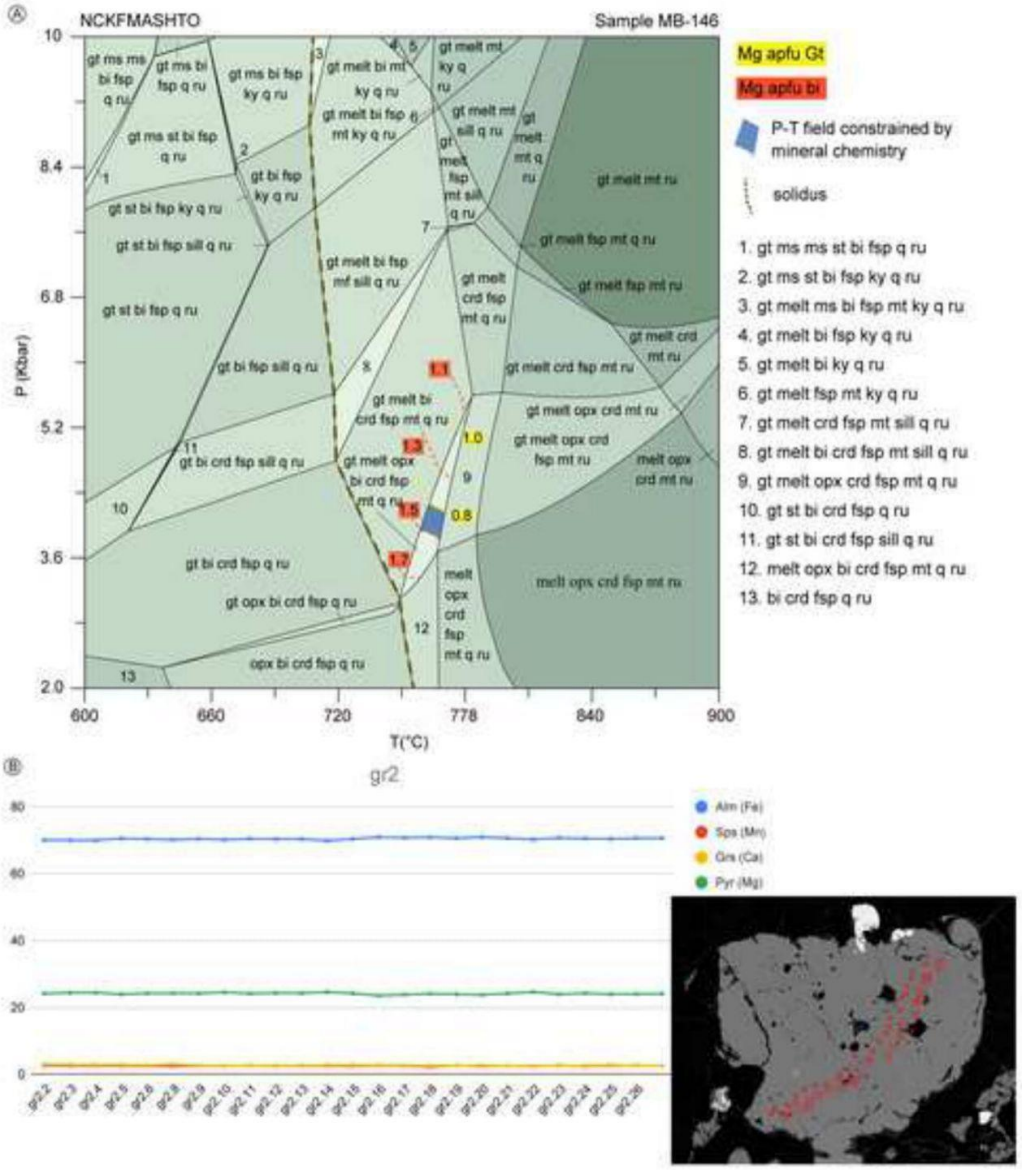

Figure 10

Click here to access/download;Figure;Figure 10.tif

Figure 11

Click here to access/download;Figure;Figure 11.tif

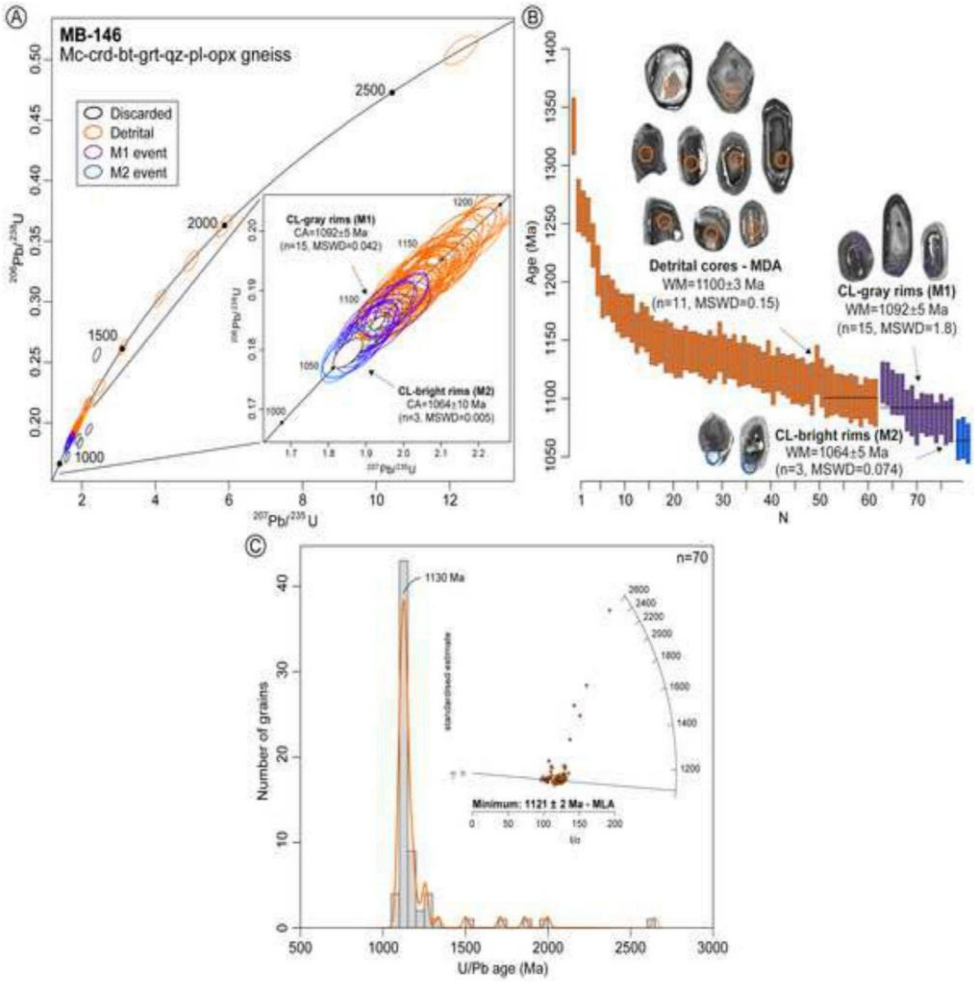

Figure 12

Click here to access/download;Figure;Figure 12.tif

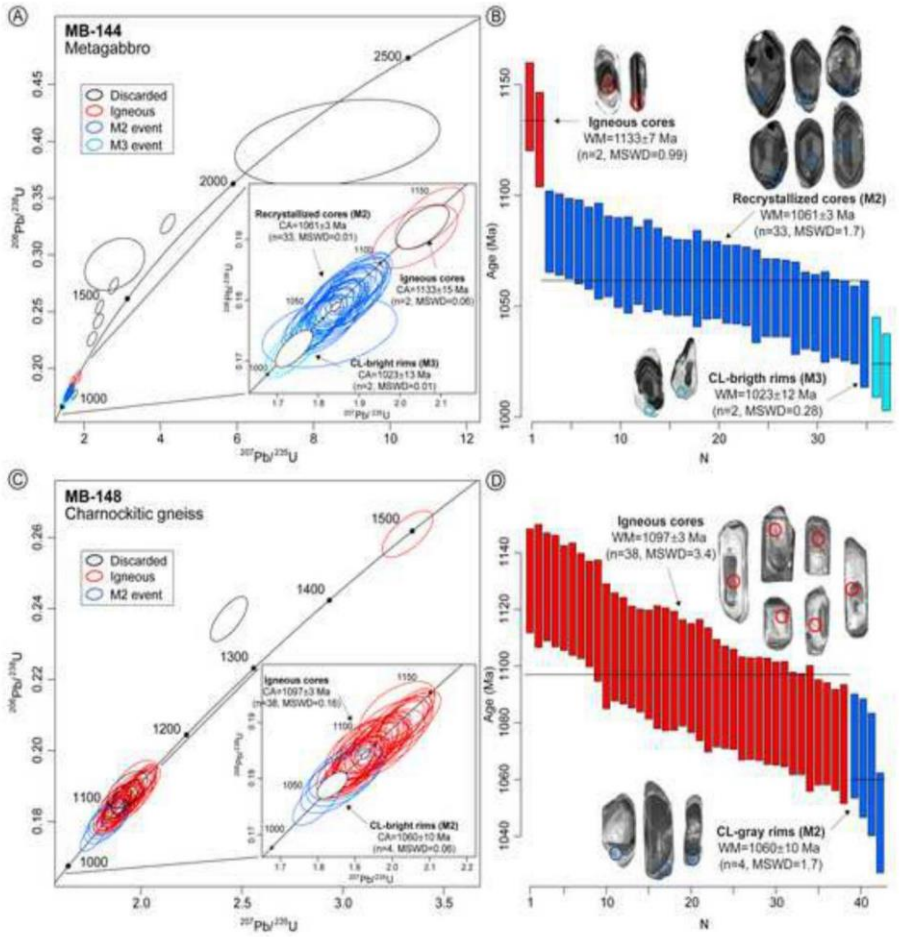

Figure 13

Click here to access/download;Figure;Figure 13.tif

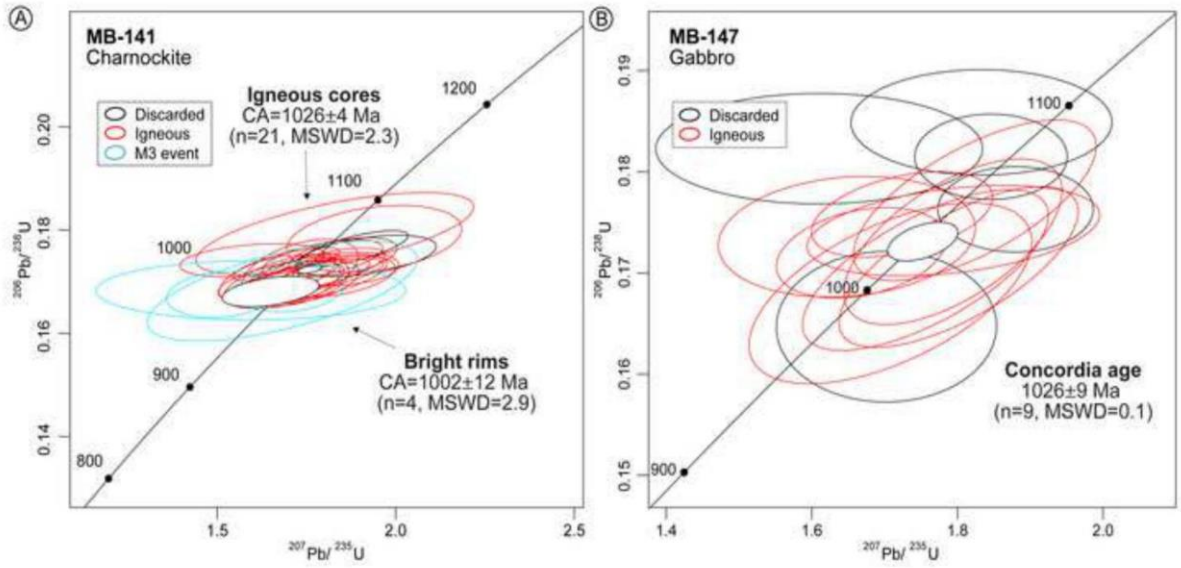

Figure 14

Click here to access/download;Figure;Figure 14.tif

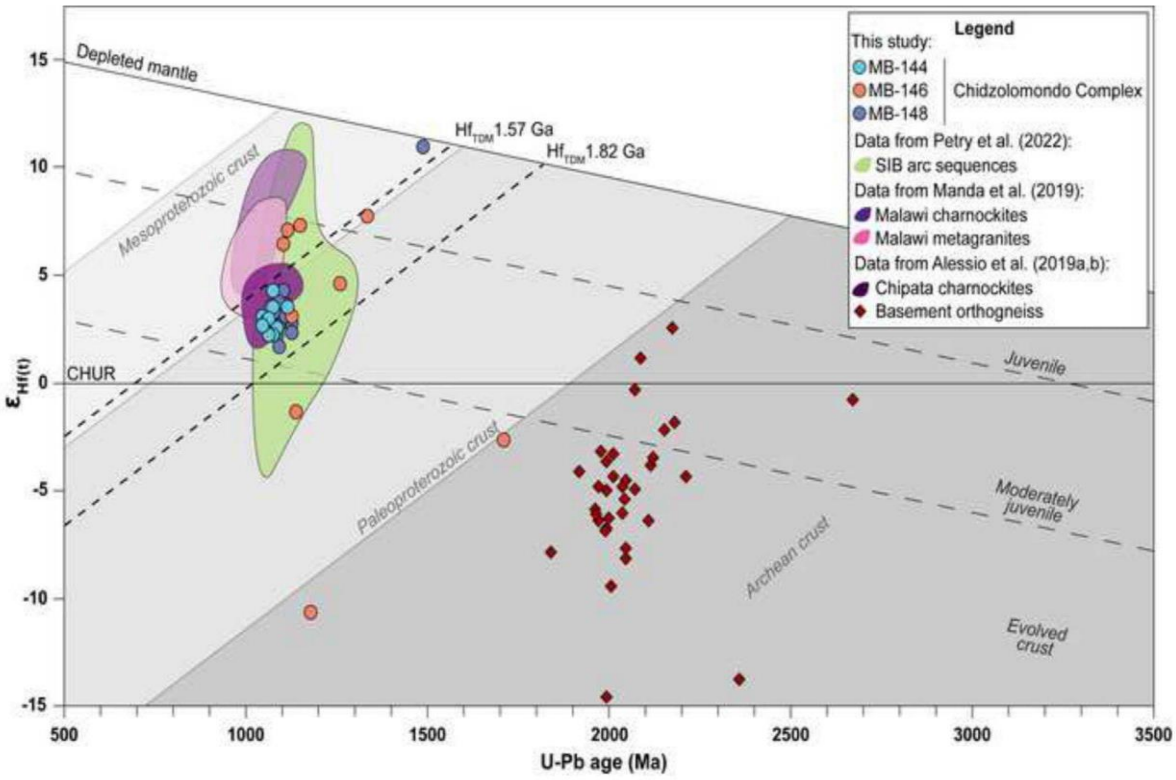

Figure 15

Click here to access/download;Figure;Figure 15.tif

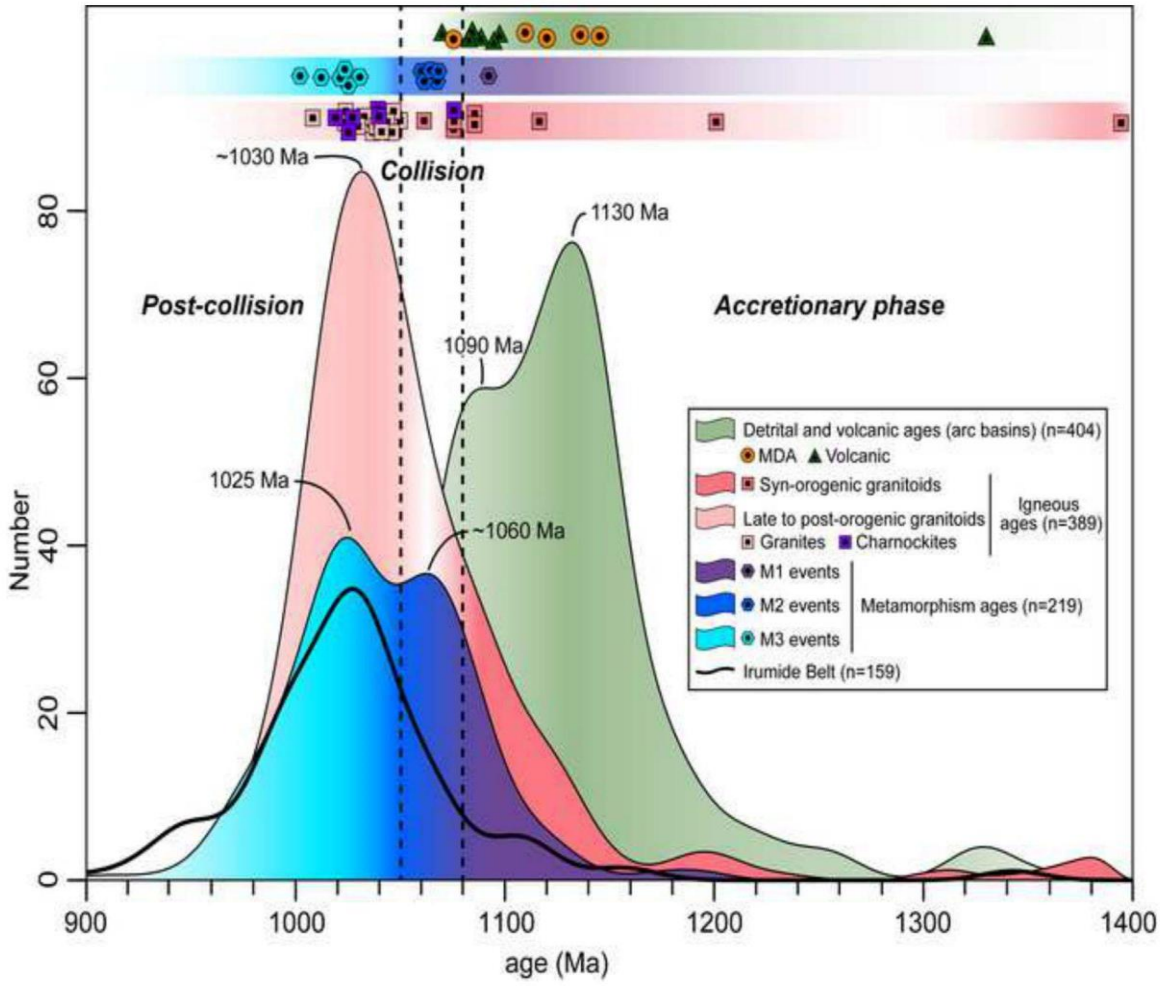

Declaration of interests

☒The authors declare that they have no known competing financial interests or personal relationships that could have appeared to influence the work reported in this paper.

☐The authors declare the following financial interests/personal relationships which may be considered as potential competing interests:

Thales Sebben Petry: Conceptualization, Data curation, Formal analysis, Investigation, Methodology, Validation, Visualization, Writing – original draft, Writing – review & editing.

Ruy Paulo Philipp: Conceptualization, Data curation, Formal analysis, Investigation, Methodology, Validation, Visualization, Writing – original draft, Writing – review & editing, Funding acquisition.

Dina Cabrita: Data curation, Formal analysis, Investigation, Methodology, Validation, Visualization, Writing – original draft

Daud Liace Jamal: Conceptualization, Investigation

Romulo Machado: Conceptualization, Investigation

Cristiano de Carvalho Lana: Methodology, Data curation

7. ANEXOS

Artigo 1.

Supplementary Data Table S1. Results of the LA-ICP-MS U-Pb zircon analysis

* concentration uncertainty ca. 10%
** data corrected/not corrected for common-Pb
*** Concordance calculated as (206Pb-238U age/207Pb-206Pb age)*100
Decay constants of Jaffey et al. (1971) used
The bold typed analysis were used to calculate the MDAs

Session	U-Pb spot	Comm 206Pb	U (µg g-1)*	Th/U	Isotope ratio** 207Pb 206Pb	±2s (%)	207Pb 235U	±2s (%)	206Pb 238U	±2s (%)	Rho	Ages 207Pb 206Pb	±2s (Ma)	206Pb 238U	±2s (Ma)	207Pb 235U	±2s (Ma)	Conc***
MB-182																		
2	**115**	**0,0079**	**235,68**	**0,59**	**0,07567**	**2,03515**	**1,91053**	**3,73384**	**0,18311**	**3,13045**	**0,83840**	**1086**	**41**	**1084**	**31**	**1085**	**25**	**100**
2	**7**	**1,0000**	**314,39**	**0,51**	**0,07575**	**3,31630**	**1,94494**	**4,63504**	**0,18622**	**3,23816**	**0,69863**	**1088**	**66**	**1101**	**33**	**1097**	**32**	**101**
2	89	0,0008	187,11	0,52	0,07576	2,05915	1,86996	3,69541	0,17902	3,06854	0,83037	1089	41	1062	30	1071	25	99
2	92	0,0609	200,83	0,49	0,07597	2,03335	1,88213	3,71861	0,17967	3,11344	0,83726	1094	41	1065	31	1075	25	99
2	**9**	**1,0000**	**161,94**	**0,45**	**0,07599**	**3,32170**	**1,94086**	**4,64384**	**0,18524**	**3,24524**	**0,69883**	**1095**	**67**	**1096**	**33**	**1095**	**32**	**100**
2	111	0,0000	82,43	0,58	0,07608	2,05047	1,85335	3,74325	0,17668	3,13169	0,83662	1097	41	1049	31	1065	25	99
2	**30**	**1,0000**	**339,85**	**0,50**	**0,07612**	**3,31622**	**1,98877**	**4,64445**	**0,18950**	**3,25171**	**0,70013**	**1098**	**66**	**1119**	**34**	**1112**	**32**	**101**
2	90	0,0000	154,76	0,70	0,07615	2,04859	1,90437	3,72945	0,18138	3,11643	0,83563	1099	41	1074	31	1083	25	99
2	**53**	**0,0056**	**298,06**	**0,44**	**0,07621**	**2,02090**	**1,99370**	**3,69582**	**0,18975**	**3,09436**	**0,83726**	**1100**	**40**	**1120**	**32**	**1113**	**25**	**101**
2	**88**	**1,0000**	**242,76**	**0,51**	**0,07626**	**3,32590**	**1,90868**	**4,67172**	**0,18152**	**3,28076**	**0,70226**	**1102**	**67**	**1075**	**33**	**1084**	**32**	**99**
2	31	1,0000	95,61	0,81	0,07629	3,32492	1,86360	4,66806	0,17718	3,27654	0,70191	1103	66	1052	32	1068	31	99
2	**34**	**0,1054**	**139,97**	**0,42**	**0,07631**	**2,06289**	**1,93359**	**3,70524**	**0,18377**	**3,07787**	**0,83068**	**1103**	**41**	**1088**	**31**	**1093**	**25**	**100**
2	**52**	**1,0000**	**209,74**	**0,48**	**0,07632**	**3,30732**	**2,00700**	**4,64426**	**0,19072**	**3,26048**	**0,70205**	**1104**	**66**	**1125**	**34**	**1118**	**32**	**101**
2	135	0,0066	219,67	0,95	0,07638	2,04236	1,89054	3,74396	0,17951	3,13783	0,83811	1105	41	1064	31	1078	25	99
2	**36**	**0,1002**	**232,10**	**0,55**	**0,07639**	**2,03289**	**1,96077**	**3,69131**	**0,18615**	**3,08109**	**0,83469**	**1105**	**41**	**1101**	**31**	**1102**	**25**	**100**
2	70	1,0000	113,71	0,91	0,07640	3,33597	1,87601	4,66428	0,17808	3,25988	0,69890	1106	67	1056	32	1073	31	99
2	**38**	**0,0246**	**339,53**	**0,43**	**0,07642**	**2,01618**	**2,00154**	**3,67294**	**0,18995**	**3,07010**	**0,83587**	**1106**	**40**	**1121**	**32**	**1116**	**25**	**101**
2	**118**	**1,0000**	**229,56**	**0,46**	**0,07647**	**3,31712**	**1,95832**	**4,69130**	**0,18574**	**3,31738**	**0,70714**	**1107**	**66**	**1098**	**34**	**1101**	**32**	**100**
2	131	0,0000	164,14	0,52	0,07647	2,04002	1,89842	3,74394	0,18005	3,13934	0,83851	1107	41	1067	31	1081	25	99
2	**100**	**0,0261**	**408,36**	**0,59**	**0,07647**	**2,01502**	**1,99086**	**3,71428**	**0,18882**	**3,12018**	**0,84005**	**1107**	**40**	**1115**	**32**	**1112**	**25**	**100**
2	119	0,0004	77,67	0,82	0,07659	2,06294	1,90244	3,75503	0,18015	3,13760	0,83557	1111	41	1068	31	1082	25	99
2	**137**	**0,0080**	**322,67**	**0,61**	**0,07661**	**2,03629**	**1,98798**	**3,75222**	**0,18819**	**3,15162**	**0,83993**	**1111**	**41**	**1112**	**32**	**1111**	**26**	**100**
2	112	0,1194	51,11	0,44	0,07663	2,11115	1,88311	3,78434	0,17823	3,14075	0,82993	1112	42	1057	31	1075	25	98
2	**13**	**0,0444**	**442,53**	**0,53**	**0,07664**	**2,03889**	**1,97635**	**3,57561**	**0,18704**	**2,93733**	**0,82149**	**1112**	**41**	**1105**	**30**	**1107**	**24**	**100**
2	74	0,1097	110,88	0,39	0,07668	2,05455	1,86029	3,72985	0,17596	3,11298	0,83461	1113	41	1045	30	1067	25	98
2	130	0,0000	44,54	0,76	0,07670	2,11213	1,89844	3,79152	0,17952	3,14873	0,83047	1113	42	1064	31	1081	26	99
2	**55**	**1,0000**	**276,11**	**0,36**	**0,07672**	**3,30605**	**1,99467**	**4,64852**	**0,18856**	**3,26784**	**0,70298**	**1114**	**66**	**1114**	**34**	**1114**	**32**	**100**
2	8	0,0449	189,99	0,51	0,07673	2,03659	1,95224	3,67858	0,18454	3,06337	0,83276	1114	41	1092	31	1099	25	99
2	**97**	**0,0402**	**413,96**	**0,52**	**0,07676**	**2,00901**	**2,01534**	**3,70666**	**0,19042**	**3,11499**	**0,84038**	**1115**	**40**	**1124**	**32**	**1121**	**26**	**100**
2	110	0,0000	90,02	0,48	0,07681	2,05702	1,86512	3,77421	0,17611	3,16438	0,83842	1116	41	1046	31	1069	25	98
2	**19**	**0,0771**	**212,90**	**0,39**	**0,07682**	**2,04060**	**1,98713**	**3,68389**	**0,18761**	**3,06708**	**0,83257**	**1117**	**41**	**1108**	**31**	**1111**	**25**	**100**
2	73	0,0195	216,30	0,51	0,07693	2,02832	1,94585	3,70729	0,18344	3,10320	0,83706	1120	40	1086	31	1097	25	99

2	**120**	**0,0517**	**213,60**	**0,49**	**0,07694**	**2,03200**	**1,97713**	**3,73132**	**0,18637**	**3,12949**	**0,83871**	**1120**	**41**	**1102**	**32**	**1108**	**26**	**100**
2	**15**	**0,0601**	**293,08**	**0,49**	**0,07695**	**2,03321**	**1,97652**	**3,67980**	**0,18628**	**3,06708**	**0,83349**	**1120**	**41**	**1101**	**31**	**1108**	**25**	**100**
2	**33**	**0,0005**	**358,46**	**0,44**	**0,07696**	**2,02704**	**2,01786**	**3,68474**	**0,19016**	**3,07708**	**0,83509**	**1120**	**40**	**1122**	**32**	**1122**	**25**	**100**
2	**109**	**0,0000**	**165,30**	**0,50**	**0,07701**	**2,02571**	**1,98135**	**3,72427**	**0,18660**	**3,12517**	**0,83914**	**1121**	**40**	**1103**	**32**	**1109**	**25**	**100**
2	**108**	**1,0000**	**278,70**	**0,50**	**0,07703**	**3,29285**	**2,01218**	**4,65632**	**0,18946**	**3,29219**	**0,70704**	**1122**	**66**	**1118**	**34**	**1120**	**32**	**100**
2	**47**	**0,0044**	**510,65**	**0,53**	**0,07704**	**2,02504**	**2,02844**	**3,62080**	**0,19097**	**3,00157**	**0,82898**	**1122**	**40**	**1127**	**31**	**1125**	**25**	**100**
2	87	0,1098	81,89	0,51	0,07706	2,07017	1,87425	3,76009	0,17641	3,13890	0,83479	1123	41	1047	31	1072	25	98
2	91	0,1513	120,90	0,40	0,07707	2,08724	1,88050	3,81011	0,17696	3,18754	0,83660	1123	42	1050	31	1074	26	98
2	**99**	**0,0168**	**240,21**	**1,02**	**0,07711**	**2,02363**	**2,00120**	**3,71819**	**0,18823**	**3,11927**	**0,83892**	**1124**	**40**	**1112**	**32**	**1116**	**26**	**100**
2	39	1,0000	162,66	0,54	0,07711	3,28951	1,96333	4,64940	0,18467	3,28574	0,70670	1124	66	1092	33	1103	32	99
2	**49**	**0,0402**	**316,29**	**0,74**	**0,07711**	**2,02580**	**1,99892**	**3,67832**	**0,18801**	**3,07022**	**0,83468**	**1124**	**40**	**1111**	**32**	**1115**	**25**	**100**
2	132	1,0000	210,87	0,51	0,07715	3,28764	1,96540	4,67583	0,18476	3,32488	0,71108	1125	66	1093	34	1104	32	99
2	94	0,0295	142,08	0,45	0,07719	2,02250	1,91929	3,71182	0,18034	3,11241	0,83851	1126	40	1069	31	1088	25	98
2	**96**	**0,0341**	**406,84**	**0,50**	**0,07734**	**2,01891**	**2,03440**	**3,71595**	**0,19077**	**3,11966**	**0,83953**	**1130**	**40**	**1126**	**32**	**1127**	**26**	**100**
2	**77**	**0,0173**	**537,84**	**0,57**	**0,07736**	**2,01713**	**2,03952**	**3,69999**	**0,19122**	**3,10180**	**0,83832**	**1130**	**40**	**1128**	**32**	**1129**	**26**	**100**
2	35	0,0326	156,78	0,48	0,07752	2,03980	1,97491	3,69513	0,18476	3,08110	0,83383	1135	41	1093	31	1107	25	99
2	58	0,0670	90,57	0,74	0,07763	2,06834	1,88637	3,72269	0,17624	3,09522	0,83145	1137	41	1046	30	1076	25	97
2	**79**	**0,0253**	**482,32**	**0,46**	**0,07770**	**2,00877**	**2,04698**	**3,69753**	**0,19107**	**3,10428**	**0,83955**	**1139**	**40**	**1127**	**32**	**1131**	**26**	**100**
2	136	1,0000	206,73	0,66	0,07773	3,29512	2,00421	4,65278	0,18701	3,28489	0,70601	1140	66	1105	34	1117	32	99
2	134	1,0000	85,23	0,46	0,07776	3,30980	1,96551	4,70272	0,18332	3,34078	0,71039	1141	66	1085	34	1104	32	98
2	72	0,1121	133,06	0,73	0,07780	2,05113	2,03858	3,71910	0,19003	3,10235	0,83417	1142	41	1122	32	1128	26	100
2	114	0,0326	475,65	0,57	0,07781	2,03219	2,01049	3,72587	0,18739	3,12287	0,83816	1142	40	1107	32	1119	26	99
2	93	0,0325	285,34	0,67	0,07782	2,03192	1,93429	3,71814	0,18026	3,11382	0,83747	1142	40	1068	31	1093	25	98
2	117	0,0124	72,17	0,73	0,07785	2,13253	1,96815	3,75744	0,18336	3,09365	0,82334	1143	42	1085	31	1105	26	98
2	71	0,0826	472,97	0,66	0,07786	2,01491	1,99755	3,77184	0,18608	3,18856	0,84536	1143	40	1100	32	1115	26	99
2	57	0,0531	273,87	0,46	0,07795	2,03155	1,99619	3,70419	0,18573	3,09739	0,83619	1146	40	1098	31	1114	25	99
2	60	0,0595	182,80	0,56	0,07802	2,03076	2,04115	3,79886	0,18974	3,21051	0,84512	1147	40	1120	33	1129	26	99
2	80	0,0047	516,26	0,42	0,07814	2,02214	2,03692	3,70577	0,18907	3,10543	0,83800	1150	40	1116	32	1128	26	99
2	128	0,0554	353,84	0,48	0,07822	2,02498	2,00843	3,74749	0,18623	3,15328	0,84144	1152	40	1101	32	1118	26	99
2	20	0,1615	81,75	0,61	0,07845	2,10559	2,01525	3,73225	0,18630	3,08159	0,82567	1158	42	1101	31	1121	26	98
2	56	0,2855	75,91	0,57	0,07933	2,18894	2,24402	3,80081	0,20515	3,10720	0,81751	1180	43	1203	34	1195	27	101
2	78	0,0482	284,92	0,50	0,07944	2,04283	2,25549	3,64274	0,20592	3,01602	0,82795	1183	40	1207	33	1198	26	101
2	32	0,0125	567,84	0,61	0,07963	2,00954	2,04406	3,67669	0,18617	3,07893	0,83742	1188	40	1101	31	1130	25	98
2	14	0,0589	417,21	0,54	0,07996	2,03129	2,05831	3,73552	0,18669	3,13496	0,83923	1196	40	1103	32	1135	26	97
2	50	0,1014	324,25	0,52	0,08044	2,02967	2,07044	3,70902	0,18668	3,10439	0,83698	1208	40	1103	32	1139	26	97
2	75	0,2177	48,04	0,88	0,11420	2,08418	5,25027	3,77076	0,33343	3,14242	0,83337	1867	38	1855	51	1861	33	100
Rejected data																		
2	~~40~~	~~0,1144~~	~~265,79~~	~~0,51~~	~~0,07846~~	~~2,03477~~	~~1,82692~~	~~3,68076~~	~~0,16888~~	~~3,06720~~	~~0,83331~~	~~1159~~	~~40~~	~~1006~~	~~29~~	~~1055~~	~~24~~	~~95~~
2	~~11~~	~~0,2771~~	~~467,31~~	~~1,00~~	~~0,09060~~	~~2,12104~~	~~1,66403~~	~~3,76075~~	~~0,13321~~	~~3,10555~~	~~0,82578~~	~~1438~~	~~40~~	~~806~~	~~24~~	~~995~~	~~24~~	~~81~~
2	~~12~~	~~0,0337~~	~~260,02~~	~~0,47~~	~~0,08173~~	~~2,00824~~	~~1,87150~~	~~3,66711~~	~~0,16607~~	~~3,06834~~	~~0,83672~~	~~1239~~	~~39~~	~~990~~	~~28~~	~~1071~~	~~25~~	~~93~~
2	~~16~~	~~0,4888~~	~~973,49~~	~~0,56~~	~~0,12573~~	~~2,16460~~	~~2,06868~~	~~3,84300~~	~~0,11933~~	~~3,17540~~	~~0,82628~~	~~2039~~	~~38~~	~~727~~	~~22~~	~~1138~~	~~27~~	~~64~~
2	~~17~~	~~0,0284~~	~~303,56~~	~~0,55~~	~~0,08110~~	~~2,02348~~	~~2,08617~~	~~3,67894~~	~~0,18657~~	~~3,07248~~	~~0,83515~~	~~1224~~	~~40~~	~~1103~~	~~31~~	~~1144~~	~~26~~	~~97~~
2	~~18~~	~~1,0000~~	~~846,53~~	~~0,49~~	~~0,11007~~	~~2,71478~~	~~2,06750~~	~~4,34931~~	~~0,13624~~	~~3,39801~~	~~0,78128~~	~~1800~~	~~49~~	~~823~~	~~26~~	~~1138~~	~~30~~	~~72~~
2	~~27~~	~~0,5946~~	~~187,87~~	~~0,38~~	~~0,10435~~	~~2,32949~~	~~2,65488~~	~~3,90984~~	~~0,18453~~	~~3,14012~~	~~0,80313~~	~~1703~~	~~43~~	~~1092~~	~~32~~	~~1316~~	~~29~~	~~83~~
2	~~28~~	~~0,0000~~	~~78,07~~	~~0,59~~	~~0,07982~~	~~2,05462~~	~~1,94106~~	~~3,71243~~	~~0,17637~~	~~3,09203~~	~~0,83289~~	~~1193~~	~~41~~	~~1047~~	~~30~~	~~1095~~	~~25~~	~~96~~

2	~~29~~	~~13,5358~~	~~877,43~~	~~0,54~~	~~0,12233~~	~~22,25153~~	~~2,34604~~	~~29,66045~~	~~0,13909~~	~~19,61151~~	~~0,66120~~	~~1990~~	~~396~~	~~840~~	~~157~~	~~1226~~	~~237~~	~~69~~
2	~~37~~	~~21,7508~~	~~455,27~~	~~0,31~~	~~0,43382~~	~~10,35340~~	~~14,79975~~	~~20,55882~~	~~0,24742~~	~~17,76153~~	~~0,86394~~	~~4031~~	~~155~~	~~1425~~	~~232~~	~~2802~~	~~217~~	~~51~~
2	~~40~~	~~0,6210~~	~~820,29~~	~~0,73~~	~~0,11502~~	~~2,30321~~	~~2,01539~~	~~3,97116~~	~~0,12708~~	~~3,23502~~	~~0,81463~~	~~1880~~	~~41~~	~~771~~	~~24~~	~~1121~~	~~27~~	~~69~~
2	~~48~~	~~0,4784~~	~~132,31~~	~~0,59~~	~~0,09176~~	~~2,29895~~	~~2,04442~~	~~3,89742~~	~~0,16159~~	~~3,14717~~	~~0,80750~~	~~1462~~	~~44~~	~~966~~	~~28~~	~~1130~~	~~27~~	~~86~~
2	~~51~~	~~0,3521~~	~~242,08~~	~~0,63~~	~~0,09148~~	~~2,17414~~	~~2,07805~~	~~3,77474~~	~~0,16476~~	~~3,08575~~	~~0,81747~~	~~1457~~	~~41~~	~~983~~	~~28~~	~~1142~~	~~26~~	~~86~~
2	~~54~~	~~0,0643~~	~~240,66~~	~~0,44~~	~~0,08116~~	~~2,02697~~	~~2,06925~~	~~3,69532~~	~~0,18492~~	~~3,08979~~	~~0,83614~~	~~1225~~	~~40~~	~~1094~~	~~31~~	~~1139~~	~~26~~	~~96~~
2	~~59~~	~~0,3523~~	~~528,39~~	~~0,51~~	~~0,09016~~	~~2,16459~~	~~1,66825~~	~~3,81665~~	~~0,13420~~	~~3,14347~~	~~0,82362~~	~~1429~~	~~41~~	~~812~~	~~24~~	~~997~~	~~25~~	~~82~~
2	~~67~~	~~0,3572~~	~~327,27~~	~~0,80~~	~~0,08941~~	~~2,16598~~	~~2,09071~~	~~3,80345~~	~~0,16959~~	~~3,12646~~	~~0,82201~~	~~1413~~	~~41~~	~~1010~~	~~29~~	~~1146~~	~~27~~	~~88~~
2	~~68~~	~~0,1119~~	~~176,71~~	~~0,50~~	~~0,08206~~	~~2,04125~~	~~2,03737~~	~~3,70940~~	~~0,18007~~	~~3,09725~~	~~0,83497~~	~~1247~~	~~40~~	~~1067~~	~~31~~	~~1128~~	~~26~~	~~95~~
2	~~69~~	~~1,0000~~	~~76,55~~	~~0,43~~	~~0,08220~~	~~3,17756~~	~~2,07497~~	~~4,57667~~	~~0,18308~~	~~3,29378~~	~~0,71969~~	~~1250~~	~~62~~	~~1084~~	~~33~~	~~1141~~	~~32~~	~~95~~
2	~~76~~	~~2,7720~~	~~207,53~~	~~0,48~~	~~0,21267~~	~~3,33990~~	~~6,31957~~	~~5,19573~~	~~0,21552~~	~~3,98004~~	~~0,76602~~	~~2926~~	~~54~~	~~1258~~	~~46~~	~~2021~~	~~47~~	~~62~~
2	~~95~~	~~0,2186~~	~~347,70~~	~~0,78~~	~~0,08643~~	~~2,09818~~	~~2,14380~~	~~3,76765~~	~~0,17989~~	~~3,12934~~	~~0,83058~~	~~1348~~	~~41~~	~~1066~~	~~31~~	~~1163~~	~~26~~	~~92~~
2	~~98~~	~~0,2174~~	~~446,04~~	~~0,39~~	~~0,08699~~	~~2,08405~~	~~2,12999~~	~~3,75638~~	~~0,17758~~	~~3,12523~~	~~0,83198~~	~~1360~~	~~40~~	~~1054~~	~~31~~	~~1159~~	~~26~~	~~91~~
2	~~107~~	~~0,9822~~	~~426,95~~	~~0,55~~	~~0,12611~~	~~2,57141~~	~~3,10807~~	~~4,22830~~	~~0,17875~~	~~3,35655~~	~~0,79383~~	~~2044~~	~~45~~	~~1060~~	~~33~~	~~1435~~	~~33~~	~~74~~
2	~~113~~	~~0,1986~~	~~377,52~~	~~0,58~~	~~0,08581~~	~~2,07992~~	~~1,97391~~	~~3,77174~~	~~0,16684~~	~~3,14642~~	~~0,83421~~	~~1334~~	~~40~~	~~995~~	~~29~~	~~1107~~	~~26~~	~~90~~
2	~~116~~	~~0,1209~~	~~167,02~~	~~0,39~~	~~0,08047~~	~~2,08458~~	~~1,15541~~	~~3,77151~~	~~0,10413~~	~~3,14306~~	~~0,83337~~	~~1209~~	~~41~~	~~639~~	~~19~~	~~780~~	~~21~~	~~82~~
2	~~127~~	~~0,0767~~	~~624,45~~	~~0,73~~	~~0,08316~~	~~2,02871~~	~~1,94369~~	~~3,73501~~	~~0,16952~~	~~3,13602~~	~~0,83963~~	~~1273~~	~~40~~	~~1009~~	~~29~~	~~1096~~	~~25~~	~~92~~
2	~~129~~	~~0,1927~~	~~93,08~~	~~0,47~~	~~0,08246~~	~~2,11390~~	~~2,01218~~	~~3,79883~~	~~0,17698~~	~~3,15635~~	~~0,83087~~	~~1256~~	~~41~~	~~1050~~	~~31~~	~~1120~~	~~26~~	~~94~~
2	~~133~~	~~0,3675~~	~~836,82~~	~~0,53~~	~~0,10232~~	~~2,15597~~	~~1,96768~~	~~3,83278~~	~~0,13947~~	~~3,16892~~	~~0,82679~~	~~1667~~	~~40~~	~~842~~	~~25~~	~~1105~~	~~26~~	~~76~~
2	~~139~~	~~1,0029~~	~~618,98~~	~~0,74~~	~~0,12504~~	~~2,60091~~	~~2,29994~~	~~4,34905~~	~~0,13340~~	~~3,48562~~	~~0,80147~~	~~2029~~	~~46~~	~~807~~	~~27~~	~~1212~~	~~31~~	~~67~~
MB-179																		
2	151	0,0000	50,36	0,32	0,07642	2,09369	1,84947	3,79369	0,17552	3,16362	0,83392	1106	42	1042	31	1063	25	98
2	**170**	**0,0675**	**103,74**	**0,37**	**0,07687**	**2,06297**	**1,99204**	**3,78853**	**0,18795**	**3,17759**	**0,83874**	**1118**	**41**	**1110**	**33**	**1113**	**26**	**100**
2	**213**	**0,0266**	**90,72**	**0,46**	**0,07691**	**2,08152**	**1,96188**	**3,81342**	**0,18501**	**3,19522**	**0,83789**	**1119**	**42**	**1094**	**32**	**1103**	**26**	**99**
2	155	0,0475	84,21	0,45	0,07717	2,07691	1,95887	3,77920	0,18409	3,15735	0,83545	1126	41	1089	32	1101	26	99
2	**188**	**1,0000**	**89,05**	**0,35**	**0,07721**	**3,31742**	**1,98078**	**4,72330**	**0,18607**	**3,36219**	**0,71183**	**1127**	**66**	**1100**	**34**	**1109**	**32**	**99**
2	**180**	**0,0170**	**258,36**	**0,62**	**0,07741**	**2,04163**	**2,07218**	**3,76859**	**0,19415**	**3,16765**	**0,84054**	**1132**	**41**	**1144**	**33**	**1140**	**26**	**101**
2	160	0,0000	47,75	0,39	0,07759	2,11367	1,92995	3,78871	0,18040	3,14431	0,82992	1136	42	1069	31	1092	26	98
2	**207**	**1,0000**	**106,18**	**0,38**	**0,07765**	**3,29844**	**1,99250**	**4,71685**	**0,18610**	**3,37179**	**0,71484**	**1138**	**66**	**1100**	**34**	**1113**	**32**	**99**
2	212	0,1391	66,36	0,36	0,07766	2,11650	1,97713	3,84076	0,18464	3,20498	0,83446	1138	42	1092	32	1108	26	99
2	**199**	**0,0454**	**103,14**	**0,51**	**0,07788**	**2,05762**	**2,06669**	**3,80105**	**0,19245**	**3,19596**	**0,84081**	**1144**	**41**	**1135**	**33**	**1138**	**26**	**100**
2	**197**	**0,0306**	**260,67**	**0,77**	**0,07809**	**2,05052**	**2,08822**	**3,78486**	**0,19395**	**3,18127**	**0,84053**	**1149**	**41**	**1143**	**34**	**1145**	**26**	**100**
2	168	1,0000	108,80	0,66	0,07809	3,27995	1,97223	4,69092	0,18318	3,35360	0,71491	1149	65	1084	34	1106	32	98
2	**172**	**1,0000**	**83,67**	**0,63**	**0,07815**	**3,29349**	**2,14316**	**4,64709**	**0,19890**	**3,27847**	**0,70549**	**1151**	**65**	**1169**	**35**	**1163**	**33**	**101**
2	**176**	**0,0357**	**406,54**	**0,42**	**0,07823**	**2,04723**	**2,12379**	**3,77724**	**0,19689**	**3,17433**	**0,84038**	**1153**	**41**	**1159**	**34**	**1157**	**26**	**100**
2	**189**	**1,0000**	**296,84**	**0,54**	**0,07823**	**3,27384**	**2,05331**	**4,68131**	**0,19035**	**3,34614**	**0,71479**	**1153**	**65**	**1123**	**35**	**1133**	**33**	**99**
2	**210**	**0,0547**	**254,25**	**0,62**	**0,07833**	**2,07295**	**2,14421**	**3,87887**	**0,19854**	**3,27849**	**0,84522**	**1155**	**41**	**1167**	**35**	**1163**	**27**	**101**
2	216	1,0000	64,35	0,36	0,07834	3,31792	1,98915	4,74855	0,18416	3,39707	0,71539	1155	66	1090	34	1112	33	98
2	198	0,0221	130,36	0,51	0,07846	2,06545	2,03089	3,80142	0,18773	3,19135	0,83952	1159	41	1109	33	1126	26	99
2	217	0,0116	156,62	0,50	0,07850	2,06388	2,25409	3,75315	0,20826	3,13473	0,83523	1160	41	1220	35	1198	27	102
2	179	0,1594	47,04	0,39	0,07853	2,12732	2,00463	3,83168	0,18513	3,18689	0,83172	1160	42	1095	32	1117	26	98
2	**192**	**0,1157**	**119,09**	**1,03**	**0,07865**	**2,08069**	**2,12863**	**3,80519**	**0,19629**	**3,18594**	**0,83726**	**1163**	**41**	**1155**	**34**	**1158**	**27**	**100**
2	**177**	**0,0271**	**173,77**	**0,79**	**0,07866**	**2,06068**	**2,15404**	**3,78661**	**0,19861**	**3,17679**	**0,83895**	**1164**	**41**	**1168**	**34**	**1166**	**27**	**100**
2	215	1,0000	49,86	0,52	0,07877	3,29965	2,00460	4,73042	0,18457	3,38956	0,71655	1166	65	1092	34	1117	33	98
2	194	0,2150	47,47	0,40	0,07891	2,17313	1,97144	3,86331	0,18120	3,19416	0,82679	1170	43	1074	32	1106	26	97

2	187	0,0592	453,82	0,50	0,07901	2,05576	2,09783	3,74673	0,19256	3,13238	0,83603	1172	41	1135	33	1148	26	99
2	193	0,0094	119,16	0,56	0,07934	2,06712	2,08121	3,80195	0,19024	3,19089	0,83928	1181	41	1123	33	1143	26	98
2	156	0,0983	55,41	0,38	0,07942	2,10470	2,02226	3,80541	0,18467	3,17039	0,83313	1183	42	1092	32	1123	26	97
2	154	0,0172	245,76	1,10	0,07963	2,03496	2,13345	3,75405	0,19432	3,15466	0,84033	1188	40	1145	33	1160	26	99
2	169	1,0000	57,43	0,52	0,08007	3,24603	2,00223	4,66909	0,18136	3,35615	0,71880	1199	64	1074	33	1116	32	96
2	**167**	**0,1288**	**247,14**	**0,54**	**0,08148**	**2,08581**	**2,36169**	**3,73519**	**0,21021**	**3,09855**	**0,82956**	**1233**	**41**	**1230**	**35**	**1231**	**27**	**100**
2	159	1,0000	137,11	0,70	0,11415	2,69665	5,28117	4,15743	0,33554	3,16422	0,76110	1867	49	1865	52	1866	36	100
2	175	0,0190	201,19	0,78	0,11921	2,04710	5,76439	3,77075	0,35071	3,16669	0,83980	1944	37	1938	53	1941	33	100
2	173	0,1432	95,49	0,36	0,12224	2,05846	6,06625	3,74245	0,35991	3,12549	0,83514	1989	37	1982	54	1985	33	100
2	174	0,0000	74,85	0,31	0,12235	2,04332	6,05418	3,75472	0,35888	3,15004	0,83896	1991	36	1977	54	1984	33	100
2	158	0,0132	158,17	0,26	0,12601	2,03164	6,44934	3,75522	0,37119	3,15818	0,84101	2043	36	2035	56	2039	34	100
2	211	0,1094	50,90	3,05	0,13866	2,06866	7,67525	3,85056	0,40146	3,24769	0,84343	2211	36	2176	60	2194	35	99
2	171	0,0254	112,41	0,26	0,17808	2,04417	12,23179	3,74373	0,49815	3,13638	0,83777	2635	34	2606	68	2622	36	100
Rejected data																		
2	~~152~~	~~0,2285~~	~~50,34~~	~~0,32~~	~~0,08287~~	~~2,17091~~	~~2,02183~~	~~3,84302~~	~~0,17695~~	~~3,17411~~	~~0,82516~~	~~1266~~	~~42~~	~~1050~~	~~31~~	~~1123~~	~~26~~	~~94~~
2	~~153~~	~~0,2040~~	~~63,46~~	~~0,68~~	~~0,08088~~	~~2,13738~~	~~2,04242~~	~~3,82349~~	~~0,18314~~	~~3,17029~~	~~0,82916~~	~~1219~~	~~42~~	~~1084~~	~~32~~	~~1130~~	~~26~~	~~96~~
2	~~157~~	~~0,2461~~	~~77,41~~	~~0,49~~	~~0,09633~~	~~2,11796~~	~~2,45363~~	~~3,81072~~	~~0,18473~~	~~3,16794~~	~~0,83132~~	~~1554~~	~~40~~	~~1093~~	~~32~~	~~1258~~	~~28~~	~~87~~
2	~~178~~	~~0,3037~~	~~76,82~~	~~0,38~~	~~0,08467~~	~~2,19894~~	~~2,20102~~	~~3,87756~~	~~0,18853~~	~~3,19376~~	~~0,82365~~	~~1308~~	~~43~~	~~1113~~	~~33~~	~~1181~~	~~27~~	~~94~~
2	~~190~~	~~0,5956~~	~~46,47~~	~~0,44~~	~~0,08808~~	~~2,50755~~	~~2,24374~~	~~4,11542~~	~~0,18475~~	~~3,26326~~	~~0,79294~~	~~1384~~	~~48~~	~~1093~~	~~33~~	~~1195~~	~~29~~	~~92~~
2	~~191~~	~~0,2577~~	~~85,87~~	~~0,42~~	~~0,08547~~	~~2,14569~~	~~2,19008~~	~~3,85557~~	~~0,18584~~	~~3,20334~~	~~0,83084~~	~~1326~~	~~42~~	~~1099~~	~~33~~	~~1178~~	~~27~~	~~93~~
2	~~195~~	~~0,1121~~	~~185,57~~	~~0,49~~	~~0,08044~~	~~2,05775~~	~~1,99123~~	~~3,80043~~	~~0,17953~~	~~3,19514~~	~~0,84073~~	~~1208~~	~~41~~	~~1064~~	~~32~~	~~1113~~	~~26~~	~~96~~
2	~~196~~	~~0,0012~~	~~77,45~~	~~0,66~~	~~0,11373~~	~~2,03994~~	~~5,80532~~	~~3,77575~~	~~0,37022~~	~~3,17725~~	~~0,84149~~	~~1860~~	~~37~~	~~2030~~	~~56~~	~~1947~~	~~33~~	~~104~~
2	~~200~~	~~0,0459~~	~~90,59~~	~~0,21~~	~~0,10683~~	~~2,06112~~	~~3,72895~~	~~3,80635~~	~~0,25316~~	~~3,20001~~	~~0,84070~~	~~1746~~	~~38~~	~~1455~~	~~42~~	~~1578~~	~~31~~	~~92~~
2	~~206~~	~~0,4443~~	~~416,41~~	~~0,39~~	~~0,09678~~	~~2,28027~~	~~2,57999~~	~~3,91546~~	~~0,19335~~	~~3,18296~~	~~0,81292~~	~~1563~~	~~43~~	~~1139~~	~~33~~	~~1295~~	~~29~~	~~88~~
2	~~209~~	~~1,1537~~	~~170,82~~	~~0,28~~	~~0,16226~~	~~2,52224~~	~~8,53867~~	~~4,05162~~	~~0,38167~~	~~3,17078~~	~~0,78260~~	~~2479~~	~~43~~	~~2084~~	~~57~~	~~2290~~	~~38~~	~~91~~
2	~~214~~	~~0,7574~~	~~60,03~~	~~0,30~~	~~0,11430~~	~~2,46830~~	~~2,96596~~	~~4,12332~~	~~0,18820~~	~~3,30291~~	~~0,80103~~	~~1869~~	~~45~~	~~1112~~	~~34~~	~~1399~~	~~32~~	~~80~~
2	~~218~~	~~1,0000~~	~~49,61~~	~~0,45~~	~~0,08640~~	~~3,11437~~	~~2,25262~~	~~4,59483~~	~~0,18910~~	~~3,37833~~	~~0,73525~~	~~1347~~	~~60~~	~~1116~~	~~35~~	~~1198~~	~~33~~	~~93~~
2	~~150~~	~~0,0646~~	~~100,51~~	~~0,77~~	~~0,07771~~	~~2,06564~~	~~1,94700~~	~~3,76209~~	~~0,18171~~	~~3,14428~~	~~0,83578~~	~~1139~~	~~41~~	~~1076~~	~~31~~	~~1097~~	~~26~~	~~98~~
MB-181																		
2	140	0,1329	126,94	1,14	0,07631	2,07377	1,92006	3,77573	0,18249	3,15525	0,83567	1103	41	1081	32	1088	26	99
2	139	1,0000	187,91	1,18	0,07683	3,30153	1,97146	4,69001	0,18611	3,33107	0,71025	1117	66	1100	34	1106	32	100
2	150	0,0646	100,51	0,77	0,07771	2,06564	1,94700	3,76209	0,18171	3,14428	0,83578	1139	41	1076	31	1097	26	98
2	148	0,0434	166,88	0,69	0,07786	2,05810	1,96253	3,77816	0,18282	3,16839	0,83861	1143	41	1082	32	1103	26	98
Rejected data																		
2	~~147~~	~~0,1211~~	~~167,76~~	~~0,53~~	~~0,07868~~	~~2,08172~~	~~1,71220~~	~~3,78112~~	~~0,15782~~	~~3,15648~~	~~0,83480~~	~~1164~~	~~41~~	~~945~~	~~28~~	~~1013~~	~~25~~	~~93~~
2	~~149~~	~~0,2099~~	~~149,72~~	~~0,51~~	~~0,08441~~	~~2,09740~~	~~2,12606~~	~~3,79032~~	~~0,18267~~	~~3,15712~~	~~0,83294~~	~~1302~~	~~41~~	~~1082~~	~~32~~	~~1157~~	~~27~~	~~94~~
MB-135																		
1	291	0,0000	462,48	0,49	0,07440	1,06937	1,87046	4,22482	0,18234	4,08724	0,96744	1052	22	1080	41	1071	28	102
1	290	0,0677	673,46	0,06	0,07447	1,26011	1,95527	4,16230	0,19042	3,96697	0,95307	1054	26	1124	41	1100	28	103
1	**289**	**0,0000**	**120,55**	**0,67**	**0,07459**	**1,21701**	**1,83721**	**4,39978**	**0,17863**	**4,22812**	**0,96098**	**1058**	**25**	**1060**	**41**	**1059**	**29**	**101**
1	**288**	**0,0000**	**105,09**	**0,63**	**0,07460**	**1,27153**	**1,85879**	**4,41118**	**0,18071**	**4,22395**	**0,95755**	**1058**	**26**	**1071**	**42**	**1067**	**29**	**102**
1	**287**	**0,0000**	**117,61**	**0,74**	**0,07461**	**1,16200**	**1,83854**	**4,22116**	**0,17871**	**4,05807**	**0,96136**	**1058**	**24**	**1060**	**40**	**1059**	**28**	**101**
1	**279**	**0,0246**	**727,28**	**0,13**	**0,07463**	**1,05460**	**1,84925**	**4,30040**	**0,17972**	**4,16908**	**0,96946**	**1058**	**21**	**1065**	**41**	**1063**	**29**	**101**
1	**278**	**0,0368**	**797,51**	**0,52**	**0,07468**	**1,01574**	**1,83785**	**4,19921**	**0,17849**	**4,07451**	**0,97030**	**1060**	**21**	**1059**	**40**	**1059**	**28**	**101**
1	**277**	**0,0000**	**357,15**	**0,50**	**0,07478**	**1,03669**	**1,88387**	**4,20841**	**0,18272**	**4,07872**	**0,96918**	**1062**	**21**	**1082**	**41**	**1075**	**28**	**102**

1	**276**	**0,0000**	**135,13**	**0,72**	**0,07489**	**1,10324**	**1,85608**	**4,27951**	**0,17975**	**4,13486**	**0,96620**	**1066**	**22**	**1066**	**41**	**1066**	**28**	**101**
1	**275**	**0,0000**	**70,70**	**0,65**	**0,07489**	**1,23944**	**1,88690**	**4,26246**	**0,18274**	**4,07828**	**0,95679**	**1066**	**25**	**1082**	**41**	**1076**	**28**	**102**
1	274	0,1373	181,19	0,54	0,07492	1,17739	1,90638	4,21941	0,18455	4,05181	0,96028	1066	24	1092	41	1083	28	102
1	**273**	**0,0709**	**231,23**	**0,52**	**0,07495**	**1,33416**	**1,85092**	**4,49820**	**0,17911**	**4,29579**	**0,95500**	**1067**	**27**	**1062**	**42**	**1064**	**30**	**101**
1	**272**	**0,0470**	**740,17**	**0,54**	**0,07498**	**1,01481**	**1,83857**	**4,27899**	**0,17785**	**4,15691**	**0,97147**	**1068**	**21**	**1055**	**41**	**1059**	**28**	**101**
1	**271**	**0,0000**	**85,47**	**0,80**	**0,07498**	**1,21072**	**1,88777**	**4,26772**	**0,18260**	**4,09238**	**0,95892**	**1068**	**24**	**1081**	**41**	**1077**	**29**	**102**
1	**270**	**0,2287**	**102,01**	**0,66**	**0,07498**	**1,50829**	**1,90365**	**4,31632**	**0,18413**	**4,04422**	**0,93696**	**1068**	**31**	**1090**	**41**	**1082**	**29**	**102**
1	**269**	**0,4965**	**87,47**	**0,63**	**0,07501**	**2,09704**	**1,85670**	**4,74346**	**0,17951**	**4,25475**	**0,89697**	**1069**	**42**	**1064**	**42**	**1066**	**32**	**101**
1	**268**	**0,0000**	**96,53**	**0,66**	**0,07506**	**1,30453**	**1,86753**	**4,32066**	**0,18045**	**4,11902**	**0,95333**	**1070**	**26**	**1069**	**41**	**1070**	**29**	**101**
1	**267**	**0,0152**	**639,27**	**0,44**	**0,07508**	**1,04688**	**1,91208**	**4,09511**	**0,18470**	**3,95903**	**0,96677**	**1071**	**21**	**1093**	**40**	**1085**	**27**	**102**
1	**260**	**0,2589**	**96,52**	**0,68**	**0,07511**	**1,30546**	**1,87365**	**4,29919**	**0,18092**	**4,09620**	**0,95278**	**1071**	**26**	**1072**	**41**	**1072**	**29**	**101**
1	**259**	**0,0000**	**78,72**	**0,90**	**0,07511**	**1,20858**	**1,87938**	**4,31279**	**0,18147**	**4,13999**	**0,95993**	**1072**	**24**	**1075**	**41**	**1074**	**29**	**101**
1	**258**	**0,0000**	**95,42**	**0,70**	**0,07511**	**1,16784**	**1,88000**	**4,27899**	**0,18153**	**4,11654**	**0,96204**	**1072**	**24**	**1075**	**41**	**1074**	**29**	**101**
1	**257**	**0,0000**	**172,84**	**0,60**	**0,07514**	**1,08592**	**1,88855**	**4,21972**	**0,18228**	**4,07760**	**0,96632**	**1072**	**22**	**1079**	**41**	**1077**	**28**	**101**
1	**256**	**0,0000**	**94,70**	**0,77**	**0,07514**	**1,14022**	**1,89603**	**4,29237**	**0,18300**	**4,13816**	**0,96407**	**1072**	**23**	**1083**	**41**	**1080**	**29**	**102**
1	255	0,1833	332,88	0,43	0,07515	1,16979	1,92656	4,26279	0,18594	4,09915	0,96161	1072	24	1099	42	1090	29	102
1	**254**	**0,0000**	**109,78**	**0,57**	**0,07519**	**1,15301**	**1,87104**	**4,26622**	**0,18047**	**4,10746**	**0,96279**	**1074**	**23**	**1070**	**41**	**1071**	**28**	**101**
1	**253**	**0,1797**	**267,25**	**0,52**	**0,07520**	**1,54384**	**1,88618**	**4,62028**	**0,18191**	**4,35472**	**0,94252**	**1074**	**31**	**1077**	**43**	**1076**	**31**	**101**
1	**252**	**0,0000**	**77,48**	**0,62**	**0,07520**	**1,61400**	**1,85260**	**4,32666**	**0,17866**	**4,01435**	**0,92782**	**1074**	**33**	**1060**	**39**	**1064**	**29**	**101**
1	**251**	**0,0656**	**838,94**	**0,59**	**0,07522**	**1,04589**	**1,84343**	**4,32185**	**0,17775**	**4,19338**	**0,97028**	**1074**	**21**	**1055**	**41**	**1061**	**29**	**101**
1	**250**	**0,0421**	**508,21**	**0,33**	**0,07523**	**1,06364**	**1,89655**	**4,25543**	**0,18283**	**4,12035**	**0,96826**	**1075**	**21**	**1082**	**41**	**1080**	**28**	**101**
1	**249**	**0,0000**	**116,56**	**0,79**	**0,07525**	**1,11156**	**1,89184**	**4,23548**	**0,18235**	**4,08701**	**0,96495**	**1075**	**22**	**1080**	**41**	**1078**	**28**	**101**
1	**248**	**0,0000**	**99,32**	**0,75**	**0,07526**	**1,15207**	**1,89127**	**4,27976**	**0,18227**	**4,12179**	**0,96309**	**1075**	**23**	**1079**	**41**	**1078**	**29**	**101**
1	**247**	**0,0000**	**132,09**	**0,56**	**0,07527**	**1,16547**	**1,87988**	**4,33991**	**0,18115**	**4,18049**	**0,96327**	**1076**	**24**	**1073**	**41**	**1074**	**29**	**101**
1	**240**	**0,0000**	**77,64**	**0,60**	**0,07528**	**1,43631**	**1,87639**	**4,42824**	**0,18079**	**4,18883**	**0,94594**	**1076**	**29**	**1071**	**41**	**1073**	**30**	**101**
1	**239**	**0,1556**	**174,27**	**0,67**	**0,07528**	**1,15041**	**1,88941**	**4,23504**	**0,18203**	**4,07580**	**0,96240**	**1076**	**23**	**1078**	**41**	**1077**	**28**	**101**
1	**238**	**0,0702**	**104,14**	**0,51**	**0,07530**	**1,16691**	**1,88502**	**4,33210**	**0,18155**	**4,17198**	**0,96304**	**1077**	**24**	**1075**	**41**	**1076**	**29**	**101**
1	**237**	**0,0715**	**179,38**	**0,60**	**0,07531**	**1,10065**	**1,89201**	**4,20477**	**0,18220**	**4,05816**	**0,96513**	**1077**	**22**	**1079**	**40**	**1078**	**28**	**101**
1	**236**	**0,0000**	**176,84**	**0,41**	**0,07532**	**1,17822**	**1,85421**	**4,26149**	**0,17855**	**4,09537**	**0,96102**	**1077**	**24**	**1059**	**40**	**1065**	**28**	**101**
1	**235**	**0,0000**	**68,34**	**0,67**	**0,07539**	**1,17711**	**1,86545**	**4,30558**	**0,17946**	**4,14155**	**0,96190**	**1079**	**24**	**1064**	**41**	**1069**	**29**	**101**
1	**234**	**0,0000**	**123,93**	**0,45**	**0,07540**	**1,16342**	**1,90204**	**4,33110**	**0,18296**	**4,17191**	**0,96325**	**1079**	**23**	**1083**	**42**	**1082**	**29**	**101**
1	**233**	**0,1739**	**85,16**	**0,70**	**0,07543**	**1,20442**	**1,89555**	**4,25648**	**0,18226**	**4,08252**	**0,95913**	**1080**	**24**	**1079**	**41**	**1080**	**28**	**101**
1	**232**	**0,0000**	**196,48**	**1,01**	**0,07548**	**1,04054**	**1,93100**	**4,21197**	**0,18554**	**4,08141**	**0,96900**	**1081**	**21**	**1097**	**41**	**1092**	**28**	**102**
1	**231**	**0,0000**	**175,15**	**0,64**	**0,07549**	**1,09445**	**1,91906**	**4,26117**	**0,18437**	**4,11822**	**0,96645**	**1082**	**22**	**1091**	**41**	**1088**	**29**	**101**
1	**230**	**0,0000**	**121,99**	**0,69**	**0,07552**	**1,13452**	**1,91973**	**4,32426**	**0,18436**	**4,17278**	**0,96497**	**1082**	**23**	**1091**	**42**	**1088**	**29**	**101**
1	**229**	**0,1799**	**221,96**	**0,60**	**0,07555**	**1,20899**	**1,90498**	**4,23430**	**0,18288**	**4,05803**	**0,95837**	**1083**	**24**	**1083**	**41**	**1083**	**28**	**101**
1	**228**	**0,0000**	**74,56**	**0,66**	**0,07555**	**1,33657**	**1,90204**	**4,30533**	**0,18259**	**4,09260**	**0,95059**	**1083**	**27**	**1081**	**41**	**1082**	**29**	**101**
1	**227**	**0,0000**	**80,05**	**0,76**	**0,07558**	**1,36302**	**1,90072**	**4,23459**	**0,18239**	**4,00923**	**0,94678**	**1084**	**27**	**1080**	**40**	**1081**	**28**	**101**
1	**220**	**0,0000**	**138,00**	**0,90**	**0,07559**	**1,16044**	**1,88094**	**4,18284**	**0,18047**	**4,01865**	**0,96075**	**1084**	**23**	**1070**	**40**	**1074**	**28**	**101**
1	**218**	**0,0000**	**130,81**	**0,58**	**0,07559**	**1,09297**	**1,90912**	**4,22350**	**0,18317**	**4,07962**	**0,96594**	**1084**	**22**	**1084**	**41**	**1084**	**28**	**101**
1	**217**	**0,0000**	**326,60**	**1,58**	**0,07560**	**1,07933**	**1,92609**	**4,32212**	**0,18477**	**4,18519**	**0,96832**	**1085**	**22**	**1093**	**42**	**1090**	**29**	**101**
1	**216**	**0,0000**	**97,80**	**0,72**	**0,07563**	**1,28119**	**1,90357**	**4,42590**	**0,18254**	**4,23640**	**0,95719**	**1085**	**26**	**1081**	**42**	**1082**	**30**	**101**
1	**215**	**0,0000**	**105,16**	**1,06**	**0,07566**	**1,29415**	**1,89379**	**4,26257**	**0,18153**	**4,06136**	**0,95280**	**1086**	**26**	**1075**	**40**	**1079**	**29**	**101**
1	**214**	**0,0000**	**181,68**	**0,65**	**0,07567**	**1,06483**	**1,91829**	**4,21222**	**0,18385**	**4,07541**	**0,96752**	**1086**	**21**	**1088**	**41**	**1087**	**28**	**101**
1	**213**	**0,0000**	**78,71**	**0,78**	**0,07568**	**1,32075**	**1,89576**	**4,22582**	**0,18167**	**4,01412**	**0,94990**	**1087**	**27**	**1076**	**40**	**1080**	**28**	**101**

1	**212**	**0,0000**	**132,33**	**0,73**	**0,07570**	**1,10482**	**1,91342**	**4,25522**	**0,18331**	**4,10929**	**0,96571**	**1087**	**22**	**1085**	**41**	**1086**	**29**	**101**
1	**211**	**0,2364**	**206,38**	**0,37**	**0,07575**	**1,32150**	**1,89217**	**4,42332**	**0,18117**	**4,22131**	**0,95433**	**1088**	**27**	**1073**	**42**	**1078**	**30**	**101**
1	**210**	**0,0000**	**115,76**	**0,85**	**0,07579**	**1,26514**	**1,89811**	**4,46235**	**0,18165**	**4,27925**	**0,95897**	**1089**	**26**	**1076**	**42**	**1080**	**30**	**101**
1	**209**	**0,0000**	**122,17**	**0,97**	**0,07585**	**1,23722**	**1,93044**	**4,32654**	**0,18459**	**4,14586**	**0,95824**	**1091**	**25**	**1092**	**42**	**1092**	**29**	**101**
1	**208**	**0,0000**	**190,69**	**0,27**	**0,07590**	**1,20951**	**1,93142**	**4,20485**	**0,18456**	**4,02714**	**0,95774**	**1092**	**24**	**1092**	**41**	**1092**	**28**	**101**
1	**207**	**0,0000**	**117,94**	**0,82**	**0,07592**	**1,12858**	**1,89409**	**4,22782**	**0,18095**	**4,07440**	**0,96371**	**1093**	**23**	**1072**	**40**	**1079**	**28**	**101**
1	**200**	**0,0000**	**146,11**	**0,68**	**0,07592**	**1,23606**	**1,89556**	**4,27593**	**0,18109**	**4,09337**	**0,95731**	**1093**	**25**	**1073**	**41**	**1080**	**29**	**101**
1	**199**	**0,0000**	**81,30**	**0,51**	**0,07593**	**1,26276**	**1,92664**	**4,33558**	**0,18403**	**4,14762**	**0,95665**	**1093**	**25**	**1089**	**42**	**1090**	**29**	**101**
1	**198**	**0,0000**	**68,71**	**0,73**	**0,07610**	**1,62177**	**1,90908**	**4,61108**	**0,18194**	**4,31647**	**0,93611**	**1098**	**33**	**1078**	**43**	**1084**	**31**	**101**
1	**197**	**0,0000**	**103,91**	**0,75**	**0,07611**	**1,15251**	**1,90523**	**4,31692**	**0,18155**	**4,16023**	**0,96370**	**1098**	**23**	**1075**	**41**	**1083**	**29**	**100**
1	196	0,0000	285,11	0,61	0,07617	1,08463	1,99819	4,10523	0,19025	3,95935	0,96447	1100	22	1123	41	1115	28	102
1	**195**	**0,0000**	**97,67**	**0,88**	**0,07635**	**1,17568**	**2,00706**	**4,27335**	**0,19066**	**4,10844**	**0,96141**	**1104**	**24**	**1125**	**42**	**1118**	**29**	**102**
1	**194**	**0,0000**	**75,54**	**0,86**	**0,07641**	**1,16139**	**1,97089**	**4,29370**	**0,18708**	**4,13365**	**0,96272**	**1106**	**23**	**1106**	**42**	**1106**	**29**	**101**
1	**193**	**0,0000**	**68,47**	**0,94**	**0,07643**	**1,21447**	**1,99791**	**4,24567**	**0,18959**	**4,06826**	**0,95822**	**1106**	**24**	**1119**	**42**	**1115**	**29**	**102**
1	**192**	**0,0000**	**180,77**	**0,72**	**0,07658**	**1,17208**	**1,99990**	**4,38017**	**0,18940**	**4,22044**	**0,96353**	**1110**	**24**	**1118**	**43**	**1115**	**30**	**101**
1	**191**	**0,0000**	**204,77**	**1,65**	**0,07663**	**1,05151**	**2,04166**	**4,20814**	**0,19323**	**4,07465**	**0,96828**	**1112**	**21**	**1139**	**43**	**1130**	**29**	**102**
1	**190**	**0,2216**	**150,62**	**0,92**	**0,07676**	**1,23864**	**2,01744**	**4,31834**	**0,19062**	**4,13688**	**0,95798**	**1115**	**25**	**1125**	**43**	**1121**	**30**	**101**
1	**189**	**0,0000**	**278,98**	**0,71**	**0,07736**	**1,04167**	**2,06598**	**4,23619**	**0,19370**	**4,10612**	**0,96930**	**1130**	**21**	**1141**	**43**	**1138**	**29**	**101**
1	**188**	**0,0000**	**231,03**	**0,96**	**0,07762**	**1,06439**	**2,08196**	**4,22485**	**0,19453**	**4,08857**	**0,96774**	**1137**	**21**	**1146**	**43**	**1143**	**29**	**101**
1	**187**	**0,0000**	**236,74**	**1,99**	**0,07842**	**1,10562**	**2,10817**	**4,25606**	**0,19498**	**4,10994**	**0,96567**	**1157**	**22**	**1148**	**43**	**1151**	**30**	**101**
Rejected data																		
1	~~294~~	~~0,0000~~	~~552,86~~	~~0,48~~	~~0,07534~~	~~1,08313~~	~~1,60156~~	~~4,35966~~	~~0,15418~~	~~4,22297~~	~~0,96865~~	~~1078~~	~~22~~	~~924~~	~~36~~	~~971~~	~~27~~	~~96~~
1	~~280~~	~~0,0000~~	~~54,63~~	~~0,72~~	~~0,07615~~	~~1,62068~~	~~1,91572~~	~~4,60966~~	~~0,18245~~	~~4,31536~~	~~0,93616~~	~~1099~~	~~33~~	~~1080~~	~~43~~	~~1087~~	~~31~~	~~101~~
1	~~219~~	~~0,0000~~	~~79,62~~	~~0,59~~	~~0,07570~~	~~1,37429~~	~~1,93109~~	~~4,49279~~	~~0,18500~~	~~4,27744~~	~~0,95207~~	~~1087~~	~~28~~	~~1094~~	~~43~~	~~1092~~	~~30~~	~~101~~
MB-138																		
1	36	0,0301	1846,93	0,30	0,07371	0,99977	1,79760	4,05597	0,17687	3,93082	0,96914	1034	20	1050	38	1045	27	101
1	78	0,0000	413,47	0,67	0,07671	1,05039	2,04411	4,16731	0,19325	4,03276	0,96771	1114	21	1139	42	1130	29	101
1	30	0,0000	239,35	0,81	0,07682	1,04900	2,00206	4,13116	0,18903	3,99576	0,96722	1116	21	1116	41	1116	28	100
1	**97**	**0,0000**	**149,57**	**0,77**	**0,07692**	**1,20674**	**2,01120**	**4,33388**	**0,18964**	**4,16248**	**0,96045**	**1119**	**24**	**1119**	**43**	**1119**	**30**	**100**
1	**67**	**0,0000**	**126,51**	**0,53**	**0,07698**	**1,08652**	**2,01641**	**4,16224**	**0,18998**	**4,01793**	**0,96533**	**1121**	**22**	**1121**	**41**	**1121**	**28**	**100**
1	114	0,0000	358,33	0,52	0,07700	1,04650	2,06502	4,17111	0,19451	4,03770	0,96802	1121	21	1146	42	1137	29	101
1	27	0,0000	152,83	0,96	0,07703	1,05932	2,06180	4,06232	0,19413	3,92177	0,96540	1122	21	1144	41	1136	28	101
1	131	0,0000	282,21	0,32	0,07705	1,15171	2,04723	4,12515	0,19270	3,96112	0,96024	1123	23	1136	41	1131	28	100
1	**110**	**0,1259**	**126,00**	**0,92**	**0,07706**	**1,22434**	**2,02916**	**4,31257**	**0,19099**	**4,13512**	**0,95885**	**1123**	**25**	**1127**	**43**	**1125**	**30**	**100**
1	**130**	**0,2120**	**154,25**	**0,89**	**0,07708**	**1,42510**	**2,03376**	**4,25149**	**0,19136**	**4,00552**	**0,94215**	**1123**	**29**	**1129**	**42**	**1127**	**29**	**100**
1	9	0,0000	197,14	0,47	0,07711	1,03175	2,06249	4,04797	0,19399	3,91428	0,96697	1124	21	1143	41	1136	28	101
1	56	0,0744	434,75	0,40	0,07714	1,05003	2,08689	4,05965	0,19622	3,92150	0,96597	1125	21	1155	42	1145	28	101
1	75	0,0000	337,79	0,39	0,07717	1,03093	2,06668	4,11294	0,19423	3,98164	0,96808	1126	21	1144	42	1138	28	101
1	113	0,0351	608,84	0,88	0,07720	1,03477	2,04941	4,15783	0,19254	4,02701	0,96854	1126	21	1135	42	1132	29	100
1	48	0,0000	246,52	0,32	0,07722	1,03025	2,05013	4,08602	0,19254	3,95401	0,96769	1127	21	1135	41	1132	28	100
1	76	0,0000	265,57	1,40	0,07724	1,02997	2,08151	4,11857	0,19544	3,98770	0,96822	1128	21	1151	42	1143	28	101
1	**129**	**0,0000**	**97,35**	**0,79**	**0,07725**	**1,12226**	**2,04689**	**4,21813**	**0,19216**	**4,06610**	**0,96396**	**1128**	**22**	**1133**	**42**	**1131**	**29**	**100**
1	72	1,0000	345,65	0,18	0,07727	2,82914	2,07803	4,98589	0,19506	4,10550	0,82342	1128	57	1149	43	1142	35	101
1	**112**	**0,0388**	**138,55**	**0,39**	**0,07730**	**1,08689**	**2,05258**	**4,18018**	**0,19259**	**4,03640**	**0,96561**	**1129**	**22**	**1135**	**42**	**1133**	**29**	**100**
1	**118**	**1,0000**	**105,42**	**0,80**	**0,07731**	**2,85709**	**2,04621**	**5,05610**	**0,19197**	**4,17148**	**0,82504**	**1129**	**57**	**1132**	**43**	**1131**	**35**	**100**

1	79	0,0575	278,56	1,21	0,07732	1,05310	2,08489	4,13237	0,19556	3,99593	0,96698	1130	21	1151	42	1144	29	101
1	**128**	**0,0000**	**120,89**	**1,05**	**0,07733**	**1,10803**	**2,05209**	**4,20804**	**0,19247**	**4,05954**	**0,96471**	**1130**	**22**	**1135**	**42**	**1133**	**29**	**100**
1	60	0,0000	551,15	0,61	0,07733	1,04208	2,08232	3,99530	0,19531	3,85700	0,96539	1130	21	1150	41	1143	28	101
1	49	0,0007	448,90	0,32	0,07735	1,02863	2,11629	4,03049	0,19844	3,89702	0,96689	1130	21	1167	42	1154	28	101
1	28	0,0000	328,36	0,53	0,07735	1,01543	2,10626	4,05494	0,19750	3,92575	0,96814	1130	20	1162	42	1151	28	101
1	32	0,0000	294,00	0,64	0,07739	1,01489	2,07434	4,06544	0,19441	3,93672	0,96834	1131	20	1145	41	1140	28	100
1	52	0,0713	587,29	0,35	0,07753	1,01735	2,08780	4,07872	0,19532	3,94980	0,96839	1135	20	1150	42	1145	28	100
1	73	0,0000	143,60	0,63	0,07753	1,10512	2,10955	4,11073	0,19734	3,95939	0,96319	1135	22	1161	42	1152	29	101
1	14	0,0000	803,53	0,35	0,07753	1,01302	2,12358	3,97376	0,19865	3,84247	0,96696	1135	20	1168	41	1156	28	101
1	**77**	**0,0000**	**113,65**	**1,06**	**0,07756**	**1,13098**	**2,05189**	**4,08573**	**0,19187**	**3,92607**	**0,96092**	**1136**	**23**	**1132**	**41**	**1133**	**28**	**100**
1	57	0,0000	60,28	0,53	0,07758	1,27531	2,09100	4,08839	0,19548	3,88439	0,95010	1136	26	1151	41	1146	28	100
1	**59**	**0,0000**	**130,13**	**0,89**	**0,07761**	**1,06453**	**2,05217**	**4,11016**	**0,19177**	**3,96991**	**0,96588**	**1137**	**21**	**1131**	**41**	**1133**	**28**	**100**
1	**70**	**0,0000**	**97,97**	**0,55**	**0,07761**	**1,11710**	**2,08014**	**4,11238**	**0,19439**	**3,95774**	**0,96240**	**1137**	**22**	**1145**	**42**	**1142**	**28**	**100**
1	15	0,0244	531,90	0,46	0,07763	1,01370	2,15472	4,04072	0,20130	3,91150	0,96802	1138	20	1182	42	1167	28	101
1	50	0,0000	366,41	0,51	0,07766	1,02443	2,13504	4,07967	0,19938	3,94895	0,96796	1138	20	1172	42	1160	28	101
1	**31**	**0,0000**	**77,66**	**1,57**	**0,07768**	**1,27363**	**2,06081**	**4,02817**	**0,19240**	**3,82152**	**0,94870**	**1139**	**25**	**1134**	**40**	**1136**	**28**	**100**
1	37	0,0000	321,76	0,32	0,07771	1,03688	2,09823	4,16232	0,19582	4,03110	0,96847	1140	21	1153	43	1148	29	100
1	115	0,0000	434,47	0,84	0,07776	1,03620	2,10036	4,16075	0,19589	4,02966	0,96849	1141	21	1153	43	1149	29	100
1	98	0,0000	419,67	0,49	0,07776	1,03620	2,11496	4,14364	0,19725	4,01199	0,96823	1141	21	1161	43	1154	29	101
1	39	0,0000	740,90	0,19	0,07776	1,02308	2,12968	3,98665	0,19862	3,85314	0,96651	1141	20	1168	41	1158	28	101
1	71	0,0000	214,49	0,64	0,07778	1,07541	2,04080	4,18313	0,19031	4,04253	0,96639	1141	22	1123	42	1129	29	99
1	10	0,0000	196,44	0,84	0,07782	1,03552	2,05466	4,04746	0,19150	3,91275	0,96672	1142	21	1130	41	1134	28	100
1	91	0,0000	79,36	0,55	0,07782	1,21903	2,11205	4,20091	0,19685	4,02015	0,95697	1142	24	1158	43	1153	29	100
1	**8**	**0,0000**	**332,96**	**0,48**	**0,07785**	**1,02201**	**2,08708**	**4,07641**	**0,19445**	**3,94622**	**0,96806**	**1143**	**20**	**1145**	**41**	**1145**	**28**	**100**
1	**54**	**0,0000**	**183,93**	**0,71**	**0,07786**	**1,08738**	**2,09800**	**4,08387**	**0,19544**	**3,93644**	**0,96390**	**1143**	**22**	**1151**	**42**	**1148**	**28**	**100**
1	13	0,0000	558,89	0,41	0,07789	1,00838	2,13841	4,04169	0,19912	3,91387	0,96838	1144	20	1171	42	1161	28	101
1	**132**	**0,1056**	**242,94**	**0,93**	**0,07792**	**1,46630**	**2,09876**	**4,21319**	**0,19536**	**3,94980**	**0,93748**	**1145**	**29**	**1150**	**42**	**1148**	**29**	**100**
1	**100**	**0,0000**	**164,90**	**0,39**	**0,07793**	**1,13874**	**2,10842**	**4,27907**	**0,19623**	**4,12476**	**0,96394**	**1145**	**23**	**1155**	**44**	**1152**	**30**	**100**
1	**20**	**0,0000**	**511,57**	**0,28**	**0,07796**	**1,00746**	**2,09881**	**4,04696**	**0,19526**	**3,91956**	**0,96852**	**1146**	**20**	**1150**	**41**	**1148**	**28**	**100**
1	99	0,0000	215,89	1,17	0,07796	1,05979	2,16018	4,15498	0,20097	4,01755	0,96692	1146	21	1181	43	1168	29	101
1	40	0,0000	234,55	0,76	0,07798	1,02027	2,11745	4,06698	0,19694	3,93693	0,96802	1146	20	1159	42	1155	28	100
1	**16**	**0,0000**	**170,39**	**0,76**	**0,07799**	**1,04630**	**2,10889**	**4,05991**	**0,19612**	**3,92277**	**0,96622**	**1147**	**21**	**1154**	**42**	**1152**	**28**	**100**
1	**117**	**0,0000**	**128,17**	**0,55**	**0,07800**	**1,20309**	**2,10734**	**4,14549**	**0,19595**	**3,96708**	**0,95696**	**1147**	**24**	**1154**	**42**	**1151**	**29**	**100**
1	**19**	**1,0000**	**564,10**	**0,33**	**0,07801**	**2,80224**	**2,11845**	**4,92176**	**0,19696**	**4,04613**	**0,82209**	**1147**	**56**	**1159**	**43**	**1155**	**34**	**100**
1	**35**	**0,0000**	**306,38**	**0,90**	**0,07802**	**1,20277**	**2,11155**	**4,34435**	**0,19629**	**4,17453**	**0,96091**	**1147**	**24**	**1155**	**44**	**1153**	**30**	**100**
1	**127**	**0,0000**	**89,25**	**0,45**	**0,07803**	**1,29412**	**2,10903**	**4,18100**	**0,19603**	**3,97568**	**0,95089**	**1148**	**26**	**1154**	**42**	**1152**	**29**	**100**
1	69	0,0000	394,49	0,49	0,07805	1,00627	2,15356	4,09027	0,20012	3,96456	0,96927	1148	20	1176	43	1166	29	101
1	53	0,0400	713,84	0,49	0,07810	1,02402	2,15452	4,08594	0,20008	3,95554	0,96809	1149	20	1176	43	1167	29	101
1	80	0,0000	134,28	0,58	0,07810	1,12316	2,12509	4,06680	0,19734	3,90863	0,96111	1149	22	1161	42	1157	28	100
1	68	0,0000	200,33	0,87	0,07818	1,04371	2,15528	4,11279	0,19994	3,97816	0,96726	1152	21	1175	43	1167	29	101
1	89	0,0000	269,57	0,90	0,07820	1,04343	2,15476	4,13405	0,19984	4,00020	0,96762	1152	21	1174	43	1167	29	101
1	119	0,0000	76,99	0,54	0,07832	1,21125	2,19019	4,16084	0,20283	3,98064	0,95669	1155	24	1191	43	1178	29	101
1	93	0,0000	350,97	1,68	0,07868	1,15375	2,19231	4,32086	0,20208	4,16398	0,96369	1164	23	1186	45	1179	30	101
1	18	0,0000	341,81	0,37	0,07868	1,15375	2,21546	3,88376	0,20421	3,70843	0,95486	1164	23	1198	41	1186	27	101
1	55	0,0000	116,25	0,33	0,07890	1,07304	2,19795	4,10888	0,20205	3,96629	0,96530	1170	21	1186	43	1180	29	101

1	95	0,0000	480,03	0,42	0,07896	1,11097	2,21176	4,10754	0,20316	3,95444	0,96273	1171	22	1192	43	1185	29	101
1	74	0,0000	81,27	0,85	0,07917	1,28833	2,23865	4,09612	0,20507	3,88824	0,94925	1176	26	1203	43	1193	29	101
1	94	0,0000	186,61	0,88	0,07934	1,07997	2,21795	4,12587	0,20276	3,98202	0,96513	1181	21	1190	43	1187	29	100
1	92	0,0000	52,41	0,51	0,07961	1,17873	2,24731	4,19109	0,20473	4,02192	0,95964	1187	23	1201	44	1196	30	100
1	58	0,1050	166,92	0,35	0,08026	1,07572	2,28950	4,10543	0,20689	3,96199	0,96506	1203	21	1212	44	1209	29	100
1	90	0,5377	100,23	0,73	0,08043	1,88850	2,35533	4,61373	0,21239	4,20953	0,91239	1208	37	1242	48	1229	33	101
1	87	0,0000	250,71	0,34	0,08078	1,09848	2,37605	4,26686	0,21332	4,12303	0,96629	1216	22	1246	47	1235	31	101
1	12	0,0000	191,02	0,81	0,08094	1,03340	2,19140	4,05177	0,19637	3,91777	0,96693	1220	20	1156	42	1178	28	98
1	34	0,0000	202,48	1,17	0,08096	1,07093	2,35845	4,20650	0,21128	4,06789	0,96705	1220	21	1236	46	1230	30	100
1	108	0,0000	350,83	1,24	0,08101	1,08285	2,38041	4,08503	0,21312	3,93890	0,96423	1222	21	1245	45	1237	29	101
1	33	0,0024	473,06	0,67	0,08103	0,99450	2,26232	4,05172	0,20250	3,92778	0,96941	1222	20	1189	43	1201	29	99
1	111	0,0000	80,08	1,33	0,08200	1,11954	2,43576	4,18830	0,21544	4,03590	0,96361	1245	22	1258	46	1253	30	100
1	38	0,0000	379,57	0,52	0,08226	1,02914	2,45545	4,04769	0,21648	3,91467	0,96714	1252	20	1263	45	1259	29	100
1	109	0,0000	259,32	0,40	0,08557	1,03707	2,71483	4,14557	0,23011	4,01376	0,96820	1328	20	1335	49	1333	31	100
1	96	0,0000	214,22	0,80	0,08718	1,05300	2,85880	4,13758	0,23783	4,00135	0,96707	1364	20	1375	50	1371	31	100
1	120	0,0000	291,88	1,75	0,11466	1,08531	5,48701	4,10030	0,34708	3,95405	0,96433	1875	20	1921	66	1899	36	101
Rejected data																		
1	~~17~~	~~0,1088~~	~~604,81~~	~~0,39~~	~~0,07908~~	~~1,09435~~	~~1,92826~~	~~4,23518~~	~~0,17686~~	~~4,09135~~	~~0,96604~~	~~1174~~	~~22~~	~~1050~~	~~40~~	~~1091~~	~~29~~	~~96~~
1	~~29~~	~~0,1444~~	~~297,60~~	~~0,41~~	~~0,08532~~	~~1,11857~~	~~2,26935~~	~~4,22478~~	~~0,19290~~	~~4,07401~~	~~0,96431~~	~~1323~~	~~22~~	~~1137~~	~~43~~	~~1203~~	~~30~~	~~95~~
1	~~51~~	~~0,1881~~	~~371,91~~	~~1,03~~	~~0,08701~~	~~1,11120~~	~~2,28600~~	~~4,11108~~	~~0,19056~~	~~3,95805~~	~~0,96278~~	~~1361~~	~~22~~	~~1124~~	~~41~~	~~1208~~	~~29~~	~~93~~
1	~~7~~	~~0,1693~~	~~839,23~~	~~0,44~~	~~0,08337~~	~~1,08547~~	~~2,02262~~	~~4,05790~~	~~0,17596~~	~~3,91003~~	~~0,96356~~	~~1278~~	~~21~~	~~1045~~	~~38~~	~~1123~~	~~28~~	~~93~~
1	~~47~~	~~0,4556~~	~~233,86~~	~~0,79~~	~~0,09067~~	~~1,48080~~	~~2,43141~~	~~4,19231~~	~~0,19449~~	~~3,92208~~	~~0,93554~~	~~1440~~	~~28~~	~~1146~~	~~41~~	~~1252~~	~~30~~	~~92~~
1	~~11~~	~~0,5247~~	~~450,98~~	~~2,18~~	~~0,10298~~	~~1,49154~~	~~2,45958~~	~~4,06789~~	~~0,17323~~	~~3,78458~~	~~0,93035~~	~~1678~~	~~28~~	~~1030~~	~~36~~	~~1260~~	~~30~~	~~82~~
1	~~107~~	~~0,0000~~	~~83,92~~	~~0,51~~	~~0,07764~~	~~1,14293~~	~~2,09437~~	~~4,18372~~	~~0,19564~~	~~4,02458~~	~~0,96196~~	~~1138~~	~~23~~	~~1152~~	~~43~~	~~1147~~	~~29~~	~~100~~
1	~~88~~	~~0,0000~~	~~302,41~~	~~0,01~~	~~0,07880~~	~~1,13916~~	~~2,18880~~	~~4,30999~~	~~0,20147~~	~~4,15672~~	~~0,96444~~	~~1167~~	~~23~~	~~1183~~	~~45~~	~~1177~~	~~30~~	~~100~~
1	~~116~~	~~0,0000~~	~~463,19~~	~~0,40~~	~~0,08855~~	~~1,15194~~	~~2,72347~~	~~4,08168~~	~~0,22308~~	~~3,91576~~	~~0,95935~~	~~1394~~	~~22~~	~~1298~~	~~46~~	~~1335~~	~~31~~	~~97~~
MB-137																		
1	151	0,0000	282,56	0,47	0,07403	1,15962	1,87491	4,12181	0,18368	3,95533	0,95961	1042	23	1087	40	1072	28	102
1	**150**	**0,0000**	**287,69**	**0,77**	**0,07506**	**1,35899**	**1,88122**	**4,39927**	**0,18177**	**4,18410**	**0,95109**	**1070**	**27**	**1077**	**42**	**1074**	**29**	**101**
1	**140**	**0,0000**	**296,59**	**0,81**	**0,07509**	**1,18359**	**1,91679**	**4,31678**	**0,18513**	**4,15135**	**0,96168**	**1071**	**24**	**1095**	**42**	**1087**	**29**	**101**
1	148	0,0753	396,24	0,71	0,07526	1,14528	1,83348	4,11655	0,17669	3,95403	0,96052	1075	23	1049	38	1058	27	100
1	**180**	**0,0000**	**344,44**	**0,36**	**0,07528**	**1,32832**	**1,90336**	**4,17835**	**0,18339**	**3,96158**	**0,94812**	**1076**	**27**	**1085**	**40**	**1082**	**28**	**101**
1	**157**	**0,0000**	**309,35**	**0,43**	**0,07528**	**1,31491**	**1,91053**	**4,14969**	**0,18408**	**3,93585**	**0,94847**	**1076**	**26**	**1089**	**40**	**1085**	**28**	**101**
1	179	0,1209	346,27	0,45	0,07531	1,19814	1,83502	4,26226	0,17673	4,09039	0,95968	1077	24	1049	40	1058	28	100
1	**171**	**0,0588**	**280,77**	**0,64**	**0,07535**	**1,30970**	**1,90197**	**4,38769**	**0,18307**	**4,18766**	**0,95441**	**1078**	**26**	**1084**	**42**	**1082**	**30**	**101**
1	**136**	**0,0000**	**270,35**	**0,49**	**0,07536**	**1,20627**	**1,88450**	**4,41621**	**0,18137**	**4,24828**	**0,96197**	**1078**	**24**	**1074**	**42**	**1076**	**30**	**100**
1	173	0,0000	351,60	0,51	0,07536	1,08565	1,97340	4,19965	0,18993	4,05690	0,96601	1078	22	1121	42	1106	29	102
1	155	0,0243	888,67	0,68	0,07536	1,19462	1,84681	4,19366	0,17774	4,01991	0,95857	1078	24	1055	39	1062	28	100
1	**156**	**0,0000**	**537,79**	**0,55**	**0,07541**	**1,16528**	**1,89794**	**4,30499**	**0,18255**	**4,14428**	**0,96267**	**1079**	**23**	**1081**	**41**	**1080**	**29**	**101**
1	**133**	**0,1464**	**114,26**	**0,54**	**0,07544**	**1,21636**	**1,86385**	**4,33228**	**0,17919**	**4,15802**	**0,95978**	**1080**	**24**	**1063**	**41**	**1068**	**29**	**100**
1	**178**	**0,0000**	**648,60**	**0,41**	**0,07546**	**1,31174**	**1,91285**	**4,36027**	**0,18386**	**4,15828**	**0,95367**	**1081**	**26**	**1088**	**42**	**1086**	**29**	**101**
1	**153**	**0,0000**	**300,63**	**0,53**	**0,07547**	**1,33833**	**1,87114**	**4,16100**	**0,17982**	**3,93990**	**0,94686**	**1081**	**27**	**1066**	**39**	**1071**	**28**	**100**
1	**168**	**0,0000**	**143,39**	**0,61**	**0,07554**	**1,36382**	**1,89051**	**4,43771**	**0,18152**	**4,22295**	**0,95160**	**1083**	**27**	**1075**	**42**	**1078**	**30**	**100**
1	**152**	**0,0000**	**143,64**	**0,94**	**0,07558**	**1,26954**	**1,87536**	**4,15765**	**0,17996**	**3,95907**	**0,95224**	**1084**	**26**	**1067**	**39**	**1072**	**28**	**100**
1	**188**	**0,1451**	**349,17**	**0,46**	**0,07559**	**1,75371**	**1,89660**	**4,54525**	**0,18198**	**4,19331**	**0,92257**	**1084**	**35**	**1078**	**42**	**1080**	**31**	**100**

1	**175**	**0,0000**	**223,20**	**0,38**	**0,07564**	**1,26853**	**1,90671**	**4,34894**	**0,18283**	**4,15982**	**0,95651**	**1086**	**26**	**1082**	**42**	**1083**	**29**	**100**
1	**189**	**0,0058**	**614,27**	**0,44**	**0,07567**	**1,42817**	**1,92693**	**4,22589**	**0,18468**	**3,97725**	**0,94116**	**1086**	**29**	**1092**	**40**	**1090**	**29**	**101**
1	**137**	**0,0492**	**641,60**	**0,83**	**0,07582**	**1,03399**	**1,91608**	**4,19212**	**0,18328**	**4,06260**	**0,96910**	**1090**	**21**	**1085**	**41**	**1087**	**28**	**100**
1	**169**	**0,0000**	**206,51**	**0,49**	**0,07584**	**1,46491**	**1,92771**	**4,50085**	**0,18435**	**4,25578**	**0,94555**	**1091**	**29**	**1091**	**43**	**1091**	**30**	**101**
1	159	0,0000	154,98	0,79	0,07596	1,17006	1,89085	4,16953	0,18053	4,00200	0,95982	1094	23	1070	40	1078	28	100
1	**158**	**0,0000**	**188,20**	**0,33**	**0,07597**	**1,13002**	**1,92119**	**4,17168**	**0,18341**	**4,01571**	**0,96261**	**1094**	**23**	**1086**	**40**	**1088**	**28**	**100**
1	**154**	**0,0000**	**311,32**	**0,50**	**0,07631**	**1,20450**	**1,92709**	**4,14520**	**0,18317**	**3,96635**	**0,95685**	**1103**	**24**	**1084**	**40**	**1091**	**28**	**100**
1	**187**	**0,0000**	**184,78**	**1,01**	**0,07635**	**1,34938**	**1,92390**	**4,19782**	**0,18277**	**3,97503**	**0,94693**	**1104**	**27**	**1082**	**40**	**1089**	**28**	**100**
1	129	0,2357	106,68	0,76	0,07700	1,40284	2,02373	4,47471	0,19061	4,24913	0,94959	1121	28	1125	44	1124	31	101
1	177	0,0864	140,97	0,40	0,07730	1,35171	2,04306	4,28137	0,19169	4,06239	0,94885	1129	27	1131	42	1130	30	101
1	131	0,0000	304,18	0,33	0,07753	1,34184	2,04278	4,16014	0,19110	3,93779	0,94655	1135	27	1127	41	1130	29	100
1	130	0,1876	181,06	0,84	0,07757	1,28154	2,03351	4,27528	0,19012	4,07868	0,95402	1136	26	1122	42	1127	29	100
1	138	0,0000	135,88	0,34	0,07763	1,30107	2,02841	4,46052	0,18951	4,26655	0,95651	1137	26	1119	44	1125	31	100
1	**191**	**0,0000**	**277,27**	**0,62**	**0,07766**	**1,45663**	**2,02385**	**4,24941**	**0,18901**	**3,99195**	**0,93941**	**1138**	**29**	**1116**	**41**	**1124**	**29**	**100**
1	128	0,0000	148,67	1,01	0,07783	1,25876	2,06118	4,44376	0,19207	4,26175	0,95904	1143	25	1133	44	1136	31	100
1	132	0,2290	294,46	0,92	0,07797	1,35445	2,06242	4,14708	0,19183	3,91965	0,94516	1146	27	1131	41	1136	29	100
1	174	0,0000	475,98	0,65	0,07821	1,14928	2,07502	4,15623	0,19241	3,99418	0,96101	1152	23	1134	42	1141	29	100
1	135	0,0093	381,33	0,84	0,07892	1,11360	2,12934	4,21050	0,19567	4,06056	0,96439	1170	22	1152	43	1158	29	100
1	127	0,0000	117,35	0,40	0,07953	1,15570	2,16636	4,34045	0,19757	4,18376	0,96390	1185	23	1162	45	1170	31	100
1	167	1,0000	198,94	0,23	0,07968	2,78010	2,17835	5,05377	0,19829	4,22038	0,83510	1189	55	1166	45	1174	36	100
Rejected data																		
1	~~160~~	~~0,0000~~	~~186,44~~	~~0,76~~	~~0,07382~~	~~1,14927~~	~~2,19618~~	~~4,23998~~	~~0,21577~~	~~4,08125~~	~~0,96256~~	~~1037~~	~~23~~	~~1259~~	~~47~~	~~1180~~	~~30~~	~~107~~
1	~~190~~	~~0,0000~~	~~586,12~~	~~0,46~~	~~0,07559~~	~~1,13576~~	~~1,57076~~	~~4,20643~~	~~0,15071~~	~~4,05020~~	~~0,96286~~	~~1084~~	~~23~~	~~905~~	~~34~~	~~959~~	~~26~~	~~95~~
1	~~147~~	~~0,0599~~	~~957,12~~	~~0,60~~	~~0,07764~~	~~1,02654~~	~~1,63241~~	~~4,17157~~	~~0,15249~~	~~4,04329~~	~~0,96925~~	~~1138~~	~~20~~	~~915~~	~~35~~	~~983~~	~~27~~	~~94~~
1	~~170~~	~~0,0000~~	~~464,15~~	~~0,68~~	~~0,07675~~	~~1,13173~~	~~2,12321~~	~~4,14742~~	~~0,20064~~	~~3,99002~~	~~0,96205~~	~~1115~~	~~23~~	~~1179~~	~~43~~	~~1156~~	~~29~~	~~103~~
1	~~176~~	~~0,0000~~	~~235,96~~	~~0,66~~	~~0,07452~~	~~1,21984~~	~~1,93459~~	~~4,16845~~	~~0,18829~~	~~3,98597~~	~~0,95622~~	~~1056~~	~~25~~	~~1112~~	~~41~~	~~1093~~	~~28~~	~~102~~
1	~~172~~	~~0,0000~~	~~749,57~~	~~0,48~~	~~0,07428~~	~~1,37340~~	~~1,90103~~	~~4,46448~~	~~0,18563~~	~~4,24798~~	~~0,95151~~	~~1049~~	~~28~~	~~1098~~	~~43~~	~~1081~~	~~30~~	~~102~~
1	~~149~~	~~0,0328~~	~~293,64~~	~~0,59~~	~~0,07398~~	~~1,38183~~	~~1,92987~~	~~4,47141~~	~~0,18920~~	~~4,25254~~	~~0,95105~~	~~1041~~	~~28~~	~~1117~~	~~44~~	~~1091~~	~~30~~	~~103~~
1	~~139~~	~~0,0208~~	~~237,07~~	~~0,60~~	~~0,07344~~	~~1,07420~~	~~1,83643~~	~~4,20087~~	~~0,18135~~	~~4,06120~~	~~0,96675~~	~~1026~~	~~22~~	~~1074~~	~~40~~	~~1059~~	~~28~~	~~102~~
1	~~134~~	~~0,1230~~	~~285,24~~	~~0,47~~	~~0,07297~~	~~1,10566~~	~~1,84908~~	~~4,25402~~	~~0,18378~~	~~4,10782~~	~~0,96563~~	~~1013~~	~~22~~	~~1088~~	~~41~~	~~1063~~	~~28~~	~~103~~
Reference materials																		
BB																		
1	1	0,0000	556,71	0,48	0,05928	1,04588	0,73635	4,02332	0,09009	3,88500	0,96562	577	23	556	21	560	17	99
1	2	0,0003	598,28	0,49	0,05883	1,03689	0,74431	4,01586	0,09176	3,87969	0,96609	561	23	566	21	565	18	100
1	21	0,0380	463,98	0,46	0,05917	1,05571	0,75576	4,04853	0,09264	3,90846	0,96540	573	23	571	21	572	18	100
1	~~22~~	~~0,0000~~	~~457,90~~	~~0,47~~	~~0,05836~~	~~1,06237~~	~~0,75132~~	~~4,06130~~	~~0,09337~~	~~3,91989~~	~~0,96518~~	~~543~~	~~23~~	~~575~~	~~22~~	~~569~~	~~18~~	~~101~~
1	41	0,0000	391,77	0,48	0,05871	1,07307	0,72960	4,07161	0,09013	3,92766	0,96465	556	23	556	21	556	18	100
1	42	0,0000	394,14	0,47	0,05863	1,07454	0,73749	4,08976	0,09123	3,94607	0,96487	553	23	563	21	561	18	100
1	61	0,0000	383,85	0,47	0,05934	1,07853	0,74250	4,11094	0,09075	3,96694	0,96497	580	23	560	21	564	18	99
1	62	0,0346	381,67	0,46	0,05906	1,08995	0,73476	4,11534	0,09023	3,96838	0,96429	569	24	557	21	559	18	100
1	81	0,0000	367,39	0,45	0,05867	1,09085	0,73953	4,12835	0,09142	3,98162	0,96446	555	24	564	22	562	18	100
1	82	0,1419	355,95	0,47	0,05845	1,19785	0,73487	4,17913	0,09119	4,00378	0,95804	547	26	563	22	559	18	101
1	~~101~~	~~0,0141~~	~~361,52~~	~~0,48~~	~~0,05820~~	~~1,10069~~	~~0,74230~~	~~4,16964~~	~~0,09250~~	~~4,02174~~	~~0,96453~~	~~537~~	~~24~~	~~570~~	~~22~~	~~564~~	~~18~~	~~101~~

1	102	0,1947	353,55	0,45	0,05915	1,28087	0,75266	4,23025	0,09228	4,03168	0,95306	573	28	569	22	570	19	100
1	121	0,0000	350,07	0,45	0,05886	1,10432	0,74128	4,17751	0,09134	4,02890	0,96443	562	24	563	22	563	18	100
1	122	0,0000	351,22	0,47	0,05912	1,08254	0,73852	4,18227	0,09060	4,03974	0,96592	572	24	559	22	562	18	100
1	121	0,0000	398,93	0,45	0,05862	1,09178	0,74400	4,20714	0,09205	4,06301	0,96574	553	24	568	22	565	18	101
1	122	0,0000	401,17	0,46	0,05932	1,07889	0,74855	4,20543	0,09152	4,06469	0,96653	579	23	565	22	567	18	99
1	141	0,0000	426,05	0,46	0,05893	1,08603	0,73387	4,19527	0,09032	4,05226	0,96591	565	24	557	22	559	18	100
1	142	0,0000	372,61	0,50	0,05844	1,12936	0,75751	4,29947	0,09401	4,14849	0,96488	546	25	579	23	573	19	101
1	161	0,0000	426,55	0,46	0,05901	1,11845	0,74065	4,21567	0,09103	4,06459	0,96416	567	24	562	22	563	18	100
1	162	0,0000	426,32	0,48	0,05827	1,11550	0,73851	4,19792	0,09192	4,04700	0,96405	540	24	567	22	562	18	101
1	181	0,0000	420,81	0,47	0,05928	1,14710	0,74518	4,21735	0,09117	4,05835	0,96230	577	25	562	22	565	18	99
1	182	0,0746	423,54	0,46	0,05883	1,18348	0,74531	4,22089	0,09189	4,05158	0,95989	561	26	567	22	566	18	100
GJ-1																		
1	~~3~~	~~0,0000~~	~~314,54~~	~~0,04~~	~~0,06000~~	~~1,06667~~	~~0,81263~~	~~4,05864~~	~~0,09823~~	~~3,91597~~	~~0,96485~~	~~604~~	~~23~~	~~604~~	~~23~~	~~604~~	~~19~~	~~100~~
1	4	0,0000	336,02	0,04	0,06005	1,18235	0,81315	4,09134	0,09821	3,91677	0,95733	605	26	604	23	604	19	100
1	23	0,0000	211,54	0,04	0,06015	1,36326	0,81882	4,01300	0,09873	3,77435	0,94053	609	29	607	22	607	18	100
1	~~24~~	~~0,2499~~	~~215,75~~	~~0,03~~	~~0,05991~~	~~1,49049~~	~~0,81026~~	~~4,13161~~	~~0,09809~~	~~3,85339~~	~~0,93266~~	~~600~~	~~32~~	~~603~~	~~22~~	~~603~~	~~19~~	~~100~~
1	43	0,0000	204,02	0,07	0,06079	1,11861	0,82333	4,11184	0,09823	3,95676	0,96228	632	24	604	23	610	19	99
1	44	0,0577	202,50	0,02	0,06049	1,20556	0,81219	4,22984	0,09739	4,05440	0,95852	621	26	599	23	604	19	99
1	~~63~~	~~0,0000~~	~~195,60~~	~~0,04~~	~~0,06005~~	~~1,39883~~	~~0,80668~~	~~4,26628~~	~~0,09743~~	~~4,03043~~	~~0,94472~~	~~605~~	~~30~~	~~599~~	~~23~~	~~601~~	~~20~~	~~100~~
1	~~64~~	~~0,2239~~	~~197,24~~	~~0,05~~	~~0,05968~~	~~1,71455~~	~~0,79613~~	~~4,41106~~	~~0,09676~~	~~4,06421~~	~~0,92137~~	~~592~~	~~37~~	~~595~~	~~23~~	~~595~~	~~20~~	~~100~~
1	~~83~~	~~0,0000~~	~~154,91~~	~~0,04~~	~~0,05430~~	~~2,19153~~	~~0,73701~~	~~4,78496~~	~~0,09844~~	~~4,25359~~	~~0,88895~~	~~384~~	~~49~~	~~605~~	~~25~~	~~561~~	~~21~~	~~108~~
1	84	0,0000	182,36	0,01	0,06013	1,21404	0,81049	4,11786	0,09776	3,93483	0,95555	608	26	601	23	603	19	100
1	103	0,0000	178,50	0,04	0,06076	1,15207	0,82268	4,18104	0,09820	4,01918	0,96129	631	25	604	23	610	19	99
1	~~104~~	~~0,0000~~	~~187,57~~	~~0,06~~	~~0,05999~~	~~1,30022~~	~~0,81184~~	~~4,36239~~	~~0,09815~~	~~4,16412~~	~~0,95455~~	~~603~~	~~28~~	~~604~~	~~24~~	~~603~~	~~20~~	~~100~~
1	~~123~~	~~0,0000~~	~~182,59~~	~~0,04~~	~~0,05987~~	~~1,20261~~	~~0,80492~~	~~4,18317~~	~~0,09751~~	~~4,00657~~	~~0,95778~~	~~599~~	~~26~~	~~600~~	~~23~~	~~600~~	~~19~~	~~100~~
1	124	0,0000	183,20	0,08	0,06034	1,17667	0,82266	4,20020	0,09888	4,03201	0,95996	616	25	608	23	610	19	100
1	123	0,0000	210,72	0,04	0,06013	1,13088	0,81206	4,24022	0,09795	4,08664	0,96378	608	24	602	24	604	19	100
1	124	0,0000	207,66	0,08	0,06011	1,28098	0,81311	4,19856	0,09811	3,99837	0,95232	608	28	603	23	604	19	100
1	143	0,0000	224,05	0,05	0,05982	1,20361	0,81043	4,28691	0,09826	4,11447	0,95978	597	26	604	24	603	20	100
1	144	0,4184	209,25	0,06	0,05970	1,84910	0,80270	4,50973	0,09752	4,11320	0,91207	593	40	600	24	598	21	100
1	163	0,0464	215,24	0,02	0,06036	1,51540	0,81277	4,37099	0,09766	4,09989	0,93798	617	33	601	24	604	20	99
1	164	0,0000	215,81	0,05	0,05998	1,16706	0,81615	4,24003	0,09869	4,07625	0,96137	603	25	607	24	606	20	100
1	183	0,0000	218,10	0,06	0,06103	1,32722	0,82337	4,26184	0,09785	4,04991	0,95027	640	29	602	23	610	20	99
1	184	0,0000	209,69	0,04	0,06022	1,32846	0,81352	4,23771	0,09798	4,02410	0,94959	611	29	603	23	604	19	100
1	183	0,5699	215,61	0,06	0,06057	2,19967	0,81560	4,76497	0,09766	4,22687	0,88707	624	47	601	24	606	22	99
1	184	1,0000	210,97	0,05	0,06053	3,49006	0,81958	5,74354	0,09821	4,56154	0,79420	622	75	604	26	608	27	99
1	203	0,0455	215,81	0,06	0,06057	1,13261	0,82731	4,24044	0,09906	4,08638	0,96367	624	24	609	24	612	20	99
1	204	0,0000	213,72	0,07	0,06031	1,12751	0,81706	4,23089	0,09826	4,07789	0,96384	615	24	604	24	606	19	100
1	223	0,0000	229,82	0,07	0,06017	1,13013	0,80909	4,24126	0,09753	4,08792	0,96385	610	24	600	23	602	19	100
1	224	0,0643	218,31	0,05	0,05932	1,15005	0,79892	4,26235	0,09768	4,10426	0,96291	579	25	601	24	596	19	101
1	243	0,0000	210,13	0,03	0,06022	1,14580	0,80769	4,25560	0,09728	4,09845	0,96307	611	25	598	23	601	19	100
1	244	0,0198	207,61	0,05	0,06008	1,15039	0,81466	4,27286	0,09835	4,11509	0,96308	606	25	605	24	605	20	100
1	263	0,0000	209,72	0,09	0,05966	1,15655	0,80059	4,27629	0,09733	4,11692	0,96273	591	25	599	24	597	19	100
1	264	1,0000	209,02	0,07	0,05994	3,52955	0,81820	5,78180	0,09900	4,57946	0,79205	601	76	609	27	607	27	100
1	283	0,0000	209,52	0,07	0,06009	1,16492	0,80852	4,28774	0,09759	4,12646	0,96239	607	25	600	24	602	20	100

1	284	0,0000	207,04	0,07	0,05965	1,17351	0,80902	4,29774	0,09837	4,13442	0,96200	591	25	605	24	602	20	100
Plesovice																		
1	~~5~~	~~0,0000~~	~~594,90~~	~~0,14~~	~~0,05324~~	~~1,08941~~	~~0,39547~~	~~4,05392~~	~~0,05387~~	~~3,90480~~	~~0,96322~~	~~339~~	~~25~~	~~338~~	~~13~~	~~338~~	~~12~~	~~100~~
1	6	~~0,0000~~	~~621,39~~	~~0,14~~	~~0,05320~~	~~1,14662~~	~~0,39436~~	~~4,18475~~	~~0,05376~~	~~4,02459~~	~~0,96173~~	~~337~~	~~26~~	~~338~~	~~13~~	~~338~~	~~12~~	~~100~~
1	25	0,0000	554,96	0,13	0,05317	1,50461	0,39678	4,30621	0,05412	4,03480	0,93697	336	34	340	13	339	12	100
1	~~26~~	~~0,0000~~	~~614,13~~	~~0,15~~	~~0,05319~~	~~1,31604~~	~~0,39524~~	~~4,26040~~	~~0,05389~~	~~4,05204~~	~~0,95109~~	~~337~~	~~30~~	~~338~~	~~13~~	~~338~~	~~12~~	~~100~~
1	45	0,0000	470,25	0,17	0,05335	1,23711	0,39555	4,13856	0,05377	3,94933	0,95428	344	28	338	13	338	12	100
1	46	0,0000	499,93	0,16	0,05324	1,22089	0,40076	4,18217	0,05459	4,00000	0,95644	339	28	343	13	342	12	100
1	65	0,0000	345,88	0,14	0,05319	1,18443	0,39546	4,11258	0,05392	3,93832	0,95763	337	27	339	13	338	12	100
1	66	0,0000	397,31	0,13	0,05321	1,18399	0,38753	4,19119	0,05282	4,02048	0,95927	338	27	332	13	333	12	100
1	~~85~~	~~0,0000~~	~~267,95~~	~~0,12~~	~~0,05336~~	~~1,21814~~	~~0,39621~~	~~4,16287~~	~~0,05385~~	~~3,98065~~	~~0,95623~~	~~344~~	~~28~~	~~338~~	~~13~~	~~339~~	~~12~~	~~100~~
1	86	0,0000	284,58	0,14	0,05320	1,20301	0,39649	4,17983	0,05405	4,00297	0,95769	337	27	339	13	339	12	100
1	105	0,0751	415,14	0,15	0,05315	1,18199	0,39436	4,20030	0,05381	4,03056	0,95959	335	27	338	13	338	12	100
1	106	0,0000	384,54	0,15	0,05329	1,20098	0,39621	4,15292	0,05392	3,97548	0,95727	341	27	339	13	339	12	100
1	125	0,0000	411,20	0,14	0,05351	1,15866	0,39806	4,21011	0,05395	4,04753	0,96138	350	26	339	13	340	12	100
1	126	0,0297	398,77	0,13	0,05354	1,16322	0,39980	4,19841	0,05415	4,03405	0,96085	352	26	340	13	342	12	100
1	125	0,0000	453,59	0,14	0,05332	1,23781	0,39514	4,13666	0,05375	3,94712	0,95418	342	28	337	13	338	12	100
1	126	0,0000	445,78	0,12	0,05333	1,27508	0,39580	4,17777	0,05383	3,97843	0,95229	343	29	338	13	339	12	100
1	145	0,0000	568,54	0,16	0,05339	1,34857	0,39691	4,44132	0,05392	4,23163	0,95279	345	31	339	14	339	13	100
1	146	0,0000	539,72	0,15	0,05335	1,12465	0,39492	4,21614	0,05369	4,06337	0,96377	344	25	337	13	338	12	100
1	165	0,0000	594,84	0,15	0,05330	1,21951	0,39903	4,26929	0,05430	4,09141	0,95833	342	28	341	14	341	12	100
1	166	0,0000	566,97	0,13	0,05323	1,44655	0,39462	4,44801	0,05377	4,20622	0,94564	339	33	338	14	338	13	100
1	~~185~~	~~0,0000~~	~~525,42~~	~~0,13~~	~~0,05337~~	~~1,46150~~	~~0,39528~~	~~4,38626~~	~~0,05372~~	~~4,13562~~	~~0,94286~~	~~345~~	~~33~~	~~337~~	~~14~~	~~338~~	~~13~~	~~100~~
1	186	0,0000	603,90	0,18	0,05335	1,25586	0,39521	4,32136	0,05373	4,13485	0,95684	344	28	337	14	338	12	100
1	185	0,0000	493,60	0,13	0,05414	1,10824	0,40528	4,20761	0,05429	4,05904	0,96469	377	25	341	13	345	12	99
1	~~186~~	~~0,0000~~	~~556,64~~	~~0,18~~	~~0,05335~~	~~1,10590~~	~~0,40268~~	~~4,21006~~	~~0,05474~~	~~4,06221~~	~~0,96488~~	~~344~~	~~25~~	~~344~~	~~14~~	~~344~~	~~12~~	~~100~~
1	205	0,0000	469,20	0,14	0,05298	1,11363	0,39477	4,22718	0,05404	4,07785	0,96467	328	25	339	13	338	12	100
1	206	0,0000	538,80	0,14	0,05301	1,11300	0,39741	4,23864	0,05437	4,08990	0,96491	329	25	341	14	340	12	100
1	225	0,3140	399,94	0,14	0,05450	1,63223	0,40337	4,57061	0,05368	4,26922	0,93406	392	37	337	14	344	13	98
1	226	0,0000	303,76	0,12	0,05421	1,18059	0,39809	4,26665	0,05326	4,10006	0,96096	380	27	335	13	340	12	98
1	245	0,0000	409,49	0,14	0,05377	1,15306	0,39746	4,26927	0,05361	4,11061	0,96284	361	26	337	13	340	12	99
1	246	0,0000	369,48	0,12	0,05409	1,16473	0,39781	4,25636	0,05334	4,09390	0,96183	375	26	335	13	340	12	98
1	~~265~~	~~0,0704~~	~~448,48~~	~~0,14~~	~~0,05592~~	~~1,17181~~	~~0,41251~~	~~4,29061~~	~~0,05350~~	~~4,12749~~	~~0,96198~~	~~449~~	~~26~~	~~336~~	~~14~~	~~351~~	~~13~~	~~96~~
1	266	0,3656	286,71	0,12	0,05379	1,83116	0,39904	4,72132	0,05380	4,35175	0,92172	362	41	338	14	341	14	99
1	285	0,0805	729,22	0,21	0,05361	1,15887	0,39640	4,27995	0,05363	4,12007	0,96264	355	26	337	14	339	12	99
1	286	0,1027	425,61	0,12	0,05403	1,22638	0,40374	4,33496	0,05419	4,15787	0,95915	372	28	340	14	344	13	99
GJ-1																		
2	1	0,0648	393,34	0,02	0,06008	2,04202	0,81365	3,65957	0,09822	3,03687	0,82984	606	44	604	18	605	17	100
2	2	0,0141	385,41	0,02	0,06003	2,03281	0,81869	3,65138	0,09891	3,03319	0,83070	605	44	608	18	607	17	100
2	21	0,0753	343,84	0,02	0,05983	2,05441	0,80850	3,67298	0,09800	3,04470	0,82894	598	44	603	18	602	17	100
2	22	0,0000	342,74	0,02	0,05995	2,03503	0,80436	3,65979	0,09731	3,04183	0,83115	602	44	599	17	599	17	100
2	41	0,0482	329,24	0,02	0,06029	2,06290	0,81259	3,69924	0,09775	3,07064	0,83007	614	45	601	18	604	17	100
2	42	0,0114	330,78	0,02	0,06024	2,05867	0,81086	3,69904	0,09762	3,07323	0,83082	612	44	600	18	603	17	100
2	61	0,0000	296,60	0,02	0,06018	2,06049	0,79367	3,70044	0,09565	3,07371	0,83063	610	45	589	17	593	17	99
2	62	0,0622	323,11	0,02	0,06002	2,04309	0,80070	3,69835	0,09675	3,08278	0,83356	604	44	595	18	597	17	100

2	81	1,0000	293,68	0,02	0,06009	3,91599	0,80883	5,39471	0,09762	3,71052	0,68781	607	85	600	21	602	25	100
2	82	1,0000	288,22	0,02	0,06048	3,89059	0,81528	5,37264	0,09776	3,70521	0,68964	621	84	601	21	605	25	99
2	101	0,0000	285,14	0,02	0,06063	2,04519	0,80980	3,72855	0,09687	3,11758	0,83614	626	44	596	18	602	17	99
2	102	1,0000	274,76	0,02	0,06054	3,88728	0,81648	5,39230	0,09782	3,73709	0,69304	623	84	602	22	606	25	99
2	121	0,0000	293,42	0,02	0,06066	2,04418	0,80945	3,74773	0,09678	3,14114	0,83815	627	44	596	18	602	17	99
2	122	0,0293	286,21	0,02	0,05989	2,07270	0,80499	3,76214	0,09748	3,13968	0,83455	600	45	600	18	600	17	100
2	141	1,0000	285,98	0,02	0,06033	3,90075	0,80817	5,40767	0,09716	3,74527	0,69258	615	84	598	21	601	25	99
2	142	0,0153	277,88	0,02	0,06026	2,05835	0,81177	3,76511	0,09770	3,15266	0,83734	613	44	601	18	603	17	100
2	161	0,0540	291,22	0,02	0,06035	2,06255	0,80869	3,78277	0,09719	3,17100	0,83827	616	45	598	18	602	17	99
2	162	0,0000	286,75	0,02	0,06064	2,04485	0,83544	3,76604	0,09992	3,16253	0,83975	626	44	614	19	617	18	100
2	181	0,0000	270,67	0,02	0,05980	2,04013	0,81199	3,76820	0,09848	3,16816	0,84076	596	44	605	18	604	17	100
2	182	1,0000	259,55	0,02	0,05970	3,94199	0,80671	5,46233	0,09801	3,78124	0,69224	593	85	603	22	601	25	100
2	201	0,0238	279,21	0,02	0,06001	2,06798	0,80883	3,78607	0,09776	3,17140	0,83765	604	45	601	18	602	17	100
2	202	0,0708	270,26	0,02	0,05973	2,08958	0,80813	3,82441	0,09813	3,20309	0,83754	594	45	603	18	601	18	100
Plesovice																		
2	3	0,0174	898,72	0,13	0,05370	2,01220	0,40172	3,65015	0,05426	3,04543	0,83433	359	45	341	10	343	11	99
2	4	0,0463	955,05	0,14	0,05200	2,04638	0,39289	3,70747	0,05480	3,09155	0,83387	285	47	344	10	336	11	102
2	23	1,0000	607,31	0,09	0,05313	4,27775	0,39355	6,44078	0,05372	4,81503	0,74759	335	97	337	16	337	19	100
2	~~24~~	~~1,0000~~	~~330,55~~	~~0,10~~	~~0,05311~~	~~4,27957~~	~~0,46036~~	~~6,14574~~	~~0,06286~~	~~4,41083~~	~~0,71771~~	~~334~~	~~97~~	~~393~~	~~17~~	~~385~~	~~20~~	~~102~~
2	43	0,0490	547,87	0,09	0,05284	2,05213	0,39053	3,70721	0,05360	3,08742	0,83282	322	47	337	10	335	11	101
2	44	0,1246	516,29	0,09	0,05309	2,12433	0,39019	3,75568	0,05330	3,09715	0,82466	333	48	335	10	335	11	100
2	63	0,0856	521,03	0,09	0,05304	2,06144	0,39143	3,72535	0,05352	3,10302	0,83295	331	47	336	10	335	11	100
2	64	1,0000	509,11	0,08	0,05305	4,28481	0,39167	6,45684	0,05355	4,83024	0,74808	331	97	336	16	336	19	100
2	83	0,0412	476,18	0,08	0,05299	2,04410	0,39203	3,72953	0,05366	3,11946	0,83642	328	46	337	10	336	11	100
2	84	1,0000	493,08	0,08	0,05350	4,26604	0,39402	6,47179	0,05341	4,86673	0,75199	350	96	335	16	337	19	100
2	103	0,0658	455,65	0,09	0,05331	2,07795	0,39262	3,76517	0,05341	3,13984	0,83392	342	47	335	10	336	11	100
2	104	0,0200	460,71	0,09	0,05292	2,04224	0,38927	3,74121	0,05335	3,13463	0,83787	325	46	335	10	334	11	100
2	123	0,0000	453,65	0,08	0,05328	2,06456	0,39229	3,75026	0,05340	3,13082	0,83483	341	47	335	10	336	11	100
2	124	0,1214	444,57	0,08	0,05347	2,10694	0,39372	3,80030	0,05341	3,16276	0,83224	349	48	335	10	337	11	100
2	143	0,0193	417,41	0,09	0,05320	2,06896	0,39250	3,77910	0,05351	3,16243	0,83682	337	47	336	10	336	11	100
2	144	0,0000	400,31	0,08	0,05379	2,04499	0,39302	3,75973	0,05299	3,15493	0,83914	362	46	333	10	337	11	99
2	163	0,0838	444,70	0,09	0,05297	2,10077	0,39303	3,82421	0,05382	3,19553	0,83560	327	48	338	11	337	11	100
2	164	1,0000	425,48	0,08	0,05314	4,29551	0,39204	6,50248	0,05351	4,88168	0,75074	335	97	336	16	336	19	100
2	183	1,0000	361,90	0,08	0,05391	4,25216	0,40150	6,45741	0,05402	4,85976	0,75259	367	96	339	16	343	19	99
2	184	1,0000	390,05	0,08	0,05311	4,29800	0,39218	6,51886	0,05356	4,90130	0,75186	333	97	336	16	336	19	100
2	203	0,0000	400,99	0,08	0,05352	2,05531	0,39303	3,78334	0,05326	3,17638	0,83957	351	46	335	10	337	11	99
2	204	0,0395	384,81	0,08	0,05363	2,09361	0,39257	3,81561	0,05309	3,18994	0,83602	355	47	333	10	336	11	99
GJ-1																		
2	5	0,0703	376,56	0,02	0,05979	2,05404	0,80820	3,73917	0,09804	3,12447	0,83560	596	45	603	18	601	17	100
2	6	0,0635	373,06	0,01	0,05925	2,03656	0,80594	3,67912	0,09865	3,06404	0,83282	576	44	606	18	600	17	101
2	25	0,0709	341,76	0,01	0,05950	2,03093	0,80739	3,68253	0,09842	3,07187	0,83417	585	44	605	18	601	17	101
2	~~26~~	~~1,0000~~	~~205,26~~	~~0,02~~	~~0,05993~~	~~3,90915~~	~~0,90596~~	~~5,30215~~	~~0,10964~~	~~3,58208~~	~~0,67559~~	~~601~~	~~85~~	~~671~~	~~23~~	~~655~~	~~26~~	~~102~~
2	45	0,0044	307,38	0,01	0,06035	2,02168	0,80869	3,67269	0,09719	3,06617	0,83486	616	44	598	18	602	17	99
2	46	1,0000	308,19	0,02	0,06035	3,89926	0,80981	5,37867	0,09732	3,70484	0,68880	616	84	599	21	602	25	99
2	65	1,0000	306,48	0,02	0,06044	3,87619	0,80283	5,37611	0,09634	3,72527	0,69293	619	84	593	21	598	25	99

2	66	1,0000	308,19	0,01	0,05992	3,90998	0,80110	5,39565	0,09697	3,71821	0,68911	601	85	597	21	597	25	100
2	85	0,0362	284,67	0,02	0,05976	2,04515	0,80805	3,71444	0,09807	3,10071	0,83477	595	44	603	18	601	17	100
2	86	1,0000	226,96	0,02	0,06003	3,91988	0,81233	5,41922	0,09814	3,74198	0,69050	605	85	603	22	604	25	100
2	105	0,0935	247,29	0,02	0,05946	2,07564	0,80358	3,75399	0,09801	3,12796	0,83324	584	45	603	18	599	17	101
2	106	0,0251	278,89	0,02	0,05870	2,04625	0,79060	3,75901	0,09769	3,15325	0,83885	556	45	601	18	592	17	102
2	125	1,0000	280,40	0,02	0,06012	3,89665	0,81130	5,39773	0,09787	3,73519	0,69199	608	84	602	22	603	25	100
2	126	0,0563	281,41	0,02	0,06030	2,06497	0,80717	3,76972	0,09709	3,15384	0,83662	614	45	597	18	601	17	99
2	~~145~~	~~0,0000~~	~~162,60~~	~~0,02~~	~~0,05985~~	~~2,07185~~	~~0,89181~~	~~3,76703~~	~~0,10807~~	~~3,14611~~	~~0,83517~~	~~598~~	~~45~~	~~662~~	~~20~~	~~647~~	~~18~~	~~102~~
2	146	1,0000	271,12	0,02	0,06027	3,90430	0,80993	5,43803	0,09746	3,78532	0,69608	613	84	600	22	602	25	100
2	165	0,0796	278,96	0,02	0,05988	2,08771	0,80675	3,80142	0,09771	3,17683	0,83570	599	45	601	18	601	17	100
2	166	1,0000	263,85	0,02	0,06003	3,92000	0,81148	5,45763	0,09804	3,79727	0,69577	605	85	603	22	603	25	100
2	185	0,0773	272,15	0,02	0,05999	2,08290	0,80775	3,80022	0,09765	3,17855	0,83641	603	45	601	18	601	17	100
2	186	0,0000	256,90	0,02	0,06020	2,05980	0,81103	3,78266	0,09771	3,17265	0,83874	611	45	601	18	603	17	100
2	205	0,0657	268,63	0,02	0,05958	2,09285	0,80803	3,83656	0,09836	3,21546	0,83811	588	45	605	19	601	18	101
2	206	0,0013	260,22	0,02	0,06042	2,05233	0,81365	3,79690	0,09767	3,19443	0,84133	619	44	601	18	604	17	99

Supplementary Data Table S2. Lu-Hf isotope composition of the investigated zircons

Lu-Hf spot	U-Pb spot	207Pb/206Pb age (Ma)	±2s	176Yb/177Hf	±2s	176Lu/177Hf	±2s	178Hf/177Hf	180Hf/177Hf	SigHf b	176Hf/177Hf	±2s	176Hf/177Hf(t)	eHf(t)	±2s	TDM2
MB-182																
49	88	1102	64	0,0242	20	0,000817	5	1,46515	1,8884	11	0,282222	15	0,282205	4,21	1,0	1,57
26	31	1103	66	0,0345	28	0,001135	7	1,46720	1,8869	11	0,282388	19	0,282364	9,88	1,0	1,26
23	34	1103	41	0,0358	29	0,001167	7	1,46519	1,8886	11	0,282231	20	0,282207	4,29	1,0	1,57
36	135	1105	41	0,0873	72	0,002753	17	1,46542	1,8881	8	0,282312	14	0,282254	6,02	1,2	1,47
31	38	1106	40	0,0402	33	0,001364	8	1,46518	1,8882	18	0,282248	21	0,282220	4,82	1,0	1,54
35	137	1111	41	0,0644	52	0,001993	12	1,46542	1,8882	10	0,282286	16	0,282245	5,81	1,1	1,49
46	119	1111	41	0,0289	23	0,001005	6	1,46520	1,8883	15	0,282245	20	0,282224	5,08	1,0	1,53
47	112	1112	42	0,0179	19	0,000573	5	1,46513	1,8884	10	0,282149	17	0,282137	2,03	1,0	1,70
38	130	1113	42	0,0302	24	0,001038	6	1,46543	1,8882	11	0,282282	16	0,282260	6,40	1,0	1,46
41	110	1116	41	0,0387	31	0,001242	7	1,46540	1,8883	10	0,282231	18	0,282205	4,52	1,0	1,56
27	19	1117	41	0,0262	21	0,000853	5	1,46725	1,8868	11	0,282351	16	0,282333	9,08	1,0	1,31
43	120	1120	41	0,0452	36	0,001404	8	1,46530	1,8883	9	0,282227	16	0,282197	4,33	1,1	1,58
44	108	1122	66	0,0485	39	0,001493	9	1,46534	1,8882	9	0,282304	15	0,282273	7,06	1,1	1,43
48	87	1123	41	0,0227	19	0,000729	4	1,46529	1,8885	7	0,282211	16	0,282196	4,35	1,0	1,58
45	91	1123	42	0,0290	23	0,000975	6	1,46533	1,8883	13	0,282169	19	0,282149	2,68	1,0	1,67
29	49	1124	40	0,0302	25	0,001038	6	1,46525	1,8878	12	0,282225	15	0,282203	4,62	1,0	1,57
37	132	1125	66	0,0662	53	0,002160	13	1,46543	1,8882	7	0,282220	15	0,282174	3,64	1,1	1,62
24	35	1135	41	0,0280	23	0,000872	5	1,46720	1,8869	15	0,282330	17	0,282311	8,71	1,0	1,35
33	58	1137	41	0,0383	32	0,001311	8	1,46530	1,8884	8	0,282252	24	0,282224	5,67	1,0	1,52
34	136	1140	66	0,0307	25	0,001052	6	1,46542	1,8881	12	0,282206	24	0,282183	4,28	1,0	1,60
39	72	1142	41	0,0509	41	0,001751	11	1,46551	1,8882	6	0,282261	20	0,282223	5,74	1,1	1,52
40	71	1143	40	0,0318	26	0,001035	6	1,46540	1,8882	9	0,282233	18	0,282211	5,35	1,0	1,54
42	128	1152	40	0,0342	27	0,001182	7	1,46540	1,8881	13	0,282224	15	0,282198	5,09	1,0	1,56
30	56	1180	43	0,0231	19	0,000793	5	1,46517	1,8882	17	0,282194	16	0,282176	4,96	1,0	1,59
MB-179																
59	213	1119	42	0,0278	22	0,000874	5	1,46529	1,8881	12	0,282213	11	0,282194	4,21	1,0	1,58
56	155	1126	41	0,0492	39	0,001570	9	1,46524	1,8883	9	0,282245	18	0,282211	4,96	1,1	1,55
53	168	1149	65	0,0323	26	0,001171	7	1,46523	1,8884	10	0,282337	16	0,282312	9,04	1,0	1,34
57	172	1151	65	0,0352	29	0,001242	8	1,46527	1,8883	11	0,282138	16	0,282111	1,97	1,0	1,73
65	176	1153	41	0,0378	32	0,001201	8	1,46518	1,8883	14	0,282067	19	0,282041	-0,46	1,0	1,87
63	216	1155	66	0,0213	18	0,000660	4	1,46519	1,8883	12	0,282048	16	0,282034	-0,67	1,0	1,88
51	198	1159	41	0,0477	39	0,001534	9	1,46509	1,8885	10	0,282188	14	0,282155	3,71	1,1	1,64
64	179	1160	42	0,0210	18	0,000764	5	1,46513	1,8882	9	0,282208	15	0,282191	5,03	1,0	1,57
69	217	1160	35	0,0240	19	0,000964	6	1,46526	1,8882	15	0,282186	16	0,282165	4,10	1,0	1,62
67	177	1164	41	0,0171	14	0,000604	4	1,46515	1,8883	12	0,282103	17	0,282089	1,50	1,0	1,77
50	194	1170	43	0,0261	21	0,000908	5	1,46514	1,8884	11	0,282047	15	0,282027	-0,56	1,0	1,89
60	187	1172	41	0,0327	27	0,001203	8	1,46532	1,8882	13	0,282061	15	0,282034	-0,26	1,0	1,87
54	169	1199	64	0,0284	23	0,000935	6	1,46524	1,8884	14	0,282213	18	0,282192	5,95	1,0	1,55
61	174	1991	36	0,0160	13	0,000515	3	1,46529	1,8883	12	0,281315	11	0,281295	-7,71	1,0	2,94
58	211	2211	36	0,0058	5	0,000180	1	1,46531	1,8882	15	0,281322	15	0,281314	-1,94	1,0	2,80
MB-181																
72	148	1148	32	0,0157	13	0,000572	3	1,46531	1,8881	13	0,282155	15	0,282143	4,31	1,0	1,60
73	139	1117	34	0,0323	26	0,001092	7	1,46524	1,8883	11	0,282202	15	0,282180	2,34	1,0	1,69
70	150	1139	31	0,0151	12	0,000562	3	1,46521	1,8882	9	0,282155	16	0,282143	2,83	1,0	1,68
MB-135																
108	278	1060	23	0,0237	19	0,000762	5	1,46509	1,8883	13	0,282254	16	0,282238	4.64	1.00	1,52
107	277	1062	24	0,0119	10	0,000410	2	1,46512	1,8884	15	0,282211	15	0,282203	3.93	1.01	1,59
111	274	1066	24	0,0229	19	0,000756	5	1,46498	1,8885	15	0,282259	14	0,282244	0.79	1.00	1,51
112	272	1068	25	0,0137	12	0,000438	3	1,46498	1,8884	14	0,282231	15	0,282222	3.83	0.99	1,54
113	271	1068	21	0,0134	21	0,000455	6	1,46502	1,8884	15	0,282232	27	0,282223	3.99	1.00	1,55
114	269	1069	21	0,0199	17	0,000628	4	1,46502	1,8884	13	0,282257	18	0,282244	4.30	1.00	1,51
115	267	1071	25	0,0140	11	0,000455	3	1,46496	1,8884	10	0,282226	18	0,282217	3.44	1.00	1,56
116	259	1072	23	0,0137	11	0,000468	3	1,46495	1,8884	15	0,282220	16	0,282211	3.80	1.00	1,56
117	258	1072	24	0,0204	16	0,000620	4	1,46495	1,8885	12	0,282144	17	0,282132	2.90	1.00	1,73
118	257	1072	21	0,0120	10	0,000401	2	1,46497	1,8883	11	0,282224	17	0,282216	3.29	0.99	1,56
119	255	1072	24	0,0197	16	0,000617	4	1,46493	1,8883	10	0,282233	14	0,282221	4.16	0.99	1,56
104	251	1074	23	0,0102	8	0,000341	2	1,46506	1,8883	14	0,282217	18	0,282210	-3.31	1.04	1,56
102	248	1075	23	0,0261	21	0,000837	5	1,46512	1,8884	15	0,282213	20	0,282196	4.76	1.01	1,60
103	249	1075	24	0,0150	12	0,000497	3	1,46507	1,8883	17	0,282235	19	0,282225	4.22	1.00	1,53
100	247	1076	24	0,0160	13	0,000591	4	1,46507	1,8883	18	0,282254	16	0,282241	6.46	1.02	1,50
96	239	1076	26	0,0213	17	0,000845	5	1,46500	1,8883	15	0,282074	13	0,282057	3.27	1.01	1,87
99	240	1076	26	0,0135	11	0,000471	3	1,46503	1,8882	15	0,282223	19	0,282213	-12.24	1.00	1,56
105	236	1077	29	0,0165	13	0,000552	3	1,46511	1,8884	12	0,281769	20	0,281758	5.00	1.01	2,45
109	238	1077	22	0,0175	14	0,000611	4	1,46507	1,8883	13	0,282235	15	0,282223	4.06	1.00	1,55
101	233	1080	27	0,0165	13	0,000561	3	1,46504	1,8882	15	0,282233	15	0,282222	3.61	0.99	1,55
95	228	1083	22	0,0179	15	0,000607	4	1,46492	1,8883	16	0,282236	15	0,282224	4.35	1.00	1,54
120	218	1084	42	0,0153	12	0,000531	3	1,46496	1,8884	15	0,282240	14	0,282229	4.45	1.00	1,54
121	216	1085	21	0,0186	15	0,000596	4	1,46492	1,8884	12	0,282215	16	0,282203	-1.43	1.00	1,59
122	213	1087	24	0,0167	13	0,000543	3	1,46502	1,8884	13	0,282224	21	0,282213	4.67	1.01	1,57
123	212	1087	24	0,0152	12	0,000557	3	1,46500	1,8885	12	0,282199	21	0,282188	3.96	1.00	1,62
124	210	1089	22	0,0120	10	0,000417	3	1,46494	1,8885	17	0,282207	19	0,282198	4.18	0.99	1,60
106	199	1093	24	0,0292	24	0,001005	6	1,46505	1,8884	12	0,282306	13	0,282285	4.59	1.00	1,43
110	207	1093	21	0,0319	33	0,001065	9	1,46499	1,8884	11	0,282033	16	0,282011	4.20	0.99	1,96
97	193	1106	27	0,0228	21	0,000760	5	1,46497	1,8883	14	0,282244	17	0,282228	5.00	1.00	1,53
98	194	1106	22	0,0169	14	0,000575	4	1,46501	1,8883	11	0,282220	14	0,282208	4.48	0.99	1,57
94	192	1110	24	0,0136	11	0,000450	3	1,46502	1,8884	14	0,282232	14	0,282223	5.67	1.00	1,55
MB-138																
170	36	1034	20	0,0275	22	0,000850	5	1,46493	1,8884	14	0,282258	24	0,282241	3.93	1.01	1,53
171	30	1116	21	0,0371	31	0,001156	7	1,46497	1,8883	10	0,282226	23	0,282202	4.40	1.03	1,57

143	67	1121	22	0,0058	5	0,000155	1	1,46494	1,8884	19	0,282122	15	0,282119	1.58	0.99	1,73
164	27	1122	21	0,0192	15	0,000616	4	1,46500	1,8883	13	0,282297	17	0,282283	7.44	1.00	1,41
148	131	1123	23	0,0377	31	0,001338	8	1,46494	1,8884	15	0,282248	15	0,282219	5.19	1.04	1,53
161	110	1123	25	0,0216	18	0,000786	5	1,46506	1,8882	13	0,282364	19	0,282347	9.72	1.01	1,28
159	113	1126	21	0,1030	103	0,003138	24	1,46507	1,8883	11	0,282259	19	0,282192	4.28	1.43	1,59
153	118	1129	57	0,0266	24	0,000954	7	1,46501	1,8881	12	0,282183	19	0,282163	3.32	1.02	1,64
160	112	1129	22	0,0224	18	0,000742	5	1,46508	1,8883	15	0,282325	18	0,282310	8.52	1.01	1,35
145	60	1130	21	0,0208	17	0,000854	5	1,46492	1,8883	15	0,282361	19	0,282343	9.73	1.00	1,29
147	10	1130	21	0,0337	27	0,001063	6	1,46500	1,8883	13	0,282307	20	0,282285	7.66	1.03	1,40
158	49	1130	21	0,0226	18	0,000763	5	1,46506	1,8882	16	0,282234	15	0,282218	5.29	1.01	1,53
168	32	1131	20	0,0293	24	0,000966	6	1,46501	1,8883	12	0,282253	13	0,282232	5.81	1.02	1,51
149	73	1135	22	0,0135	13	0,000389	3	1,46502	1,8883	13	0,282104	18	0,282096	1.08	1.00	1,77
155	52	1135	20	0,0456	37	0,001524	9	1,46505	1,8883	15	0,282295	21	0,282262	6.98	1.06	1,44
151	77	1136	23	0,0167	14	0,000677	4	1,46501	1,8883	12	0,282203	19	0,282188	4.38	1.00	1,59
144	70	1137	22	0,0154	13	0,000574	3	1,46493	1,8883	14	0,282282	16	0,282270	7.29	1.00	1,43
146	59	1137	21	0,0232	20	0,000743	5	1,46497	1,8884	14	0,282231	16	0,282215	5.35	1.01	1,54
157	50	1138	20	0,0388	32	0,001283	8	1,46504	1,8882	14	0,282203	15	0,282175	3.97	1.04	1,61
169	31	1139	25	0,0292	24	0,001024	6	1,46498	1,8884	9	0,282266	15	0,282244	6.44	1.02	1,48
163	40	1146	20	0,0423	44	0,001358	11	1,46497	1,8883	13	0,282296	18	0,282266	7.37	1.08	1,43
165	20	1146	20	0,0541	53	0,001667	11	1,46494	1,8881	10	0,282225	14	0,282189	4.62	1.12	1,58
167	99	1146	21	0,0201	16	0,000712	4	1,46495	1,8883	13	0,282056	16	0,282040	-0.64	1.00	1,87
154	117	1147	24	0,0375	30	0,001171	7	1,46506	1,8883	12	0,282338	17	0,282313	9.04	1.03	1,34
152	127	1148	26	0,0464	37	0,001914	12	1,46494	1,8883	15	0,282420	19	0,282379	11.40	1.06	1,21
150	12	1220	20	0,0210	17	0,000781	5	1,46504	1,8884	11	0,282220	20	0,282202	6.78	1.00	1,52
166	34	1220	21	0,0192	16	0,000665	4	1,46498	1,8883	15	0,282079	14	0,282063	1.86	1.00	1,80
172	38	1252	20	0,0386	32	0,001222	7	1,46492	1,8885	11	0,282155	24	0,282126	4.82	1.04	1,66
162	109	1328	20	0,0445	102	0,001539	30	1,46502	1,8882	13	0,282103	911	0,282064	4.35	1.42	1,75
MB-137																
138	140	1071	24	0,0343	28	0,001189	7	1,46510	1,8882	8	0,282192	17	0,282168	2,18	1,0	1,66
139	157	1076	26	0,0172	17	0,000636	4	1,46491	1,8883	14	0,282174	22	0,282161	2,05	1	1,67
132	155	1078	26	0,0239	19	0,000769	5	1,46502	1,8883	15	0,282252	21	0,282236	4,75	1,0	1,52
128	156	1079	23	0,027	24	0,000940	6	1,46492	1,8884	15	0,282182	19	0,282163	2,19	1	1,66
136	133	1080	24	0,0289	23	0,000909	5	1,46496	1,8884	12	0,282206	18	0,282188	3,08	1	1,62
140	178	1081	26	0,0192	16	0,000628	4	1,46500	1,8883	16	0,282192	15	0,282179	2,81	1,0	1,63
129	168	1083	27	0,0208	17	0,000681	5	1,46500	1,8884	14	0,282181	14	0,282167	2,43	1,0	1,65
137	152	1084	35	0,0156	13	0,000533	3	1,46495	1,8884	19	0,282145	17	0,282134	1,29	1	1,72
125	188	1084	26	0,0465	37	0,001437	9	1,46492	1,8884	11	0,282221	14	0,282192	3,32	1,1	1,61
131	175	1086	26	0,0163	13	0,000542	3	1,46501	1,8883	15	0,282200	15	0,282189	3,28	1,0	1,61
142	189	1086	29	0,0248	20	0,000814	5	1,46498	1,8883	20	0,282201	14	0,282184	3,10	1	1,62
135	159	1094	23	0,0247	20	0,000913	6	1,46501	1,8883	12	0,282144	16	0,282125	1,19	1,0	1,73
126	187	1104	27	0,036	29	0,001244	8	1,46495	1,8883	14	0,282165	19	0,282139	1,90	1	1,70
133	177	1129	27	0,0121	10	0,000452	3	1,46499	1,8881	8	0,282150	13	0,282140	2,52	1,0	1,69
130	191	1138	29	0,0182	15	0,000628	4	1,46498	1,8883	16	0,282198	15	0,282184	4,28	1	1,60

141	135	1170	22	0,0291	24	0,001092	7	1,46494	1,8883	15	0,282242	17	0,282218	6,20	1	1,52
Reference materials																
TEMORA																
1		416	1	0,0233	19	0,000846	5	1,46526	1,8887	15	0,282703	16	0,282697	6,15	1,0	0,75
2		416	1	0,0301	29	0,001097	8	1,46480	1,8890	20	0,282651	17	0,282643	4,24	1,0	0,85
BB																
3		560	1	0,0049	5	0,000154	1	1,46517	1,8886	15	0,281698	18	0,281696	-26,06	1,0	2,62
5		560	1	0,0050	4	0,000156	1	1,46468	1,8892	15	0,281629	17	0,281627	-28,48	1,0	2,75
4		560	1	0,0049	4	0,000155	1	1,46455	1,8894	15	0,281617	18	0,281616	-28,90	1,0	2,78
74		560	1	0,0050	4	0,000157	1	1,46519	1,8885	15	0,281680	16	0,281678	-26,68	1,0	2,66
75		560	1	0,0049	4	0,000158	1	1,46518	1,8882	15	0,281699	20	0,281697	-26,02	1,0	2,62
76		560	1	0,0048	4	0,000155	1	1,46522	1,8884	15	0,281683	16	0,281681	-26,57	1,0	2,65
77		560	1	0,0049	5	0,000152	1	1,46515	1,8883	15	0,281690	15	0,281688	-26,32	1,0	2,64
173		560	1	0,0047	4	0,000153	1	1,46499	1,8882	13	0,281681	17	0,281680	-26,63	1,0	2,65
174		560	1	0,0047	4	0,000151	1	1,46499	1,8883	12	0,281673	17	0,281672	-26,92	1,0	2,67
175		560	1	0,0051	4	0,000162	1	1,46499	1,8884	12	0,281637	18	0,281635	-28,20	1,0	2,74
176		560	1	0,0048	4	0,000154	1	1,46496	1,8882	12	0,281643	17	0,281641	-27,99	1,0	2,73
6		560	1	0,0049	4	0,000155	1	1,46537	1,8885	15	0,281706	19	0,281704	-25,76	1,0	2,61
91500																
7		1065	1	0,0135	13	0,000481	3	1,46545	1,8883	8	0,282356	18	0,282347	8,38	1,0	1,16
8		1065	1	0,0133	14	0,000474	4	1,46534	1,8884	8	0,282345	22	0,282335	7,97	1,0	1,18
9		1065	1	0,0133	11	0,000472	3	1,46530	1,8887	8	0,282330	21	0,282320	7,45	1,0	1,21
10		1065	1	0,0145	15	0,000518	5	1,46519	1,8885	8	0,282341	19	0,282330	7,80	1,0	1,19
78		1065	1	0,0128	12	0,000445	3	1,46510	1,8883	8	0,282324	17	0,282315	7,26	1,0	1,22
79		1065	1	0,0129	12	0,000451	3	1,46514	1,8886	9	0,282320	20	0,282311	7,10	1,0	1,23
80		1065	1	0,0127	12	0,000449	3	1,46514	1,8884	9	0,282331	15	0,282322	7,49	1,0	1,21
81		1065	1	0,0125	11	0,000444	3	1,46512	1,8884	8	0,282319	18	0,282311	7,10	1,0	1,23
177		1065	1	0,0132	11	0,000460	3	1,46506	1,8884	7	0,282295	18	0,282286	6,23	1,0	1,28
178		1065	1	0,0146	12	0,000508	3	1,46502	1,8884	7	0,282314	17	0,282304	6,87	1,0	1,24
179		1065	1	0,0149	12	0,000522	3	1,46500	1,8884	7	0,282294	18	0,282283	6,14	1,0	1,28
180		1065	1	0,0143	12	0,000505	3	1,46500	1,8883	7	0,282328	18	0,282318	7,36	1,0	1,21
Mudtank																
11		732	1	0,0011	1	0,000033	0	1,46510	1,8888	18	0,282479	17	0,282479	5,53	1,0	1,04
12		732	1	0,0010	1	0,000032	0	1,46493	1,8891	18	0,282469	20	0,282469	5,17	1,0	1,06
13		732	1	0,0010	1	0,000032	0	1,46476	1,8891	18	0,282463	17	0,282462	4,94	1,0	1,07
14		732	1	0,0011	1	0,000033	0	1,46509	1,8888	18	0,282501	19	0,282501	6,32	1,0	1,00
82		732	1	0,0011	1	0,000034	0	1,46510	1,8884	17	0,282510	19	0,282509	6,61	1,0	0,98
83		732	1	0,0011	1	0,000034	0	1,46509	1,8884	17	0,282509	15	0,282509	6,60	1,0	0,98
84		732	1	0,0012	1	0,000037	0	1,46507	1,8884	18	0,282506	18	0,282505	6,47	1,0	0,99
85		732	1	0,0012	1	0,000035	0	1,46507	1,8884	17	0,282504	12	0,282503	6,39	1,0	0,99
181		732	1	0,0012	1	0,000035	0	1,46503	1,8883	13	0,282494	21	0,282494	6,05	1,0	1,01

182	732	1	0,0010	1	0,000030	0	1,46504	1,8883	14	0,282514	12	0,282513	6,75	1,0	0,97
183	732	1	0,0011	1	0,000033	0	1,46512	1,8883	14	0,282516	15	0,282516	6,84	1,0	0,97
184	732	1	0,0011	1	0,000034	0	1,46506	1,8883	14	0,282494	14	0,282494	6,05	1,0	1,01
GJ-1															
15	602	1	0,0068	6	0,000258	2	1,46502	1,8889	13	0,282002	18	0,281999	-14,39	1,0	2,03
16	602	1	0,0068	5	0,000257	2	1,46484	1,8891	13	0,281988	21	0,281985	-14,88	1,0	2,05
17	602	1	0,0069	9	0,000257	3	1,46496	1,8890	12	0,282006	19	0,282003	-14,23	1,0	2,02
18	602	1	0,0068	7	0,000258	2	1,46481	1,8891	13	0,281992	18	0,281989	-14,74	1,0	2,05
87	602	1	0,0069	11	0,000258	4	1,46502	1,8882	12	0,282025	18	0,282022	-13,57	1,0	1,98
88	602	1	0,0068	5	0,000257	2	1,46504	1,8884	12	0,282016	15	0,282013	-13,90	1,0	2,00
186	602	1	0,0068	5	0,000256	2	1,46508	1,8882	11	0,282006	21	0,282003	-14,25	1,0	2,02
187	602	1	0,0068	6	0,000258	2	1,46511	1,8882	11	0,282026	18	0,282023	-13,55	1,0	1,98
Plesovice															
19	337	1	0,0032	3	0,000081	1	1,46482	1,8891	22	0,282440	20	0,282439	-4,74	1,0	1,28
20	337	1	0,0038	4	0,000094	1	1,46487	1,8890	21	0,282442	21	0,282441	-4,67	1,0	1,28
21	337	1	0,0036	4	0,000089	1	1,46487	1,8891	22	0,282451	25	0,282450	-4,34	1,0	1,26
22	337	1	0,0028	2	0,000069	0	1,46501	1,8888	21	0,282488	17	0,282487	-3,03	1,0	1,19
90	337	1	0,0080	6	0,000198	1	1,46510	1,8885	19	0,282492	16	0,282490	-2,92	1,0	1,18
91	337	1	0,0076	6	0,000190	1	1,46506	1,8884	19	0,282492	15	0,282491	-2,90	1,0	1,18
92	337	1	0,0056	5	0,000136	1	1,46504	1,8884	19	0,282482	17	0,282481	-3,26	1,0	1,20
93	337	1	0,0054	4	0,000133	1	1,46509	1,8884	19	0,282483	17	0,282482	-3,21	1,0	1,20
189	337	1	0,0051	4	0,000126	1	1,46513	1,8883	17	0,282485	14	0,282484	-3,14	1,0	1,19
190	337	1	0,0029	2	0,000071	0	1,46509	1,8882	17	0,282479	17	0,282478	-3,36	1,0	1,21

Artigo 2.

Supplementary Data Table S1. Whole-rock geochemistry

Sample name	Reference	Unidade	Lithology	SiO2	Al2O3	CaO	FeO	MgO	TiO2	Na2O	K2O	P2O5	MnO	LOI	Sum	Rb
MB-72			Syenite	61,9	17,9	1,8	4,6	0,4	0,6	4,6	7,4	0,1	0,1	0,6	99,8	117,8
MB-68A			Syenite	62,6	14,7	3,8	7,2	1,4	1	3,5	4,6	0,3	0,1	0,5	99,7	138,7
MB-69			Syenite	62,2	14,8	3,8	7,6	1,4	1,1	3,7	4,4	0,3	0,1	0,4	99,7	116,8
MB-44	This study	Castanho Suite	Diorite	59,6	15,7	4,6	7,8	1,9	1,2	3,8	3,8	0,3	0,1	0,9	99,7	109,3
MB-47			Diorite	50,4	14,4	10,7	11,5	8	1,4	2,2	0,7	0,1	0,2	0,2	99,7	18,4
MB-63A			Qz-diorite	63,4	14,6	3,5	7	1,3	1	3,5	4,6	0,3	0,1	0,5	99,7	165,5
MB-45A			Qz diorite	63,6	14,7	3,4	6,8	1,2	1	3,4	4,7	0,3	0,1	0,5	99,7	125,3
MB-67			Granite	64,1	15,1	3,3	6	1,1	0,9	3,6	4,9	0,3	0,1	0,5	99,7	148,5
MB-71A			Granite	70,7	14,4	1,6	2,2	0,3	0,3	3,8	5,3	0,1	0	1,2	99,9	111,1
MB-45B			Mafic enclave	49	17,2	8	10,5	10,5	0,8	2,6	0,7	0,2	0,1		99,7	20
MB-68B			Mafic enclave	49,5	22,3	9,9	6,3	8,1	0,4	2,9	0,3	0,1	0,1		99,7	0
MB-63B			Mafic enclave	51,4	21,2	9,4	6	8	0,4	2,8	0,3	0,1	0,1		99,7	0
36			Olivine-hy gabbro	59,9	15,7	4	9,2	1,2	1,2	4,7	3,3	0,4	0,2		99,7	63
37	GTK		Gabbro	65,1	15,2	2,9	6,1	0,6	0,8	3,9	4,8	0,3	0,1		99,7	120
38	Consortium,		Gabbro	49,7	16,6	8,7	11,1	6,1	1,7	3,5	1,3	0,5	0,2	0,3	99,7	29,3
39	2006		Qz diorite	53,8	14,3	5,8	12,3	2,6	2,3	3,8	3,6	1	0,2		99,6	100,2
40			Pyroxene granite	54,7	14,1	5,2	11,8	2,2	2,1	3,1	5,4	0,5	0,2	0,5	99,6	167,7
MB-143A			Pelitic gneiss	60,9	16,2	4,6	7,3	4,6	0,7	4,1	0,9	0,2	0,2		99,7	16
MB-143B			Pelitic gneiss	48,6	18,1	8,5	12	6	2,1	3,5	0,5	0,3	0,2		99,7	12
MB-145A			Pelitic gneiss	64,7	16	3	7,4	2,8	1	3,2	1,5	0,1	0,1		99,7	20
MB-145B	This study		Pelitic gneiss	51,1	16,5	7,4	10,4	5	1,9	3,7	2,1	0,5	0,2		98,8	80
MB-146			Pelitic gneiss	52,6	17,9	7,7	9,8	4,9	1,3	4,3	0,7	0,3	0,1		99,7	
MB-148			Charnockitic gneiss	56,3	16,2	7,8	9,2	6,9	1	1,3	0,6	0,1	0,1		99,7	26
MB-144			Metagabbro	54,8	17,1	4,7	12,1	3,6	1,3	3,6	1,4	0,3	0,4		99,3	21
1			Diabase	67,2	14,2	2,5	7,3	2,8	0,9	2,6	1,9	0	0,1		99,6	45
2			Amphibolite	71,8	15,7	3,4	1,9	0,5	0,3	4,8	1,3	0,1	0		99,7	16
3			Hb-bt gneiss	72,1	16	3,5	1,5	0,5	0,1	5,3	0,6	0	0		99,7	
5		Chidzolomond	Hb-bt gneiss	72,4	15,5	3,1	1,9	0,5	0,2	5,2	0,8	0	0		99,6	
4		o Complex	Granulite	76,9	12	0,4	1,6	0,2	0,2	2,6	5,6	0	0		99,6	252
7	GTK		Granulite	48,5	15,7	8,8	7,5	10,7	0,9	1,8	1,2	0,1	0,2		98,3	26,6
6	Consortium		Granite gneiss	55,9	16,3	5,6	7,6	3,2	1,7	3,5	1,4	0,5	0,2		99,7	41,9
8	(2006)		Qz-feld. gneiss	57,7	19,7	2,9	1,9	0,3	0,4	5	7,5	0,1	0,2		97,9	161,7
9			Arkosic gneiss	54,6	20,5	6,8	9,5	1	0,9	4,7	1,3	0,4	0,1		99,6	10
10			Meta-arkose	62	15,9	2,7	8,1	3,6	1	3,2	1,9	0,1	0,1	0,3	98,9	37
11			Granulite	65,4	15,7	2,1	7,7	2,7	1	2,5	2,1	0	0,1	0,3	99,6	33
12			Qz-feld. gneiss	67,4	15	2,5	4,1	0,7	0,6	3,6	3,7	0,2	0,1	0,3	98,3	75
GW11				66,6	14,1	2,9	6,8	2,9	0,8	2,5	1,2	0,1	0,1	0,5	98,3	19
GW12	Grantham et al. (2007)			68,4	13	2,7	6,8	2,8	0,9	2,9	1,5	0	0,1	0,6	99,6	24
GW14				73	11,5	5,3	4,2	1,3	0,7	1,3	1,2	0,1	0,1	1,1	99,7	28

Sample name	Ba	Zr	Sr	Ga	La	Ce	Pr	Nd	Sm	Eu	Gd	Tb	Dy	Ho	Er	Tm	Yb	Lu
MB-72	903	130,6	102,6	19	13,6	32,1	3,6	16,4	3,9	2,3	3,4	0,5	2,8	0,6	1,7	0,3	1,7	0,3
MB-68A	897	486,5	236,6	21,8	45,8	109,9	13,1	54,3	11,8	2,7	11,5	1,8	10,3	2	5,5	0,8	5,3	0,8
MB-69	932	539,7	257,3	22,7	42,9	108,3	13,4	58,7	13,1	3,1	12,7	2	11,6	2,4	6,7	0,9	5,7	0,8
MB-44	772	468,7	329,5	22,7	44	97,6	11,8	47,4	9,6	2,2	9,2	1,5	8,6	1,7	4,7	0,7	4,3	0,6
MB-47	271	90,7	424,4	16,8	10,7	28	3,6	18	4,2	1,3	4,6	0,8	4,6	1	2,7	0,4	2,4	0,4
MB-63A	921	482,7	252,8	22,4	51,4	125,7	14,9	62,9	13,1	2,7	12,8	2	11,3	2,3	6,5	0,9	6	0,9
MB-45A	903	552,3	238,7	23,8	41,2	96,8	11,4	48,7	11,3	2,5	10,7	1,7	9,5	1,8	4,9	0,7	4,4	0,7
MB-67	896	455,2	235,7	22,6	46	109,1	13,6	56,4	12,1	2,6	11,6	1,9	11,2	2,2	5,8	0,9	5,5	0,8
MB-71A	546	197,8	205,6	18,3	21,1	41,4	4,8	20	4	1,1	4	0,6	3,4	0,6	1,7	0,2	1,5	0,2
MB-45B	220	70	330			30												
MB-68B	126	16	511															
MB-63B	107	20	477			32												
36	904	516	212		34	85												
37	950	520	200		40	90												
38	533	207,5	594,3		29,1	70,8	8,5	34,1	7,5	2,4	6,1	0,9	4,9	0,9	2,4	0,3	2	0,3
39	856	577,6	260,8	23	89,8	236,2	28,7	121,9	26,6	3,5	24,4	3,7	21,4	4,1	11,2	1,6	9,7	1,4
40	1068	527,4	247,8	22,8	65	168,5	21,8	97,8	22,4	3,2	21,5	3,6	19,8	3,9	11,1	1,6	9,8	1,4
MB-143A	466	56	322			37												
MB-143B	386	92	398			40												
MB-145A	530	210	330		40	70												
MB-145B	560	150	480		18,1	41												
MB-146	285	106	351			52												
MB-148	395	86	260		36	97												
MB-144	760	109	112			54												
1	568	268	269		38	85												
2	132	120	320			46												
3	189	53	440			30												
5	600	96	626			39												
4	344	247	47		51	105												
7	238	82,5	275,5	15,7	7,4	16,7	2	10,5	2,6	1,1	2,6	0	2,8	0,6	1,7	0.3	1,7	0,3
6	672	266,2	314,5	30	22	53,4	6,5	33,2	7,7	2,6	6,7	0	6,5	1,3	3,7	0.5	3,4	0,5
8	1215	598,4	3353	35	222,1	408,2	36,3	136,1	16,8	4,6	11,6	0	6,7	1,2	3,5	0.4	3,2	0,5
9	720	144	554	23	19,6	40,5		22,2	5,1	3,4	5,5	0,9	5,4	1	3	0,4	2,6	0,4
10	513	254	210	18	39,2	77,9		34,1	6,3	1,6	6	1,1	7,1	1,5	4,7	0,7	4,9	0,8
11	591	266	246	17	40	83,3		37,6	7,6	2,1	7,6	1,4	8,4	1,7	5,1	0,8	5,4	0,8
12	1101	308	178	20	44,1	88,8		38,3	7	1,9	5,8	0,8	4,2	0,8	2,1	0,3	1,9	0,3
GW11	425	282	302	17	43,2	87,6		39,5	7,6	2	5,9	0,8	4,7	1	3	0,5	3,3	0,6
GW12	319	333	186	16	46,1	98,6		44,8	8,1	1,4	7,4	1,1	6,5	1,4	4,2	0,6	4	0,6
GW14	339	466	198	15	50,2	103		42,9	8,6	1,4	7,4	1	5,5	1,2	3,6	0,6	3,8	0,6

Sample name	Y	V	Hf	Nb	Ta	Sc	Th	U	Cu	Pb	Zn	Mo	Ni	Co	As	Au	Cr2O3	Cs
MB-72	16,9	<8	2,7	6,9	0,4	19	1,7	0,5	1,8	6	32	1	0,1	1,1	0,4	11,1	0	0,7
MB-68A	51,4	62	11,9	15	1	14	4,9	1,5	8,4	1,5	36	1,5	3	11,2	1,3	12,7	0	2,6
MB-69	60,4	59	12,7	18,4	1,2	15	2,3	0,8	9,2	1,1	30	1,4	3	11,4	0,4	25,7	0	0,9
MB-44	41,4	101	11,3	15,5	0,9	16	4	1,2	10,9	1,2	58	1,5	3	13,3	0,3	14,1	0	1,2
MB-47	24,2	309	2,3	3,8	0,2	45	0,3	0,2	24,8	1	18	0,2	4,1	46,3	0,3	18,4	0	0,2
MB-63A	62,6	63	12,3	18,2	1,3	14	11,7	3,8	7,6	6,9	68	2,4	3,4	10	5,7	7,3	0	5,1
MB-45A	48,4	63	13,8	17,3	0,8	13	1,9	0,7	8,7	1,3	31	1,6	3,4	10,6	0,5	15,7	0	0,5
MB-67	57,8	55	11,4	15,2	1	12	7,3	2	7,1	3,7	46	1,4	2,6	8,8	0,3	13,2	0	1,5
MB-71A	16,8	13	5,4	2,5	0	3	0,4	0,4	0,5	4,1	34	0,6	0,5	1,9	0,3	9,2	0	0,2
MB-45B	20	110											300					
MB-68B	0	64											114					
MB-63B	0	99											68					
36	67	117		25														
37	50	60		20														
38	21,5	225	5,2	6,5	0,4	24	1	0,4	31,7	0,9	53	0,3	38,3	35,1	0,8	10,1	0	0,4
39	105,7	139	14,1	27,8	1,9	22	5,1	1,9	14,9	1,2	38	1,6	4,9	21	0,4	37,9	0	0,7
40	100,5	139	12,7	31,7	2	31	4,5	1,5	16,9	2,2	102	3,5	7,3	17,4	0,4	50,8	0	1,8
MB-143A	36	155				35							43					
MB-143B	23	278				31							77					
MB-145A	30	150											70					
MB-145B	20	193		5,5		18,8	1	0,5					60					
MB-146	25	204											48					
MB-148	25	204					18						64					
MB-144	38	218											75					
1	49	159											55					
2																		
3																		
5																		
4	40																	
7	18,9	157	1,7	4,1	1,6	27		0,6	32	3,3	75	0,5	91,5	41				0,8
6	39,4	149	5,8	13,3	1,1	25		0,7	37	8,4	129	1,1	34,5	34				1,3
8	39,6	24	11,3	97,3	4,8	2		14,7	8	74,9	96	0,4	6	2				11,1
9	26	28	3,3	7	0,3	11	0,3	0,1	20		90	2		13				
10	40	162	6,8	10	0,4	23	5,5	0,6	10	12	100	2	70	22				
11	45	150	6,9	9	0,3	22	4,6	0,7	10	10	110		60	20				
12	20	40	7,7	8	0,5	9	0,9	0,5	10	11	80	2		6				
GW11	24	110	7,5	6	0,4	20	9,3	1,1		13	100	2	40	17				
GW12	38	134	9,3	8	0,3	18	11,9	1,1	10	11	90	1	50	15				
GW14	32	67	11,9	12	0,9	9	18,7	3,9	40	11	60	2	30	9				

Sample name	W	Be
MB-72	3,5	1
MB-68A	1,1	3
MB-69	0,9	5
MB-44	1	2
MB-47	1,6	3
MB-63A	2,4	3
MB-45A	1	3
MB-67	1,4	2
MB-71A	0,8	1
MB-45B		
MB-68B		
MB-63B		
36		
37		
38	1,6	1
39	1,7	3
40	2	3
MB-143A		
MB-143B		
MB-145A		
MB-145B		
MB-146		
MB-148		
MB-144		
1		
2		
3		
5		
4		
7		
6		
8		
9		
10		
11		
12		
GW11		
GW12		
GW14		

Supplementary Data Table S2. Mineral chemistry (EPMA)

Garnet compositions (EMPA). Cations are calculated based on 12 oxygens.

Mineral	gr1.1	gr1.2	gr1.3	gr1.4	gr1.5	gr1.6	gr1.7	gr1.8	gr1.9	gr1.10	gr1.11	gr1.12	gr1.13	gr1.14	gr1.15	gr1.16	gr1.17	gr1.18	gr1.19
SiO2	37,73	38	37,89	38,04	38,17	38,09	38,27	38,37	38,35	38,31	38,5	38,2	38,44	38,33	38,07	38,19	38,04	38,41	38,34
Al2O3	21,78	21,4	21,77	21,62	21,4	21,63	21,59	21,42	21,22	21,57	21,57	21,28	21,45	21,35	21,63	21,59	21,26	21,37	21,28
FeO	32,63	31,79	31,97	31,83	31,69	31,58	31,1	31,35	31,42	31,35	31,43	31,45	31,53	31,34	31,23	31,37	31,46	31,15	31,4
MnO	1,25	1,17	1,17	1,18	1,15	1,16	1,18	1,07	1,22	1,12	1,17	1,17	1,17	1,13	1,15	1,11	1,12	1,15	1,15
CaO	1,07	1,05	1,02	1,03	0,93	0,98	0,92	0,96	0,91	0,98	1	0,96	0,91	1,01	0,96	0,98	0,99	0,98	0,96
Cr2O3	0,14	0,13	0,11	0,18	0,21	0,1	0,04	0,12	0,04	0,06	0,03	0,12	0,11	0,12	0,1	0,04	0,07	0,13	0,19
TiO2	0,02	0,02	0,03	0,05	0,04	0,06	0,06	0,05	0,05	0,03	0,07	0,07	0,07	0,05	0,05	0,05	0,03	0,02	0,03
MgO	5,31	5,42	5,78	5,87	5,97	6,03	6,07	6,15	6,1	6,1	6,29	6,09	6,15	6,13	6,22	5,98	6,06	6,06	6,06
Total	99,93	98,98	99,73	99,8	99,57	99,64	99,22	99,49	99,31	99,51	100,05	99,34	99,82	99,45	99,42	99,31	99,02	99,29	99,4
Si	2,987	3,024	2,994	3,002	3,016	3,006	3,023	3,026	3,033	3,021	3,019	3,022	3,024	3,026	3,006	3,019	3,02	3,034	3,029
Al	2,033	2,008	2,028	2,011	1,994	2,012	2,011	1,992	1,979	2,005	1,994	1,985	1,989	1,987	2,014	2,012	1,99	1,99	1,982
Fe2+	2,16	2,116	2,112	2,101	2,094	2,084	2,055	2,068	2,078	2,067	2,062	2,081	2,074	2,069	2,062	2,074	2,089	2,058	2,075
Mn	0,084	0,079	0,078	0,079	0,077	0,078	0,079	0,071	0,082	0,075	0,078	0,078	0,078	0,076	0,077	0,074	0,075	0,077	0,077
Ca	0,091	0,09	0,086	0,087	0,079	0,083	0,078	0,081	0,077	0,083	0,084	0,081	0,077	0,085	0,081	0,083	0,084	0,083	0,081
Cr	0,009	0,008	0,007	0,011	0,013	0,006	0,002	0,007	0,003	0,004	0,002	0,008	0,007	0,007	0,006	0,002	0,004	0,008	0,012
Ti	0,001	0,001	0,002	0,003	0,002	0,004	0,004	0,003	0,003	0,002	0,004	0,004	0,004	0,003	0,003	0,003	0,002	0,001	0,002
Mg	0,626	0,643	0,681	0,69	0,703	0,709	0,715	0,723	0,719	0,717	0,735	0,718	0,721	0,721	0,732	0,704	0,717	0,713	0,714
Total	7,991	7,967	7,987	7,984	7,978	7,981	7,966	7,971	7,973	7,973	7,978	7,977	7,974	7,974	7,981	7,971	7,981	7,965	7,972
XAlm	45,41	44,38	45,09	43,89	45,03	45,61	48,47	43,83	49,7	45,73	46,43	45,61	46,99	44,44	46,11	45,68	45,45	45,56	44,77
XPyr	4,86	4,49	4,05	6,11	7,6	3,51	1,23	4,32	1,82	2,44	1,19	4,68	4,22	4,09	3,59	1,23	2,42	4,73	6,98
XGros	0,54	0,56	1,16	1,67	1,17	2,34	2,45	1,85	1,82	1,22	2,38	2,34	2,41	1,75	1,8	1,85	1,21	0,59	1,16
XSps	49,19	50,56	49,71	48,33	46,2	48,54	47,85	50	46,67	50,61	50	47,37	46,39	49,71	48,5	51,23	50,91	49,11	47,09

XAlm = Fe2+/(Fe2+ + Mg + Mn + Ca); XPyr = Mg/(Fe2+ + Mg + Mn + Ca); XGros = Ca/(Fe2+ + Mg + Mn + Ca); XSps = Mn/(Fe2+ + Mg + Mn + Ca)

Garnet comp

Mineral	gr1.20	gr2.1	gr2.2	gr2.3	gr2.4	gr2.5	gr2.6	gr2.8	gr2.9	gr2.10	gr2.11	gr2.12	gr2.13	gr2.14	gr2.15	gr2.16	gr2.17	gr2.18	gr2.19
SiO2	38,51	38,34	38,11	38,1	38,15	38,2	38,13	38,18	38,36	38,4	38,04	38,15	38,28	38,13	37,87	38,1	37,98	38,05	38,22
Al2O3	21,17	21,61	21,49	21,44	21,64	21,48	21,59	21,6	21,31	21,26	21,47	21,56	19,61	21,48	21,58	21,45	21,44	21,78	21,59
FeO	31,29	31,41	30,85	31,27	31,27	31,39	31,04	31,34	31,06	31,53	31,16	31,53	31,35	31,45	31,44	31,32	31,54	31,51	31,51
MnO	1,18	1,19	1,13	1,16	1,14	1,13	1,09	1,15	1,14	1,2	1,13	1,16	1,16	1,13	1,17	1,15	1,01	1,19	1,1
CaO	1,03	1,07	1,01	1,02	1	0,97	1,06	0,95	0,92	0,93	0,93	0,95	1	0,98	0,98	0,95	0,92	0,95	0,95
Cr2O3	0,1	0,14	0,21	0,2	0,17	0,17	0,06	0,09	0,05	0,1	0,08	0,14	0,03	0	0,11	0,17	0,11	0	0,05
TiO2	0,04	0,02	0,02	0,07	0,03	0,04	0,07	0,04	0,03	0,03	0,06	0,06	0,03	0,09	0,06	0,05	0,06	0,05	0,06
MgO	6,18	6,08	6,03	6,13	5,96	6,07	6,03	6,05	6,1	6,07	6,05	6,11	6,2	6,07	5,86	5,93	6,02	6	5,93
Total	99,5	99,86	98,86	99,39	99,37	99,45	99,07	99,39	98,98	99,51	98,92	99,65	97,66	99,32	99,06	99,1	99,08	99,53	99,41
Si	3,038	3,015	3,022	3,011	3,014	3,017	3,018	3,015	3,038	3,032	3,018	3,009	3,086	3,015	3,006	3,019	3,013	3,004	3,019
Al	1,969	2,004	2,009	1,998	2,016	2	2,014	2,011	1,99	1,979	2,008	2,005	1,864	2,003	2,019	2,004	2,005	2,027	2,011
Fe2+	2,064	2,066	2,046	2,067	2,066	2,073	2,055	2,07	2,057	2,082	2,067	2,08	2,114	2,08	2,087	2,076	2,092	2,08	2,082
Mn	0,079	0,079	0,076	0,078	0,076	0,076	0,073	0,077	0,076	0,08	0,076	0,077	0,079	0,076	0,079	0,077	0,068	0,08	0,074
Ca	0,087	0,09	0,086	0,086	0,085	0,082	0,09	0,08	0,078	0,079	0,079	0,08	0,086	0,083	0,083	0,081	0,078	0,08	0,08
Cr	0,006	0,009	0,013	0,012	0,011	0,011	0,004	0,006	0,003	0,006	0,005	0,009	0,002	0	0,007	0,011	0,007	0	0,003
Ti	0,002	0,001	0,001	0,004	0,002	0,002	0,004	0,002	0,002	0,002	0,004	0,004	0,002	0,005	0,004	0,003	0,004	0,003	0,004
Mg	0,727	0,713	0,713	0,722	0,702	0,714	0,711	0,712	0,72	0,714	0,715	0,718	0,745	0,715	0,693	0,7	0,712	0,706	0,698
Total	7,972	7,977	7,966	7,979	7,971	7,975	7,969	7,974	7,964	7,974	7,972	7,981	7,979	7,978	7,978	7,971	7,978	7,98	7,97
XAlm	45,4	44,13	43,18	43,33	43,68	44,44	42,69	46,67	47,8	47,9	46,34	45,29	46,75	46,34	45,66	44,77	43,31	49,08	45,96
XPyr	3,45	5,03	7,39	6,67	6,32	6,43	2,34	3,64	1,89	3,59	3,05	5,29	1,18	0	4,05	6,4	4,46	0	1,86
XGros	1,15	0,56	0,57	2,22	1,15	1,17	2,34	1,21	1,26	1,2	2,44	2,35	1,18	3,05	2,31	1,74	2,55	1,84	2,48
XSps	50	50,28	48,86	47,78	48,85	47,95	52,63	48,48	49,06	47,31	48,17	47,06	50,89	50,61	47,98	47,09	49,68	49,08	49,69

XAlm = Fe2+/(F

Garnet comp

Mineral	gr2.20	gr2.21	gr2.22	gr2.23	gr2.24	gr2.25	gr2.26
SiO2	37,91	38,26	38,27	38,11	38,31	37,96	37,93
Al2O3	21,63	21,54	21,42	21,56	21,31	21,5	21,5
FeO	31,44	31,21	31,39	31,34	31,39	31,39	31,45
MnO	1,15	1,08	1,19	1,1	1,19	1,19	1,14
CaO	0,91	0,9	0,91	0,93	1	0,92	0,91
Cr2O3	0,12	0,07	0,04	0,04	0,14	0,12	0,18
TiO2	0,06	0,03	0,06	0,06	0,05	0,05	0,04
MgO	6,04	6,15	5,97	6,05	6	6	6,03
Total	99,27	99,24	99,26	99,19	99,38	99,13	99,18
Si	3,002	3,023	3,028	3,016	3,028	3,01	3,007
Al	2,019	2,006	1,998	2,011	1,986	2,01	2,009
Fe2+	2,082	2,062	2,077	2,074	2,075	2,082	2,085
Mn	0,077	0,072	0,08	0,074	0,08	0,08	0,077
Ca	0,077	0,076	0,077	0,079	0,085	0,078	0,077
Cr	0,008	0,004	0,003	0,003	0,009	0,008	0,011
Ti	0,004	0,002	0,004	0,004	0,003	0,003	0,002
Mg	0,713	0,724	0,704	0,714	0,707	0,709	0,712
Total	7,981	7,97	7,969	7,974	7,972	7,979	7,981
XAlm	46,39	46,75	48,78	46,25	45,2	47,34	46,11
XPyr	4,82	2,6	1,83	1,88	5,08	4,73	6,59
XGros	2,41	1,3	2,44	2,5	1,69	1,78	1,2
XSps	46,39	49,35	46,95	49,38	48,02	46,15	46,11

XAlm = Fe2+/(Fe

Biotite compositions (EMPA). Cations are calculated bas

Mineral	bt1	bt2	bt3	bt4	bt5
SiO2	36.57	36.52	36.79	36.65	36.44
TiO2	4.74	5.38	5.34	4.53	4.16
Al2O3	15.04	14.94	14.79	15.09	15.15
FeO	16.74	17.23	14.07	17.12	17.28
MnO	0.03	0.00	0.00	0.00	0.00
MgO	12.15	11.89	14.14	12.17	12.09
CaO	0.00	0.00	0.00	9.98	0.01
Na2O	0.02	0.05	0.04	0.04	0.03
K2O	9.93	9.88	10.06	9.98	9.87
Si	2.768	2.751	2.752	2.578	2.770
Ti	0.270	0.305	0.300	0.240	0.238
Al	1.341	1.326	1.304	1.251	1.357
Fe+3	0.000	0.000	0.000	0.000	0.000
Fe+2	1.059	1.085	0.880	1.007	1.098
Mn	0.002	0.000	0.000	0.000	0.000
Mg	1.371	1.335	1.577	1.276	1.370
Ca	0.000	0.000	0.000	0.752	0.001
Na	0.003	0.007	0.006	0.005	0.004
K	0.959	0.949	0.960	0.896	0.957
H	2.000	2.000	2.000	2.000	2.000
Total	9.773	9.759	9.779	10.007	9.795
XFe					
XMg					

XFe = Fe2+/(Fe2+ + Mg); XMg = Mg/(Mg+Fe2+)

Supplementary Data Table S3. Results of the LA-ICP-MS U-Pb zircon analysis

* concentration uncertainty ca. 10%
** data corrected/not corrected for common-Pb
*** Concordance calculated as (206Pb-238U age/207Pb-206Pb age)*100
Decay constants of Jaffey et al. (1971) used
The bold type analysis were used to calculate de MDA and the concordia ages

SESSION A					Isotope ratio**							Ages						
Analysis	Domain	Comm 206Pb	U (µg g-1)*	Th/U	207Pb 206Pb	±2s (%)	207Pb 235U	±2s (%)	206Pb 238U	±2s (%)	Rho	207Pb 206Pb	±2s (Ma)	206Pb 238U	±2s (Ma)	207Pb 235U	±2s (Ma)	Conc***
MB-146B																		
132	CL-bright rim (M2)	0.0410	520	1.18	0.0748	2.0353	1.8453	2.8370	0.1789	1.9764	0.6966	1063	41	1061	19	1062	19	100
80	CL-bright rim (M2)	0.0000	275	0.37	0.0750	2.3736	1.8557	3.0718	0.1795	1.9499	0.6348	1068	48	1064	19	1065	20	100
87	CL-bright rim (M2)	0.0724	142	0.69	0.0748	2.5199	1.8560	3.2050	0.1799	1.9803	0.6179	1064	51	1066	19	1066	21	100
73	CL-gray rim (M1)	0.0051	718	4.13	0.0759	2.0286	1.8939	2.9277	0.1809	2.1110	0.7210	1093	41	1072	21	1079	20	99
178	CL-gray rim (M1)	0.0578	768	0.05	0.0758	2.3283	1.9010	3.2080	0.1820	2.2070	0.6880	1089	47	1078	22	1081	22	100
148	CL-gray rim (M1)	0.0058	503	0.56	0.0755	2.7301	1.8954	3.2996	0.1822	1.8531	0.5616	1081	55	1079	18	1079	22	100
137	CL-gray rim (M1)	0.0560	832	4.50	0.0752	2.1070	1.8917	3.0311	0.1825	2.1791	0.7189	1073	42	1081	22	1078	20	100
88	CL-gray rim (M1)	0.0054	286	2.32	0.0757	2.4582	1.9132	3.1525	0.1834	1.9737	0.6261	1086	49	1085	20	1086	21	100
175	CL-gray rim (M1)	0.0014	889	0.09	0.0757	2.0605	1.9160	2.8280	0.1840	1.9370	0.6850	1087	41	1086	19	1087	19	100
79	CL-gray rim (M1)	0.0114	722	0.16	0.0755	2.0934	1.9114	2.8977	0.1837	2.0035	0.6914	1081	42	1087	20	1085	20	100
60	CL-gray rim (M1)	0.0479	588	0.63	0.0754	2.6275	1.9108	3.2269	0.1837	1.8731	0.5805	1080	53	1087	19	1085	22	100
72	CL-gray rim (M1)	1.0000	434	0.70	0.0758	3.3607	1.9250	4.0908	0.1841	2.3324	0.5702	1091	67	1089	23	1090	28	100
95	CL-gray rim (M1)	0.0152	774	0.08	0.0758	2.1626	1.9270	2.9360	0.1840	1.9860	0.6760	1091	43	1090	20	1091	20	100
140	CL-gray rim (M1)	0.0301	717	0.17	0.0763	2.0713	1.9647	2.8654	0.1867	1.9800	0.6910	1104	41	1103	20	1103	19	100
70	CL-gray rim (M1)	0.1248	193	1.83	0.0760	2.0794	1.9586	2.8882	0.1870	2.0044	0.6940	1094	42	1105	20	1101	20	100
179	CL-gray rim (M1)	0.0559	237	0.91	0.0765	3.5312	1.9736	4.0520	0.1870	1.9873	0.4905	1109	71	1105	20	1107	28	100
156	CL-gray rim (M1)	0.0886	450	0.11	0.0768	2.0963	1.9950	2.9310	0.1880	2.0490	0.6990	1116	42	1113	21	1114	20	100
38	CL-gray rim (M1)	0.1423	258	0.80	0.0768	2.0384	1.9964	2.8266	0.1885	1.9583	0.6928	1117	41	1113	20	1114	19	100
30	Detrital core	0.0000	245	1.00	0.0761	1.9966	1.9392	2.8509	0.1847	2.0350	0.7138	1098	40	1093	20	1095	19	100
150	Detrital core	1.0000	282	0.41	0.0761	3.4157	1.9450	4.0427	0.1854	2.1625	0.5349	1098	68	1096	22	1097	27	100
91	Detrital core	0.0748	662	0.89	0.0761	2.0854	1.9469	3.0158	0.1855	2.1786	0.7224	1098	42	1097	22	1097	20	100
35	Detrital core	1.0000	261	0.82	0.0763	3.3231	1.9580	3.9927	0.1860	2.2133	0.5543	1104	66	1100	22	1101	27	100
50	Detrital core	0.2113	134	1.55	0.0761	2.1994	1.9547	2.9156	0.1862	1.9140	0.6565	1098	44	1101	19	1100	20	100
28	Detrital core	0.1014	258	0.59	0.0762	2.1700	1.9557	2.9729	0.1863	2.0321	0.6835	1099	43	1101	21	1100	20	100
158	Detrital core	0.0292	312	0.56	0.0764	3.0131	1.9616	3.5554	0.1863	1.8873	0.5308	1104	60	1101	19	1102	24	100
127	Detrital core	0.0588	786	0.91	0.0764	2.0739	1.9631	2.9299	0.1864	2.0696	0.7064	1105	41	1102	21	1103	20	100
52	Detrital core	0.1066	159	1.04	0.0764	2.1641	1.9675	2.8791	0.1867	1.8989	0.6595	1106	43	1104	19	1104	20	100
147	Detrital core	1.0000	583	1.60	0.0766	3.3610	1.9734	4.0538	0.1869	2.2664	0.5591	1110	67	1105	23	1106	28	100
135	Detrital core	1.0000	670	0.22	0.0765	3.3156	1.9755	4.0189	0.1873	2.2713	0.5651	1108	66	1107	23	1107	27	100
94	Detrital core	1.0000	231	1.36	0.0767	3.4584	1.9816	4.2118	0.1875	2.4040	0.5708	1112	69	1108	25	1109	29	100
31	Detrital core	0.1523	135	1.38	0.0767	2.1479	1.9922	2.8451	0.1883	1.8658	0.6558	1115	43	1112	19	1113	19	100
53	Detrital core	1.0000	653	1.23	0.0766	3.3259	1.9928	3.9786	0.1886	2.1834	0.5488	1112	66	1114	22	1113	27	100
169	Detrital core	1.0000	359	0.40	0.0769	3.4828	1.9993	4.0946	0.1886	2.1530	0.5258	1118	69	1114	22	1115	28	100
78	Detrital core	0.0779	526	0.82	0.0769	2.1169	1.9996	3.0123	0.1886	2.1430	0.7114	1118	42	1114	22	1115	21	100
139	Detrital core	1.0000	176	1.17	0.0771	3.3224	2.0065	3.9834	0.1888	2.1975	0.5517	1124	66	1115	23	1118	27	100
39	Detrital core	1.0000	123	0.55	0.0769	3.3145	2.0053	3.9913	0.1891	2.2236	0.5571	1119	66	1117	23	1117	27	100
47	Detrital core	0.0771	456	0.81	0.0770	2.0630	2.0102	2.8856	0.1895	2.0176	0.6992	1120	41	1118	21	1119	20	100
171	Detrital core	0.0459	253	0.52	0.0770	2.3155	2.0154	2.9849	0.1899	1.8836	0.6311	1121	46	1121	19	1121	20	100
151	Detrital core	0.0000	192	1.18	0.0771	2.3075	2.0219	2.9704	0.1901	1.8704	0.6297	1125	46	1122	19	1123	20	100
56	Detrital core	0.0583	385	0.95	0.0771	2.0561	2.0266	2.9223	0.1908	2.0766	0.7106	1123	41	1125	21	1124	20	100
55	Detrital core	1.0000	583	0.70	0.0766	3.3419	2.0170	3.9977	0.1909	2.1940	0.5488	1112	67	1126	23	1121	28	100
20	Detrital core	0.0000	362	1.14	0.0772	2.0464	2.0336	2.8392	0.1910	1.9681	0.6932	1127	41	1127	20	1127	20	100
77	Detrital core	1.0000	615	1.48	0.0771	3.3531	2.0335	4.0775	0.1912	2.3200	0.5690	1125	67	1128	24	1127	28	100

69	Detrital core	0.0142	598	0.22	0.0774	2.0665	2.0417	2.9181	0.1912	2.0603	0.7060	1133	41	1128	21	1130	20	100
14	Detrital core	0.1865	456	0.38	0.0773	2.1266	2.0370	2.9240	0.1912	2.0068	0.6863	1128	42	1128	21	1128	20	100
49	Detrital core	0.0037	194	1.46	0.0773	2.0702	2.0413	2.8170	0.1916	1.9104	0.6782	1129	41	1130	20	1129	19	100
7	Detrital core	1.0000	701	0.68	0.0774	3.2765	2.0503	3.9509	0.1921	2.2077	0.5588	1132	65	1133	23	1132	27	100
19	Detrital core	1.0000	365	0.70	0.0775	3.2723	2.0547	3.9361	0.1923	2.1874	0.5557	1134	65	1134	23	1134	27	100
71	Detrital core	0.0234	534	1.09	0.0776	2.0364	2.0591	2.8732	0.1924	2.0270	0.7055	1137	41	1134	21	1135	20	100
27	Detrital core	0.0088	805	0.17	0.0775	2.1162	2.0564	2.7902	0.1924	1.8186	0.6518	1134	42	1135	19	1134	19	100
154	Detrital core	0.1091	130	0.74	0.0777	2.1047	2.0617	2.9145	0.1925	2.0160	0.6917	1138	42	1135	21	1136	20	100
170	Detrital core	1.0000	212	1.36	0.0777	3.3798	2.0621	4.1150	0.1926	2.3474	0.5705	1138	67	1135	25	1136	29	100
89	Detrital core	0.1280	196	2.27	0.0775	2.9099	2.0589	3.5290	0.1927	1.9966	0.5658	1134	58	1136	21	1135	24	100
173	Detrital core	0.0200	873	2.02	0.0777	2.0343	2.0665	2.8446	0.1929	1.9883	0.6990	1139	40	1137	21	1138	20	100
48	Detrital core	1.0000	728	1.21	0.0779	3.3050	2.0733	3.9382	0.1931	2.1415	0.5438	1144	66	1138	22	1140	27	100
29	Detrital core	1.0000	632	0.06	0.0778	3.5087	2.0750	4.0770	0.1930	2.0760	0.5090	1143	70	1139	22	1140	28	100
176	Detrital core	0.0685	612	1.08	0.0777	2.3219	2.0733	2.9883	0.1934	1.8811	0.6295	1140	46	1140	20	1140	21	100
15	Detrital core	0.1168	255	1.19	0.0777	2.0553	2.0734	2.7886	0.1935	1.8846	0.6758	1139	41	1140	20	1140	19	100
75	Detrital core	1.0000	891	0.41	0.0780	3.3468	2.0876	4.0124	0.1940	2.2132	0.5516	1148	66	1143	23	1145	28	100
93	Detrital core	0.0127	687	1.90	0.0778	2.0558	2.0829	2.9255	0.1941	2.0814	0.7115	1143	41	1143	22	1143	20	100
168	Detrital core	1.0000	710	0.37	0.0781	3.3458	2.0918	4.0961	0.1943	2.3630	0.5769	1149	66	1145	25	1146	29	100
131	Detrital core	1.0000	493	0.76	0.0776	3.2685	2.0803	3.9433	0.1944	2.2060	0.5594	1137	65	1145	23	1142	27	100
96	Detrital core	0.0748	491	1.56	0.0782	2.5633	2.0997	3.2480	0.1946	1.9947	0.6141	1153	51	1146	21	1149	23	100
34	Detrital core	0.0175	820	1.32	0.0781	2.0490	2.0988	2.7863	0.1949	1.8881	0.6777	1150	41	1148	20	1148	19	100
159	Detrital core	1.0000	717	1.96	0.0783	3.3526	2.1067	3.9697	0.1952	2.1256	0.5355	1154	67	1149	22	1151	28	100
16	Detrital core	0.0066	757	0.09	0.0787	2.0073	2.1280	2.7340	0.1960	1.8560	0.6790	1165	40	1154	20	1158	19	100
153	Detrital core	0.0183	695	0.80	0.0786	2.0869	2.1335	2.9755	0.1969	2.1209	0.7128	1162	41	1158	23	1160	21	100
90	Detrital core	0.0270	267	2.63	0.0786	2.4686	2.1444	3.1591	0.1978	1.9714	0.6240	1163	49	1164	21	1163	22	100
57	Detrital core	0.0361	743	0.30	0.0779	2.3119	2.1325	2.9826	0.1985	1.8844	0.6318	1145	46	1167	20	1159	21	101
9	Detrital core	1.0000	788	1.27	0.0788	3.2483	2.1615	3.8571	0.1988	2.0798	0.5392	1168	64	1169	22	1169	27	100
133	Detrital core	0.0076	819	0.35	0.0791	2.0478	2.1708	2.8818	0.1990	2.0276	0.7036	1175	41	1170	22	1172	20	100
152	Detrital core	0.0087	755	1.29	0.0790	2.0266	2.1685	2.8024	0.1992	1.9354	0.6906	1171	40	1171	21	1171	20	100
174	Detrital core	0.0146	776	3.49	0.0793	2.1189	2.1851	2.8723	0.1998	1.9392	0.6751	1180	42	1175	21	1176	20	100
36	Detrital core	0.1087	139	3.75	0.0795	2.1050	2.2095	2.8282	0.2015	1.8888	0.6679	1185	42	1183	20	1184	20	100
149	Detrital core	0.0000	518	0.58	0.0798	2.3323	2.2220	2.9822	0.2021	1.8584	0.6232	1191	46	1186	20	1188	21	100
10	Detrital core	0.0478	617	0.82	0.0797	2.0852	2.2253	2.7474	0.2024	1.7890	0.6511	1191	41	1188	19	1189	19	100
12	Detrital core	1.0000	438	1.00	0.0807	3.2364	2.2960	3.8711	0.2063	2.1239	0.5487	1214	64	1209	23	1211	28	100
8	Detrital core	0.1312	177	1.89	0.0813	2.0671	2.3611	2.8161	0.2106	1.9124	0.6791	1229	41	1232	21	1231	20	100
130	Detrital core	1.0000	150	1.21	0.0815	3.2534	2.4132	3.8747	0.2148	2.1045	0.5431	1233	64	1254	24	1247	28	101
17	Detrital core	0.0004	538	0.78	0.0823	2.1375	2.4367	2.8603	0.2146	1.9007	0.6645	1254	42	1253	22	1254	21	100
160	Detrital core	0.0126	821	1.17	0.0826	2.0346	2.4547	2.8346	0.2156	1.9736	0.6963	1259	40	1259	23	1259	21	100
167	Detrital core	1.0000	680	4.31	0.0830	3.1615	2.4814	3.8243	0.2168	2.1519	0.5627	1270	62	1265	25	1267	28	100
180	Detrital core	1.0000	356	2.75	0.0863	4.2181	2.7307	4.7419	0.2296	2.1663	0.4569	1344	81	1332	26	1337	36	100
58	Detrital core	0.0532	258	1.00	0.0935	2.0348	2.3830	2.8514	0.2624	1.9974	0.7005	1498	38	1502	27	1500	23	100
11	Detrital core	0.0000	278	3.88	0.1051	2.0360	4.3899	2.7812	0.3029	1.8947	0.6813	1716	37	1706	28	1710	23	100
157	Detrital core	0.0000	223	1.97	0.1139	2.2470	5.2375	3.0653	0.3334	2.0850	0.6802	1863	41	1855	34	1859	26	100
128	Detrital core	0.0490	290	1.71	0.1229	2.0357	6.1405	2.8508	0.3624	1.9957	0.7001	1999	36	1993	34	1996	25	100
129	Detrital core	0.0000	61	1.14	0.1796	2.2275	12.5703	2.9229	0.5077	1.8925	0.6475	2649	37	2647	41	2648	28	100
Rejected data																		
138		0.0143	157	0.06	0.0746	2.4145	2.6329	3.0552	0.2561	1.8720	0.6127	1057	49	1470	25	1310	23	112
37		0.1025	789	0.65	0.0773	1.9836	1.8278	2.9078	0.1714	2.1262	0.7312	1129	40	1020	20	1055	19	97
155		0.0046	802	0.79	0.0822	2.0437	2.1150	2.8016	0.1866	1.9163	0.6840	1250	40	1103	19	1154	20	96
136		0.0170	816	0.73	0.0865	2.0819	2.1843	2.7949	0.1832	1.8647	0.6572	1349	40	1084	19	1176	20	92
40		0.3170	584	0.66	0.0902	2.1997	2.4175	2.9004	0.1944	1.8903	0.6517	1430	42	1145	20	1248	21	92
32		0.0333	1053	0.33	0.0738	2.0609	1.2871	2.7702	0.1254	1.8511	0.6682	1037	42	768	13	840	16	91
59		0.0004	860	0.28	0.2182	2.0168	3.0425	2.8395	0.1311	1.9088	0.7039	2967	33	794	15	1622	23	49
74		1.0000	1356	0.65	0.2333	2.2051	2.1077	4.2702	0.0655	3.6568	0.8564	3075	35	409	15	1151	30	36
134		0.0297	1697	0.84	0.2829	2.0223	2.0260	2.8462	0.0519	2.0029	0.7037	3379	32	326	6	1124	20	29

18		0.0895	1465	0.48	0.3461	2.0116	2.1195	2.7902	0.0444	1.9335	0.6930	3690	31	280	5	1155	19	24
172		0.0272	1788	0.54	0.3470	2.0577	2.0343	2.8537	0.0425	1.9773	0.6929	3694	31	268	5	1127	20	24
67		0.1148	2389	0.23	0.9028	2.0251	1.9029	3.1944	0.0153	2.4705	0.7734	5093	29	98	2	1082	21	9
51		0.0064	2095	0.81	0.9778	2.0189	2.0219	2.8431	0.0150	2.0018	0.7041	5206	28	96	2	1123	20	9
54		0.1883	2021	0.68	1.0397	2.0260	2.0252	3.8899	0.0141	3.3207	0.8537	5292	28	90	3	1124	27	8
33		0.1277	1972	0.45	1.1721	2.0171	2.3607	3.2858	0.0146	2.5938	0.7894	5459	28	93	2	1231	24	8
13		1.0000	1633	1.31	1.4947	2.0168	3.2208	13.0953	0.0156	12.9391	0.9881	5796	28	100	13	1462	107	7
76		0.2818	2348	0.53	1.5188	2.0401	2.1337	6.2133	0.0102	5.8689	0.9446	5818	28	65	4	1160	44	6
177		0.2472	3167	1.17	1.8723	2.1046	2.0214	5.9534	0.0078	5.6272	0.9531	6105	29	50	3	1123	48	4
68		0.0615	3442	0.22	2.0251	2.0295	1.8594	3.4567	0.0067	2.7982	0.8095	6211	28	43	1	1067	23	4
92		0.1358	3695	1.02	2.2966	2.0465	2.0833	5.0758	0.0066	4.6450	0.9151	6382	28	42	2	1143	35	4
MB-144																		
153	CL-bright rim (M3)	0.1571	67	2.12	0.0732	2.2009	1.7312	2.9980	0.1715	2.0357	0.6790	1019	45	1021	19	1020	19	100
150	CL-bright rim (M3)	0.0218	96	2.57	0.0736	2.1755	1.7512	3.0451	0.1726	2.1306	0.6997	1030	44	1027	20	1028	20	100
117	Recryst. core (M2)	0.0105	549	0.48	0.0759	6.7492	1.8276	7.2522	0.1747	2.6540	0.3660	1091	135	1038	26	1055	49	98
147	Recryst. core (M2)	0.1952	199	1.21	0.0739	2.1243	1.7879	2.9524	0.1755	2.0505	0.6945	1038	43	1042	20	1041	19	100
116	Recryst. core (M2)	0.0126	797	0.18	0.0741	2.1592	1.7950	3.0235	0.1757	2.1165	0.7000	1044	44	1043	20	1044	20	100
107	Recryst. core (M2)	1.0000	186	2.13	0.0744	3.4270	1.8040	4.1054	0.1759	2.2605	0.5506	1052	69	1045	22	1047	27	100
108	Recryst. core (M2)	0.0621	301	0.82	0.0740	2.0608	1.7961	2.9194	0.1760	2.0679	0.7083	1042	42	1045	20	1044	19	100
138	Recryst. core (M2)	0.0270	398	0.97	0.0743	2.0479	1.8055	2.8672	0.1763	2.0068	0.6999	1049	41	1047	19	1047	19	100
140	Recryst. core (M2)	0.0514	263	1.14	0.0742	2.0803	1.8069	2.8963	0.1766	2.0151	0.6958	1047	42	1049	20	1048	19	100
128	Recryst. core (M2)	1.0000	218	1.54	0.0744	3.3939	1.8122	4.1050	0.1767	2.3093	0.5626	1052	68	1049	22	1050	27	100
158	Recryst. core (M2)	0.0897	278	1.08	0.0744	2.0571	1.8217	2.8734	0.1776	2.0061	0.6982	1052	41	1054	20	1053	19	100
113	Recryst. core (M2)	0.0000	248	1.81	0.0744	2.0427	1.8227	2.8924	0.1777	2.0477	0.7080	1053	41	1054	20	1054	19	100
156	Recryst. core (M2)	1.0000	304	1.13	0.0746	3.3691	1.8264	4.0888	0.1777	2.3167	0.5666	1057	68	1054	23	1055	27	100
134	Recryst. core (M2)	0.1328	193	1.23	0.0744	2.0748	1.8222	2.9106	0.1777	2.0414	0.7013	1052	42	1054	20	1053	19	100
111	Recryst. core (M2)	0.0076	299	2.08	0.0748	2.0326	1.8411	2.8938	0.1786	2.0598	0.7118	1063	41	1059	20	1060	19	100
127	Recryst. core (M2)	0.0000	158	1.43	0.0754	2.1217	1.8575	2.8871	0.1787	1.9579	0.6782	1079	43	1060	19	1066	19	99
154	Recryst. core (M2)	0.0000	218	1.17	0.0745	2.0685	1.8350	2.9253	0.1788	2.0685	0.7071	1054	42	1060	20	1058	19	100
110	Recryst. core (M2)	0.1077	181	1.65	0.0745	2.0593	1.8384	2.8969	0.1789	2.0375	0.7033	1056	41	1061	20	1059	19	100
149	Recryst. core (M2)	0.0000	120	1.21	0.0748	2.2985	1.8472	3.0240	0.1790	1.9649	0.6498	1064	46	1062	19	1062	20	100
139	Recryst. core (M2)	0.0000	187	1.23	0.0747	2.0605	1.8456	2.9012	0.1791	2.0424	0.7040	1062	41	1062	20	1062	19	100
137	Recryst. core (M2)	1.0000	279	1.13	0.0749	3.3689	1.8507	4.1282	0.1791	2.3858	0.5779	1067	68	1062	23	1064	28	100
132	Recryst. core (M2)	0.1150	264	1.56	0.0750	2.1015	1.8543	2.9013	0.1792	2.0003	0.6894	1069	42	1063	20	1065	19	100
100	Recryst. core (M2)	0.0000	224	1.92	0.0748	2.1131	1.8482	2.8686	0.1793	1.9400	0.6763	1062	43	1063	19	1063	19	100
98	Recryst. core (M2)	1.0000	262	1.90	0.0751	3.3471	1.8647	4.0412	0.1802	2.2646	0.5604	1070	67	1068	22	1069	27	100
118	Recryst. core (M2)	0.1962	156	1.33	0.0749	2.1484	1.8618	2.9248	0.1804	1.9847	0.6786	1065	43	1069	20	1068	20	100
148	Recryst. core (M2)	0.0000	273	0.98	0.0746	2.0638	1.8560	2.9719	0.1804	2.1385	0.7196	1058	42	1069	21	1066	20	100
151	Recryst. core (M2)	1.0000	405	1.15	0.0748	3.3567	1.8619	4.1139	0.1804	2.3784	0.5781	1064	68	1069	23	1068	28	100
99	Recryst. core (M2)	1.0000	210	1.70	0.0751	3.5480	1.8685	4.1665	0.1805	2.1844	0.5243	1071	71	1070	22	1070	28	100
112	Recryst. core (M2)	0.1172	279	1.16	0.0750	2.1033	1.8736	2.9644	0.1812	2.0891	0.7047	1069	42	1073	21	1072	20	100
114	Recryst. core (M2)	0.0000	204	1.38	0.0755	2.1446	1.8896	3.0123	0.1814	2.1154	0.7022	1083	43	1075	21	1077	20	100
97	Recryst. core (M2)	1.0000	246	1.41	0.0752	3.3582	1.8813	4.1013	0.1815	2.3545	0.5741	1073	67	1075	23	1075	28	100
157	Recryst. core (M2)	0.4009	118	1.84	0.0752	2.4277	1.8913	3.2211	0.1824	2.1171	0.6573	1074	49	1080	21	1078	22	100
152	Recryst. core (M2)	0.1814	63	4.14	0.0755	2.2235	1.9001	3.0080	0.1824	2.0259	0.6735	1083	45	1080	20	1081	20	100
155	Recryst. core (M2)	0.1198	236	1.85	0.0755	2.0910	1.9030	2.9577	0.1829	2.0919	0.7073	1081	42	1083	21	1082	20	100
136	Recryst. core (M2)	0.3784	110	1.63	0.0752	2.6695	1.9015	3.3388	0.1833	2.0054	0.6006	1074	54	1085	20	1082	22	100
135	Igneous core	0.1180	471	2.34	0.0742	2.1544	1.9302	2.8931	0.1888	1.9310	0.6674	1046	43	1115	20	1092	20	102
133	Igneous core	1.0000	129	1.69	0.0776	3.4510	2.0375	4.1013	0.1905	2.2162	0.5404	1136	69	1124	23	1128	28	100
130	Igneous core	0.5016	55	3.90	0.0777	2.5184	2.0726	3.2921	0.1935	2.1203	0.6441	1139	50	1140	22	1140	23	100
Rejected data																		
120		0.0000	33	3.18	0.0755	19.7721	3.0350	20.7610	0.2917	6.3314	0.3050	1081	397	1650	93	1416	172	117
194		0.0199	68	1.91	0.0753	2.4161	2.6425	3.1240	0.2544	1.9803	0.6339	1078	48	1461	26	1313	23	111
109		0.0000	12	4.09	0.0799	2.6520	3.0062	3.3666	0.2727	2.0739	0.6160	1196	52	1555	29	1409	26	110
129		1.0000	68	2.49	0.0782	3.2742	2.6051	3.9562	0.2415	2.2205	0.5613	1153	65	1395	28	1302	29	107

~~115~~		~~0.5272~~	~~18~~	~~2.90~~	~~0.0981~~	~~2.6524~~	~~4.4269~~	~~3.4222~~	~~0.3272~~	~~2.1625~~	~~0.6319~~	~~1589~~	~~50~~	~~1825~~	~~34~~	~~1717~~	~~29~~	~~106~~
~~119~~		~~1.0000~~	~~117~~	~~2.44~~	~~0.0784~~	~~3.3492~~	~~2.4422~~	~~4.0442~~	~~0.2260~~	~~2.2668~~	~~0.5605~~	~~1156~~	~~66~~	~~1314~~	~~27~~	~~1255~~	~~30~~	~~105~~
~~177~~		~~0.0075~~	~~889~~	~~1.96~~	~~0.0813~~	~~2.1415~~	~~1.9850~~	~~2.8898~~	~~0.1772~~	~~1.9403~~	~~0.6714~~	~~1228~~	~~42~~	~~1052~~	~~19~~	~~1110~~	~~20~~	~~95~~
~~131~~		~~0.0000~~	~~1~~	~~11.11~~	~~0.1612~~	~~23.1213~~	~~8.8559~~	~~24.3675~~	~~0.3986~~	~~7.6929~~	~~0.3157~~	~~2468~~	~~390~~	~~2162~~	~~143~~	~~2323~~	~~251~~	~~93~~
MB-148																		
175	CL-bright rim (M2)	0.0878	203	1.69	0.0739	2.1241	1.7970	2.9160	0.1760	1.9970	0.6850	1039	43	1047	19	1044	19	100
~~159~~	CL-bright rim (M2)	1.0000	610	0.92	0.0747	3.3618	1.8470	4.0880	0.1790	2.3250	0.5690	1061	68	1063	23	1062	27	100
169	CL-bright rim (M2)	1.0000	189	3.30	0.0752	3.5432	1.8660	4.1800	0.1800	2.2190	0.5310	1074	71	1067	22	1069	28	100
173	CL-bright rim (M2)	1.0000	147	2.28	0.0753	3.6804	1.8760	4.2940	0.1810	2.2110	0.5150	1077	74	1070	22	1073	29	100
208	Igneous core	0.0000	129	2.11	0.0752	2.1557	1.8720	2.9730	0.1810	2.0470	0.6890	1073	43	1071	20	1071	20	100
227	Igneous core	0.0162	287	2.02	0.0754	2.2810	1.8850	3.0020	0.1810	1.9510	0.6500	1080	46	1074	19	1076	20	100
187	Igneous core	0.0664	470	1.57	0.0753	2.0800	1.8850	2.9500	0.1820	2.0930	0.7090	1076	42	1076	21	1076	20	100
160	Igneous core	0.0000	239	1.78	0.0751	2.1044	1.8820	2.9120	0.1820	2.0120	0.6910	1071	42	1077	20	1075	19	100
214	Igneous core	0.0000	259	2.69	0.0757	2.1139	1.9010	2.9080	0.1820	1.9980	0.6870	1087	42	1078	20	1081	20	100
193	Igneous core	1.0000	194	2.03	0.0753	3.3524	1.8920	4.1030	0.1820	2.3650	0.5760	1076	67	1079	24	1078	28	100
188	Igneous core	0.0956	363	2.23	0.0755	2.1069	1.9000	2.8800	0.1820	1.9640	0.6820	1083	42	1080	20	1081	19	100
229	Igneous core	0.0688	~~264~~	1.94	0.0761	2.2669	1.9170	2.9900	0.1830	1.9490	0.6520	1098	45	1081	19	1087	20	100
189	Igneous core	0.0000	112	2.23	0.0756	2.1164	1.9050	2.9590	0.1830	2.0680	0.6990	1084	42	1082	21	1083	20	100
178	Igneous core	0.0011	407	1.64	0.0758	2.0850	1.9100	2.9590	0.1830	2.0990	0.7090	1089	42	1082	21	1085	20	100
230	Igneous core	0.1287	146	2.29	0.0756	2.2234	1.9060	2.9860	0.1830	1.9930	0.6670	1083	45	1083	20	1083	20	100
231	Igneous core	0.0546	401	2.20	0.0759	2.4808	1.9190	3.1570	0.1830	1.9530	0.6180	1093	50	1085	20	1088	21	100
167	Igneous core	0.0340	554	1.49	0.0757	2.2219	1.9190	2.9390	0.1840	1.9240	0.6550	1086	45	1088	19	1088	20	100
200	Igneous core	0.0355	388	2.19	0.0751	2.0264	1.9040	2.8780	0.1840	2.0440	0.7100	1071	41	1088	21	1083	19	101
210	Igneous core	0.0245	351	1.61	0.0757	2.5358	1.9240	3.1880	0.1840	1.9320	0.6060	1088	51	1090	19	1089	22	100
168	Igneous core	0.0000	290	1.82	0.0760	2.0789	1.9300	2.9660	0.1840	2.1160	0.7130	1095	42	1090	21	1092	20	100
211	Igneous core	1.0000	223	2.91	0.0752	3.3549	1.9150	4.0760	0.1850	2.3150	0.5680	1075	67	1092	23	1086	28	101
191	Igneous core	0.0261	615	2.00	0.0761	2.1025	1.9450	2.9970	0.1850	2.1360	0.7130	1099	42	1096	22	1097	20	100
219	Igneous core	1.0000	335	2.02	0.0763	3.7273	1.9480	4.3340	0.1850	2.2120	0.5100	1102	75	1096	22	1098	30	100
176	Igneous core	1.0000	757	1.56	0.0758	3.6049	1.9390	4.2130	0.1860	2.1800	0.5170	1089	72	1098	22	1095	29	100
190	Igneous core	0.1899	138	1.87	0.0759	2.1664	1.9430	2.9940	0.1860	2.0660	0.6900	1093	43	1098	21	1096	20	100
174	Igneous core	1.0000	260	1.81	0.0763	3.3416	1.9530	4.0360	0.1860	2.2640	0.5610	1102	67	1098	23	1099	27	100
170	Igneous core	1.0000	384	2.30	0.0757	3.3814	1.9460	4.0700	0.1860	2.2650	0.5570	1088	68	1102	23	1097	28	100
195	Igneous core	0.0620	321	1.98	0.0762	2.1589	1.9580	3.0210	0.1860	2.1130	0.7000	1100	43	1102	21	1101	21	100
209	Igneous core	0.1115	475	1.57	0.0766	2.2656	1.9680	2.9850	0.1860	1.9440	0.6510	1110	45	1102	20	1105	20	100
197	Igneous core	0.0286	~~384~~	2.70	0.0759	2.1105	1.9590	2.8830	0.1870	1.9640	0.6810	1091	42	1107	20	1102	20	101
213	Igneous core	0.0126	302	2.19	0.0763	2.0448	1.9710	2.9170	0.1870	2.0810	0.7130	1103	41	1107	21	1106	20	100
220	Igneous core	0.0118	234	2.08	0.0765	2.0400	1.9770	2.9360	0.1870	2.1110	0.7190	1108	41	1108	22	1108	20	100
228	Igneous core	1.0000	736	1.69	0.0769	3.3159	1.9870	4.0290	0.1870	2.2890	0.5680	1118	66	1108	23	1111	28	100
192	Igneous core	1.0000	575	1.64	0.0770	3.5993	2.0020	4.2100	0.1890	2.1830	0.5190	1122	72	1113	22	1116	29	100
207	Igneous core	0.0085	755	1.04	0.0771	2.0234	2.0130	2.8720	0.1890	2.0380	0.7100	1124	40	1118	21	1120	20	100
218	Igneous core	0.0282	692	2.36	0.0775	2.0403	2.0270	2.9940	0.1900	2.1910	0.7320	1134	41	1120	23	1125	21	100
212	Igneous core	0.0848	295	2.89	0.0770	2.5031	2.0160	3.1660	0.1900	1.9390	0.6120	1121	50	1121	20	1121	22	100
215	Igneous core	0.1764	289	3.26	0.0776	2.2640	2.0340	2.9900	0.1900	1.9530	0.6530	1135	45	1123	20	1127	21	100
171	Igneous core	0.0000	838	1.70	0.0774	2.0421	2.0320	2.9810	0.1910	2.1720	0.7280	1131	41	1124	22	1126	20	100
179	Igneous core	0.0082	741	2.29	0.0780	2.2296	2.0540	2.9470	0.1910	1.9270	0.6540	1148	44	1126	20	1133	20	99
199	Igneous core	0.0999	504	1.84	0.0773	2.0612	2.0390	2.9220	0.1910	2.0710	0.7090	1128	41	1129	21	1128	20	100
180	Igneous core	1.0000	929	1.31	0.0760	3.3888	2.0130	4.0530	0.1920	2.2230	0.5490	1094	68	1134	23	1120	28	101
217	Inherited	0.0000	38	2.28	0.0934	2.2494	3.3540	3.0220	0.2610	2.0180	0.6680	1495	43	1493	27	1494	24	100
Rejected data																		
~~216~~		~~0.0452~~	~~442~~	~~3.41~~	~~0.0745~~	~~2.1247~~	~~2.4353~~	~~3.0106~~	~~0.2371~~	~~2.1329~~	~~0.7085~~	~~1055~~	~~43~~	~~1372~~	~~26~~	~~1253~~	~~22~~	~~109~~
~~172~~		~~0.0270~~	~~364~~	~~1.20~~	~~0.0747~~	~~2.1172~~	~~1.9240~~	~~2.9950~~	~~0.1870~~	~~2.1180~~	~~0.7070~~	~~1060~~	~~43~~	~~1104~~	~~22~~	~~1089~~	~~20~~	~~101~~
~~196~~		~~1.0000~~	~~678~~	~~2.50~~	~~0.0743~~	~~3.4646~~	~~1.9320~~	~~4.1100~~	~~0.1890~~	~~2.2100~~	~~0.5380~~	~~1049~~	~~70~~	~~1114~~	~~23~~	~~1092~~	~~28~~	~~102~~
~~198~~		~~0.0403~~	~~490~~	~~1.32~~	~~0.0740~~	~~2.0558~~	~~1.8840~~	~~2.8560~~	~~0.1850~~	~~1.9830~~	~~0.6940~~	~~1043~~	~~44~~	~~1092~~	~~20~~	~~1075~~	~~19~~	~~102~~
Reference materials																		
BB																		
121		0.0191	414	0.44	0.0591	2.0636	0.7419	2.8593	0.0910	1.9791	0.6922	573	45	561	11	564	12	100
122		0.0355	414	0.44	0.0586	2.0844	0.7402	2.8661	0.0916	1.9672	0.6864	553	45	565	11	563	12	100
141		0.1487	421	0.44	0.0586	2.1417	0.7417	2.9371	0.0918	2.0100	0.6843	553	47	566	11	563	13	100
142		0.0991	428	0.45	0.0589	2.0998	0.7458	2.8946	0.0919	1.9923	0.6883	562	46	567	11	566	13	100
161		1.0000	404	0.43	0.0588	3.9868	0.7404	4.9651	0.0914	2.9592	0.5960	558	87	564	16	563	22	100
162		1.0000	399	0.43	0.0592	3.9734	0.7406	4.9678	0.0907	2.9817	0.6002	575	86	560	16	563	22	99
181		1.0000	416	0.45	0.0587	4.0057	0.7435	4.9811	0.0918	2.9607	0.5944	558	87	566	16	564	22	100
182		0.0849	417	0.45	0.0589	2.1249	0.7416	2.9342	0.0913	2.0234	0.6896	563	46	563	11	563	13	100
001		1.0000	501	0.46	0.0589	3.9585	0.7508	4.8802	0.0924	2.8542	0.5849	564	86	570	16	569	21	100
002		0.0285	515	0.45	0.0589	2.0406	0.7432	2.7743	0.0916	1.8796	0.6775	562	44	565	10	564	12	100
021		1.0000	419	0.45	0.0589	3.9581	0.7460	4.9077	0.0918	2.9015	0.5912	564	86	566	16	566	22	100
022		0.0000	423	0.44	0.0588	2.0419	0.7399	2.7929	0.0913	1.9056	0.6823	559	45	563	10	562	12	100
041		0.0830	401	0.45	0.0584	2.0747	0.7332	2.8562	0.0911	1.9630	0.6873	544	45	562	11	558	12	101
042		0.0393	400	0.45	0.0593	2.0607	0.7370	2.8407	0.0901	1.9553	0.6883	579	45	556	10	561	12	99
062		0.0478	366	0.47	0.0587	2.0832	0.7418	2.8960	0.0916	2.0117	0.6946	558	45	565	11	563	13	100
082		1.0000	375	0.48	0.0587	3.9935	0.7483	4.9838	0.0925	2.9817	0.5983	555	87	570	16	567	22	101
101		1.0000	443	0.79	0.0591	3.9669	0.7461	4.9620	0.0916	2.9807	0.6007	569	86	565	16	566	22	100
102		0.0133	459	0.79	0.0591	2.0644	0.7471	2.8947	0.0917	2.0292	0.7010	571	45	565	11	567	13	100
202		0.0000	399	0.82	0.0590	2.0696	0.7477	2.9393	0.0920	2.0872	0.7101	565	45	567	11	567	13	100
221		0.0100	388	0.82	0.0589	2.0714	0.7393	2.9407	0.0910	2.0873	0.7098	564	45	562	11	562	13	100
~~081~~		~~0.0092~~	~~365~~	~~0.47~~	~~0.0589~~	~~2.0699~~	~~0.7589~~	~~2.9176~~	~~0.0934~~	~~2.0561~~	~~0.7047~~	~~565~~	~~45~~	~~575~~	~~11~~	~~573~~	~~13~~	~~100~~
~~061~~		~~0.0935~~	~~365~~	~~0.46~~	~~0.0594~~	~~2.1121~~	~~0.7227~~	~~2.9121~~	~~0.0883~~	~~2.0049~~	~~0.6885~~	~~581~~	~~46~~	~~545~~	~~10~~	~~552~~	~~12~~	~~99~~
~~201~~		~~0.0439~~	~~395~~	~~0.82~~	~~0.0587~~	~~2.0819~~	~~0.7472~~	~~2.9453~~	~~0.0923~~	~~2.0834~~	~~0.7074~~	~~558~~	~~45~~	~~569~~	~~11~~	~~557~~	~~13~~	~~100~~
~~222~~		~~0.0582~~	~~387~~	~~0.82~~	~~0.0598~~	~~2.0832~~	~~0.7618~~	~~2.9447~~	~~0.0924~~	~~2.0813~~	~~0.7068~~	~~596~~	~~45~~	~~570~~	~~11~~	~~575~~	~~13~~	~~99~~
PLESOVICE																		
105		1.0000	1340	0.42	0.0532	4.3249	0.3967	6.0324	0.0541	4.2053	0.6971	339	98	339	14	339	18	100
106		0.0000	1118	0.41	0.0531	2.1833	0.3921	2.8981	0.0535	1.9058	0.6576	334	49	336	6	336	8	100
125		0.0472	880	0.37	0.0532	2.2253	0.3936	3.0814	0.0537	2.1314	0.6917	337	50	337	7	337	9	100
126		0.0223	943	0.38	0.0532	2.0683	0.3935	2.9407	0.0536	2.0904	0.7109	339	47	337	7	337	8	100
145		0.1053	774	0.39	0.0532	2.1408	0.3964	2.9304	0.0540	2.0010	0.6828	339	48	339	7	339	8	100
146		1.0000	823	0.41	0.0533	4.3011	0.3947	6.0211	0.0537	4.2136	0.6998	341	97	337	14	338	17	100
165		1.0000	1813	0.61	0.0532	4.3087	0.3949	6.0579	0.0538	4.2583	0.7029	337	98	338	14	338	18	100
166		1.0000	1295	0.43	0.0533	4.2988	0.3964	6.0332	0.0539	4.2332	0.7017	343	97	339	14	339	18	100
185		1.0000	1189	0.38	0.0533	4.2860	0.3929	6.0344	0.0535	4.2478	0.7039	340	97	336	14	336	17	100
186		0.0549	910	0.38	0.0533	2.1540	0.3967	2.9237	0.0540	1.9769	0.6762	340	49	339	7	339	8	100
205		0.0003	1117	0.39	0.0532	2.0677	0.3940	2.9100	0.0537	2.0477	0.7037	337	47	337	7	337	8	100
123		0.0589	1151	0.23	0.0528	2.1723	0.3900	2.9689	0.0536	2.0238	0.6817	318	49	337	7	334	9	101
124		1.0000	802	0.20	0.0534	4.3133	0.3946	6.0443	0.0536	4.2343	0.7005	345	98	337	14	338	18	100
143		0.0000	900	0.21	0.0536	2.2744	0.3968	3.0857	0.0536	2.0853	0.6758	356	51	337	7	339	9	99
144		0.0000	850	0.23	0.0532	2.1441	0.3947	3.0376	0.0538	2.1517	0.7084	336	49	338	7	338	9	100
163		0.0043	1023	0.24	0.0533	2.3270	0.3954	3.1703	0.0538	2.1530	0.6791	341	53	338	7	338	9	100
164		1.0000	836	0.22	0.0533	4.3394	0.3942	6.0854	0.0537	4.2662	0.7011	341	98	337	14	337	18	100
005		1.0000	1243	0.22	0.0532	4.2865	0.3946	5.9975	0.0537	4.1947	0.6994	339	97	337	14	338	17	100
006		0.0006	975	0.22	0.0533	2.0998	0.3971	2.8747	0.0540	1.9633	0.6830	343	48	339	6	340	8	100
025		1.0000	827	0.24	0.0533	4.3209	0.3976	5.9778	0.0541	4.1309	0.6910	341	98	340	14	340	17	100
026		1.0000	930	0.22	0.0531	4.3344	0.3935	6.0200	0.0537	4.1777	0.6940	334	98	337	14	337	17	100
045		1.0000	786	0.21	0.0532	4.3097	0.3942	6.0256	0.0538	4.2112	0.6989	337	98	338	14	337	17	100
046		1.0000	692	0.21	0.0533	4.2845	0.3952	6.0049	0.0538	4.2073	0.7006	340	97	338	14	338	17	100
065		1.0000	803	0.24	0.0533	4.2855	0.3968	5.9930	0.0540	4.1894	0.6990	340	97	339	14	339	17	100
066		1.0000	635	0.23	0.0534	4.3278	0.3981	6.0223	0.0541	4.1879	0.6954	347	98	339	14	340	18	100
085		0.0179	906	0.25	0.0532	2.3676	0.3926	3.1865	0.0535	2.1327	0.6693	339	54	336	7	336	9	100
086		1.0000	1042	0.26	0.0532	4.7886	0.3942	6.3790	0.0537	4.2144	0.6607	338	108	337	14	337	18	100
~~206~~		~~0.1138~~	~~1238~~	~~0.56~~	~~0.0584~~	~~2.3285~~	~~0.4332~~	~~3.0553~~	~~0.0538~~	~~1.9781~~	~~0.6474~~	~~544~~	~~51~~	~~338~~	~~7~~	~~365~~	~~9~~	~~92~~

GJ-1																		
103		0.0279	732	0.09	0.0593	2.0587	0.8028	2.9107	0.0982	2.0576	0.7069	579	45	604	12	598	13	101
104		0.1059	697	0.09	0.0592	2.1258	0.8024	3.0199	0.0983	2.1450	0.7103	574	46	605	12	598	14	101
183		1.0000	657	0.09	0.0599	3.9303	0.8050	4.8752	0.0975	2.8844	0.5917	599	85	600	17	600	22	100
184		1.0000	609	0.09	0.0600	3.9190	0.8063	4.8511	0.0974	2.8592	0.5894	605	85	599	16	600	22	100
203		1.0000	647	0.09	0.0600	3.9226	0.8123	4.9178	0.0982	2.9661	0.6031	603	85	604	17	604	23	100
204		1.0000	682	0.09	0.0598	3.9525	0.8083	4.9097	0.0980	2.9125	0.5932	597	86	603	17	602	23	100
223		0.1022	669	0.09	0.0596	2.0745	0.8070	2.9575	0.0982	2.1078	0.7127	590	45	604	12	601	14	100
224		0.0329	682	0.09	0.0596	2.0496	0.8178	2.9274	0.0995	2.0902	0.7140	589	44	611	12	607	13	101
125		0.0165	684	0.05	0.0604	2.0209	0.8142	2.8180	0.0978	1.9639	0.6969	618	44	601	11	605	13	99
126		0.0027	673	0.05	0.0599	2.0358	0.8089	2.8269	0.0979	1.9614	0.6938	601	44	602	11	602	13	100
145		0.0000	727	0.05	0.0600	2.1344	0.8116	2.9369	0.0982	2.0173	0.6869	602	46	604	12	603	13	100
146		0.0135	703	0.05	0.0601	2.0633	0.8129	2.8164	0.0981	1.9170	0.6807	608	45	603	11	604	13	100
165		0.0186	679	0.05	0.0602	2.1279	0.8134	2.9623	0.0980	2.0609	0.6957	610	46	603	12	604	14	100
166		0.0842	698	0.05	0.0599	2.1215	0.8087	2.9364	0.0979	2.0302	0.6914	601	46	602	12	602	13	100
003		0.0086	804	0.05	0.0601	2.0293	0.8075	2.7863	0.0974	1.9093	0.6852	608	44	599	11	601	13	100
004		1.0000	800	0.05	0.0599	3.8927	0.8095	4.7957	0.0980	2.8009	0.5840	601	84	603	16	602	22	100
023		0.0000	642	0.05	0.0598	2.0732	0.8061	2.7864	0.0977	1.8617	0.6681	597	45	601	11	600	13	100
024		1.0000	642	0.05	0.0598	3.9173	0.8119	4.7998	0.0985	2.7737	0.5779	597	85	605	16	603	22	100
043		1.0000	607	0.05	0.0600	3.9248	0.8079	4.8179	0.0977	2.7944	0.5800	602	85	601	16	601	22	100
044		1.0000	632	0.05	0.0600	3.9410	0.8060	4.8519	0.0975	2.8302	0.5833	603	85	599	16	600	22	100
063		0.0000	592	0.06	0.0601	2.0979	0.8130	2.8540	0.0982	1.9350	0.6780	606	45	604	11	604	13	100
064		0.0000	600	0.05	0.0599	2.0687	0.8196	2.9031	0.0992	2.0367	0.7016	601	45	610	12	608	13	100
083		0.0360	633	0.06	0.0600	2.2348	0.8111	3.0002	0.0980	2.0018	0.6672	605	48	602	12	603	14	100
084		1.0000	627	0.06	0.0600	4.2690	0.8099	5.1463	0.0979	2.8741	0.5585	603	92	602	17	602	24	100

SESSION B					Isotope ratio**							Ages						
Analysis	Domain	Comm 206Pb (%)	U ppm	Th/U	207Pb 206Pb	±1s abs	207Pb 235U	±1s abs	206Pb 238U	±1s abs	Rho	207Pb 206Pb	±1s (Ma)	206Pb 238U	±1s (Ma)	207Pb 235U	±1s (Ma)	Conc***
MB-141																		
16	CL-bright rim	0.2	52	0.7	0.0723	0.0042	1.6368	0.0864	0.1642	0.0019	0.45	994	119	980	11	984	33	99
2	CL-bright rim	0.0	43	0.7	0.0725	0.0070	1.6821	0.1524	0.1682	0.0039	0.63	1001	176	1002	21	1002	58	100
13	CL-bright rim	3.4	37	0.9	0.0687	0.0075	1.5945	0.1748	0.1683	0.0023	0.01	890	216	1003	13	968	70	103
28	CL-bright rim	1.8	112	0.8	0.0732	0.0031	1.7007	0.0626	0.1686	0.0018	0.17	1018	88	1004	10	1009	24	99
11	Igneous core	2.7	130	0.7	0.0714	0.0030	1.6745	0.0681	0.1700	0.0021	0.38	970	85	1012	12	999	25	101
7	Igneous core	0.4	96	0.9	0.0716	0.0029	1.6781	0.0710	0.1700	0.0016	0.53	975	79	1012	9	1000	26	101
10	Igneous core	5.9	43	-	0.0735	0.0026	1.7220	0.0593	0.1700	0.0019	0.43	1027	72	1012	10	1017	22	99
31	Igneous core	0.8	100	0.6	0.0747	0.0026	1.7508	0.0590	0.1700	0.0017	0.46	1060	70	1012	10	1027	21	98
9	Igneous core	3.3	92	0.7	0.0712	0.0028	1.6749	0.0628	0.1706	0.0019	0.69	963	80	1016	10	999	23	101
4	Igneous core	0.0	102	0.6	0.0739	0.0030	1.7383	0.0761	0.1707	0.0015	0.75	1038	82	1016	8	1023	28	99
35	Igneous core	1.2	164	0.6	0.0758	0.0034	1.7850	0.0767	0.1708	0.0018	0.61	1090	87	1016	10	1040	27	97
32	Igneous core	1.8	107	0.6	0.0778	0.0028	1.8344	0.0660	0.1710	0.0016	0.43	1142	73	1018	9	1058	24	96
34	Igneous core	0.8	141	0.7	0.0751	0.0034	1.7709	0.0786	0.1710	0.0014	0.71	1071	92	1018	8	1035	30	98
1	Igneous core	2.2	59	1.0	0.0730	0.0031	1.7312	0.0658	0.1720	0.0025	0.45	1014	86	1023	14	1020	25	100
3	Igneous core	0.0	209	0.5	0.0733	0.0017	1.7388	0.0433	0.1720	0.0014	0.63	1022	46	1023	8	1023	16	100
8	Igneous core	0.0	-	0.1	0.0751	0.0032	1.7847	0.0746	0.1723	0.0017	0.68	1072	83	1025	9	1040	27	98
18	Igneous core	1.7	170	0.7	0.0782	0.0027	1.8600	0.0600	0.1725	0.0013	0.23	1152	72	1026	7	1067	22	96
25	Igneous core	0.0	152	0.8	0.0709	0.0027	1.6939	0.0601	0.1734	0.0013	0.74	954	77	1031	7	1006	22	102
24	Igneous core	4.0	116	0.6	0.0666	0.0036	1.5982	0.0819	0.1741	0.0013	0.31	824	108	1035	7	970	32	106
33	Igneous core	0.0	135	0.5	0.0747	0.0029	1.7953	0.0679	0.1744	0.0015	0.57	1060	81	1036	8	1044	25	99
29	Igneous core	1.2	206	0.7	0.0768	0.0026	1.8524	0.0610	0.1748	0.0015	0.46	1117	68	1039	8	1064	22	97
30	Igneous core	1.7	86	0.7	0.0794	0.0033	1.9166	0.0793	0.1750	0.0016	0.46	1183	88	1040	9	1087	28	95
17	Igneous core	0.0	94	0.5	0.0774	0.0028	1.8827	0.0611	0.1764	0.0014	0.72	1131	73	1047	8	1075	22	97
14	Igneous core	0.0	55	0.8	0.0789	0.0043	1.9395	0.0987	0.1783	0.0026	0.30	1170	109	1057	14	1095	35	96
5	Igneous core	0.5	45	0.8	0.0740	0.0070	1.8290	0.1567	0.1793	0.0032	0.65	1041	182	1063	18	1056	62	100

~~*Rejected data*~~																		
~~6~~		~~1.3~~	~~82~~	~~0.7~~	~~0.0754~~	~~0.0031~~	~~1.9401~~	~~0.0787~~	~~0.1866~~	~~0.0020~~	~~0.67~~	~~1080~~	~~86~~	~~1103~~	~~11~~	~~1095~~	~~29~~	~~100~~
~~15~~		~~0.0~~	~~8~~	~~45017~~	~~0.0799~~	~~0.0088~~	~~2.0277~~	~~0.2161~~	~~0.1841~~	~~0.0038~~	~~0.53~~	~~1194~~	~~140~~	~~1089~~	~~21~~	~~1125~~	~~89~~	~~96~~
~~22~~		~~0.0~~	~~-~~	~~45078~~	~~0.0411~~	~~0.0060~~	~~1.1946~~	~~0.1670~~	~~0.2107~~	~~0.0033~~	~~0.98~~	~~0~~	~~167~~	~~1233~~	~~18~~	~~798~~	~~57~~	~~154~~
~~21~~		~~0.0~~	~~-~~	~~44986~~	~~0.0707~~	~~0.0043~~	~~1.7781~~	~~0.1108~~	~~0.1823~~	~~0.0017~~	~~0.75~~	~~950~~	~~112~~	~~1080~~	~~9~~	~~1037~~	~~40~~	~~104~~
~~26~~		~~2.3~~	~~47~~	~~44958~~	~~0.0871~~	~~0.0034~~	~~2.1701~~	~~0.0715~~	~~0.1807~~	~~0.0026~~	~~0.34~~	~~1363~~	~~87~~	~~1071~~	~~14~~	~~1172~~	~~26~~	~~91~~
~~12~~		~~2.9~~	~~102~~	~~0.8~~	~~0.0662~~	~~0.0028~~	~~1.5335~~	~~0.0630~~	~~0.1680~~	~~0.0020~~	~~0.41~~	~~813~~	~~81~~	~~1001~~	~~11~~	~~944~~	~~25~~	~~106~~
~~27~~		~~0.2~~	~~289~~	~~44958~~	~~0.0745~~	~~0.0023~~	~~1.8273~~	~~0.0501~~	~~0.1779~~	~~0.0015~~	~~0.51~~	~~1054~~	~~63~~	~~1056~~	~~8~~	~~1055~~	~~18~~	~~100~~
~~19~~		~~12.7~~	~~67~~	~~0.7~~	~~0.0744~~	~~0.0026~~	~~1.7394~~	~~0.0529~~	~~0.1697~~	~~0.0017~~	~~0.49~~	~~1051~~	~~72~~	~~1010~~	~~10~~	~~1023~~	~~19~~	~~98~~
~~20~~		~~17.6~~	~~44~~	~~45139~~	~~0.0703~~	~~0.0060~~	~~1.7103~~	~~0.1381~~	~~0.1764~~	~~0.0047~~	~~0.75~~	~~938~~	~~177~~	~~1047~~	~~25~~	~~1012~~	~~49~~	~~103~~
~~23~~		~~24.3~~	~~36~~	~~45078~~	~~0.0733~~	~~0.0056~~	~~1.7941~~	~~0.1352~~	~~0.1775~~	~~0.0023~~	~~0.27~~	~~1023~~	~~156~~	~~1053~~	~~13~~	~~1043~~	~~51~~	~~100~~
MB-147																		
11	Igneous core	5.0	46	1.05	0.0740	0.0028	1.7079	0.0782	0.1674	0.0036	0.90	1042	76	998	20	1011	29	98
9	Igneous core	0.5	350	0.14	0.0751	0.0022	1.7560	0.0680	0.1697	0.0032	0.85	1070	59	1010	18	1029	25	98
10	Igneous core	4.0	157	0.53	0.0768	0.0021	1.8015	0.0662	0.1700	0.0032	0.61	1117	56	1012	17	1046	24	96
3	Igneous core	2.6	244	0.49	0.0706	0.0019	1.6677	0.0469	0.1714	0.0018	0.34	945	51	1020	10	996	17	102
13	Igneous core	1.0	227	0.66	0.0754	0.0020	1.7939	0.0604	0.1725	0.0033	0.73	1079	53	1026	18	1043	22	98
15	Igneous core	0.8	142	0.47	0.0691	0.0030	1.6480	0.0711	0.1730	0.0024	0.40	902	87	1029	13	989	27	104
6	Igneous core	0.7	134	0.72	0.0750	0.0032	1.7944	0.0810	0.1736	0.0018	0.36	1068	92	1032	10	1043	31	98
2	Igneous core	0.0	503	0.10	0.0714	0.0019	1.7239	0.0501	0.1752	0.0017	0.40	968	54	1041	9	1017	18	102
12	Igneous core	0.9	204	0.71	0.0749	0.0021	1.8238	0.0672	0.1766	0.0032	0.77	1066	57	1048	18	1054	24	99
~~*Rejected data*~~																		
~~1~~		~~1.6~~	~~423~~	~~0.10~~	~~0.0776~~	~~0.0016~~	~~1.8798~~	~~0.0430~~	~~0.1757~~	~~0.0017~~	~~0.20~~	~~1136~~	~~42~~	~~1044~~	~~10~~	~~1074~~	~~15~~	~~97~~
~~8~~		~~0.3~~	~~162~~	~~0.2~~	~~0.0740~~	~~0.0016~~	~~1.8461~~	~~0.0422~~	~~0.1809~~	~~0.0017~~	~~0.95~~	~~1042~~	~~44~~	~~1072~~	~~9~~	~~1062~~	~~15~~	~~100~~
~~5~~		~~0.0~~	~~114~~	~~1.4~~	~~0.0698~~	~~0.0070~~	~~0.9211~~	~~0.0776~~	~~0.0957~~	~~0.0015~~	~~0.31~~	~~924~~	~~171~~	~~589~~	~~9~~	~~663~~	~~44~~	~~88~~
~~4~~		~~1.8~~	~~56~~	~~1.1~~	~~0.0643~~	~~0.0035~~	~~1.6101~~	~~0.0904~~	~~0.1817~~	~~0.0022~~	~~0.47~~	~~751~~	~~109~~	~~1076~~	~~12~~	~~974~~	~~34~~	~~110~~
~~7~~		~~0.0~~	~~167~~	~~0.9~~	~~0.0721~~	~~0.0026~~	~~1.8330~~	~~0.0722~~	~~0.1843~~	~~0.0021~~	~~0.47~~	~~990~~	~~75~~	~~1090~~	~~11~~	~~1057~~	~~26~~	~~103~~
~~14~~		~~0.1~~	~~443~~	~~0.1~~	~~0.0753~~	~~0.0020~~	~~1.7025~~	~~0.0609~~	~~0.1641~~	~~0.0030~~	~~0.78~~	~~1075~~	~~55~~	~~979~~	~~16~~	~~1009~~	~~23~~	~~97~~

Supplementary Data Table S3. Lu-Hf isotope composition of the investigated zircons

Analysis	Domain	Age (Ma)	±2s	176Yb/177Hf	±2s	176Lu/177Hf	±2s	178Hf/177Hf	180Hf/177Hf	SigHf b (V)	176Hf/177Hf	±2s	176Hf/177Hf(t)	eHf(t)	±2s	TDM (Ga)
MB-146B																
35	Detrital core	1104	66	0.014054	11	0.000507	3	1.467210	1.88687	16	0.282282	15	0.282271	6.60	1.00	1.44
31	Detrital core	1115	43	0.025486	20	0.001038	6	1.467287	1.88672	16	0.282306	15	0.282285	7.32	1.01	1.41
20	Detrital core	1127	41	0.032780	26	0.001249	8	1.467228	1.88690	14	0.282186	18	0.282160	3.16	1.02	1.65
27	Detrital core	1134	42	0.039691	32	0.001383	8	1.467222	1.88681	21	0.282061	16	0.282031	-1.23	1.04	1.90
96	Detrital core	1153	51	0.021416	17	0.000870	5	1.467195	1.88673	19	0.282288	18	0.282269	7.64	1.00	1.42
174	Detrital core	1180	42	0.048214	40	0.001929	12	1.467226	1.88677	18	0.281784	22	0.281741	-10.46	1.06	2.44
160	Detrital core	1259	40	0.028875	24	0.001141	7	1.467150	1.88660	19	0.282145	14	0.282118	4.68	1.02	1.67
180	Detrital core	1344	81	0.011166	9	0.000453	3	1.467232	1.88683	10	0.282173	19	0.282161	8.15	0.99	1.55
11	Detrital core	1716	37	0.016224	13	0.000612	4	1.467285	1.88677	17	0.281645	17	0.281625	-2.35	1.00	2.43
MB-144																
135	Igneous core	1046	43	0.034187	27	0.001300	8	1.467194	1.886810	15	0.282209	19	0.282183	2.17	1.03	1.64
138	Recryst. core	1049	41	0.018608	15	0.000742	5	1.467237	1.886739	15	0.282226	13	0.282211	3.21	1.00	1.58
158	Recryst. core	1052	41	0.023210	29	0.000943	8	1.467244	1.886709	14	0.282220	17	0.282201	2.92	1.03	1.60
107	Recryst. core	1052	69	0.024005	19	0.000940	6	1.467231	1.886734	16	0.282220	15	0.282201	2.93	1.01	1.60
148	Recryst. core	1058	42	0.010354	9	0.000413	3	1.467211	1.886853	16	0.282219	14	0.282211	3.40	0.99	1.58
100	Recryst. core	1062	43	0.010865	9	0.000435	3	1.467237	1.886766	9	0.282207	26	0.282198	3.04	0.99	1.60
111	Recryst. core	1063	41	0.030676	25	0.001152	7	1.467256	1.886778	13	0.282201	15	0.282178	2.37	1.02	1.64
149	Recryst. core	1064	46	0.023079	19	0.000920	6	1.467244	1.886867	12	0.282197	17	0.282178	2.39	1.01	1.64
112	Recryst. core	1069	42	0.029929	24	0.001167	7	1.467202	1.886761	16	0.282194	16	0.282170	2.23	1.02	1.65
97	Recryst. core	1073	67	0.007866	7	0.000305	2	1.467268	1.886905	12	0.282213	18	0.282206	3.59	0.99	1.58
155	Recryst. core	1081	42	0.027664	22	0.001135	7	1.467249	1.886764	16	0.282198	12	0.282174	2.64	1.01	1.64
114	Recryst. core	1083	43	0.009006	7	0.000345	2	1.467256	1.886976	8	0.282234	24	0.282227	4.56	0.99	1.54
MB-148																
198	Igneous core	1043	41	0.015425	12	0.000583	3	1.467224	1.88683	16	0.282212	15	0.282201	2.70	1.00	1.61
200	Igneous core	1071	41	0.019520	16	0.000729	4	1.467203	1.88688	21	0.282187	13	0.282173	2.34	1.00	1.65
211	Igneous core	1075	67	0.027602	22	0.000928	6	1.467260	1.88678	18	0.282163	17	0.282144	1.44	1.01	1.70
193	Igneous core	1076	67	0.019558	16	0.000717	4	1.467229	1.88694	16	0.282188	14	0.282173	2.48	1.00	1.65
227	Igneous core	1080	46	0.024622	20	0.000891	5	1.467237	1.88681	20	0.282207	17	0.282189	3.13	1.01	1.61
230	Igneous core	1083	45	0.017898	14	0.000675	4	1.467285	1.88700	12	0.282178	17	0.282164	2.32	1.00	1.66
214	Igneous core	1087	42	0.018719	15	0.000682	4	1.467247	1.88679	18	0.282211	14	0.282197	3.58	1.00	1.59
231	Igneous core	1093	50	0.018030	14	0.000688	4	1.467265	1.88675	19	0.282219	15	0.282204	3.97	1.00	1.58
195	Igneous core	1100	43	0.015630	13	0.000570	3	1.467225	1.88679	21	0.282222	16	0.282210	4.33	1.00	1.56
220	Igneous core	1108	41	0.016732	13	0.000607	4	1.467211	1.88670	18	0.282186	15	0.282173	3.20	1.00	1.63
228	Igneous core	1118	66	0.017108	14	0.000603	4	1.467230	1.88670	18	0.282202	16	0.282189	4.01	1.00	1.59
192	Igneous core	1122	72	0.023878	19	0.000882	5	1.467205	1.88675	22	0.282198	15	0.282180	3.76	1.01	1.61
171	Igneous core	1131	41	0.022621	18	0.000821	5	1.467241	1.88684	19	0.282170	13	0.282153	3.01	1.00	1.66
179	Igneous core	1148	44	0.021711	18	0.000769	5	1.467197	1.88671	20	0.282157	14	0.282140	2.96	1.00	1.68
217	Igneous core	1495	43	0.010553	8	0.000394	2	1.467285	1.88645	11	0.282172	27	0.282160	11.59	0.99	1.48
Reference materials																
BB																
3		560	1	0.0046	4	0.00016	1	1.46720	1.88671	15	0.281693	14	0.281691	-26.23	0.60	2.6
5		560	1	0.0045	4	0.00015	1	1.46722	1.88673	16	0.281666	17	0.281664	-27.18	0.60	2.7
62		560	1	0.0047	4	0.00016	1	1.46728	1.88691	17	0.281672	14	0.281670	-26.96	0.60	2.6
63		560	1	0.0047	4	0.00016	1	1.46723	1.88685	16	0.281675	14	0.281673	-26.86	0.60	2.6
65		560	1	0.0048	4	0.00016	1	1.46724	1.88683	16	0.281661	14	0.281659	-27.35	0.60	2.7
122		560	1	0.0047	4	0.00016	1	1.46721	1.88677	19	0.281685	14	0.281683	-26.50	0.60	2.6
123		560	1	0.0046	4	0.00015	1	1.46724	1.88674	18	0.281668	15	0.281667	-27.09	0.60	2.6
124		560	1	0.0048	4	0.00016	1	1.46725	1.88679	19	0.281674	14	0.281672	-26.90	0.60	2.6
~~6~~		~~560~~	~~1~~	~~0.0044~~	~~4~~	~~0.00015~~	~~1~~	~~1.46719~~	~~1.88674~~	~~15~~	~~0.281635~~	~~16~~	~~0.281633~~	~~-28.29~~	~~0.60~~	~~2.7~~
~~64~~		~~560~~	~~1~~	~~0.0048~~	~~4~~	~~0.00016~~	~~1~~	~~1.46725~~	~~1.88685~~	~~16~~	~~0.281650~~	~~16~~	~~0.281648~~	~~-27.76~~	~~0.60~~	~~2.7~~
Mudtank																
7		732	1	0.0011	1	0.00004	0	1.46728	1.88686	16	0.282506	12	0.282505	6.47	0.60	1.0
8		732	1	0.0010	1	0.00003	0	1.46722	1.88679	17	0.282510	16	0.282509	6.62	0.60	0.9
9		732	1	0.0011	1	0.00003	0	1.46725	1.88681	17	0.282492	13	0.282491	5.97	0.60	1.0
10		732	1	0.0010	1	0.00003	0	1.46719	1.88689	17	0.282510	16	0.282510	6.63	0.60	0.9
66		732	1	0.0010	1	0.00003	0	1.46725	1.88683	18	0.282517	16	0.282516	6.86	0.60	0.9
67		732	1	0.0010	1	0.00003	0	1.46724	1.88681	18	0.282521	13	0.282520	7.01	0.60	0.9
68		732	1	0.0010	1	0.00003	0	1.46722	1.88679	19	0.282508	12	0.282507	6.54	0.60	0.9
69		732	1	0.0010	1	0.00003	0	1.46726	1.88684	20	0.282499	13	0.282499	6.24	0.60	1.0
125		732	1	0.0010	1	0.00003	0	1.46723	1.88681	19	0.282504	14	0.282504	6.42	0.60	1.0
126		732	1	0.0010	1	0.00003	0	1.46722	1.88676	20	0.282518	14	0.282517	6.90	0.60	0.9
127		732	1	0.0010	1	0.00003	0	1.46721	1.88680	19	0.282511	14	0.282510	6.65	0.60	0.9
GJ-1																
12		602	1	0.0065	5	0.00026	2	1.46728	1.88694	10	0.282004	23	0.282001	-14.31	0.60	2.0
13		602	1	0.0066	5	0.00026	2	1.46726	1.88685	10	0.282008	17	0.282006	-14.15	0.60	2.0
14		602	1	0.0066	5	0.00026	2	1.46719	1.88663	11	0.282012	21	0.282009	-14.04	0.60	2.0
70		602	1	0.0065	5	0.00026	2	1.46725	1.88668	12	0.282018	22	0.282015	-13.80	0.60	2.0
71		602	1	0.0066	5	0.00026	2	1.46725	1.88682	12	0.281992	14	0.281989	-14.72	0.60	2.0
72		602	1	0.0066	5	0.00026	2	1.46724	1.88680	12	0.282000	17	0.281997	-14.45	0.60	2.0
73		602	1	0.0066	5	0.00026	2	1.46720	1.88684	12	0.281997	16	0.281994	-14.55	0.60	2.0
11		602	1	0.0066	5	0.00026	2	1.46724	1.88672	10	0.282032	20	0.282029	-13.31	0.60	1.9
129		602	1	0.0067	5	0.00026	2	1.46724	1.88680	13	0.282029	19	0.282027	-13.41	0.60	1.9
130		602	1	0.0066	5	0.00026	2	1.46725	1.88682	13	0.282025	14	0.282022	-13.57	0.60	2.0
Plesovice																
16		337	1	0.0083	7	0.00022	1	1.46723	1.88679	16	0.282463	17	0.282462	-3.94	0.60	1.2
17		337	1	0.0060	5	0.00015	1	1.46724	1.88682	17	0.282482	16	0.282481	-3.24	0.60	1.2
18		337	1	0.0075	7	0.00020	1	1.46722	1.88677	16	0.282481	17	0.282479	-3.32	0.60	1.2
74		337	1	0.0049	4	0.00012	1	1.46721	1.88678	20	0.282488	12	0.282487	-3.03	0.60	1.2

75	337	1	0.0050	4	0.00013	1	1.46725	1.88672	19	0.282483	17	0.282482	-3.21	0.60	1.2
76	337	1	0.0088	7	0.00023	1	1.46723	1.88683	19	0.282462	12	0.282461	-3.97	0.60	1.2
76	337	1	0.0073	6	0.00018	1	1.46722	1.88670	19	0.282461	15	0.282459	-4.02	0.60	1.2
132	337	1	0.0059	5	0.00015	1	1.46728	1.88686	19	0.282467	13	0.282466	-3.77	0.60	1.2
133	337	1	0.0067	5	0.00017	1	1.46724	1.88671	19	0.282462	15	0.282461	-3.96	0.60	1.2

	Sample name	Region	Unit	Lithology	U-Pb ages (Ma)			Reference
					MDA	Crystallization	Metamorphism	
Accretionary phase	SJ106	Rufunsa		Plagiogranite		1393±22		Oliver et al. (1998)
	MOS 34	Tete Province	Fíngoè Supergroup	Meta-andesite		1327±10		Manttari (2008)
	MOS 1	Tete Province	Rio Capoche granite	Granite		1201±10		Manttari (2008)
	MB179	Tete Province	Fíngoè Supergroup	Calc-silicatic schist	1143±2			Petry et al. (2022)
	MB138	Tete Province	Cazula Complex	Grt-bt-qz schist	1137±1			Petry et al. (2022)
	MB144	Tete Province	Chidzolomondo Complex	Metagabbro		1133±15	1061±3; 1023±12	This study
	MOS 15	Tete Province	Cassacatiza Suite	Granite		1117±12		Manttari (2008)
	MB182	Tete Province	Zâmbué Supergroup	Meta-arkose	1110±2			Petry et al. (2022)
	MB148	Tete Province	Chidzolomondo Complex	Charnockitic gneiss		1110±2	1060±10	This study
	MB146	Tete Province	Chidzolomondo Complex	Paragneiss	1100±3		1092±5; 1064±5	This study
	MB181	Tete Province	Fíngoé Supergroup	Meta-andesite	1095±10			Petry et al. (2022)
	C61a	Rufunsa	Chongwe Complex	Felsic gneiss		1088±4		Johnson et al. (2007)
	ADC	Rufunsa		Granitic orthogneiss		1087±9	1068±21	Goscombe et al. (2000)
	MOS 18	Tete Province	Monte Capirimpica granite	Granite		1086±7		Manttari (2008)
	CHAK48a	Rufunsa	Chakwenga Complex	Felsic gneiss		1083±18		Johnson et al. (2007)
	MB137	Tete Province	Cazula Complex	Diabase	1082±3			Petry et al. (2022)
	MB135	Tete Province	Cazula Complex	Metasandstone	1077±1			Petry et al. (2022)
	MOS 9	Tete Province	Cassacatiza Suite	Granite		1077±2		Manttari (2008)
	CHP10	Chipata		Porphiritic granite		1076±14		Johnson et al. (2006)
	CHP4a	Chipata		Charnockitic gneiss		1076±6		Johnson et al. (2006)
	C70	Rufunsa	Chongwe Complex	Felsic gneiss		1070±3		Johnson et al. (2007)
	Z-118	Chipata		Grt-Crd-Sil gneiss			1067±15 (monazite)	Karmakar and Schenk (2016)
nal phase	CHP8	Chipata		Porphiritic granite		1061±13		Johnson et al. (2006)
	MOS 10	Tete Province	Monte Sanja Suite	Granite		1050±8		Manttari (2008)
	BM179	SW Malawi	Furacungo Suite	Granite		1047±12		Manda et al. (2019)
	CHP2a	Chipata		Augen gneiss		1046±4		Johnson et al. (2006)
	PS65	Petauke		Granite		1043±14		Johnson et al. (2006)
	MOS 11	Tete Province	Furacungo Suite	Granite		1041±4		Manttari (2008)
	Z16-41	Chipata		Charnockite		1040±5		Alessio et al. (2019)
	Z16-42	Chipata		Charnockite		1039±6		Alessio et al. (2019)
	BM163	SW Malawi	Furacungo Suite	Granite		1039±12		Manda et al. (2019)

	Sample name	Region	Unit	Lithology	U-Pb ages (Ma)			Reference
					MDA	Crystallization	Metamorphism	
Late- to post-collision	CHP12	Chipata		Porphiritic granite		1038±9		Johnson et al. (2006)
	CHP6a	Chipata		Granite		1038±6		Johnson et al. (2006)
	BM256	SW Malawi	Furacungo Suite	Granite		1033±40		Manda et al. (2019)
	Z-126	Chipata		Grt-Sil-Spl-Qz granulite			1031±4 (monazite)	Karmakar and Schenk (2016)
	BM174	SW Malawi	Furacungo Suite	Granite		1029±8		Manda et al. (2019)
	BM249	SW Malawi	Castanho Suite?	Charnockitic gneiss		1027±11		Manda et al. (2019)
	MB141	Tete Province		Charnockite		1025±4		This study
	Z-127	Chipata		Grt-Sil-Spl-Qz granulite			1024±8 (monazite)	Karmakar and Schenk (2016)
	SZ25C	Nyamadzi Shear Zone		Milonitic granite		1023±12		Johnson et al. (2006)
	BM209	SW Malawi	Furacungo Suite	Granite		1023±21		Manda et al. (2019)
	Z-115	Chipata		Grt-Sil-Spl-Qz granulite			1021±4 (monazite)	Karmakar and Schenk (2016)
	MB132	Tete Province		Charnockite		1019±17		This study
	Z-120	Chipata		Grt-Opx-Crd granulite			1013±4 (monazite)	Karmakar and Schenk (2016)
	SZ23	Nyamadzi Shear Zone		Ultramilonite		1008±17		Johnson et al. (2006)